Mechanisms of Phenotypic Variability in Myotonia Congenita

James Burge

A thesis submitted to University College London for the degree of Doctor of Philosophy

Department of Molecular Neuroscience
Institute of Neurology
Queen Square
London
WC1N 3BG

Declaration

I, James Burge, confirm that the work presented in this thesis is my original research work. Where contributions of others are involved, this has been clearly indicated in the thesis.

Acknowledgements

I am extremely grateful to my two supervisors Prof. Mike Hanna and Dr. Stephanie Schorge for giving me the opportunity, freedom, and support to explore my own ideas, and for keeping me on track. I also thank Prof Dimitri Kullmann for his guidance and for allowing me to tinker with his excellent LabView virtual instrument. My colleagues Drs. Emily Fletcher, Clare Farmer, Sanjeev Rajakulendran, Klaus Wanisch and Rahima Begum helped to teach me many of the basic laboratory techniques that were necessary for this thesis and have been great friends. Dr. Rahima Begum in addition kindly shared her muscle tissue with me (that is, tissue from her experimental subjects). Thanks also to Dr. Iris Oren for her patience with the dreaded pipette-puller and its filament, and for sharing tissue from her experimental subjects. Drs Mary Davis, Andrea Howorth, and Richa Sud in the department of clinical genetics were very kind to grant me access to the CLCN1 sequencing data (and also to their supply of tea, coffee and biscuits). A major segment of this work would not have been possible without the expert advice from Dr. John Lueck regarding whole cell patch clamp of skeletal muscle fibres. Most importantly, thanks to my family, Jennie and Finn, for everything else.

Abstract

The severity of Myotonia Congenita varies not only across individuals with different CLCN1 genotypes, but also within a pedigree, and can even fluctuate over time within a single individual in response to environmental circumstances. The functional consequences of eight naturally occurring sequence variants in the skeletal muscle chloride channel gene, CLCN1, were examined by whole cell patch-clamp of HEK293T cells expressing the gene product, ClC-1, in order to investigate potential differences in their mechanisms of pathogenicity. G276D and G523D caused complete loss of function, while S289G produced altered kinetics and a marked depolarizing shift of voltage dependence. H369P, A566T and M646T all tested normal in the HEK293T assay despite strong clinical support for pathogenicity. Their mechanism of pathogenicity may rely on muscle-specific processes that are not faithfully recapitulated in HEK293T cells. W118G and P744T were selected as examples of variants for which pathogenicity is unclear from the clinical evidence. The former is present in controls, but over-represented in the Myotonia Congenita population. The latter is present in an individual who also harbours a large deletion in CLCN1. Both variants tested normal in the HEK293T assay.

A potent trigger for worsening of myotonia in some female patients is pregnancy. In order to clarify the role of sex hormones in non-genomic modulation of skeletal muscle excitability, the effects of progesterone and oestrogen on endogenous chloride currents through the wildtype ClC-1 of mouse skeletal muscle were tested by whole cell patch clamp. Progesterone and oestrogen rapidly reduced the chloride conductance and shifted its voltage dependence, thus a non-genomic mechanism exists in skeletal muscle linking sex

hormones to ClC-1. However the effect was only significant at 500 times the highest physiological concentration encountered in pregnancy.

The macroscopic chloride conductance of a membrane expressing wildtype ClC-1 was simulated in Matlab. The simulation improves on published models by recapitulating both time-dependence and voltage-dependence of the channel through a method based on independent representations of the fast and the slow gates. The applicability of the model for the purposes of exploring the effects of specific mutations was assessed by attempting to simulate the currents through S289G channels; the effects of S289G could be mimicked by slowing and inverting the kinetics of the fast gate and shifting the fast gate opening probability to more depolarized potentials. The mechanism of low chloride conductance myotonia and electrical factors likely to impact on its severity are discussed in the context of experiments conducted in a model of myotonic muscle. Slowing of ClC-1 kinetics alone did not produce myotonia, but could lower the threshold for myotonia caused by shifts in voltage dependence. Muscle fibre diameter is an important factor in the propensity to myotonia, which can be driven by asynchrony between surface and t-tubular action potentials in large muscle fibres. Increasing muscle fibre diameter could underly the age-dependence of symptom onset in Myotonia Congenita, and differences in diameter could contribute to phenotypic variability, including male-female differences.

Table of Contents

List of Tables

List of Figures

List of abbreviations

ATP	Adenosine triphosphate
BSA	Bovine serum albumin
BTS	N-benzyl-p-toluene sulphonamide
CLCN1	Gene encoding the skeletal muscle chloride channel, ClC-1
ClC-1	The skeletal muscle chloride channel
CsCl	Caesium chloride
CsOH	Cesium hydroxide
DMEM	Dulbecco's modified Eagle's medium
DMSO	Dimethyl sulphoxide
dNTP	Deoxynucleotide triphosphatases
DNA	Deoxyribonucleic acid
EDTA	Ethylenediaminetetraacetic acid
EMG	Electromyography
E_{ion}	Equilibrium potential for an ion
F	Faraday's constant (96485.3383 coulombs per mole)
HCl	Hydrochloric acid

HEK293T	Human Embryonic Kidney Cells expressing the SV40 large T antigen
HEPES	4-(2-hydroxyethyl)-1-piperazineethanesulfonic acid
KCL	Potassium chloride
Kir2.1	Inward rectifier potassium channel 2.1
Kb	Kilobase (1000 base pairs of a DNA or RNA molecule)
LB	Luria Bertani medium
MC	Myotonia Congenita
mRNA	Messenger ribonucleic acid
NaCl	Sodium chloride
NaOH	Sodium hydroxide
PCR	Polymerase chain reaction
PBS	Phosphate-Buffered Saline
PKC	Protein kinase C
R	The gas constant (8.314472 Joules per Mole per Kelvin)
SEM	Standard error of the mean
S.O.C	Super optimal broth with Catabolite repression
T	Temperature (in Kelvin for equations of chapter 5)

UV	Ultraviolet
UCSC	University of California Santa Cruz
V_{50}	Voltage that produces half maximal activation/inactivation
V_m	Membrane potential

Chapter 1 Introduction

1.1 Clinical aspects of Myotonia Congenita

Autosomal dominant Myotonia Congenita (Thomsen's disease) was identified in the 19th century by the Danish physician, Julius Thomsen, who suffered from the disease himself, while the recessive variant (Becker's disease) was not recognised until 100 years later. Myotonia is a temporary inability of the skeletal muscle fibres to relax after a contraction, leading to symptoms of stiffness, pain and muscle locking that can cause falls. The relaxation time shortens and may normalize during a series of repeated contractions so that stiffness wears off with exercise (warm-up phenomenon). In addition to myotonia, more severely affected patients with Myotonia Congenita experience transient muscle weakness at the onset of muscle activity. Myotonia Congenita is one of the Non-Dystrophic Myotonias, so named to distinguish them from Myotonic Dystrophy, in which low chloride conductance myotonia (Lueck, Lungu et al. 2007) is part of a wider syndrome affecting many systems (including the eyes, heart, brain, and endocrine glands). In the latter there is muscle wasting and weakness owing to structural damage to muscle fibres (dystrophy). In contrast the Non-Dystrophic Myotonias are classically associated with muscle hypertrophy in response to the involuntary exercise associated with myotonia, although the most severely affected individuals with Myotonia Congenita may develop permanent weakness and muscle wasting (Colding-Jorgensen 2005). The Non-Dystrophic Myotonias are ion channelopathies (diseases caused by mutations in ion channel genes) whereas in Myotonic Dystrophy chloride ion channel expression is disrupted along with expression of many other proteins, but not as a result of an ion channel mutation (Mankodi, Takahashi et al.

2002; Cooper 2007; Lueck, Lungu et al. 2007). Mutations in CLCN1, the gene for the skeletal muscle voltage-gated chloride channel, ClC-1, cause Myotonia Congenita. Mutations in SCN4A, the gene that codes for the alpha subunit of the skeletal muscle voltage-gated sodium channel, NaV1.4, cause a spectrum of phenotypes from pure myotonia (a group of syndromes collectively known as Sodium Channel Myotonia or Potassium Aggravated Myotonia) through to overlap syndromes with varying degrees of myotonia and/or episodic weakness (Paramyotonia Congenita and Hyperkalaemic Periodic Paralysis).

In Myotonia Congenita, the onset of symptoms and/or clinical signs is typically in childhood, and usually the lower limbs are affected first. In severe cases the parents may notice manifestations of myotonia around the time that the affected infant begins to walk. Milder disease presents later in childhood or adolescence, and in some cases the symptoms go un-noticed or are put down to a curiosity or quirk of the family. Patients may complain of 'stiffness', 'muscles locking up', 'spasms', 'cramp', or 'difficulty getting started'. Muscle pain is a problem for approximately a third of patients (Fialho, Schorge et al. 2007; Trip, Drost et al. 2009). Rapid corrective movements, for example after catching a foot on an uneven surface, may cause sudden stiffness that leads to a fall. In addition to lower limb symptoms, patients may complain of difficulty letting go of objects or of their hands 'sticking'. Symptoms are often exacerbated by exposure to cold but the clinician should take care to distinguish worsening of myotonic symptoms (as occurs in Myotonia Congenita) from cold-induced muscle weakness as occurs in Paramyotonia Congenita. In Paramyotonia Congenita, which is caused by mutations in the skeletal muscle sodium channel gene SCN4A, myotonia is exacerbated rather than alleviated by exercise

(paradoxical myotonia). In Myotonia Congenita symptoms are worst after a period of rest, for example during a long journey, and are alleviated by on-going gentle muscle activity (warm-up phenomenon). Patients may prepare for disembarkation by contracting their leg muscles to produce the warm-up phenomenon in advance of a journey's end. Asking a patient suspected to have Myotonia Congenita whether and how well he plays sports may elicit a story of good performance dependent upon continued activity and difficulty or slowness to get started after any rests and at the onset of the game. A story of having to be rescued from a cold swimming pool owing to muscle weakness and of worsening symptoms with continued exercise would be more in keeping with Paramyotonia Congenita than of Myotonia Congenita.

There may be a family history of myotonia, but often there is not (sporadic and recessive disease). Careful clinical and electrophysiological examination of the parents can be helpful in determining the likely mode of inheritance. Myotonia may have gone un-noticed in an affected parent.

On clinical examination muscle hypertrophy is often striking, leading to the textbook description of the child with Myotonia Congenita as a 'mini-Hercules'. Clinical examination should seek to elicit both action myotonia (delayed relaxation after voluntary muscle contraction) and percussion myotonia (contraction of a muscle after it is struck by a tendon hammer). Action myotonia may be evident from the moment the patient is invited in from the waiting room as slowness and stiffness when rising from the waiting room chair and a stiff, labored gait, particularly if they have been waiting for some time. The warm-up phenomenon may also be observed at this stage as an improvement in the gait by the time he or she reaches the clinic room. Grip myotonia can sometimes be detected at the first

handshake as a delay or difficulty letting go, but is more consistently elicited by asking the patient to clench the fists tight for ten seconds and then snap the hands open. On repetition of this manoeuvre the slowness and difficulty in opening the fists, which may be very marked at first, typically improves, often to normality as a consequence of the warm-up phenomenon. The warm-up phenomenon can be seen in Sodium Channel Myotonia but grip myotonia that worsens with repetition of fist-clenching (paradoxical myotonia) does not occur in Myotonia Congenita (Trip, Drost et al. 2009). Action myotonia of the face is usually more pronounced in myotonia caused by sodium channel mutations than in Myotonia Congenita, where myotonia is usually worse in the lower limbs than in the face. The patient can be asked to tightly close the eyes and snap them open, analogous to the test for grip myotonia. Subtle eye-lid myotonia may only be detectable as lid-lag on rapid down-gaze. In the clinical distinction between sodium and chloride channel mutations, transient weakness is specific for the latter but not particularly sensitive as it tends only to occur in the more severely affected individuals, typically with recessive disease. Percussion myotonia is often sought by tapping the thenar eminence with a tendon hammer to elicit a myotonic contraction of thenar muscles and movement of the thumb. In more proximal upper limb muscles, and in the lower limb, there is usually not movement of a joint but local muscle contraction at the site of percussion leaves a dimple where the tendon hammer strikes. Percussion myotonia of the tongue can be elicited by holding a tongue depressor on the tongue and tapping it with a tendon hammer. Transient weakness can be elicited by repeatedly testing the strength of shoulder abduction (asking the patient to repeatedly resist firm downward pressure from the examiner on the abducted arms). The test is positive if there is mild weakness of shoulder abduction initially followed by an improvement in

strength to normal after a few repetitions (this is another manifestation of the warm-up phenomenon).

Colding-Jørgensen has proposed an arbitrary but sensible division of disease severity into 5 grades (Colding-Jorgensen 2005) based on clinical signs and symptoms:

1) no symptoms but unequivocal myotonia on clinical examination

2) mild and/or fluctuating symptoms

3) pronounced myotonia, but no transient weakness

4) pronounced myotonia with transient weakness, but without dystrophic features

5) pronounced myotonia, transient weakness, and dystrophic features.

Autosomal dominant Myotonia Congenita tends to be milder (grades 1–3) and recessive disease more severe (grades 4–5) but there is considerable variability even among patients with the same mutation, and even within a pedigree. Males tend to be more severely affected (Colding-Jorgensen 2005). In females symptoms often worsen during pregnancy or menstruation, and in some cases the disease is only manifest at these times (Lacomis, Gonzales et al. 1999).

Studies of phenotypic variability in Myotonia Congenita are hampered by the difficulty of quantifying myotonia. Clinical scales have the advantage of relatively good test-retest repeatability, but at the cost of inter-observer differences and insensitivity to small changes in severity. Objective and quantitative measures such as muscle relaxation time or duration of myotonic discharges recorded by EMG have tended to suffer from poor test-retest repeatability (Colding-Jorgensen 2005). Recently, however, the Quantitative Myotonia

Assessment (QMA) system, a commercially available method for measuring grip myotonia, has shown promise as an outcome measure in clinical trials and also in natural history studies of myotonic disorders (Statland, Bundy et al. 2012). The reproducibility of abnormalities in the short exercise test (discussed below) is good, but abnormalities tend only to occur in recessive disease (Fournier, Arzel et al. 2004).

None of the currently available drug therapies for Myotonia Congenita target the primary defect in chloride conductance. Mexiletine, considered by many to be the most effective anti-myotonic drug, is a class Ib antiarrhythmic drug, as is Phenytoin. The actions of Class I antiarrhythmics are described succinctly in the text book of pharmacology by Rang, Dale & Ritter (H.P. Rang, M.M. Dale et al. 1995). These drugs block sodium channels in a use-dependent fashion by binding with higher affinity to open channels than to closed channels. This enables these drugs to block high-frequency trains of action potentials such as occur in cardiac arrhythmias (tachycardia) or during myotonic discharges in skeletal muscle in myotonia. Members of antiarrhythmic classes Ia, Ib and Ic differ in their kinetics and affinity for inactivated sodium channels (sodium channels cycle between open, closed and inactivated states). Class Ib drugs, including mexiletine and lignocaine, associate and dissociate rapidly (within the time scale of the normal heart rate), and bind avidly to inactivated channels, as occur in persistently depolarized cells making them ideal for preventing ventricular arrhythmias after myocardial infarction. Class Ic drugs, for example fleccanide, have slower kinetics while class Ia drugs, which were the first to be developed, have intermediate kinetics. Evidence for the efficacy of anti-myotonic drugs is largely anecdotal or based on small studies owing to the difficulty of conducting randomized controlled trials in such a rare disease, and a Cochrane review in 2006 concluded that there

was insufficient evidence to determine whether any drugs were safe or effective (Trip, Drost et al. 2006). However, after a multi-national effort to recruit patients, the Consortium for Clinical Investigation of Neurologic Channelopathies has recently published the results of a randomized controlled trial of Mexiletine 200mg three times daily in the control of symptoms and signs of myotonia in patients with Non-Dystrophic Myotonia, which show that the drug is effective (Statland, Bundy et al. 2012). Unfortunately gastro-intestinal side-effects are problematic for many patients who try mexiletine and for some an alternative drug must be used. A more serious side-effect of mexiletine is prolongation of the QT interval. The corrected QT interval should be checked before starting the drug and at regular intervals (for example yearly) while on the drug.

Acetazolamide (a carbonic anhydrase inhibitor) has some anti-myotonic effect. Its mode of action may involve increasing expression levels of ClC-1, as well as activation of BK potassium channels (Camerino, Tricarico et al. 2007). Retigabine, which acts on Kv7 potassium channels (encoded by KCNQ genes), has found a place as an anti-epileptic but also has anti-myotonic properties. In neurons KCNQ2/3 are responsible for the M-current, while KCNQ5 is found in skeletal muscle (Maljevic, Wuttke et al. 2010). Retigabine shifts the voltage-dependence of activation of KCNQ channels in a hyperpolarizing direction (Camerino, Tricarico et al. 2007), meaning that more KCNQ channels are open at physiological voltages in the presence of the drug and the membrane potential is more strongly coupled to the potassium equilibrium gradient (opposing depolarizing influences).

Rather than modulating the function of channels in the membrane, it may be possible to increase the density of ClC-1 channels expressed in the membrane; insulin-like growth factor and taurine may act in this way (Camerino, Tricarico et al. 2007). Where there is no

dominant-negative interaction between ClC-1 subunits novel therapies that increase expression would be helpful, particularly where the pathology involves a defect in trafficking of a partially function mutant allele as has been suggested for F413C (Papponen, Nissinen et al. 2008). However where there is dominant-negative interaction between a mutant and a normal allele, it would be preferable to selectively increase expression of the normal allele and/or reduce expression of the mutant. At present there are no such therapies available, nor any that can uncouple mutant from wildtype alleles to prevent dominant-negative interaction.

1.2 Establishing the diagnosis and determining pathogenicity

Clinical and electrodiagnostic assessment [electromyography, repetitive stimulation and the short exercise test (Fournier, Arzel et al. 2004; Fournier, Viala et al. 2006)] can all help to guide which gene to test in a case of myotonia. Electromyography (EMG), in which action potentials are recorded *in vivo* from the extracellular space within the muscles of patients, is helpful to confirm the clinical suspicion of myotonia. A needle electrode is inserted into the muscle and records fluctuations in the extracellular potential caused by action potentials in muscle fibres close to the recording surface. The signal is visualized on a screen, but also converted to sound. The autonomous muscle fibre action potentials in myotonia have an unmistakable modulation of frequency and amplitude leading to the term 'dive bomber potentials'. Sometimes patients with symptoms suspicious of myotonia have no detectable clinical signs, and in these cases EMG is particularly helpful to establish the diagnosis. Myotonia may be asymptomatic and is occasionally an incidental finding in patients referred for EMG for assessment of an unrelated condition. A distinctive rather high frequency 'tournado-shaped' myotonic discharge can occasionally be detected in patients

with sodium channel mutations (Tan, Matthews et al. 2012). In addition to documenting the presence of myotonia in the relaxed muscle, the electromyographer should examine the morphology and recruitment pattern of motor units when the patient is asked to contract the muscle being examined. In all but the most severe cases of Myotonia Congenita, motor unit potentials are normal. The presence of short duration polyphasic motor units potentials with early recruitment (a myopathic pattern) suggests the patient may have myotonic dystrophy, not myotonia mongenita. The choice of muscles to examine is usually based on a clinical assessment of the patient, but a standard approach is to examine one proximal and one distal muscle from the upper and lower limb.

Once the presence of myotonia has been established the electromyographer should proceed to the short exercise test, which can help to direct genetic testing towards CLCN1 or SCN4A. The short exercise test (Streib, Sun et al. 1982; Fournier, Arzel et al. 2004) was devised as a better tolerated alternative to repetitive nerve stimulation at high rates (10 Hz or more), which has been known for many years to produce a decrement in compound motor action potential (CMAP) amplitude in a subset of patients with Myotonia Congenita (Brown 1974). This electrophysiological phenomenon reflects the same process, namely depolarization-induced inactivation of sodium channels in a proportion of muscle fibres, as produces transient weakness in patients with Myotonia Congenita. The short exercise test is usually performed by recording the CMAP with surface electrodes over abductor digiti minimi in response to supramaximal stimulation of the ulnar nerve at the wrist before and at 10 second intervals over a minute after ten seconds of maximal contraction of the muscle (Figure 1.1). A fall in CMAP amplitude by 20% from the pre-exercise baseline is considered abnormal. In mild Myotonia Congenita, as exhibited by many patients with

autosomal dominant disease, there is usually no decrement (same response as normal subjects). In recessive Myotonia Congenita, which tends to be more severe, there is an immediate post-exercise decrement in CMAP amplitude, followed by a return to baseline over the minute of recording.

Cooling the muscle and repeating the test can sometimes reveal a CLCN1 pattern that was not apparent at room temperature. In Paramyotonia Congenita cooling produces a very marked attenuation of the post-exercise CMAP that fails to recover immediately on re-warming the muscle (Fournier, Viala et al. 2006). Concordant changes in the amplitude and area of the CMAPs are more specific in the diagnosis of Non-Dystrophic Myotonia by short exercise test than changes in amplitude alone (Tan, Matthews et al. 2012).

There is currently no technique available to clinical neurophysiologists that allows selective recording of transmembrane sodium and chloride currents *in vivo* from the myofibres of patients. It may be possible to demonstrate a specific defect of sodium or chloride channels in a patient with myotonia *in vitro* using microelectrodes to record intracellularly from myofibres of an intercostal muscle biopsy (Lipicky, Bryant et al. 1971; Kwiecinski, Lehmann-Horn et al. 1984). However the technique is too difficult for routine use in a diagnostic service. Nowadays genetic testing has the potential for establishing a diagnosis at the molecular level with a simple blood test.

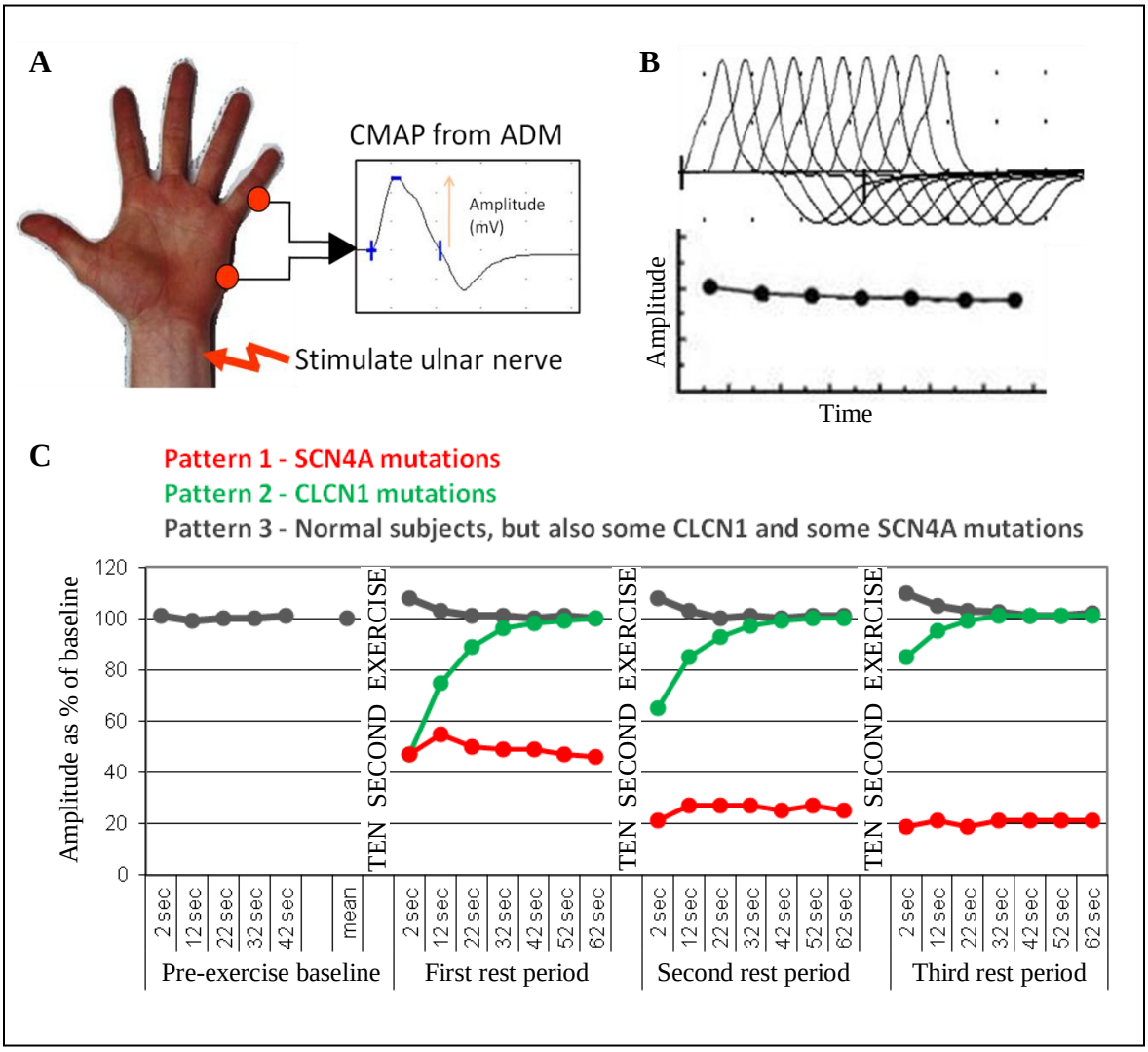

Figure 1.1 The short exercise test
(A) Illustration of the compound motor action potential (CMAP) recorded from abductor digiti minimi. **(B)** Upper panel shows a series of CMAPs to illustrate the appearance of the raw data (in the figure 10 CMAPs are shown but in the short exercise test only 7 post-exercise CMAPs are recorded). In the lower panel the amplitude of each CMAP is plotted against time. Amplitude is expressed as a percentage of a mean baseline pre-exercise CMAP. **(C)** The change in compound motor action after 10 seconds of exercise can guide genetic testing in the non-dystrophic myotonias (Fournier, Arzel et al. 2004). A 20% decrement immediately post-exercise is considered abnormal. Pattern 1 (red) is seen in Paramyotonia Congenita (SCN4A mutations). In these patients repeated exercise causes worsening myotonia and exacerbates the post-exercise CMAP decrement. Pattern 2 (green) occurs in a subset of Myotonia Congenita patients (CLCN1 mutations), usually those with recessive disease in whom transient weakness occurs. In these patients repeated exercise produces the warm-up phenomenon and the post-exercise decrement becomes less pronounced. Pattern 3 is seen in normal individuals, but also occurs in patients with more mild Myotonia Congenita (often autosomal dominant) and in some with Sodium Channel Myotonia.

For a firm diagnosis of Myotonia Congenita identification of the causative sequence variant in CLCN1 is the gold standard. Where Myotonia Congenita is suspected, sequencing of all 23 CLCN1 exons plus short regions of flanking introns is available in the NHS diagnostic laboratory of the National Hospital for Neurology & Neurosurgery (NHNN). Although sequencing all the exons increases the detection rate for known pathogenic sequence variants, it also increases the rate of detection of novel sequence variants of uncertain pathogenicity ('unclassified variants').

With increasing demand for sequencing this has become such a problem that the Clinical Molecular Genetic Society issued guidelines in 2008 for the interpretation and reporting of unclassified variants (Bell J 2008). Multiple sequence alignment should be applied with caution, and should be supported with evidence from other sources. Segregation of the variant with the disease in a family supports pathogenicity, and where possible relatives of an affected individual are tested by the clinical genetics laboratory at NHNN. The presence of a variant among control chromosomes raises doubts about pathogenicity but cannot entirely exclude that possibility. The majority of pathogenic CLCN1 mutations are recessive [two copies required to cause disease (Pusch 2002; Fialho, Schorge et al. 2007)] so unaffected heterozygotes may appear in among a random selection of healthy control individuals. The existence of unaffected homozygotes for a novel variant is stronger evidence that the variant is benign, but it is rare for unaffected individuals to undergo EMG to confirm absence of myotonia. It is recommended that "if a reliable functional assay is available it must be regarded as essential for the definitive interpretation of a variant of unclear clinical significance" (Bell J 2008).

1.3 The chloride conductance of mature skeletal muscle

Bretag (Bretag 1987) has comprehensively reviewed the experiments of Hodgkin, Katz, Adrian, Bryant and others in the mid 20th century that characterized the chloride conductance of amphibian and mammalian skeletal muscle. Unlike other excitable cells, muscle fibres have a large resting chloride conductance. This was demonstrated in 1959 by Hodgkin and Horowicz (Hodgkin and Horowicz 1959), who showed that the chloride conductance of frog semitendinosus contributes 50% to the total resting membrane conductance. In mammalian muscle the contribution from chloride channels is even higher. Rat diaphragm in a physiological environment has an average total membrane conductance of 2.45 mS/cm^2, falling to 0.34 mS/cm^2 in chloride-free environment, i.e. the chloride conductance makes up about 85% of total resting membrane conductance in this preparation (Palade and Barchi 1977). In human intercostal muscle chloride conductance contributes 76 - 82% to total membrane conductance (Rudel and Lehmann-Horn 1985; Kwiecinski, Lehmann-Horn et al. 1988). Only a small proportion of chloride ions are actively transported into the muscle cell (Harris and Betz 1987; Aickin, Betz et al. 1989), so the majority must equilibrate passively in response to the resting membrane potential set by the potassium concentration gradient. While the chloride conductance does not set the resting potential, it tends to maintain the *status quo*. For example if the cytoplasm becomes less negative (depolarization), chloride ions are drawn into the cell, making the intracellular environment more negative again. Because very few ions need to flow to change the potential, the concentration gradient is essentially unchanged and the old equilibrium is restored. In fact, only 10^{-12} mole of univalent ions (6×10^{11} individual ions) need to cross each square centimeter of membrane to produce a 100mV change. Voltage is a measure of

the force between charged particles. The closer they are the higher the force (much like when two magnets are held close to each other), and the more concentrated the charge within a region (the higher the charge density), the stronger the force field around it. The constant of proportionality that relates the quantity of charge (Q) on each unit area of membrane to the transmembrane voltage (V_m) is the membrane's capacitance (C). A square cm of membrane (a rather large cell, or one with many fine processes) would have a capacitance of only 1 microfarad (very little capacity for storing charge at a given voltage because the thin membrane means each unit of charge produces a large voltage). The amount of charge required to change V_m by 1mV is calculated as follows:

$$Q = CV_m = 10^{-6} \text{ farad per cm}^2 \text{ x } 0.1 \text{ Volt} = 10^{-7} \text{ coulomb per cm}^2$$

From Faraday's constant (96485.3399 Coulombs per mole) 1 coulomb is equivalent to about 1/100,000 mole of univalent ions. Thus 10^{-7} Coulombs corresponds to about 10^{-12} moles of univalent ions (or 6×10^{11} individual ions) crossing each square cm.

1.4 The pathophysiology of Myotonia Congenita

The physiological basis of Myotonia Congenita was elucidated from studies of the myotonic goat thirty years before the CLCN1 gene was identified. It is now known that the myotonic goat has a point mutation in ClC-1 at position 885 leading to a substitution of proline for alanine (Beck, Fahlke et al. 1996). While the goat has dominant Myotonia Congenita, the arrested development of righting (ADR) mouse has recessive disease, for example caused by a transposon inserted into ClC-1 (Steinmeyer, Klocke et al. 1991). Many of the studies on pathology of myotonia took advantage of these models, with the

myotonic goats being particularly important for early work clarifying the role of the skeletal muscle chloride conductance.

Myotonia congenita muscle differs from normal muscle in two important ways. First, when the neural stimulus (or a current stimulus *in vitro*) ceases, muscle action potentials continue to fire, delaying relaxation (a myotonic discharge). Secondly the muscle membrane is hyperexcitable (a smaller amount of current is required to depolarize the membrane to threshold) (Adrian and Bryant 1974). The mathematical model by Barchi implies that the myotonic discharge originates in the t-tubule membranes (Barchi 1975). Normally, t-tubular action potentials should not be able to propagate to the surface owing to the sparse tubular openings and the relatively low density of sodium channels in the tubular membrane. Hyperexcitability of the sarcolemma could allow a tubular myotonic discharge to spread over the muscle cell by first propagating up to the surface (Lamb 2005). Adrian and colleagues convincingly showed that asynchrony between the action potential at the surface and in the t-tubule system could drive a depolarizing current at the surface (Adrian and Peachey 1973; Adrian and Marshall 1976). Myotonic action potentials could therefore originate at the surface and yet be driven by the t-tubule. It is worth pointing out that contraction could occur simply from tubular action potentials with no surface action potential (Lamb 2005). However, such contractions would appear electrically silent to an extracellular electrode, and this is not the case in myotonia (EMG is a valuable diagnostic technique).

In the 1960s voltage clamp experiments on *in vitro* intercostal muscle fibres from the myotonic goat revealed a specific defect of chloride conductance (Lipicky and Bryant 1966; Bryant 1969). The same defect was soon demonstrated using intercostal muscle

biopsy from humans with Myotonia Congenita (Lipicky, Bryant et al. 1971). Adrian and Bryant proposed that the high chloride conductance is a specialization of muscle cells to stabilize the surface membrane by making the potential across it relatively independent of ionic concentration changes in the t-tubules (Adrian and Bryant 1974). When a t-tubule conducts an action potential into the cell the repolarization current carries potassium ions out of the cell into the tubular lumen. Long, narrow T-tubules present a significant barrier to diffusion and potassium tends to accumulate there, depolarizing the tubular membrane sufficient to trigger further tubular action potentials. The efflux of potassium associated with a single action potential has been calculated to increase the tubular concentration by 0.3 mM (Adrian and Marshall 1976). In normal muscle some of the repolarizing current is carried by chloride ions, limiting potassium accumulation (Dutka, Murphy et al. 2008). Furthermore, the chloride conductance tends to oppose changes in resting potential; depolarization caused by potassium accumulation drives an influx of chloride ions, opposing the change in resting potential. A single action potential in normal muscle is followed by a small, transient after-depolarization (Freygang, Goldstein et al. 1964) . When the chloride current is absent the after-depolarization becomes abnormally large, but is abolished when t-tubules are disconnected by glycerol shock (Adrian and Bryant 1974). Summation of abnormally large after-depolarizations during a train of impulses was suggested to be the drive for self-sustaining myotonic discharges (Adrian and Bryant 1974).

Mathematical modeling of a skeletal muscle fibre using parameters derived from experiments on amphibian muscle suggests that decreasing chloride permeability to 20% of normal is sufficient to produce myotonic discharges in response to a single stimulus (Barchi 1975). In rat extensor digitorum muscle bathed in concentrations of 9-anthracene

carboxylic acid that reduce the chloride conductance to 40% of normal, brief extracellular current stimuli elicit myotonia at 50% of sites on the muscle fibre (Furman and Barchi 1978). In human intercostal muscle, reduction to 40% produces a small prolongation of the muscle's relaxation time, possibly corresponding to mild myotonia, whereas reduction to 18% causes clear myotonia (Kwiecinski, Lehmann-Horn et al. 1988). Reduction of chloride conductance to 50% of normal apparently never causes myotonia in humans because heterozygous carriers of non-functional recessive mutations are asymptomatic. By the same logic haploinsufficiency, a mechanism of autosomal dominant inheritance in which a single copy of a gene is insufficient to maintain normal function, appears *not* to be the mechanism of dominant Myotonia Congenita. Instead, dominant Myotonia Congenita is brought about when a mutant allele impairs the normal allele (dominant negative interaction) in a heterozygote (Duffield, Rychkov et al. 2003; Fialho, Schorge et al. 2007).

1.5 The skeletal muscle chloride channel

In 1990, Jentsch and colleagues cloned an ion channel, naming it ClC0, that had been characterized electrophysiologically in the electric organ of the pacific electric ray 11 years previously (White and Miller 1979; Jentsch, Steinmeyer et al. 1990). By searching for a homologue in skeletal muscle they discovered ClC-1 (Steinmeyer, Ortland et al. 1991). Mutations of the CLCN1 gene on chromosome 7, encoding the ClC-1 protein, were soon linked to Myotonia Congenita (Koch, Steinmeyer et al. 1992).

The cloning of ClC0 and ClC-1 paved the way for the discovery of a whole family of ClC proteins that are expressed in all kingdoms of life, nine of them (ClC 1 – 7, ClC-Ka and ClC-Kb) in mammals. ClC-1, -2, -Ka, and -Kb are plasma membrane anion channels. They are called chloride channels because chloride is the most abundant anion in most

physiological conditions. ClC-1 is almost exclusively expressed in skeletal muscle, although small amounts are found in kidney, heart and smooth muscle (Steinmeyer, Ortland et al. 1991). ClCs 3 – 7 reside in endosomal/lysosomal membranes or synaptic vesicles and probably function as Cl-/H+ transporters (Jentsh 2008). The existence of secondary active transporters and ion channels in the same family was an unexpected and novel feature of the ClC family. Unlike channels, transporters have no continuous transmembrane pore, instead using conformational changes to collect ions from one side of the membrane and deposit them on the other side.

ClC proteins are dimers and in contrast to many voltage gated cation channels, where each subunit contributes equally to a single pore, each ClC subunit has its own independent ion transport path or pore (Estevez and Jentsch 2002). Although heterodimers containing subunits from different channel types (e.g. ClC-1 and ClC-2) have been described in heterologous expression systems (Lorenz, Pusch et al. 1996), the role of such channels *in vivo* is unclear.

Gating of ClC-1 and ClC-0 channels

Gating of ClC channels involves conformational changes similar to those responsible for ion transport by ClC antiporters (Lisal and Maduke 2009). Independent gates, one on each subunit of a ClC channel, regulate flow through the pore of each subunit in a process known as protopore gating. A separate process, known as common gating, opens and closes both pores simultaneously.

Gating of ClC channels is voltage-dependent, with an apparent gating charge of 1, but unlike voltage-gated cation channels, chloride channels have no in-built voltage sensor.

Voltage dependence probably arises from the interaction of either chloride ions or protons within the channel (Chen and Miller 1996; Lisal and Maduke 2009). This is reflected in the modulation of gating by chloride concentration and pH, reviewed by Chen (Chen 2005) and summarized below.

Extracellular chloride acts like an activating ligand. When the channel is bound with chloride, the protopore gate opens in response to depolarization, and the opening rate is increased by increasing the external chloride concentration. The closing rate of the protopore gate is unaffected by external chloride, but is modulated by intracellular chloride ions. Increasing intracellular chloride concentration (which has no effect on protopore gate opening), reduces the closing rate of the protopore gate (i.e. tends to maintain the protopore in an open state).

Besides a depolarization-activated opening mechanism, ClC-0 and ClC-1 protopore gating has a hyperpolarization-activated opening mechanism that becomes apparent in the absence of external chloride ions. Hyperpolarization-induced opening is modulated by external pH such that a reducing the pH raises the minimum opening probability (Rychkov, Pusch et al. 1996) without shifting the voltage dependence curve left or right.

Internal pH affects the kinetics and voltage-dependence of protopore gating. Lowering internal pH slows macroscopic current kinetics of ClC-1 and shifts the opening probability curve to the left (so that the same opening probability can be achieved by more hyperpolarized potentials) (Rychkov, Pusch et al. 1996).

The common gates of CLC-0 and ClC-1 behave rather differently from each other. The ClC-0 common gate is much slower than the ClC-0 protopore gate, closes upon membrane

depolarization (while the protopore gate opens), and opens in low external pH. Reducing the extracellular chloride concentration favours closing of the common gate (as it does with the protopore gate). The fact that the ClC-0 protopore and common gates have the opposite voltage dependence makes plotting opening probability curves for each of them relatively straightforward. For example protocols that involve progressive depolarization steps followed by measurement of tail currents measure only the protopore gate opening probability.

CLC-1 common gating is much faster than that of CLC-0, with transition times on the order of tens of milliseconds, comparable to that of the ClC-1 protopore gate (Accardi and Pusch 2000; Aromataris, Rychkov et al. 2001). Furthermore, the ClC-1 common gate is activated by depolarization, the same as its protopore gate. This means that, unlike for ClC-0, macroscopic ClC-1 current traces in response to step changes in membrane potential are composed of not one but two exponentials. Analysis of the open probability from tail currents of macroscopic recordings of CLC-1 has no mechanistic meaning because such an open probability is a combination of the open probabilities of the fast and the slow gates. However from a practical point of view, such recordings can still help with the question of whether a point mutation is likely to be pathogenic.

It is possible to dissect out the protopore and common gating relaxations from ClC-1 tail currents by imposing a 400μs activation pulse to 180 mV between the variable voltage test pulse and the -100 mV tail pulse of the voltage protocol. This fully opens the channel fast gates but is too brief to open the common gate (Accardi and Pusch 2000). The method works because the time constants of the two gates are voltage dependent to different

extents. At negative voltages protopore and common gating have similarly slow kinetics, whereas at 200 mV the time constants differ by almost two orders of magnitude.

An alternative method is to estimate the relative amplitudes of the two exponential components obtained by fitting a curve to macroscopic ClC-1 currents (Aromataris, Rychkov et al. 2001). At each voltage the time-varying current *I(t)* is fitted with a curve of the form:

$$I(t) = A_1 e^{-\frac{t}{\tau_1}} + A_2 e^{-\frac{t}{\tau_2}} + C$$

Parameters A1, A2 and C are estimated by the curve fitting process and normalized (divided by the maximal current) yielding $\alpha 1$, $\alpha 2$, and χ. The opening probability of the protopore gate at each voltage is $1 - \alpha 1$. The opening probability of the slow gate at each voltage is $\chi/(\alpha 2+\chi)$. The derivation of these equations, and assumptions are covered in the paper by Aromatis (Aromataris, Rychkov et al. 2001), who showed that results of this method are essentially the same as that that those of the first method discussed.

Structure of ClC-1

The crystal structure of a ClC protein was first described by Dutzler and colleagues (Dutzler, Campbell et al. 2002; Dutzler 2007). This bacterial homologue of ClC-1 found in *E.coli* and known as EcClC subsequently turned out to be a Cl^-/H^+ antiporter (Accardi and Miller 2004). The prokaryotic ClC proteins lack the long cytoplasmic C-terminus of eukaryotic ClC proteins, but the transmembrane moiety is structurally homologous with eukaryotic ClC channels. Briefly, each subunit of a ClC dimer has 18 alpha helices (named A to R) and cytoplasmic amino and carboxy terminals. The helices are of variable length,

tilted, and many only partially span the membrane. The two halves of a subunit protein resemble imperfect inverted copies of each other (an 'antiparallel' architecture). This facilitates apposition of helices from different parts of the protein end-to-end as the two antiparallel halves wrap around a common centre. An hourglass-shaped ion transport path at the interface of the two antiparallel halves has a selectivity filter at its neck, formed by electropositive amino acids at the ends of apposed helices.

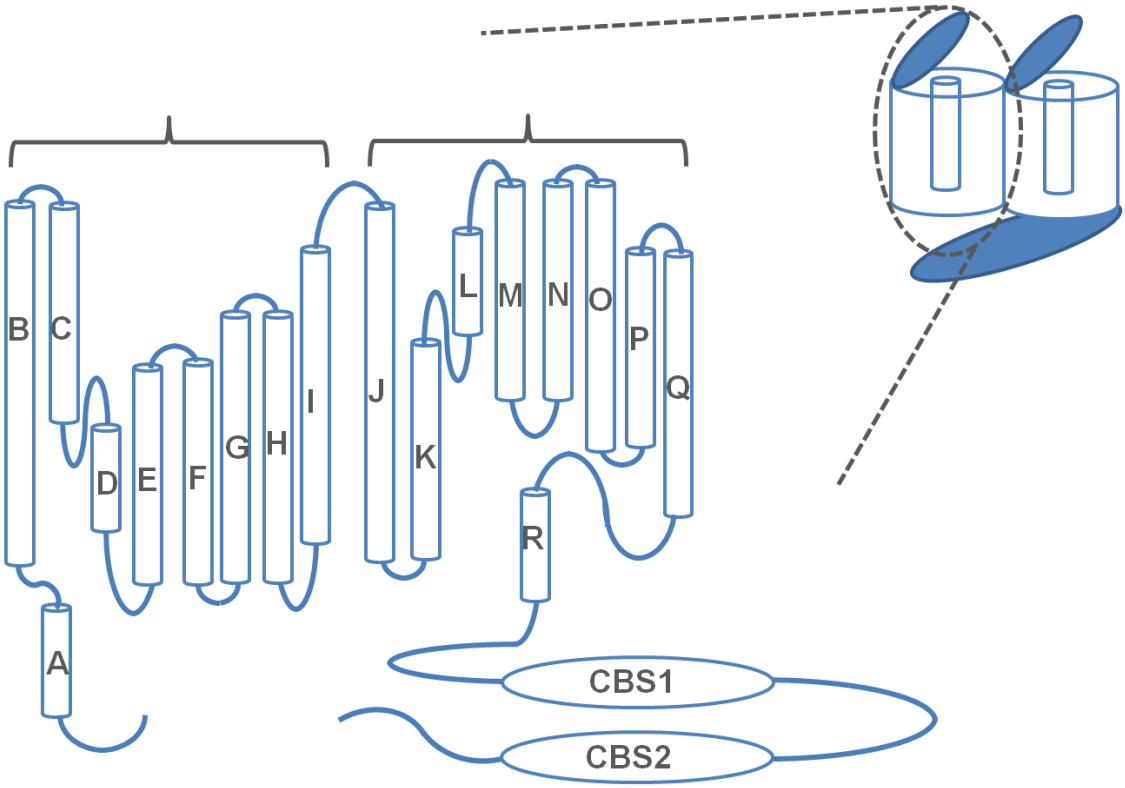

Figure 1.2 Structure of ClC-1
The cartoon illustrates the helices that make up one subunit of a ClC-1 channel. Parentheses above the diagram indicate the two antiparallel halves of the protein. Inset is a cartoon of the ClC-1 dimer, each subunit with its own independent pore and gate. A common gate regulates both pores simultaneously. Figure modified from: Dutzler, R., et al., X-ray structure of a ClC chloride channel at 3.0 A reveals the molecular basis of anion selectivity. Nature, 2002. 415(6869): p. 287-94. Dutzler, R., A structural perspective on ClC channel and transporter function. FEBS letters, 2007. 581: p. 2839-2844.

The selectivity filter at the neck of the hourglass contains three anion-binding sites that allow chloride ions to travel between the aqueous vestibules on either side. The side-chain

of a conserved glutamate residue is thought to be the structural basis of the protopore gate. This glutamate side-chain occupies the external anion binding site, blocking the pore, but when protonated it swings out of the binding site to open the channel. Voltage dependence and also pH-dependence could arise from movement of protons from the intra- to extracellular side, favoured by depolarized potentials, along a pathway that converges on this glutamate residue. In this model, the activating effect of chloride ions arises from its binding to a putative allosteric site on the outside of channel, occupancy of which opens the proton pathway (Miller 2006).

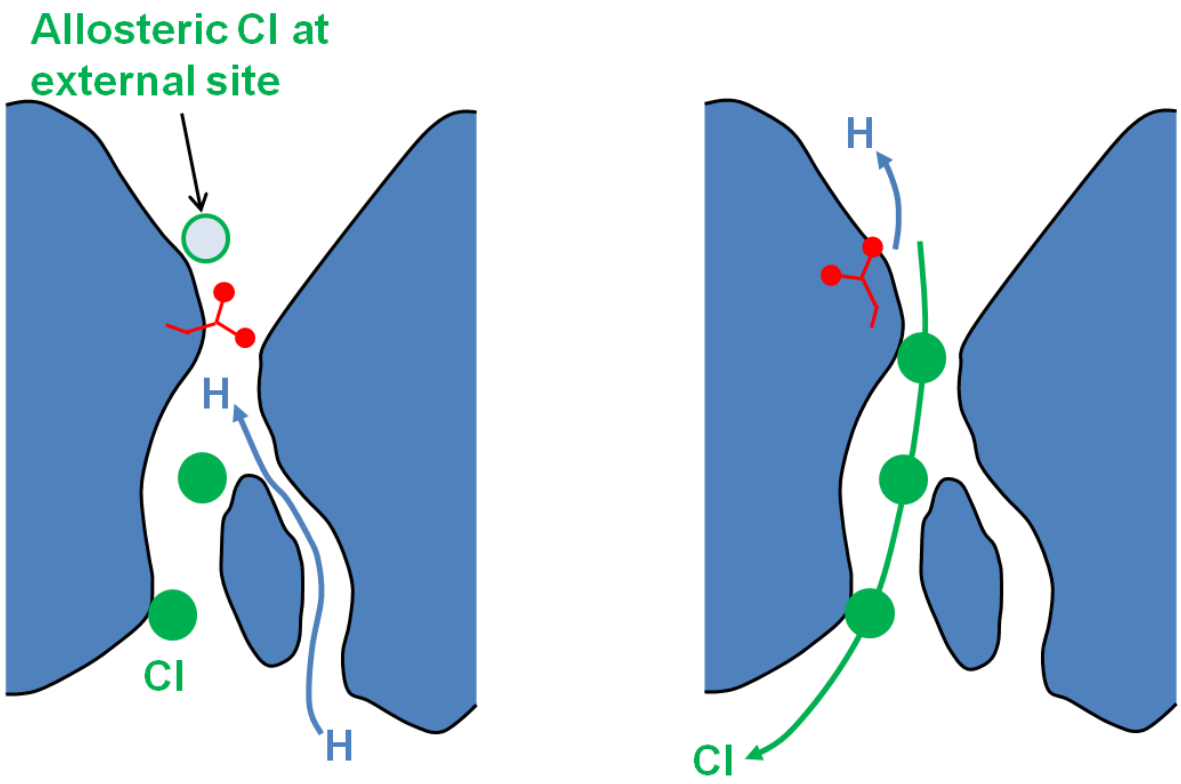

Figure 1.3 Miller's model of fast gating in ClC channels
Figure adapted from Miller, C. (2006) *Nature* **440**: 484-489. A single subunit of ClC-1 is illustrated. A glutamate side chain (red) at the external side of the channel pore functions as the fast gate. It swings out, unblocking the pore, in response to protonation by hydrogen ions flowing from inside to outside along a path that converges with the chloride permeation pathway at the external side. In this model, external chloride ions promote channel opening by binding to a putative allosteric site on the outside of channel, occupancy of which opens the proton pathway.

The mechanism of common gating remains unclear, but its exquisite temperature-sensitivity (Pusch, Ludewig et al. 1997) implies large conformational changes of the channel protein, perhaps reflecting phylogenetic origins as a transporter. Common gating probably requires concerted movements of both subunits, and mutations in helices at the intra-membrane interface of the two subunits of ClC-1 lead to autosomal dominant Myotonia Congenita by disrupting this process (Saviane, Conti et al. 1999; Duffield, Rychkov et al. 2003). The interface between subunits occurs not only between intra-membrane moieties of the channel subunits, but also between their cytoplasmic C-terminal domains (Markovic and Dutzler 2007). Unlike bacterial ClC proteins, eukaryotic ClC proteins have very long cytoplasmic C-termini containing two CBS domains (which take their name from cystathionine b-synthetase in which the domain was first described)(Bateman 1997; Markovic and Dutzler 2007). Studies of the C-terminus in relation to subcellular localization (Fong, Rehfeldt et al. 1998; Estevez, Pusch et al. 2004; Macias, Teijido et al. 2007), phosphorylation (Hsiao, Huang et al.) and ATP-binding (Bennetts, Rychkov et al. 2005) suggest it plays a role in regulation of trafficking to the plasma membrane in response to cytoplasmic signals. But it is also thought to be important for common gating (Arreola, De Santiago-Castillo et al. 2008). Movements of the carboxy terminus during common gating have actually been measured by fluorescence resonance energy transfer (FRET) (Bykova, Zhang et al. 2006). Chimeras in which ClC-0 channels were created with a carboxy tail from either ClC-1 or ClC-2 have altered common gating (Fong, Rehfeldt et al. 1998). Mutations of ClC-0's R-helix, which connects the carboxy tail to the intracellular side of the protopore, also disrupt common gating (Ludewig, Jentsch et al. 1997). One end of the R helix protrudes into the cytoplasm, while the other end

contributes a chloride-coordinating tyrosine residue to the selectivity filter of the channel. Common gating and protopore gating may well be coupled (suggested by their common sensitivity to chloride ion concentration)(Estevez and Jentsch 2002). Common gating may involve coupling of carboxy terminus movements to conformational changes in the protopore through the R-helix (Arreola, De Santiago-Castillo et al. 2008). Helix R is close to helix A of the other subunit and an interaction between these two could be important for coupling conformational changes in the two subunits (Estevez and Jentsch 2002).

Localization and mechanism of action of ClC-1

The subcellular localization of ClC-1 in skeletal myofibres remains a hotly debated topic. In 1960 Hodgkin and Horowicz noted that changes in external chloride concentration affect the membrane potential of amphibian muscle more rapidly than changes in external potassium concentration (Hodgkin and Horowicz 1960). They hypothesized that the 'chloride sensitive sites' are on the surface membrane while some of the 'potassium sensitive sites' are in a less accessible compartment (the t-tubules). Subsequent measurements of the chloride and potassium conductances before and after detubulation suggested that in amphibian muscle the chloride conductance is located entirely at the surface while potassium conductance is distributed between the surface and the t-tubules (Eisenberg and Gage 1969). In 1995 the first immunoflurorescence experiments were conducted in order to ascertain the location of ClC-1 in mouse skeletal muscle. These agreed with the conclusions from the above experiments in amphibian muscle – in sections of mouse muscle antibody against ClC-1 stained the periphery but not the internal regions of the cells (Gurnett, Kahl et al. 1995). This sarcolemmal pattern of staining has been observed subsequently by others (Mankodi, Takahashi et al. 2002). Using confocal

microscopy and immunofluorescence to examine ClC-1 in rat myofibres Papponen and colleagues noted that the distribution of ClC-1 on the surface is not uniform. They found a more intense staining of ClC-1 at the endplate than in the extrajunctional sarcolemma, and co-localization of ClC-1 with β-dystroglycan in a pattern of cross-striations and longitudinal stripes that left transverse tubule openings clear (Papponen, Kaisto et al. 2005). More recently Lueck and colleagues used a combination of electrophysiology, detubulation and immunofluorescence to show that ClC-1 localizes to the surface membrane and not to the t-tubules of mouse skeletal muscle fibres (Lueck, Rossi et al. 2010). They recorded chloride currents by whole cell patch clamp in the same cell before and after de-tubulation and showed that while the capacitance fell dramatically (indicating disconnection of t-tubules) chloride currents were not appreciably diminished. In fact the chloride current density (expressed per unit of cell capacitance) increased because of the fall in capacitance.

The use of immunofluorescence and microscopy to investigate distribution of ClC-1 has been challenged. Lamb and colleagues argue that the gain of confocal imaging is inadequate to detect immunofluorescence from antibody-bound ClC-1 channels in t-tubules because the diameter of the t-tubules is smaller than the effective pixel size set by confocal resolution (Lamb, Murphy et al. 2011). Furthermore, detubulation experiments in rat muscle have suggested that the t-tubules *do* contribute to the total chloride conductance (Palade and Barchi 1977). Although t-tubules are inaccessible to microelectrodes, the average voltage of the t-tubular system can be ascertained using voltage-sensitive dyes. A recent comparison of total chloride current measured between the intracellular and extracellular space of mouse flexor digitorum brevis muscle fibres, t-tubular optical signals from the same fibres, and predictions from a mathematical model suggested an equal

density of ClC-1 at the surface and in the tubules (Difranco, Herrera et al. 2010). In amphibian muscle fibres repolarization of the tubular action potential (measured using a voltage-sensitive dye) is slowed by removing chloride from the extracellular environment, suggesting a significant contribution of chloride currents to tubular repolarization (Heiny, Valle et al. 1990). In the skinned muscle fibre preparation, where the sarcolemma of an isolated myofibre is removed and the t-tubule system seals off, larger twitches could be elicited and at lower intensity electric stimulation in the presence of substances that inhibit ClC-1 – further (albeit indirect) evidence for ClC-1 in the tubules (Dutka, Murphy et al. 2008).

Theoretical arguments can be put forward for having a purely sarcolemmal ClC-1 or for having a ClC-1 presence in the tubules. The cable model of radial propagation of the action potential into the muscle fibre suggests that asynchrony between the surface and tubular membranes tends to drive current into the muscle cell through the tubule at a time when the surface is 'trying' to repolarize (Adrian and Peachey 1973; Adrian and Marshall 1976). The model is discussed in more detail later in this thesis (see Chapter 5, Figure 5.4 and Figure 5.5). Chloride channels at the surface would provide an alternative exit route across the surface for this inward current preventing it from re-charging the surface and limiting the early after-depolarization which might otherwise elicit a further action potential. Chloride channels in the t-tubule would be helpful in limiting the late after-depolarization, which is caused by potassium accumulation in the lumens of t-tubules. If the t-tubular repolarization current is carried in part by chloride then less potassium will flow out into the tubules than if potassium is the only charge carrier for the repolarization current. Proponents of a purely surface localization of ClC-1 argue that tubular chloride currents have the potential to alter

tubular chloride concentrations and reduce the effectiveness of chloride at maintaining the tubular resting potential (Lueck, Rossi et al. 2010; Zifarelli and Pusch 2010).

Regulation of ClC-1 in adult muscle

ClC-1 is involved in feedback that enables the muscle fibre to adapt its excitability to the properties of its motor neuron. Two lines of evidence suggest that muscle fibre electrical activity itself regulates ClC-1 expression. Firstly denervation causes the chloride conductance of adult muscle to fall dramatically (Camerino and Bryant 1976; Conte-Camerino, Bryant et al. 1985; Conte Camerino, De Luca et al. 1989; Chen and Jockusch 1999). Secondly, in wild type rodents fast muscle expresses more ClC-1 than slow muscle, whereas in myotonic animals slow muscle expresses as much as fast muscle (Klocke, Steinmeyer et al. 1994), suggesting that myotonic discharges themselves can drive chloride channel expression. Fast muscle may need a higher chloride conductance than slow muscle because the high frequency action potentials in the former should produce more marked t-tubular potassium accumulation and a higher risk of myotonia.

Immature muscle and the developmental regulation of chloride channels

Skeletal muscle contains a population of myoblasts known as satellite cells that can be cultured *in vitro* and induced to fuse into myotubes, embryonic muscle cells that are partially differentiated. In 1975 Ritchie reported that neither the membrane potential nor the input resistance of rat myotubes on day 7 of culture are influenced by changes in the external concentration of chloride ions, suggesting a very low chloride conductance (Ritchie and Fambrough 1975). The chloride conductance of wildtype mouse myotubes been estimated to be about $10\mu S/cm^2$ (Wischmeyer, Nolte et al. 1993), and cultured human

myotubes at -85 mV have a chloride conductance of about 6□ μS/cm^2 (Zachar, Fahlke et al. 1992). More recently, myotubes cultured from the dyspedic mouse, which lacks a functional ryanodine receptor (and therefore cannot disturb recordings that rely on microelectrodes by contracting), have been reported to lack chloride currents (Lueck, Mankodi et al. 2007). Thus the chloride conductance of embryonic rodent muscle cells is hundreds of times smaller than that of mature rodent muscle conductance (about 3000 □μS/cm^2 for adult rat muscle (Conte-Camerino, Bryant et al. 1985))

The small but measurable chloride conductance of cultured myotubes may not be regulated by CLCN1. Firstly the chloride conductance of wildtype mouse myotubes is the same as that of myotubes from the ADR mouse, which lacks functional ClC-1 channels (Wischmeyer, Nolte et al. 1993). Secondly SDS-PAGE fails to detect ClC-1 protein in cultured myotubes from the rat L6 cell line (Papponen 2008). Thirdly ClC-1 mRNA is undetectable by northern blot in cultured rodent myotubes (although it is measurable by RT-PCR at concentrations 100-200 fold lower than in mature myofibres) (Bardouille, Vullhorst et al. 1996). The small amount of ClC-1 mRNA in myotubes exists as a number of splice variants containing exons that are absent from adult ClC-1 mRNA. These extra exons disrupt the reading frame, introducing premature stop codons that lead to nonsense mediated decay (Cooper 2007; Lueck, Lungu et al. 2007). In the first few weeks after birth rodent muscle ClC-1 mRNA levels rise steeply (Steinmeyer, Ortland et al. 1991; Wischmeyer, Nolte et al. 1993) in parallel with a rise in the membrane chloride conductance (Conte Camerino, De Luca et al. 1989). This post-natal rise in ClC-1 expression is brought about by a splicing switch that restores the reading frame. This rise

in ClC-1 expression with development is dependent upon electrical activity of the muscle cell (Conte-Camerino, Bryant et al. 1985; Klocke, Steinmeyer et al. 1994).

The search for the major skeletal muscle chloride channel by patch clamp before the CLCN1 gene was cloned revealed a variety of putative chloride channels in embryonic and adult skeletal muscle cells. Cultured myotubes can be converted into spherical cells known as 'myosacs' or 'myoballs', which facilitates electrophysiological studies (Bischoff and Holtzer 1968; Fukada 1975; Boldin, Jager et al. 1987). Single channel studies of rat myoballs in the 1980s revealed three different putative chloride channels in the sarcolemma with conductances of 45 pS, 61 pS and 430 pS (Blatz and Magleby 1983; Blatz and Magleby 1985). On the surface of adult rat skeletal muscle fibres, a 60 pS chloride channel was identified (Chua and Betz 1991). In human myoballs 3 different putative chloride channels with conductances of 10 pS, 31 pS and 250 pS were described (Fahlke, Zachar et al. 1992). Comparisons of macroscopic and single channel chloride conductances of human myotubes from normal and myotonic muscle suggested that reduced conductance of the 31pS channel might be responsible for the reduced chloride current in recessive Myotonia Congenita (Fahlke, Zachar et al. 1993). Unfortunately however, none of these putative channels corresponds to ClC-1, which was found to have a much lower single channel conductance (about 1pS) when it was cloned and expressed in HEK293 (Pusch, Steinmeyer et al. 1994; Saviane, Conti et al. 1999). Channels can behave differently in different cell types, further complicating unambiguous attribution of a single cDNA to a particular conductance. The molecular identity of the various conductances identified in single channel studies of cultured myotubes is not clear.

The role of phosphorylation in regulating chloride channels

In slow muscle fibres phosphorylation of chloride channels appears to maintain the chloride conductance at lower levels than in fast muscle fibres. Inhibiting protein kinase C increases the chloride conductance of rat soleus (slow muscle) but has no effect on extensor digitorum longus (fast muscle) (Desaphy, Pierno et al. 2005) presumably because the ClC-1 channels are not phosphorylated in fast muscle. When intact myofibres are dissociated enzymatically and maintained in culture their membrane resistance begins to rise after about two days in culture as the chloride conductance falls (Bekoff and Betz 1977). The fall in chloride conductance can be attenuated by incubation in a protein-kinase inhibitor (Chen and Jockusch 1999) or by electrical stimulation of the fibre (Papponen, Kaisto et al. 2005). These effects may be caused by changes in the density of chloride channels at the membrane (Papponen, Kaisto et al. 2005). However, phosphorylation also affects the function of ClC-1, producing a right-shift in the voltage dependence of activation in *Xenopus* oocytes (Hsiao, Huang et al. 2010) and altering kinetics of channel deactivation in HEK cells (Rosenbohm, Rudel et al. 1999).

Regulation of chloride channel expression in Myotonia Congenita

The effect of CLCN1 mutations on expression and cellular localization of ClC-1 protein has received little attention. A number of missense mutations, for example F413C, produce only minor changes of channel function in heterologous expression systems (Zhang, Bendahhou et al. 2000). The pathomechanism in such cases may well be altered membrane density of ClC-1. The F413C mutation may not be exported properly from the endoplasmic reticulum (Papponen, Nissinen et al. 2008).

The CBS domains in the cytoplasmic carboxy tail of the subunits may play a role in the cellular localization of ClC-1. Heterologously expressed channels that have been truncated after first CBS domain so as to remove a carboxy tail fragment containing the second CBS domain do not produce chloride current in *Xenopus* oocytes (Schmidt-Rose and Jentsch 1997). Function of these truncated subunits can be restored by co-expressing the missing carboxy tail fragment containing the second CBS domain. Tagging the tail fragments and using antibodies to measure their surface expression suggests the loss of function is caused by reduced trafficking to membrane (at least in *Xenopus* oocytes)(Estevez, Pusch et al. 2004). However, altered sub-cellular localization is not the only way that ClC-1 mutations might alter surface expression. Differential allelic expression has been shown for the R894X mutation (Duno, Colding-Jorgensen et al. 2004) suggesting that R894X shows dominant inheritance in some families because in herozygotes from these pedigrees the mutant allele is more highly expressed than the wildtype allele.

1.6 Functional expression of Myotonia Congenita mutations

Soon after the CLCN1 gene was cloned, it was linked to Myotonia Congenita (Koch, Steinmeyer et al. 1992). However, the possibility remained that the causative gene was not CLCN1 itself, but another gene in linkage disequilibrium with it. Also, patch clamping studies in skeletal muscle at that time were uncovering a variety of putative chloride channels (Fahlke, Zachar et al. 1992). By expressing mutant ClC-1 channels in *Xenopus* oocytes, Steinmeyer et. al. proved that mutations carried by patients with Myotonia Congenita reduced channel conductance at physiological voltages (Steinmeyer, Lorenz et al. 1994), lending essential physiological support to the ClC-1 hypothesis.

Pusch et. al. used single channel data from ClC-1 expressed in HEK293 cells to show that ClC-1, and not the putative chloride channels identified by patch clamping of cultured skeletal muscle, is responsible for the large macroscopic chloride conductance of adult muscle fibres. Interestingly, although muscle has a high macroscopic chloride conductance, the single channel conductance of ClC-1 is very low (around 1 pS) (Pusch, Steinmeyer et al. 1994), so the channel must be expressed at very high density. The low single channel conductance may also have contributed to the difficulty of identifying these channels in single channel patch clamp experiments, which are highly biased towards identifying channels with larger conductances.

Since the publication of the CLCN1 gene, over 100 mutations in it have been reported, distributed throughout the channel (Pusch 2002; Fialho, Schorge et al. 2007). The majority of these mutations are associated with recessive inheritance, and patients with recessive disease are usually compound heterozygotes. Dominant mutations cluster at the interface between the two subunits (Duffield, Rychkov et al. 2003) where they impair the function of the normal subunit as well as the mutant subunit.

1.7 Heterologous expression systems

The most commonly used heterologous expression systems for studies of CLCN1 are *Xenopus* oocytes and HEK293 cells. Both have endogenous chloride currents, but currents through heterologously expressed CLCN1 (Zhu, Zhang et al. 1998) can be distinguished by their magnitude and pattern of voltage-dependence. Expressing a mutant CLCN1 cDNA mimics the situation in a homozygous patient in which both subunits of every channel contain the mutation. However the vast majority of Myotonia Congenita sufferers are heterozygotes (two different mutant alleles in recessive disease, or one mutant and one

normal allele in dominant disease). Unless one of the alleles is never translated into protein *in vivo* (for example RNA carrying a premature stop codon may undergo nonsense mediated decay), co-expression of two different alleles is necessary to model a heterozygous patient.

HEK293 cells are human somatic cells and therefore may recapitulate human muscle cell biology more closely than *Xenopus* oocytes can. They are also more convenient to work with than *Xenopus* oocytes. On the other hand *Xenopus* oocytes are large enough that a known quantity of ClC-1 mRNA can be micro-injected into the cell. HEK293 cells must be transfected by mixing a plasmid vector into the culture medium surrounding a plate of cells, and the quantity of DNA entering a given cell is unknown. Plasmids containing fluorescent markers e.g. green fluorescent protein are used to identify cells that have taken up DNA, but the level of GPP expression estimated visually by the brightness of fluorescence does not necessarily correlate with the quantity of channel gene expressed unless the GFP is attached to the channel protein. Unlike in *Xenopus* oocytes, comparisons of current density between HEK293 cells containing wildtype or mutant ClC-1 are confounded by differing quantities of DNA expressed by each cell. To look for a reduction of current density through mutant channels, a comparison of the most fluorescent cells expressing the mutation against the least fluorescent cells expressing the wildtype helps avoid false positive results (i.e. comparing cells where mutant is as high as possible, but wildtype is as low as possible).

In *Xenopus* oocytes co-expression of mutant and wildtype alleles predicts disease inheritance from the presence or absence of a dominant negative interaction. A dominant negative interaction is implied when injecting oocytes with wildtype CLCN1 yields larger

chloride currents than injecting the same quantity of wildtype CLCN1 plus additional mutant CLCN1.

Transfection of HEK cells with two plasmids produces an inhomogeneous population of cells expressing different amounts of each plasmid. It is possible to design a concatameric construct linking two CLCN1 genes in a single open reading frame so as to produce two ClC-1 subunits covalently linked together, and to insert a sequence variant into one of the subunits (Wu, Ryan et al. 2002). Although this elegantly overcomes the problem of ensuring equal proportions of mutant and wildtype alleles being taken up by each HEK cell, it still does not recapitulate the situation in a heterozygous patient. In the heterozygous patient, assuming the alleles are transcribed in equal quantities and associate at random, then 25% of channels will be wildtype homodimers of allele 1, 25% will be homodimers of allele 2, and 50% will be heterodimers containing one subunit of each type. However, when mutant homodimers conduct zero or negligible current, the degree to which chloride conductance is reduced in a heterozygote with one normal allele depends critically upon the behaviour of the mutant-wildtype heterodimers. Of course, the assumption of equal quantities and random association of alleles may not be accurate. Indeed differential allelic expression has been reported for CLCN1(Duno, Colding-Jorgensen et al. 2004).

Xenopus oocytes have the distinct advantage that, because genetic material is introduced by microinjection rather than transfection, a known quantity of CLCN1 can be expressed. In co-expression experiments, equal proportions of two different alleles can be studied, and the subunits are assumed to associate in the same proportions as they would in a heterozygous patient (although the degree to which a frog egg cell recapitulates a human skeletal muscle cell is uncertain).

1.8 Membrane-associated signalling and steroid hormones

The observations that myotonia tends to be more severe in males and in pregnant females inspired an experiment in *Xenopus* oocytes to determine the effects of testosterone, progesterone and oestrogen on heterologously expressed ClC-1 (Fialho, Kullmann et al. 2008). Progesterone and testosterone, but not oestrogen, caused a significant right shift in the voltage dependence of activation of ClC-1 in this system. This raised the possibility that sex hormones might modulate ClC-1 in a non-genomic fashion. However, progesterone and testosterone, but not oestrogen, induce maturation of *Xenopus* oocytes (Hammes and Levin 2007) so it is unclear to what extent the effect on heterologously expressed ClC-1 is oocyte-specific. Furthermore, the concentrations of hormone employed were significantly higher than physiological serum levels in humans. Confirmation that sex hormones modulate the severity of Myotonia Congenita through an effect on ClC-1 awaits demonstration of the same effect in a somatic mammalian cell.

The action of steroid hormones mediated by membrane receptors has been comprehensively reviewed by Hammes & Levin (Hammes and Levin 2007). Briefly, classical nuclear sex hormone receptors are also present on the surface of several cell types where they associate with a variety of other proteins that facilitate signalling through g-proteins and protein kinases. For example, an orphan g-protein coupled receptor, GPR30, binds oestrogen with high affinity and probably acts in concert with the oestrogen receptor at the surface to facilitate g-protein coupled signalling. Members of the membrane progesterone-receptor (mPR) family, structurally homologous to the g-protein coupled receptor family, may facilitate progesterone-mediated g-protein signalling outside of the nucleus. Interestingly, membrane-transmitted progesterone signals via g-proteins may

regulate the contractile state of the myometrium at the end of pregnancy (Karteris, Zervou et al. 2006).

Progesterone and androgen-mediated maturation of *Xenopus* oocytes are entirely independent of nuclear receptors. Classical androgen receptors at the surface membrane mediate the effect via inhibition of constitutive Gαs and Gβγ activity that holds the oocytes in meiotic arrest. This rapid attenuation of G-protein signalling may be mediated by a protein complexed with the androgen receptor known as 'modulator of nongenomic actions of steroid receptors' or MNAR. MNAR may also regulate androgen receptor signalling in human somatic cells.

Interestingly phorbol 12-myristate 13-acetate (PMA), an activator of protein kinase C, has a very similar effect on wildtype ClC-1 in *Xenopus* oocytes as progesterone and testosterone (a right shift in the voltage dependence of activation) (Hsiao, Huang et al.). It is possible that the hormones modulate chloride conductance by changing ClC-1 phosphorylation status.

Hormones are not the only possible mediators of increased myotonic stiffness during pregnancy. The T310M mutation was found in women with sporadic disease who develop symptoms almost exclusively during pregnancy, and T310M mutant channels show a marked shift in voltage dependence at low intracellular chloride (Wu, Ryan et al. 2002). As pregnancy reduces the intracellular chloride concentration in muscle, patients with a mutant whose abnormal voltage-dependence is exacerbated by low chloride could experience worse symptoms during pregnancy (Colding-Jorgensen 2005).

1.9 Objectives

Establish an assay in HEK293T cells for classification of novel CLCN1 variants at our centre. Use the assay to examine the functional consequences of a selection of CLCN1 variants in order to explore the idea that functional differences between variants may account for some of the differences between patients.

Determine whether a mechanism exists in skeletal muscle for rapid, non-genomic modulation of the membrane chloride conductance by oestrogen and/or progesterone.

Explore the pathogenic mechanism of Myotonia Congenita by evaluating which parameters predispose to autonomous action potentials in a mathematical model of myotonic muscle with reduced ClC-1 expression.

Chapter 2 Methods

2.1 Molecular Biology

Surfaces were cleaned with 70% ethanol before and after all bacterial cell procedures. All glassware was autoclaved. Bacterial work was conducted adjacent to a flame.

Bacterial culture media

A stock of 1ml aliquots of Ampicillin (Sigma) at a concentration of 100mg/ml in ddH20 was stored at -20°C for shared use by the scientists and students working in the lab. LB Broth and LB agar for selective bacterial grown contained 100μg/ml of Ampicillin (1μL/ml of Ampicillin stock solution).

20g LB Broth (Luria Bertani medium, Sigma) was dissolved in 1 litre of ddH2O, autoclaved and stored at room temperature. 17.5g LB agar (Sigma) was dissolved in 500 ml of ddH2O, autoclaved and stored at room temperature. To make LB agar plates for selective bacterial growth, LB agar was melted in a microwave oven and allowed to cool before addition of Ampicillin. It was then poured into 10 cm plates (VWR international). Once set the plates were stored at 4^{o}C.

Competent bacterial cells

A stock of TOP10® (Invitrogen) E.coli competent cells was shared by scientists and students working in the laboratory. New stocks were made by Dr. Klaus Wanisch, an experienced post-doctoral scientist. To make new competent cells 7 μl of TOP10® (Invitrogen) E.coli stock were grown overnight at 37^{o}C on an agar plate. 2 ml of LB broth was inoculated with a single colony and placed in a 37^{o}C shaking incubator overnight. In

the morning the resulting bacterial culture was added to 500 ml of LB broth and incubated in the same way until OD_{596nm} was 0.25 – 0.7. The resulting culture was chilled on ice for 10 minutes and then centrifuged at 6000 rpm at 4^{o}C for 10 minutes (J2-21 High-Capacity Centrifuge, Beckman). 160 ml of sterile-filtered TB buffer (10 mM PIPES, 55 mM $MnCl_2$, 15 mM $CaCl_2$, 250 mM KCl, pH 6.7) that had been chilled to 0^{o}C was used to resuspend the pellet of *E.Coli* cells, and the suspension was placed on ice for 10 minutes. The suspension of *E.coli* was centrifuged again as before, and resuspended in 40 ml of TB. 2.8 ml of DMSO was added dropwise to the suspension while swirling it continuously. The suspension was chilled on ice for 10 minutes, then aliquoted into 1.5 ml tubes (Eppendorf). Aliquots were snap-frozen in liquid nitrogen and stored at -80^{o}C.

Transformation of bacterial cells

A 50 µl aliquot of TOP10® *E.coli* was thawed on ice. 1 - 5 µl ligation reaction or plasmid DNA at approximately 10ng/µl was added to the bacterial suspension, which was maintained on ice for a further 30 minutes before application of a 30 second 42^{o}C heat shock and a return to ice for 3 minutes. Finally 250 µl of S.O.C medium (20g/l (2% w/v) bacto-tryptone, 5g/l (0.5% w/v) bacto-yeast extract, 5g/l NaCl, 10 mM $MgCl_2$, 10 mM $MgSO_4$, 2 mM glucose; Sigma), that had been pre-warmed to 37^{o}C was added and the mixture placed in an incubating shaker at 225 revolutions per minute and 37^{o}C for 1 hour . 50 – 100 µl of the resulting bacterial suspension was spread on an agar plate containing Ampicillin and incubated at 37^{o}C overnight.

Extraction of plasmid DNA from bacterial cells

Plasmid DNA was extracted from bacterial cells, leaving behind bacterial genomic DNA, using a QIAfilter Maxi Plasmid Purification Kit made by Quiagen (for a 200ml suspension of cells) or a GenElute™ Plasmid Miniprep Kit made by Sigma (for a 2.5ml suspension of cells). The procedure for extracting DNA is described in detail by the instructions supplied by the kits. Briefly, bacteria suspended in LB broth were harvested by centrifugation, resuspended in Tris buffer and lysed with an alkaline solution containing SDS. After neutralization of the solution with an acidic salt solution the plasmid DNA was adsorbed onto silica. Contaminants were washed away and the DNA eluted from the silica. For a miniprep, elution in 75μL ddH20 was the final step. Maxiprep DNA was eluted in 15ml of a solution containing 1.25 mM NaCl, 50 mM Tris/HCl pH8.5, 15% (v/v) ethanol. It was then desalted and concentrated by precipitation with 10.5 ml isopropanol, centrifugation (2 500 rpm for 90 minutes at 4^{o}C in a Falcon 6/300R machine) and washing with ethanol followed by further centrifugation (2500 rpm for 30minutes) and resuspension in 500μL ddH20. DNA was stored at -20°C.

Restriction endonucleases

The shared laboratory stock of restriction endonucleases was from New England Biosciences (NEB). The enzymes were supplied by NEB in 50% (v/v) glycerol and stored in the laboratory at -20°C. According the manufacturer's guidelines, the final concentration of glycerol was always <5% in a reaction mixture (i.e. the final reaction volume was >10 times the volume of enzyme). Buffers supplied by NEB were at 10x concentration. The final volume of the reaction mixture was 10 times greater than the volume of buffer added

so that the final concentration of buffer was 1x. 100 µg/ml BSA was used to prevent enzymes interacting with plastic and/or the air-liquid interface. For double or triple digestion reactions a buffer was selected in which all the enzymes work; XbaI, EcoRI and NheI from NEB all work with NEB buffer 2.

DNA analysis

Plasmid DNA was analysed by agarose gel electrophoresis before or after digestion with an appropriate restriction enzyme, spectrophotometry and sequencing (a service provide by the Wolfson Institute for Biomedical Research, Scientific Support Services, UCL).

DNA samples were separated by electrophoresis on 0.5% (w/v) agarose gels. 0.35g Agarose powder (Sigma) was dissolved in 75ml TBE (100 mM Tris, 83 mM Boric acid, 1mM EDTA) and boiled in a microwave oven. 1 µg/ml of ethidium bromide (Molecular Probes, Invitrogen) was added in a fume cabinet after the Agarose had cooled but not set, and the mixture was poured into an electrophoresis tray to set. Prior to loading, one fifth total volume of 6x concentration Orange G dye (10 mM Tris-HCl (pH 7.6), 0.15% orange G, 0.03% xylene cyanol FF, 60% glycerol, 60 mM EDTA; Fermentas Life sciences) was added to each DNA sample to allow assessment of DNA migration by visual inspection. A 1kb reference marker ladder (NEB) was run adjacent to the samples. Gels were electrophoresed at 100 V for an hour, and then photographed using a UV-light transilluminator and the Gene Genius BioImaging System (Syngene). The concentration of a DNA sample was measured using a spectrophotometer (Nanodrop ND-1000, Thermoscientific) based on the ratio of absorbance at 260 nm and 280 nm.

PCR reactions

Primers were designed using free web-based software (PrimerX, available at http://www.bioinformatics.org/primerx/) and ordered from Sigma. Primers were made up to 100μM concentration using ddH20 in their original tubes and this stock was used to make aliquots at 10μM concentration. The stock and the aliquots were stored at -20°C.

PCR was performed using a 2720 thermal cycler (Applied Biosystems). The thermal cycling protocols and reaction mixtures were based upon the recommendations of the manufacturer of the particular polymerase enzyme being used.

Adding restriction sites onto CLCN1

The PCR reaction mixture and temperature cycle (below) for adding restriction sites to CLCN1 were based on the AccuPrime Pfx supermix (Invitrogen) instructions:

	Vol (μL)	
Pfx supermix	22.5	
Forward primer (XbaI)	1	(5μMolar concentration)
Reverse primer (EcoRI)	1	(5μM concentration)
PTLN vector	0.5	(100ng/μL concentration)
Total	25	

95°C 5 minutes
95°C 15 seconds
60°C 30 seconds } 25 cycles
68°C 3 minutes
68°C 10 minutes

The PCR product yielded a band at about 3kb, the approximate length of CLCN1, when electrophoresed on an agarose gel (figure 2.1 below):

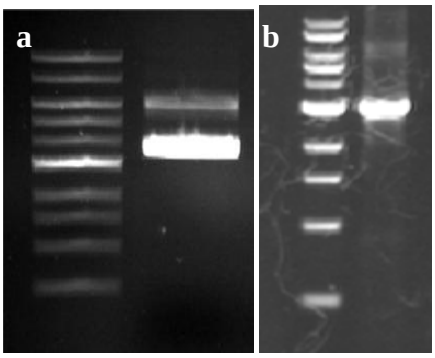

Figure 2.1 Agarose gel electrophoresis of PTLN vector (a) and the CLCN1 fragment (b).
PTLN vector produces bands at around 3.5kb and 7kb, probably representing relaxed and supercoiled states. The CLCN1 fragment produces a strong band at 3kb with some smearing above and below and an additional faint band at about 7 kb probably representing the template PTLN vector.

A double digest reaction with EcoRI-HF (NEB) and XbaI was performed:

	Vol (μL)
DNA	50
Buffer 4 (NEB)	10
BSA (10x conc)	10
EcoRI-HF	3
XbaI	6
ddH20	21
Total	100

The mixture was then incubated at 37°C for 2 hours. The DNA was cleaned with Quiaquick PCR purification kit (Quigen) according to the kit's user manual, eluted in ddH20 and stored at -20°C.

Linearization of PCDH1 in preparation for ligation

To reduce the likelihood of re-circularization NheI was used to digest the fragment excised by XbaI and EcoRI-HF in a triple digest reaction:

	Vol (μL)	
PCDH1 DNA	10	(concentration 160ng/μL)
Buffer 2	10	
BSA	10	(10x concentration)
EcoRI-HF	3	
XbaI	4	
NheI	3	
ddH20	60	
Total	100	incubated at 37°C for 4 hours.

After the restriction digest 3 μL SAP and 10 μL SAP buffer were added and the mixture incubated at 37°C for a further hour and then at 65°C for 15 minutes to inactivate the enzymes. Treatment with SAP, which removes 5' phosphate groups, was to prevent spontaneous re-joining of the cut ends of the PDCH1 vector, which would hinder insertion of the CLCN1 gene.

Finally the linearized PCDH1 vector was cleaned with a Quiaquick PCR purification kit (Quigen) according to the kit's user manual, eluted in ddH20 and stored at -20°C.

Ligation

Ligation was performed using T4 ligase (Promega) according to the instructions supplied with the enzyme. The reaction was allowed to proceed at room temperature for 3 hours. An insert:vector molar ratio of approximately 5:1 was used (a 2:1 ratio by mass).

	Vol (μl)	
Vector	3	(50ng)
Insert	5	(100ng)
Buffer	2	(supplied at 10x concentration)
T4 Ligase	1	
H20	9	
Total	20	

The following ligation reactions were performed:

1) vector, no ligase, no insert
2) vector, ligase, no insert
3) vector, no ligase, insert
4) vector, ligase, insert (the 'real' reaction)
5) no vector, no ligase, insert
6) no vector, ligase, insert

Reaction #	1	2	3	4	5	6
Vector	3	3	3	3	0	0
Insert	0	0	5	5	5	5
Buffer	2	2	2	2	2	2
Ligase	0	1	0	1	0	1
H20	15	14	10	9	13	12
Total	20	20	20	20	20	20

The 6 reaction mixtures were examined on an agarose gel (figure 2.2, below).

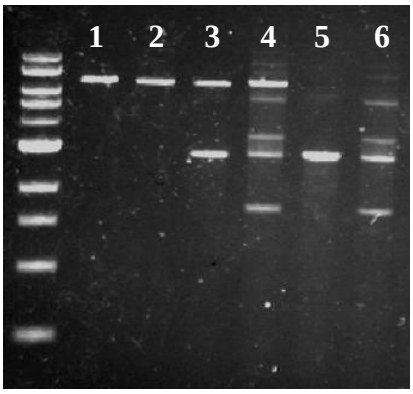

Figure 2.2 Ligation reactions analysed by gel electrophoresis
Ligation reactions analysed by gel electrophoresis. **1)** vector, no ligase, no insert **2)** vector, ligase, no insert **3)** vector, no ligase, insert **4)** vector, ligase, insert (the 'real' reaction) **5)** no vector, no ligase, insert **6)** no vector, ligase, insert.

Comparing reactions 1 and 2 there was no evidence that the PCDH1 vector was able to re-circularize – both reactions yielded a single band at about 8kb. Reaction 5 (insert only, no ligase) yielded a single band at about 3kb, while reaction 6 (insert only with ligase) produced 3 additional bands. Two of these were the same as when the un-digested PTLN vector is run (producing a band for the supercoiled and un-coiled plasmid).

Reactions 2, 4 and 6 were used to transform bacterial cells. Reaction 6 was a positive control expected to yield numerous colonies. Reaction 2 was a negative control expected to yield very few, or zero colonies. Unfortunately there were almost as many colonies grown from reaction 2 as from reaction 4, implying that a significant amount of PTLN vector was mixed in with the CLCN1 fragment in spite of the triple digest.

Colony PCR

Taq polymerase and reagents for the PCR reaction were supplied by NEB. Primers for colony PCR were the same as had been used to create a CLCN1 fragment bounded by XbaI and EcoRI restriction sites (see section 2.1). Each reaction was performed in a 20μL aliquot of the mixture specified below. The enzyme was added last and the aliquots were kept on ice. A sterile plastic pipette tip was used to lightly touch a bacterial colony, making sure that the colony was preserved on the plate, and picking up just enough bacteria to block the pipette. The bacteria were introduced to a 20μL aliquot of reaction mixture and lysed by vigorous pipetting up and down to release their DNA. The reactions were allowed to proceed on a thermal cycler according to the protocol specified beneath the reaction mixtures below:

	Vol (μL)	
Forward primer	5	(concentration 100μM)
Reverse primer	5	(concentration 100μM)
dNTP	18	
Taq buffer	44	(10x concentration)
MgCl2	27	
Taq polymerase	2	
ddH2O	339	
Total	440	

95°C	10 minutes	
95°C	15 seconds	25 cycles
60°C	30 seconds	
68°C	3 minutes	
68°C	10 minutes	

The 10 minute first step was to promote bacterial cell lysis and to inactivate DNAses.

The reaction mixtures were then electrophoresed on an agarose gel (figure 2.3 below):

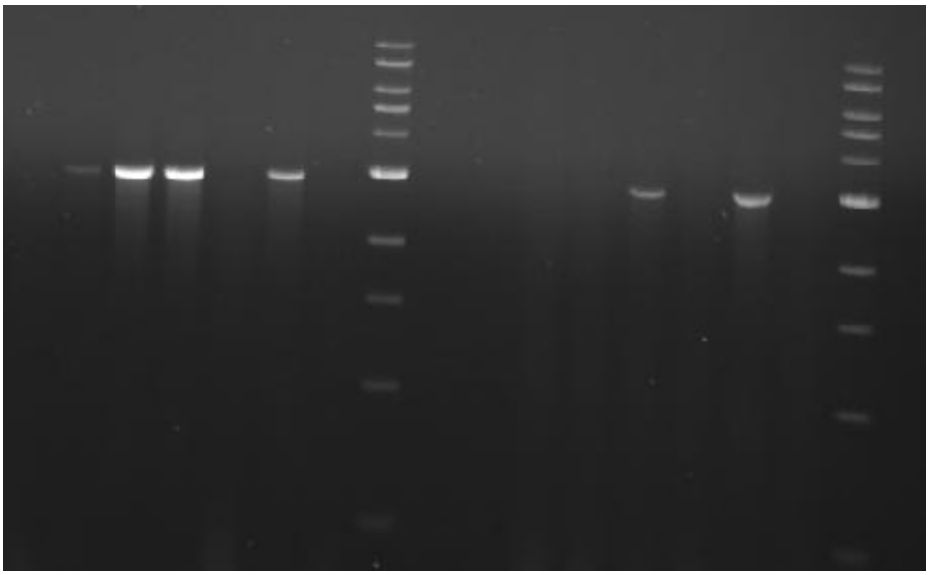

Figure 2.3 Agarose gel electrophoresis of colony PCR
Each lane represents a different colony of bacterial cells (except for lanes 7 and 16, which display the ladder). A band at approximately 3kb indicates the presence of CLCN1 in the bacterial cells.

Those colonies that yielded a band at about 3kb (indicating the presence of the CLCN1 gene) were amplified in a miniprep and the extracted DNA analysed with a diagnostic restriction digest (explained below).

Diagnostic digest

To confirm successful ligation of CLCN1 into PCDH1 the constructs identified by colony PCR were digested with ScaI (NEB) and electrophoresed on an agarose gel (figure 2.4 below). ScaI cuts PCDH1-CLCN1 in two places, once in the vector backbone and once in the CLCN1 gene, yielding a fragment of approximately 6kb and another of about 4.5 kb length. It cuts the PTLN construct into fragments of 3.7 and 2.6 kb. The empty PCDH1 vector is cut only once, producing a single fragment.

The reaction mixture and the results from the diagnostic digest are shown below:

	Vol (μL)
DNA	0.5
Buffer 4 (NEB)	1.5
BSA	1.5
ScaI-HF	0.5
ddH20	11
Total	100

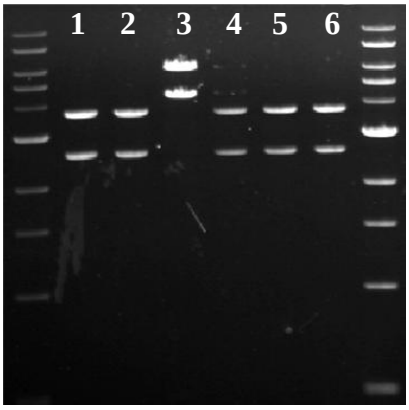

Figure 2.4 ScaI digest of constructs containing CLCN1.
Column 3 contains the intended PCDH1-CLCN1 construct. The remaining columns contain the original PTLN *Xenopus* oocytes expression vector.

Final confirmation of the presence of CLCN1 gene in the PCDH1 vector was by sequencing the entire CLCN1 gene and a short segment of PCDH1 vector at either end.

Site-directed Mutagenesis

Point mutations were introduced into plasmid DNA using a QuikChange™ mutagenesis kit (Stratagene, CA) according to the manufacturer's instructions. Mutant plasmids were amplified with a miniprep either in the *E.coli* supplied with the kit, or in the laboratory's stock Top10 *E.coli*. The whole CLCN1 gene was sequenced at the Wolfson Institute for

Biomedical Research, Scientific Support Services, UCL, to confirm the presence of the intended mutation and the absence of unintended mutations.

2.2 Preparation of HEK293T cells for voltage clamp experiments

Reagents

Dulbecco's Modified Eagles medium (D-MEM Sigma) was purchased in 500ml bottles and stored at -4 ^{o}C. GlutaMAX™ (Gibco) at 100x concentration was divided into 5ml aliquots and stored at -20 ^{o}C. Foetal calf serum (Gibco) was divided into 50ml aliquots and stored at -20 ^{o}C. Poly-D-lysine (Menzel-Glaser) was divided into 5ml aliquots and stored at -20 ^{o}C. Glass coverslips 13mm in diameter were coated by submerging them in 10ml poly-D-lysine for 1 hour in a 50ml tube on a roller. The coverslips were removed from the poly-D-lysine, transferred to a clean glass beaker covered with foil and first autoclaved then dried in an oven at 120^{o}C overnight. Sterile PDL-coated coverslips were stored in a sealed container at 4^{o}C.

Cell culture

HEK293T cells were grown in sterile polystyrene tissue culture flasks with 25mm^2 growth areas and filter caps (NUNC EasYFlask, purchased from VWR). Their culture medium (Dulbecco's Modified Eagles medium) was supplemented with 10% (v/v) foetal calf serum (one 50ml aliquot to each 500ml bottle of culture medium) and GlutaMAX™ (one 5ml aliquot of 100x concentration GlutaMAX™ to each 500ml bottle of medium). The cells were incubated at 37^{o}C in a humidified atmosphere of 5% C02, 95% air. Three times per week the cells were transferred to a new tissue culture flask at a lower density (between 1/4 and 1/8). To transfer the cells they were washed with sterile PBS before incubation in 1ml

of trypsin (Gibco / Invitrogen) for 5 minutes at 37°C. Cells were dislodged and dissociated from their neighbours by agitation of the flask followed by gentle trituration in the trypsin. The trypsin was neutralized by adding the 1ml cell suspension to 9ml of fresh medium in a 15ml tube and pelletted by centrifugation at 250 RCF for 3 minutes. The pellet was resuspended in 2ml of fresh culture medium and 0.25 to 0.5 ml of this cell suspension was transferred to a new tissue culture flask containing 3ml culture medium. On Wednesdays and Fridays 2 – 4 drops (from a plastic Pasteur pipette) of the 2ml cell suspension were swirled into each well of a 6-well plate (Nunc, Denmark) or into separate 35mm tissue culture dishes containing fresh culture medium in preparation for transfection on Friday and Monday mornings respectively.

Transfection

Cells were transfected at 50 – 70 % confluency in 35 mm dishes or a 6-well plate (Nunc, Denmark). Transfections were performed using Lipofectamine 2000 (Invitrogen) or Fugene (Roche) according the manufacturer's recommendations using 0.5 μg plasmid DNA (5 μL of a 100 ng/μL DNA solution). 6 - 8 hours after transfection the cells were transferred onto coverslips in a 4-well plate (IVF 4 well dish, Nunc). Transfected cells from each well of a 6 well plate were washed with sterile PBS before incubation in just enough trypsin to cover them for 5 minutes at 37°C. The cells were dislodged and separated from their neighbours by agitation followed by trituration before 2ml fresh culture medium was added. 1 – 3 drops of the resulting cell suspension was swirled into each well of a 4-well plate.

2.3 Preparation of skeletal muscle fibres

Reagents

500ml of ringer solution (146 NaCl, 5 KCl, 1 MgCl2, 2 CaCl2, 10 HEPES, pH 7.4) was made as required and stored at -4°C. Collagenase A (Roche) was dissolved in Ringer at 2mg/ml, divided into 1ml aliquots and stored at -20°C.

A 50 mM stock of BTS was made by adding 380uL of DMSO to the vial containing 5mg of BTS powder. The stock solution was stored in the fridge at 4 °C.

50 mM stock solutions of progesterone and oestrogen were made using DMSO as follows:

17-βoestradiol (molecular weight 272.39): 13.6 mg was dissolved in 1ml DMSO

Progesterone (molecular weight 314.47): 15.7 mg was dissolved in 1ml DMSO

To make extracellular solution containing 100μM hormone, 100μL of the hormone stock solution was added to 50ml of extracellular solution and shaken vigorously.

Animals

Colleagues in the department of experimental epilepsy regularly conducted experiments using brain tissue from mice, providing a source of muscle tissue without the need for sacrificing additional animals. Mice used for the experiments were from the C57BL/6J inbred strain. Some of the mice included in this PhD were genetically modified with a heterozygous point mutation in the voltage gated potassium channel, Kv1.1 (V408A mice - a model of Episodic Ataxia type 1) (Herson, Virk et al. 2003). Although Kv1.1 is expressed in skeletal muscle, the presence of the mutation in some but not other cells could

not directly contribute to cell to cell differences in current magnitude because potassium currents were blocked (by cesium and TEA) to enable recordings of pure chloride currents.

Isolation of single FDB muscle fibres

Mice aged 1 – 4 months were killed by isoflurane inhalation and cervical dislocation. Flexor digitorum brevis from one hind foot was excised under a dissecting microscope (20x magnification) in the following steps:

1) The dead animal was sprayed lightly with 70% ethanol, and the tail snipped off.

2) A circular incision was made just above the ankle with a scalpel.

3) With the animal supine a longitudinal incision was made along the midline of the ventral hind foot, forming a T with the first incision proximally, and extending to the toes distally.

4) With forceps and a scalpel one of the free edges of skin from the longitudinal incision was lifted and carefully separated from the underlying tissues from the ankle down to the toes. The same was performed for the other free edge. By rolling the animal onto its side first one way and then the other, and finally placing it on its front it was possible to remove the skin of the hind foot without touching the FDB. During the process the exposed tissues were intermittently wet with Ringer solution.

5) The scalpel was carefully passed either side of FDB to disrupt its attachment to adjacent structures.

6) The scalpel was slid flat underneath the tendon of FDB at the heel, and by gently cutting in a proximal direction (trying not to stretch the muscle) the proximal tendon was separated close to its attachment to the heel and then lifted slightly with forceps.

7) Without stretching the muscle the free end of tendon held by the forceps was gently lifted as the scalpel was used to cut through the tissue attaching the muscle to the plantar fascia.

8) When the FDB muscle and a portion of the FDB tendons at the toes were free, microscissors were used to snip through the distal tendons and the muscle was immediately transferred to a 35mm dish of ringer solution for cleaning

9) The muscle was cleaned of connective tissue using forceps and a scalpel, and the tendons shortened.

10) A glass Pasteur pipette that had been broken off with a wide tip and fire-polished was used to transfer the cleaned muscle from the Ringer solution to a 5ml bijou tube containing 2 ml of 1mg/ml collagenase.

11) The muscle was shaken for 1 hour in a 37 °C incubator. During the incubation period six 35mm dishes were trimmed with scissors to about half their original height – trimming increased the region of the dish accessible to the microelectrode, which approached at approximately 45° and would otherwise have tended to hit the side of the dish.

12) At the end of the incubation period the muscle was transferred to a fresh (un-trimmed) 35ml dish of Ringer solution to remove any trace of collagenase. At this stage it was sometimes possible to use forceps and a scalpel to remove further connective tissue.

13) The muscle was transferred to the first of the 6 trimmed dishes of Ringer solution where it was pulled apart slightly by its distal tendons using two pairs of forceps and then triturated. Individual myofibres were just visible under the dissecting microscope with the

light source shining from the side into the dish. With the light source sideways the muscle could be made to appear bright on a dark background and individual myofibres appeared as tiny iridescent hairs on the bottom of the dish. After at least 10 myofibres were present in the centre of the dish the muscle was transferred to the next dish and the process repeated for all 6 dishes.

14) The dishes were transferred to the electrophysiology lab and the fibres allowed to settle for about 30 minutes (a convenient time for lunch).

2.4 Electrophysiology

Solutions

The composition of solutions is shown in table 2.1 below. The pH was adjusted to 7.4 using sodium hydroxide for Ringer, and cesium hydroxide for extracellular and intracellular recording solutions. The liquid junction potential was calculated as -8.5mV, and this was used to correct the command voltage post-hoc (during analysis).

Table 2.1 Composition of patch clamp solutions in mM

	Ringer	Muscle Extracellular	HEK Extracellular	Intracellular
Cs-Aspartate	-	-	-	110
CsCl	-	-	-	30
$MgCl_2$	1	-	-	5
HEPES	10	10	10	10
TEA-Cl	-	145	145	-
CaCl2	2	10	10	-
CdCl2	-	0.25	-	-
NaCl	146	-	-	-
KCl	5	-	-	-
pH	7.4	7.4	7.4	7.4

HEK293T cells and FDB muscle fibres were studied using the same intracellular solution. The extracellular solution differed only in that for HEK293T cells there was no cadmium chloride

Patch clamp rig

Whole cell voltage clamp data were collected with an Axopatch 200B amplifier at a sampling rate of 10 kHz and low-pass filtered with a 2 kHz cutoff. Data were recorded in the LabView programming environment with a virtual instrument originally designed by Prof. D. Kullmann (Dept of Clinical and Experimental Epilepsy, Institute of Neurology, Queen Square) and adapted by the author.

The silver wire electrode was chlorinated with household bleach overnight at regular intervals. The chamber in which HEK cells were studied was cleaned with distilled water at the end of every day to prevent accumulation of salts.

Microelectrodes

Microelectrodes were pulled from 75mm long thin-walled borosilicate glass capillary tubes in 4 cycles using a Sutter P97 puller and then fire polished on a Narishige MF-830 microforge. For studying FDB muscle fibres the tip resistance was 0.5 – 1.5 MΩ. For HEK293T cells the tip resistance was 2-3 MΩ.

Whole cell patch clamp of HEK293T cells

Recording took place 24-72 hours after transfection. In the tissue culture laboratory, under sterile conditions, a glass coverslip with cells attached was transferred from its 4-well plate of incubated culture medium to a 35mm dish of external solution for transport to the patch clamp laboratory. The coverslip was then transferred to a recording chamber of an inverted microscope (Nikon eclipse Ti-U).

Successfully transfected cells were identified by GFP fluorescence owing to the presence of the GFP gene on the PCDH1 vector. Cells were selected on the basis of fluorescence intensity. Bright cells were avoided because the very large currents produced voltage errors even with low series resistance. Very faintly fluorescent cells were also avoided because in the absence of leak subtraction chloride currents were more prone to distortion by linear currents arising from un-cancelled capacitance and/or leak through the seal.

Before lowering into the bath positive pressure was applied to the electrode to prevent debris sticking to the pipette tip. Once in the bath positive pressure was released, the current offset zeroed, and the micropipette manoeuvred under fine control to hover over the cell. The tip resistance (typically 1 – 3 MΩ) was estimated from the change in current in response to a 5mV voltage step. The pipette was then lowered until a slight reduction in the current response from the seal test indicated contact with the cell membrane. Gentle suction was applied until a gigaohm seal was formed. The membrane was clamped to a holding potential of -40 mV (the approximate reversal potential of chloride ions in these solutions), and capacitance transients were cancelled using the dials on the amplifier. The whole cell configuration was achieved by applying brief, strong suction. Cell capacitance was consistently between 5 and 15 pF and the series resistance of 3 to 10 MΩ was compensated 60% to 80%.

Whole cell patch clamp of FDB fibres

Muscle fibres were prepared in the morning and studied on the afternoon of the same day within 8 hours. Before the start of an experiment two 1ml aliquots of intracellular solution were removed from the -20 °C freezer and left to thaw at room temperature. Solutions to be used on the day were removed from the fridge or freezer and allowed to equilibrate to room temperature. 10-15 microelectrodes were fabricated. The dissecting microscope was set up and focused over the dissecting mat, and the light source orientated correctly. Instruments and the mat were sprayed with 70% ethanol and allowed to dry.

A 35mm dish of muscle fibres in Ringer solution was transferred to the stage of a Nikon eclipse Ti-U inverted microscope where the Ringer solution was exchanged for recording

solution. This was performed three times by sucking off most of the ringer solution using a pump while pipetting on extracellular solution. A suitable FDB muscle fibre was identified. Only fibres with smooth membranes, without debris nearby that might stick to the electrode, and with clear striations were studied. The dish was rotated while looking down the microscope to orient the fibre so that the micro electrode would approach it from the side, perpendicular to its long axis. An empty 1 ml syringe with a rubber tube to hold an electrode was used to suck some filtered intracellular solution into the electrode tip. The electrode was then filled from the back with more intracellular solution. The first filling step was necessary to avoid bubbles (the electrode glass had no filament in order to maximize the success rate of achieving a gigaohm seal). Positive pressure was applied as the electrode was lowered through the surface of the extracellular solution but released again once in the vicinity of the FDB cell; if intracellular solution was blown onto an FDB fibre, the fibre contracted. At this stage, with zero mV applied to the pipette, the current was set to zero and the tip resistance estimated using the Axopatch 200b amplifier's 5mV seal test. The electrode was then positioned close to the fibre, and in a single movement positive pressure was applied as it was lowered onto the side of the cell. On touching the cell the positive pressure was released and gentle suction applied. The command potential was gradually taken down to -40mV as the seal formed. Once a gigaohm seal was formed, suction was increased slightly and clamped on to achieve the whole cell configuration, which often took several minutes to develop. After whole cell configuration was achieved a period of 15 minutes was allowed for the intracellular solution in the pipette to dialyze the cell before recording was started. Suction was maintained throughout the duration of the experiment. Finally, capacitance cancellation and 90% series resistance compensation were

applied, and the recording initiated. For experiments with hormone the extracellular solution was exchanged during an experiment using suction, a plastic Pasteur pipette to add the new solution, and a steady hand.

2.5 Data analysis and computer simulations

Computer simulations and data analysis were performed on a Fujitsu Siemens laptop computer in the Microsoft XP operating system. Computer simulations were written in Matlab (Mathworks), and are described in chapter 5. Data from patch clamp experiments were first converted to tab-delimited text using a LabView virtual instrument originally designed by Prof. D. Kullmann (Dept of Clinical and Experimental Epilepsy, Institute of Neurology, Queen Square) and adapted by the author. The text file was then processed in MatLab. Some figures were also produced using GraphPad prism. Statistical analysis was by t-tests or ANOVA in Matlab; each statistical comparison and its method is specified in the results sections whenever a p-value is given. Fast and slow time constants of current activation or deactivation were estimated in Matlab by fitting a double exponential function

$$I(t) = A_1 e^{-\frac{t}{\tau_1}} + A_2 e^{-\frac{t}{\tau_2}} + C$$

to the current on stepping from -40 to +60 mV (activation) or from +60mV to -80mV (deactivation). Voltage dependence of ClC-1 activation was characterized by plotting tail currents against pre-pulse voltage in Matlab and fitting with Boltzmann functions:

$$I(V) = I_{min} + \frac{I_{max} - I_{min}}{1 + \exp\left(\frac{V_{50} - V}{k}\right)}$$

The slope factor, *k*, measures the the strength of the dependency between current and voltage. V_{50}, the voltage at which current is mid way between I_{min} and I_{max}, is the 'set point' around which changes in voltage increase or decrease current. For the two ClC-1 variants (G276D and G523D) that abolished voltage dependence, statistical comparison against wildtype was made with the magnitude of the tail current after stepping to 0 mV. Normalization was performed by dividing the tail current at each voltage by I_{max}. For a channel with a single gate and pore, normalized tail current is an estimate of the gate's open probability. Each ClC-1 has two pores and three gates; the normalized ClC-1 tail current has no real physical counterpart, but can be interpreted as the open probability of an 'equivalent channel' with a single pore and gate that passes current with the same voltage dependency as ClC-1. Normalized tail current from FDB muscle fibres after hormone treatment should not, however, be interpreted in this way because normalization was against I_{max} before hormone. The fractional tail current after hormone as a proportion of peak current before hormone is a function not only of channel behaviour but also of channel abundance. Normalizing 'after-hormone' currents against the 'before-hormone' I_{max} enables a comparison before and after hormone within each cell while also preserving the shape of the Boltzmann function in the figures.

Chapter 3 Functional consequences of CLCN1 variants

3.1 Chapter summary

Eight naturally-occurring CLCN1 sequence variants, selected at different points along the channel structure, were studied by whole cell patch clamp in HEK293T cells as part of an effort to evaluate a new assay at our centre for the classification of novel variants. One variant (W118G) had been suggested to be a modifier but not pathogenic in its own right based on its presence in controls but over-representation among Myotonia Congenita patients, while the others had all been identified only in Myotonia Congenita patients. When expressed as homodimers in HEK293T cells, G276D and G523D showed complete loss of function. S289G produced a depolarizing shift in voltage-dependence that was accompanied by slowing of the channel's kinetics. The remaining variants were indistinguishable from wildtype. The results are discussed in the context of phenotypic variability and of a diagnostic service.

3.2 Aims

Test the effect on ClC-1 channel function of a selection of amino acid substitutions found in Myotonia Congenita patients by voltage clamp of HEK293T cells expressing recombinant human CLCN1.

Assess the usefulness of functional expression in HEK293T cells as an assay for the classification of novel sequence variants in the context of a diagnostic service.

3.3 Motivation

Establishing a precise genetic diagnosis is important not only for counseling the patient but provides a foundation on which to build therapeutic strategies. Phenotypic and genotypic variability make diagnosis difficult. The 'perfect disease' from the point of view of diagnosis would have the same easily recognisable phenotype in every patient, a phenotype that never occurs in unaffected individuals, and a single genetic cause. The diagnosis of Myotonia Congenita is sometimes difficult because myotonia is a feature of other diseases (associated with variants in different genes, e.g. SCN4A), previously undescribed sequence variants in CLCN1 of uncertain pathogenicity are often encountered, and the severity of the Myotonia Congenita phenotype is variable. Pathogenicity of a novel CLCN1 variant cannot be determined from the sequence alone, so an assay to test the functional consequences of such variants is desirable both for a diagnostic service and for understanding the genetic contribution to phenotypic differences between patients. Previous functional studies of ClC-1 at our centre have used two electrode voltage clamp of *Xenopus* oocytes. While these cells allow quantification of the amount of genetic material expressed, they may not recapitulate the muscle environment as faithfully as a human somatic cell line and their use requires the sacrifice of frogs to harvest the eggs. Furthermore, stably-transfected HEK293T cells could be used for automated patch clamp, with the potential for a high-throughput service.

3.4 CLCN1 sequence variants selected for functional expression

The clinical genetics laboratory of the National Hospital for Neurology & Neurosurgery sequences all exons of CLCN1 plus short regions of flanking introns as part of a diagnostic service covering the whole UK. The lab also receives occasional samples from outside the

UK. Much of this diagnostic sequencing was performed by Dr. Richa Sud. The author was kindly allowed access to the data and, where possible, collected clinical information from the referring doctors. The author did not, however, perform any sequencing of patient DNA samples but focused instead on developing a functional expression system for point mutations.

As of March 2012, among 344 patients in whom all 23 exons of CLCN1 plus flanking introns had been sequenced, 132 different sequence variants had been identified by the staff in the clinical genetics laboratory of NHNN. The distribution of variants (by exon) in the gene is shown in Figure 3.1 below.

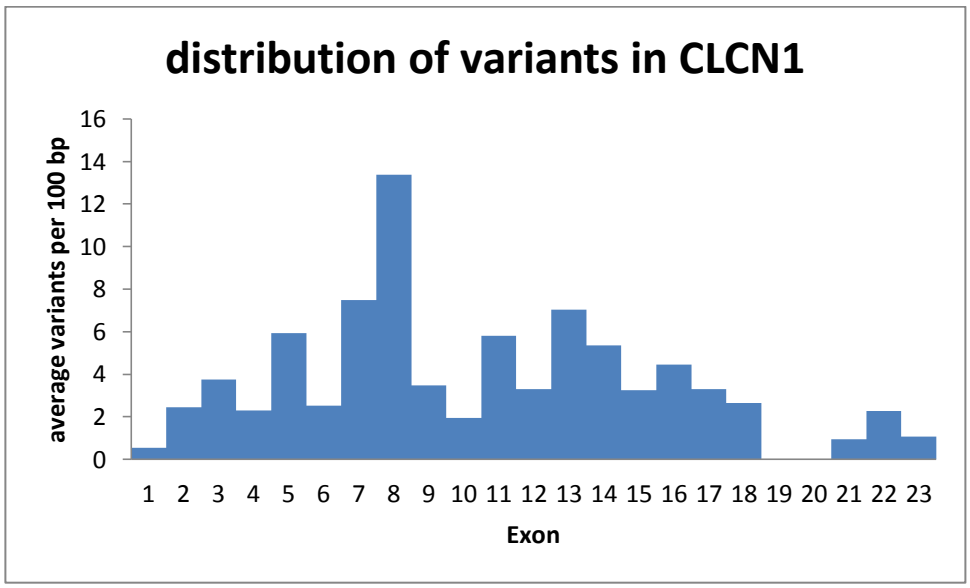

Figure 3.1 Distribution of variants in exons CLCN1.
The number of different variants in each exon was divided by the length of the exon in base pairs, and multiplied by 100 to get the average number of variants per 100pb of each exon.

At the start of the project, sequence variants whose functional effects had not at the time been reported in the literature and were located at different positions in ClC-1 were selected for study (Figure 3.2, Table 3.1).

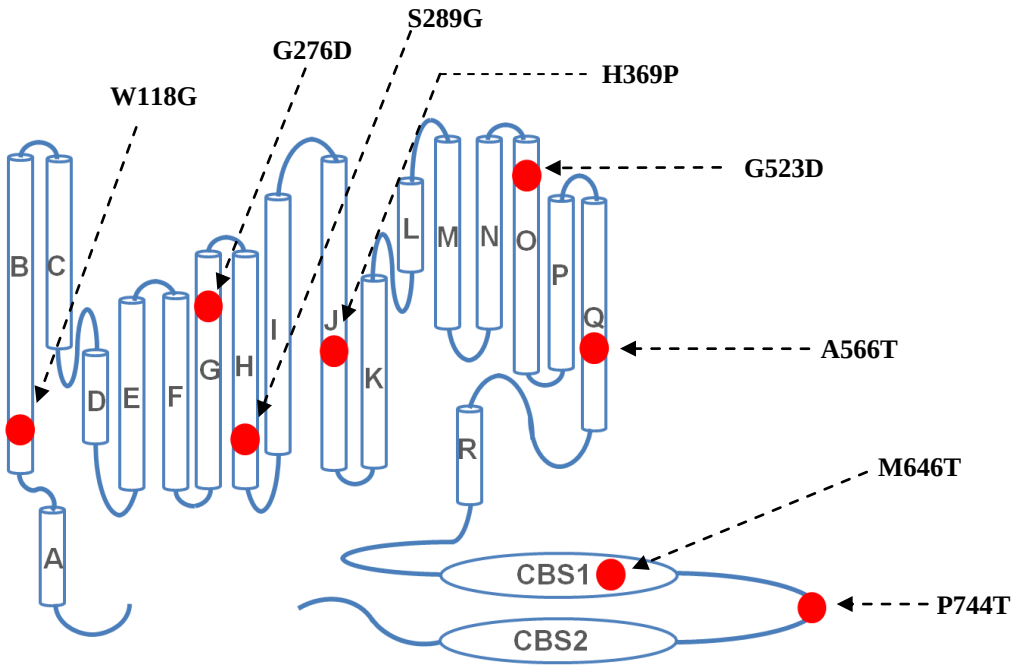

Figure 3.2 Positions of the CLCN1 sequence variants studied.
Figure adapted from Dutzler R, et al. Nature 2002;415(6869):287-94

Table 3.1 Clinical and genetic details of the patients whose variants were studied in HEK293T cells

cDNA	protein	Exon	Helix	Polyphen	HEK293T	Inheritance pattern and comments
352T>G	**W118G**	**3**	**B**	**Possibly damaging**	**As wildtype**	**Present in controls, but over-abundant in MC patients.**
				9 apparent homozygotes (see table 3.2 for details) and 37 heterozygotes.		
827G>A	**G276D**	**7**	**G**	**Possibly damaging**	**Total loss of function**	**?dominant**
		Patient ID 675		*Onset in pregnancy age 21, quite intrusive symptoms. Son affected: onset age 5 with tendency to fall, legs aching, slow to initiate movement, same genotype*		
				Other variants:	None (wildtype on other allele)	
		Patient ID 772		*Typical Myotonia Congenita. Father same genotype said to have stiffness on rising from a chair (although this could be due to arthritis)*		
				Other variants:	None (wildtype on other allele)	
865A>G	**S289G**	**8**	**H**	**Benign**	**Slow kinetics, right shift**	**Recessive**
		Patient ID 617		*stiff gait from age 1, consanguineous asymptomatic parents, 3 siblings asymptomatic, legs most affected but also eyelids, tongue, abdominal muscles. Parents carry 1 copy each of S289G.*		
				Other variants:	Apparent homozygote for S289G	
1106A>C	**H369P**	**10**	**J**	**Possibly damaging**	**As wildtype**	**Recessive**
		Patient ID 611		*severe myotonia, uses a wheelchair, no family history. No parental DNA available, but children carry H369P only so this patient's 2 variants are on different chromosomes.*		
				Other variants:	c.1872delG p.E624fs	
1568G>A	**G523D**	**14**	**O**	**Possibly damaging**	**Total loss of function**	**dominant**
		Patient ID 541		*onset age 7, worse in the cold, no family history*		
				Other variants:	None (wildtype on other allele)	
1696G>A	**A566T**	**15**	**Q**	**Benign**	**As wildtype**	**recessive**
		Patient ID 384		*Presented age 7. Severe myotonia that significantly limits walking. Florid myotonia on EMG plus occasional myopathic motor units. Unaffected, consanguineous parents No parental DNA available*		
				Other variants:	Apparent homozygote for A566T	
		Patient ID 860		*Onset age 10, severe myotonia, muscle hypertrophy, no weakness. Unaffected parents who are 1st cousins. No parental DNA available*		
				Other variants:	Apparent homozygote for A566T	
		Patient ID 998		*Typical Myotonia Congenita. No parental DNA available*		
				Other variants:	c.501C>G p.F167L	
		Patient ID 669		*Severe myotonia. One of 4 affected siblings whose parents are 1st cousins. Mother carries 1 copy of A566T, wildtype on other allele. Father is an apparent homozygote for A566T*		
				Other variants:	Apparent homozygote for A566T. NB. This family additionally has type 2 myotonic dystrophy (but members with only A566T still have severe myotonia)	
1937T>C	**M646T**	**17**	**CBS1**	**Benign**	**As wildtype**	**?dominant**
		Patient ID 222		*Onset age 10, relatively mild symptoms, parents asymptomatic. Brother with same genotype with onset age 5 and more severely affected. No parental DNA available*		
				Other variants:	Apparent homozygote for M646T	
		Patient ID 620		*Late onset mild phenotype. Referred age 51 with 20 year history of difficulty initiating movement. No recollection of school years. Myotonia on EMG but not detectable by clinical examination. Calf hypertrophy. One parent had 'difficulty with hands'. Children asymptomatic. No parental DNA available*		
				Other variants:	None: wildtype on other allele Negative tests for myotonic dystrophy types I and II	
2230C>A	**P744T**	**18**	**CBS1-2 Linker**	**Benign**	**As wildtype**	**recessive**
		Patient ID 578		*Not known to be related to 619, but same ethnicity (northern Iraq). Member of a large consanguineous family of Iraqi Kurds (parents 2nd cousins, paternal grandparents1st cousins). Father and three siblings similarly affected. No parental DNA available*		
				Other variants:	Apparent homozygote for P744T (NB. homozygous duplication of exons 8 – 14 discovered later)	
		Patient ID 619		*Not known to be related to 578, but same ethnicity (northern Iraq). Two out of six siblings affected. Children unaffected. No parental DNA available*		
				Other variants:	Apparent homozygote for P744T (NB. homozygous duplication of exons 8 – 14 discovered later)	

3.5 Choice of parameters for characterising ClC-1 in HEK293T cells

Voltage clamp in the whole cell configuration uses macroscopic current as the read-out for changes in the conductance of the cell membrane, which in turn reflects the average state of the ClC-1 channels. The conductance of a HEK293T cell to chloride ions reflects the density of ClC-1 channels in the membrane, the total area of membrane (surface are of the cell), the fraction of channels in a conductive state (one or both pores of the dimer open), and the microscopic conductance of each open pore. Voltage gating is a major aspect of ClC-1 function and as a minimum the assay should detect dysfunctional gating.

The current at different voltages does not vary in direct proportion with the fraction of open channels at those voltages, because the driving force for chloride ions also depends on voltage. A simple measure of the fraction of open channels is the conductance, obtained by dividing the steadystate current at each test potential by the driving force at each potential (driving force = membrane potential – chloride equilibrium potential).

$Current = g \times (V_m - E_{Cl})$ where g is conductance

Vm is membrane potential

E_{Cl} is chloride equilibrium potential

However, ClC-1 displays inward rectification (Figure 3.3); the open channel passes current more easily in the inward than the outward direction (in physical terms, this means negative chloride ions move *outward* more easily, see note in legend to Figure 3.3). The conductance does not therefore reflect open probability of the channel.

An alternative method (Figure 3.4) is to first open all the channels with a constant depolarization, and then to measure the instantaneous and steadystate currents on stepping

to different potentials. Immediately on stepping to the second potential the channels are still fully open, and over time at the same potential they relax into the state determined by that potential. The driving force and rectification are the same for both instantaneous and steadystate currents so the fraction steadystate/instantaneous is directly proportional to the fraction of open channels in steadystate/channels opened by pre-pulse (the prepulse should open 100% of wildtype channels).

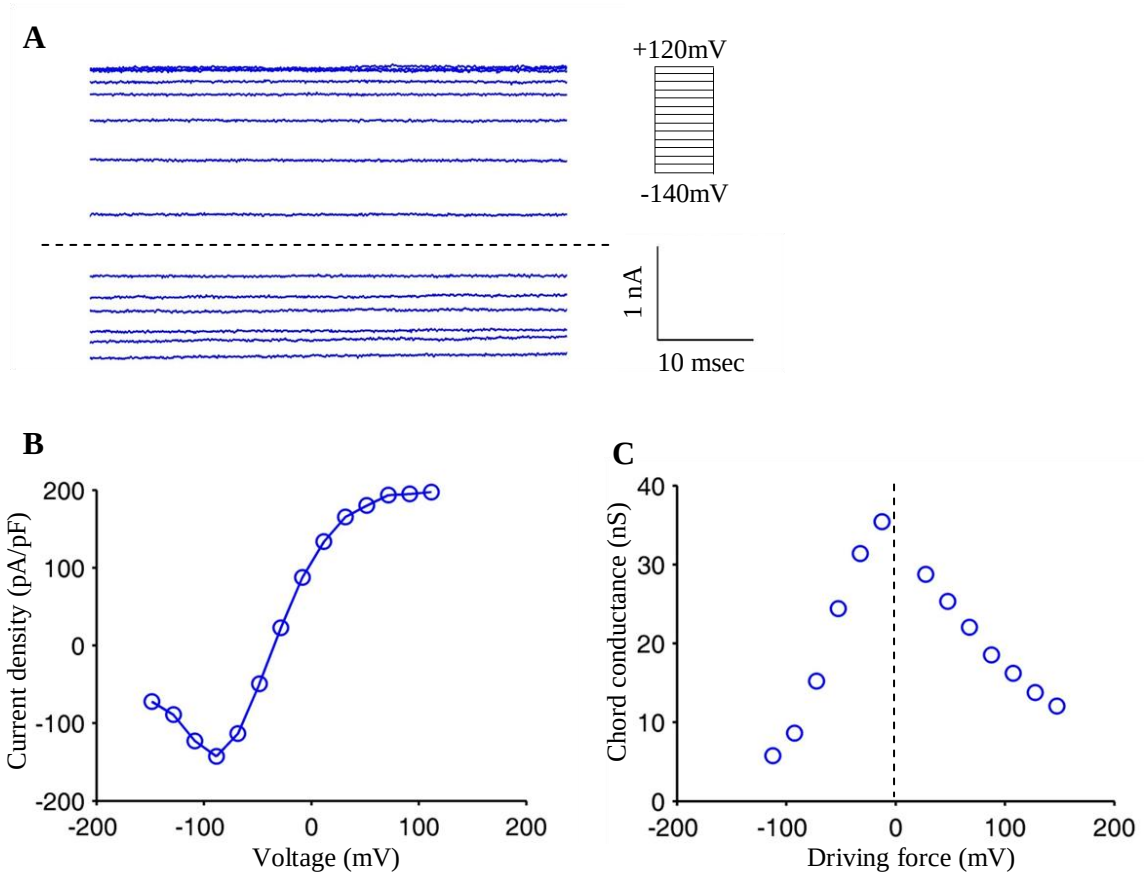

Figure 3.3 Extract from a representative wildtype ClC-1 recording showing steadystate current and conductance.
(A) Steadystate currents at different voltages between -140 and +120 mV. In the graphs below, voltages and driving force are corrected for the junction potential of -8.5 mV **(B)** Steadystate current plotted against voltage. In these recordings the chloride reversal was set to -36 mV. **(C)** Conductance plotted against driving force. Conductance was calculated as current / driving force, where driving force is the deviation of membrane potential from the chloride reversal potential. At negative driving forces the conductance plot is sigmoid resembling a Boltzmann function but instead of plateauing at positive potentials conductance falls precipitously owing to inward rectification. (Note – by convention rectification direction refers to the flow of positive charges. Thus, by convention 'inward rectification' means that negative chloride ions pass more easily in the outward direction).

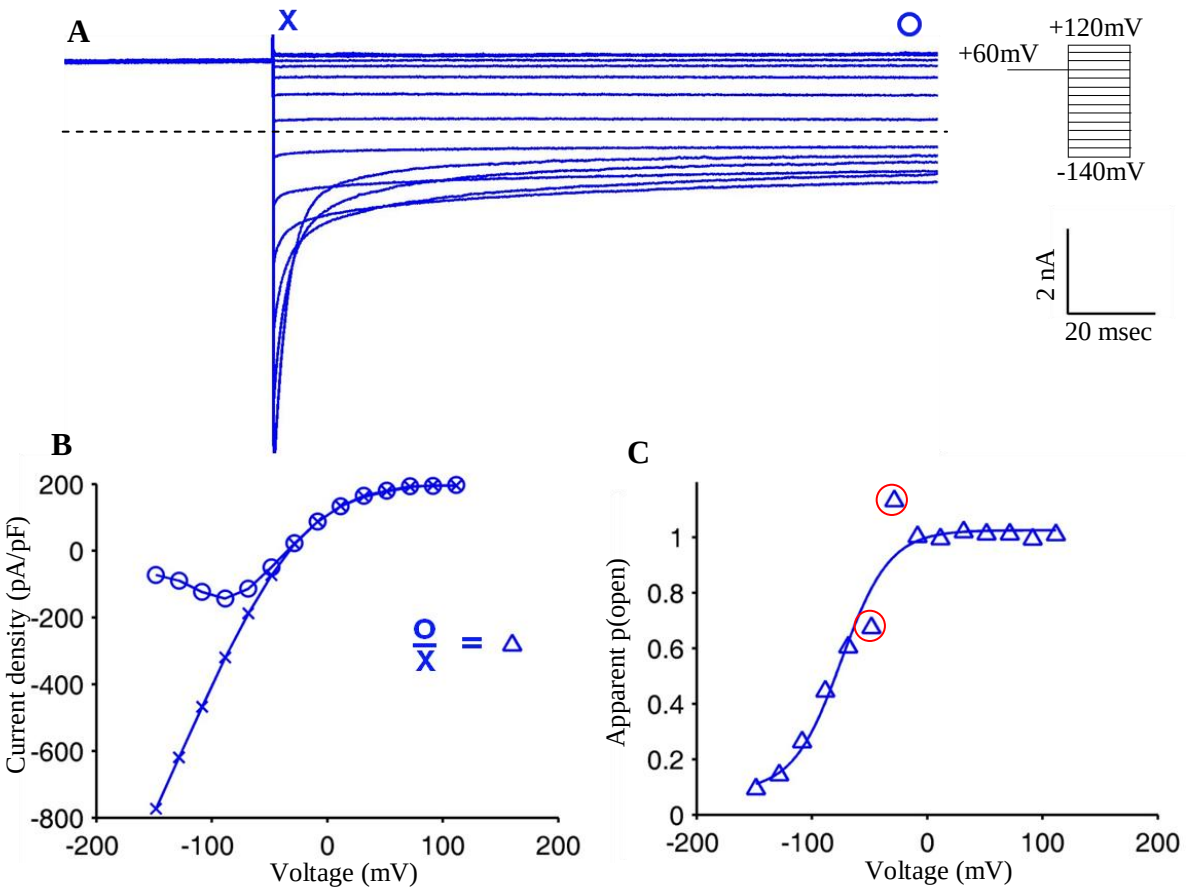

Figure 3.4 Extract from a representative wildtype ClC-1 recording illustrating the method of taking the steadystate : instantaneous current ratio.
(A) Currents in response to a constant +60 mV pulse followed by a variable step between -140 and +120 mV/ Markers indicate (approximately) the times at which the instantaneous (x) and steadystate (o) currents are measured **(B)** Instantaneous (x) and steadystate (o) current densities plotted against voltage during the variable step **(C)** Steadystate:instantaneous current ratio plotted against each voltage during the variable step produces an apparent open probability curve that is fitted with a Boltzmann function. Near the reversal potential of -36 mV the currents approach zero and a small amount of noise produces spurious values (red circles) in **(C)**. A second disadvantage is that some mutants can only be fully activated by a very strong depolarization, which is not well tolerated by the cell.

There are two disadvantages to the ratio method. Firstly, close to the reversal potential the currents approach zero and a small amount of noise produces spurious points in the apparent opening probability curve. Secondly it may be difficult to fully activate mutant ClC-1 channels whose voltage dependence is shifted to strongly depolarized potentials.

The method chosen for our assay, reflecting a standard approach for recordings from these channels, was to measure the instantaneous current (tail current) on stepping to -100mV after the variable step (Figure 3.5). The variable step sets the state of the channels, and because all tail currents are measured at the same potential (-100 mV), current amplitude is not affected by driving force or rectification. At very short latencies (< 2 msec) after stepping from the variable step to -100mV the channels have not had time to relax into a new state. Thus the same driving force can be applied and the tail current varies in direct proportion with the fraction of open channels. The curve can be fitted with a Boltzmann function and normalizing against the peak current yields an apparent open probability curve.

In the rest of this chapter the instantaneous and steadystate current densities during the variable voltage step are presented to show the magnitude of currents, along with the normalized tail currents fitted with a Boltzmann function (apparent open probability) to show the voltage dependence of channel activation. For CLCN1 sequence variants that abolish voltage dependence, tail currents are presented without normalization.

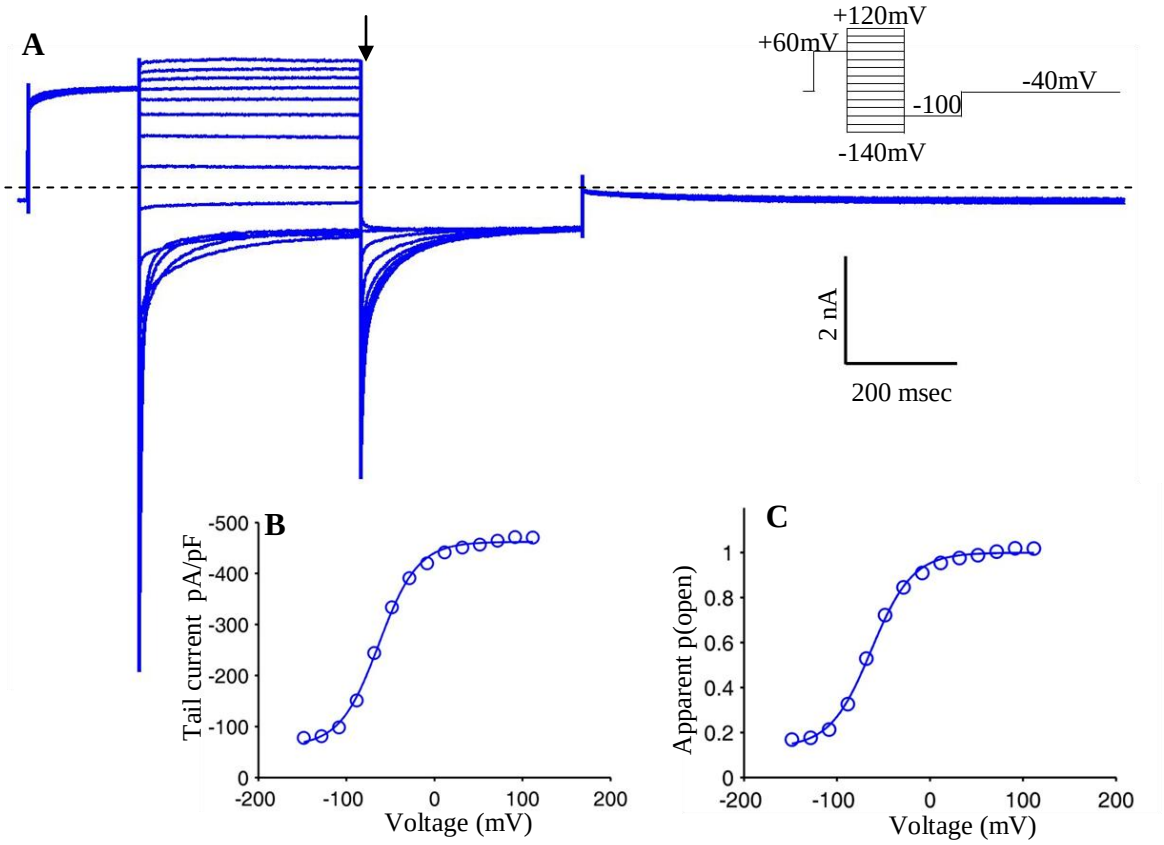

Figure 3.5 Representative wildtype ClC-1 recording illustrating the method of measuring tail currents to obtain the apparent opening probability.
(A) Currents in response to the voltage protocol shown top right. The black arrow indicates (approximately) the time at which tail currents were measured. **(B)** Tail current density plotted against voltage during the variable step and fitted with a Boltzmann function. In this and subsequent plots of tail currents the y-axis is inverted so the curve has the same orientation as the opening probability curve. **(C)** Tail currents normalized against the top of the Boltzmann function in B to produce an apparent open probability curve.

3.6 Results

Wildtype ClC-1 and untransfected HEK293T cells

HEK293T cells transfected with wildtype human ClC-1 yielded robust voltage-dependent currents that activated upon depolarization, and displayed inward rectification. The magnitude of current recorded from any given HEK293T cell expressing wildtype ClC-1 correlated approximately with the degree of fluorescence as assessed by visual inspection. Brightly fluorescent cells yielded currents an order of magnitude larger than dimly fluorescing cells. Currents from the brightest cells were measurable in tens of nA, while the currents from the faintest cells were in the range of hundreds of picoamps (Figure 3.6).

As far as was possible, cells in the moderately-fluorescent range were studied. Eight different mutations were studied during the course of this PhD. Wildtype control recordings were undertaken concurrently at the time of recording each mutant. Owing to the difficulty of recording in the absence of leak subtraction it was not possible to obtain a separate set of five high-quality wildtype recordings for each set of mutant recordings, so one high quality wildtype control recording from each session of mutant recordings was pooled with wildtype controls from all of the other sessions, and this pool was used as a group control for all the mutant recordings.

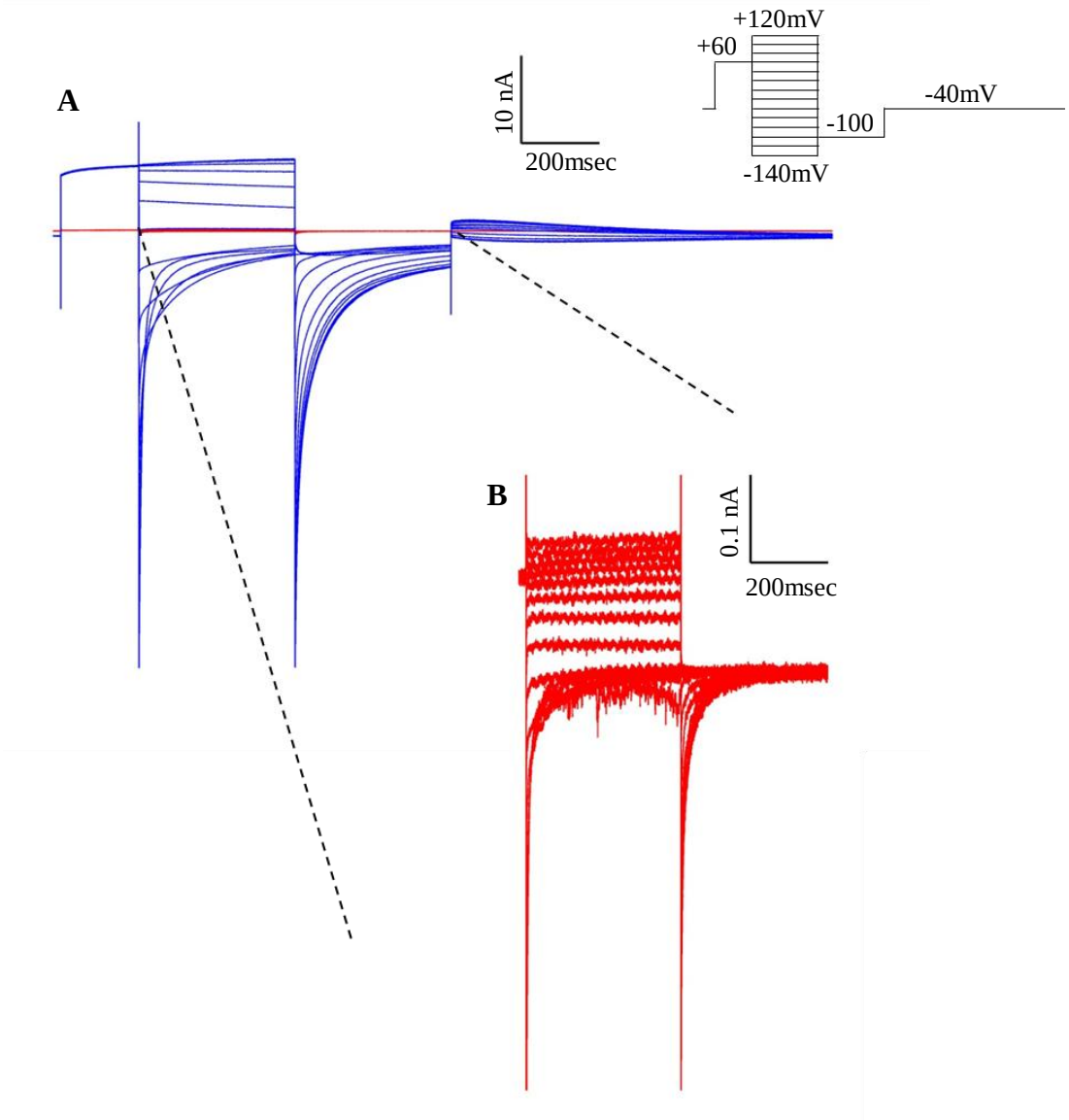

Figure 3.6 Range of current magnitude recorded from HEK293T cells expressing wildtype CLCN1.
(A) Currents from a brightly fluorescing cell (blue) and a dimly fluorescing cell (red) are superimposed.
(B) Currents of the dimly fluorescing cell magnified 100 fold relative to A. Scales as in inset.

Wildtype controls were clearly distinguishable from cells expressing no chloride channel (cells from the same transfection batch that failed to take up DNA as indicated by zero observable fluorescence). Cells from the same transfection batches that had not taken any

vector DNA (as indicated by lack of fluorescence) yielded only capacitative and leak currents (figure 3.7).

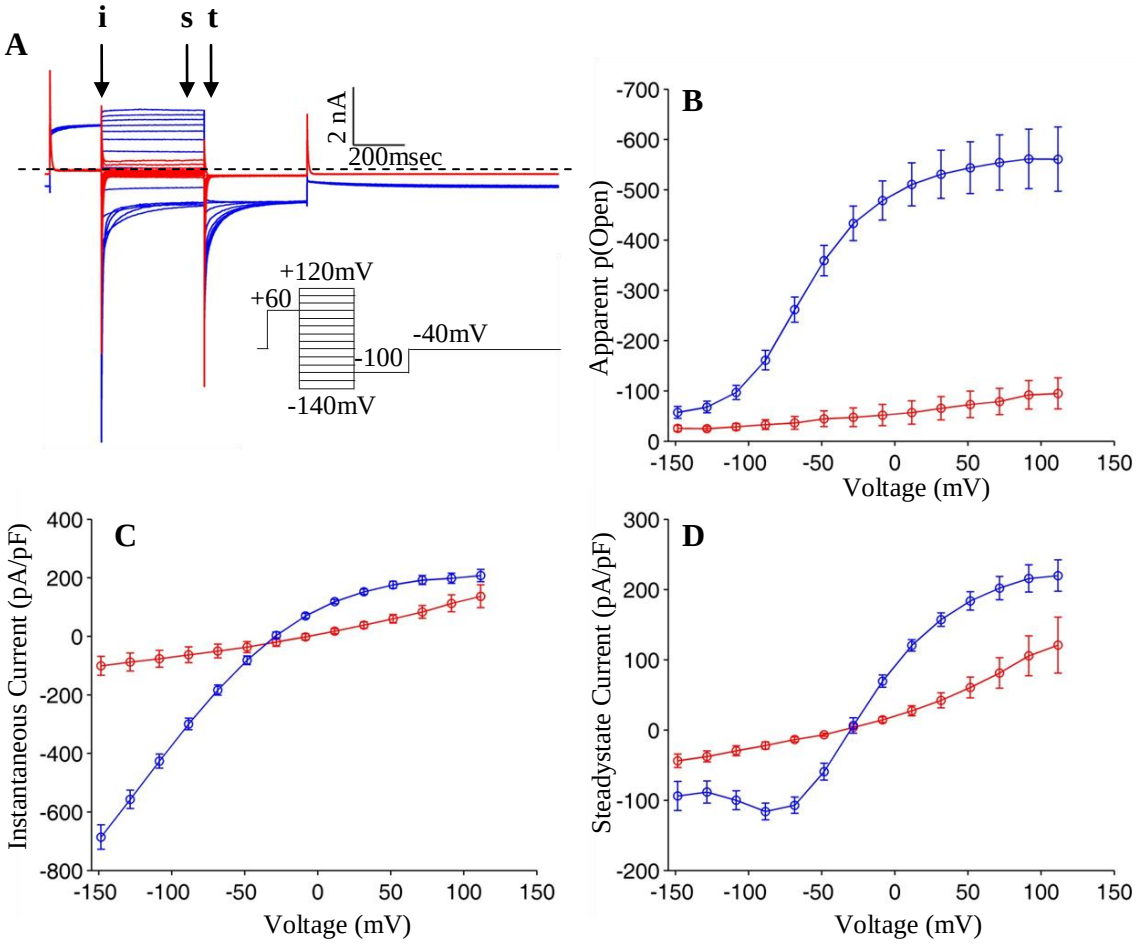

Figure 3.7 Comparison of moderately fluorescent HEK293T cells expressing wildtype ClC-1 against untransfected cells.

(A) Whole cell currents from two HEK293T cells are superimposed, one expressing ClC-1 (blue) the other not (red). For the purposes of illustration an untransfected recording that contains capacitative artifact is shown. Arrows indicate approximate times where instantaneous (i) steadystate (s) and tail currents (t) were measured. **(B)** Tail currents measured 5msec after stepping to -100 mV plotted against the prepulse voltage. The y-axis is inverted so that the blue sigmoid curve has the same orientation as an opening probability curve, but currents are presented without normalization here. Instantaneous **(C)** and steadystate **(B)** IV relationships during the variable voltage step. Voltages in **(B)**, **(C)** and **(D)** are corrected for junction potential of -8.5 mV. Wildtype ClC-1 n = 8. Untransfected cells n = 6. Error bars (S.E.M.) obscured by symbol in places.

The W118G variant

W118G was at first considered to be benign based on its occurrence in 2% (3/128) of control chromosomes sequenced by the clinical genetics laboratory of the National Hospital for Neurology & Neurosurgery. However, it is present in approximately 8% (55/688) of chromosomes from patients referred for genetic testing for Myotonia Congenita. If this over-abundance among Myotonia Congenita patients is genuine (not a chance effect of sampling), it could reflect a predisposition among patients with reduced chloride conductance myotonia who carry W118G in addition to their bona fide pathogenic genotype to a more severe phenotype. Such a predisposition would translate into a higher likelihood of presentation to a physician and subsequent referral for genetic testing (a selection bias).

There were 37 heterozygotes and 9 homozygotes for W118G recorded in the database of the clinical genetics laboratory. Eight of the 9 homozygous individuals harboured other CLCN1 variants (table 3.2). Two of the homozygotes for W118G (patient IDs 622 and 746) had incomplete genetic explanations for myotonia (unless W118G is pathogenic in its own right). In patient 746 there were no variants at all other than W118G. In patient 622 a known recessive CLCN1 variant (c.1872delG) was present together with a variant thought not to be pathogenic in its own right (c.1401+17T>C) on the basis of presence in controls and homozygosity in a patient in whom myotonia was ruled out by clinical and EMG examination. These two cases raise the possibility that W118G might in some cases act as a recessive allele. There are, however some doubts. Firstly, in patient 746, it is not absolutely certain that the symptoms are attributable to myotonia. The only clinical sign detected was a hint of percussion myotonia and when the author performed electromyography on this

patient there were one or two brief runs of spontaneous activity but no frank myotonic discharges. Such activity is open to clinical interpretation and while it could represent very mild myotonia, it is difficult to distinguish categorically from other types of EMG activity (for example, increased insertional activity or brief complex repetitive discharges). The patient did have a background of lumbar radiculopathy (‘sciatica’) that might lead to complex repetitive discharges. Patient 622 has typical Myotonia Congenita. In this case either the combination of identified CLCN1 variants (W118G homozygosity plus heterozygosity for a known recessive variant and a probable benign variant) is sufficient to produce myotonia or there is another explanation (for example a deletion/duplication on one CLCN1 allele that is not be picked up by Sanger sequencing, or an SCN4A mutation). The latter possibilities would need to be excluded before concluding that W118G is acting as a recessive allele. In the HEK293T assay W118G was indistinguishable from wildtype CLCN1 (Figure 3.8).

Table 3.2 Co-segregating variants in homozygotes for W118G

Patient	Co-segregating variants cDNA	protein	Details of co-segregating variants
Patient ID 746	*Unclear whether patient really has myotonia. If so it must be very mild (see text).*		
	No co-segregating variants		
Patient ID 622	*Typical Myotonia Congenita*		
	1872delG	E624fs	Novel ?recessive Associated with myotonia in 4 other families,
	1401+17T>C	?	Novel ?benign. Present in controls. Myotonia was excluded in one homozygote for this variant.
Patient ID 25	*Typical Myotonia Congenita*		
	1238T>G	F413C	Published recessive mutation
	1392C>T	F464=	Novel synonymous, same allele as F413C in this individual
	1930+6T>G	?	Novel ?recessive. Associated with myotonia in 1 other family
Patient ID 609	*Typical Myotonia Congenita*		
	1930+6T>G homozygote	?	Published recessive mutation
Patient ID 571	*Typical autosomal dominant Myotonia Congenita*		
	689G>A	G230E	Published dominant mutation
Patient ID 603	*Typical autosomal dominant Myotonia Congenita*		
	689G>A	G230E	Published dominant mutation
Patient ID 729	*Typical Myotonia Congenita*		
	1437_1450del homozygous	?	Published recessive mutation
Patient ID739	*Typical Myotonia Congenita*		
	1498G>A	E500K	Novel, ?recessive.
	Homozygous		Private variant not seen in any other patients.
Patient ID 186	*Typical Myotonia Congenita*		
	415delA	?	Novel, private variant not seen in any other patients
	434-2_434dupAGC	?	Novel ?recessive, associated with myotonia in 3 families.
	1401+17T>C	?	Novel ?benign. Present in controls. Myotonia was excluded in one homozygote for this variant. Also in patient ID 622 above.
	2244G>A	L748=	Published as benign

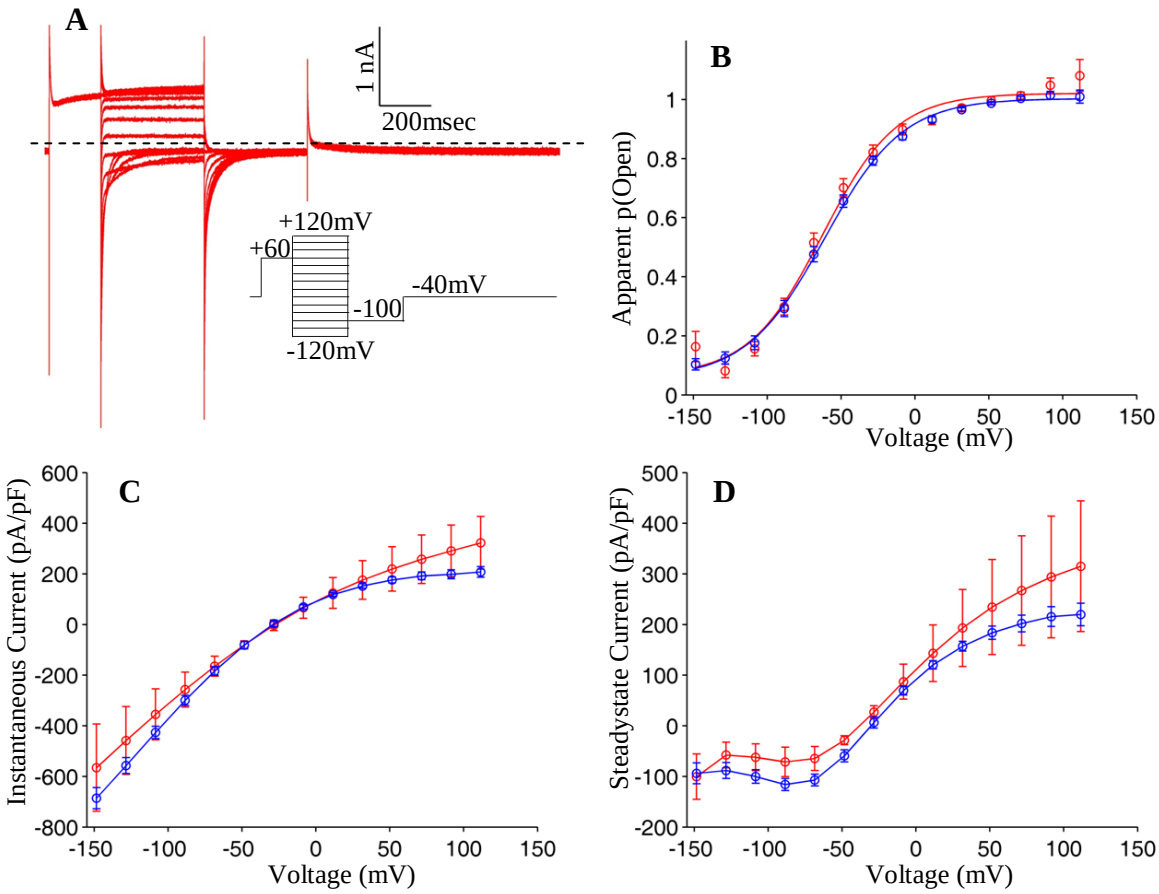

Figure 3.8 Comparison of W118G and wildtype CLCN1.
Representative currents from a HEK293T cell expressing the W118G CLCN1 mutant are shown in **(A)**. Apparent open probabilities **(B)**, instantaneous IV relationship **(C)** and steadystate IV relationship **(D)** of the mutant (red) were not significantly different from wildtype (blue). Means ± S.E.M. are shown for voltages between -140 and +120mV. Wildtype n = 8. W118G n = 5. Error bars obscured by symbol in places.

The G276D variant

The G276D variant was first discovered in a compound heterozygote and so appeared to be acting recessively (Fialho, Schorge et al. 2007). However it was subsequently identified in two dominant pedigrees, consisting of an affected parent and an affected child each with single mutations. Symptom onset for one of the probands was during pregnancy.

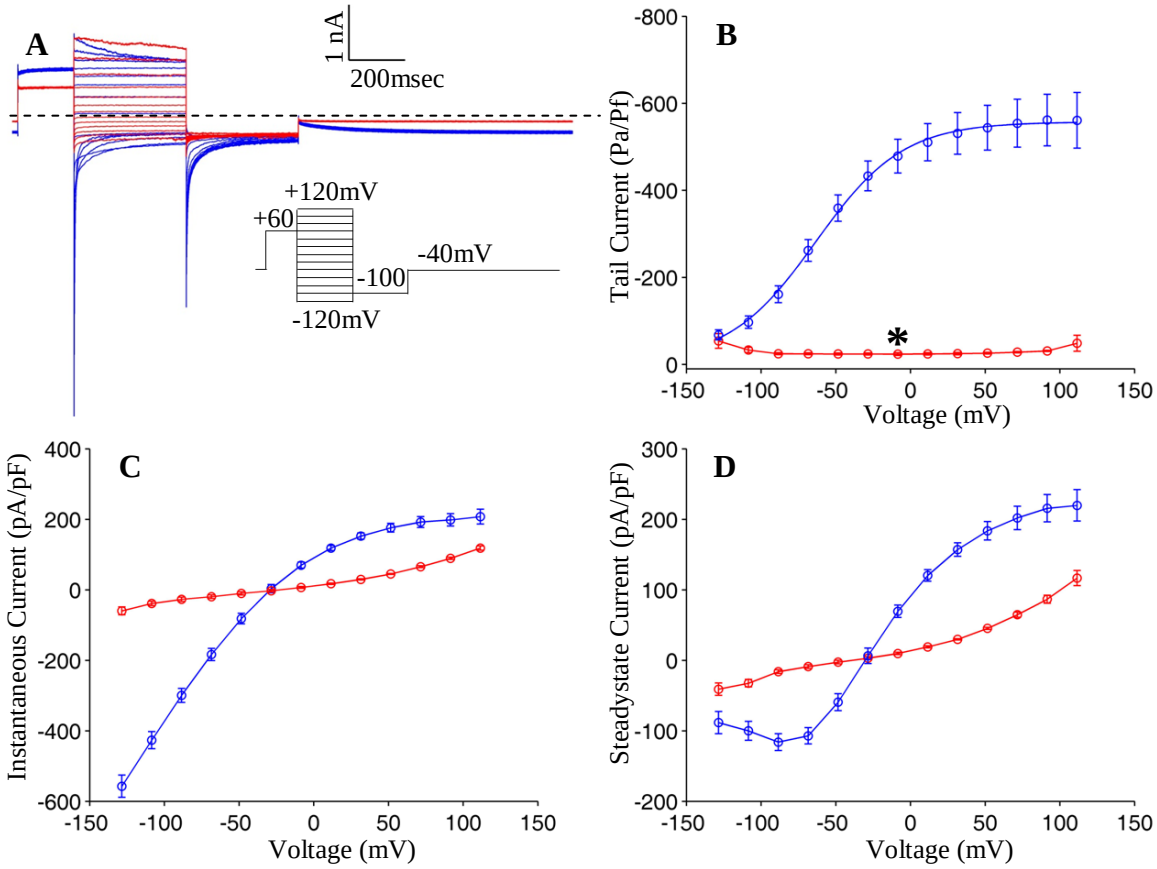

Figure 3.9 Comparison of G276D and wildtype CLCN1.
Representative currents from one HEK293T cell expressing wildtype CLCN1 (blue) and one expressing the G276D mutation (superimposed in red) are shown in **(A)**. Tail currents are presented **(B)** instead of the apparent opening probability because the mutant displayed no voltage-dependence, yielding approximately linear instantaneous **(C)** and steadystate **(D)** IV relationships indistinguishable from background leak artefact. Means ± S.E.M are shown for voltages between -120 and +120 mV (responses to the -140 mV step in this series of recordings was distorted by artefact in all but 1 of the 5 mutant recordings, not shown). Wildtype n = 8. G276D n = 5. Error bars obscured by symbol in places. Star in **(B)** indicates significant difference between WT and G276D ($p<0.01$, one way ANOVA on WT, G276D and G523D followed by post-hoc pair-wise analysis).

The individuals with G276D have typical Myotonia Congenita including the warm-up phenomenon. HEK293T cells expressing the G276D ClC-1 mutant yielded no voltage dependent chloride currents (Figure 3.9). Currents in these cells were indistinguishable from leak currents. Thus in the homozygous state the mutation appears to cause total loss of function of the ClC-1 channel.

The S289G variant

S289G was identified in the homozygous state in a single individual from a recessive pedigree with consanguineous parents of Punjabi origin. MLPA has not been performed, but the parents each carry one copy of the variant and one wildtype allele, which is against the presence of a large deletion on one allele giving the appearance of homozygosity in the proband. It is not known whether the parents are affected by myotonia; they are said to be asymptomatic but have not been formally tested by EMG. The description provided by the referring clinician of the proband's phenotype is typical of Becker type Myotonia Congenita with an early onset (age 1) and relatively severe myotonia.

HEK293T cells expressing the S289G ClC-1 mutant conducted chloride currents only at the most depolarized potentials. The apparent opening probability curve of S289G homodimeric channels is shifted very far to the right in comparison with wildtype. It was not possible to empirically measure the voltage at which S289G is fully open since HEK293T cells did not tolerate such strong depolarizations. However by fitting the available data with a Boltzmann function the mean V50 for 5 cells was estimated at 102 mV as compared with -62 mV for the wildtype V50 (Figure 3.16 and Table 3.3). S289G channels also exhibit slower activation kinetics that wildtype channels, as evident from the

failure of currents to reach steadystate during the depolarizing pulses of the variable voltage step.

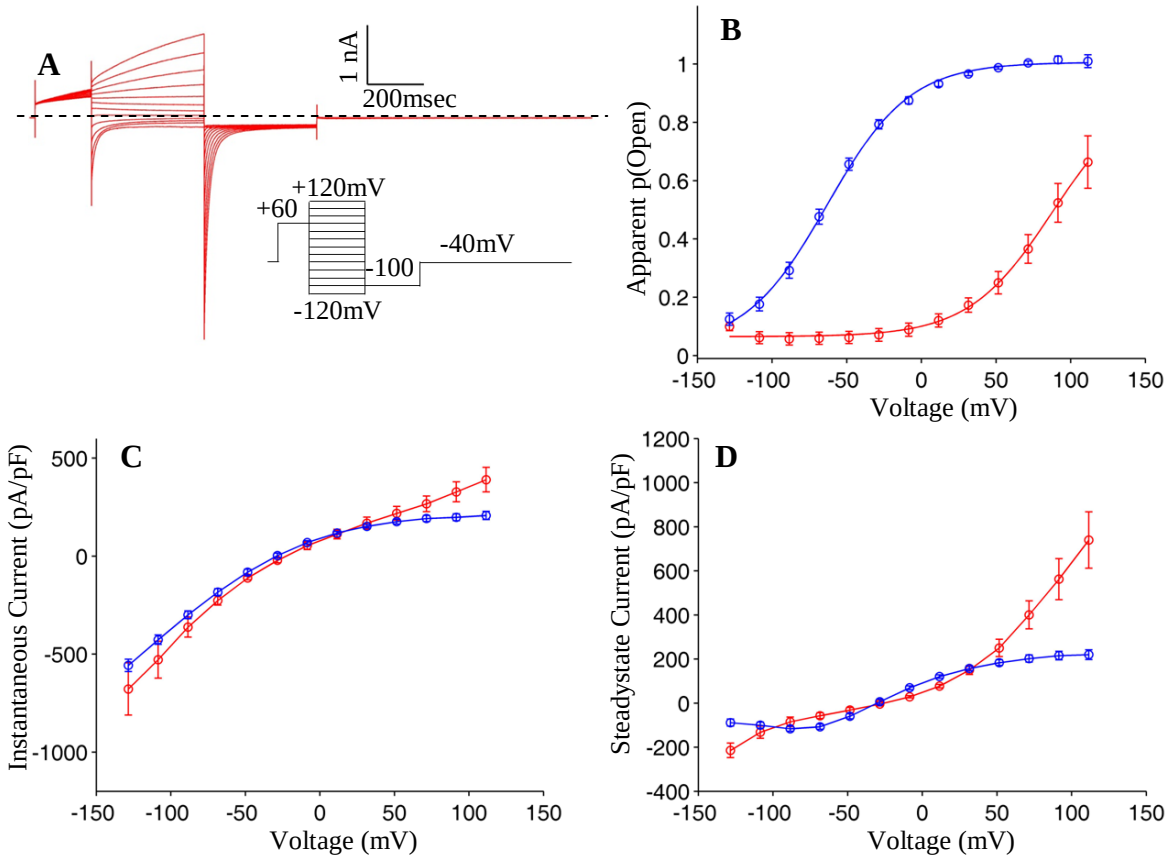

Figure 3.10 Comparison of S289G and wildtype CLCN1.
(A) Representative currents from one HEK293T cell expressing the S289G mutation. **(B)** Apparent open probabilities of wildtype (blue) and S298G (red) derived from tail currents. The V50 for S289G was +102.4 ± 18.2 mV, as compared with -62.0 ± 2.4 mV. **(C)** Instantaneous IV relationship. **(D)** Pseudo-steadystate IV relationship (steadystate was not reached for the most depolarizing pulses). Means ± S.E.M are shown for voltages between -120 and +120 mV. Wildtype n = 8. S289G n = 5. Error bars obscured by symbol in places.

The H369P variant

H369P was identified in a single individual in compound heterozygosity with c.1872delG p.E624fs. The two variants are likely to be on different chromosomes because the patient's unaffected children only carry H369P. At the time of writing MLPA has not been performed to check for a large indel *in cis* with H369P. There was no significant difference between the voltage dependence of H369P and wildtype ClC-1. However, the fast time constant of current deactivation for H369P was slower than for wildtype (see Table 3.4).

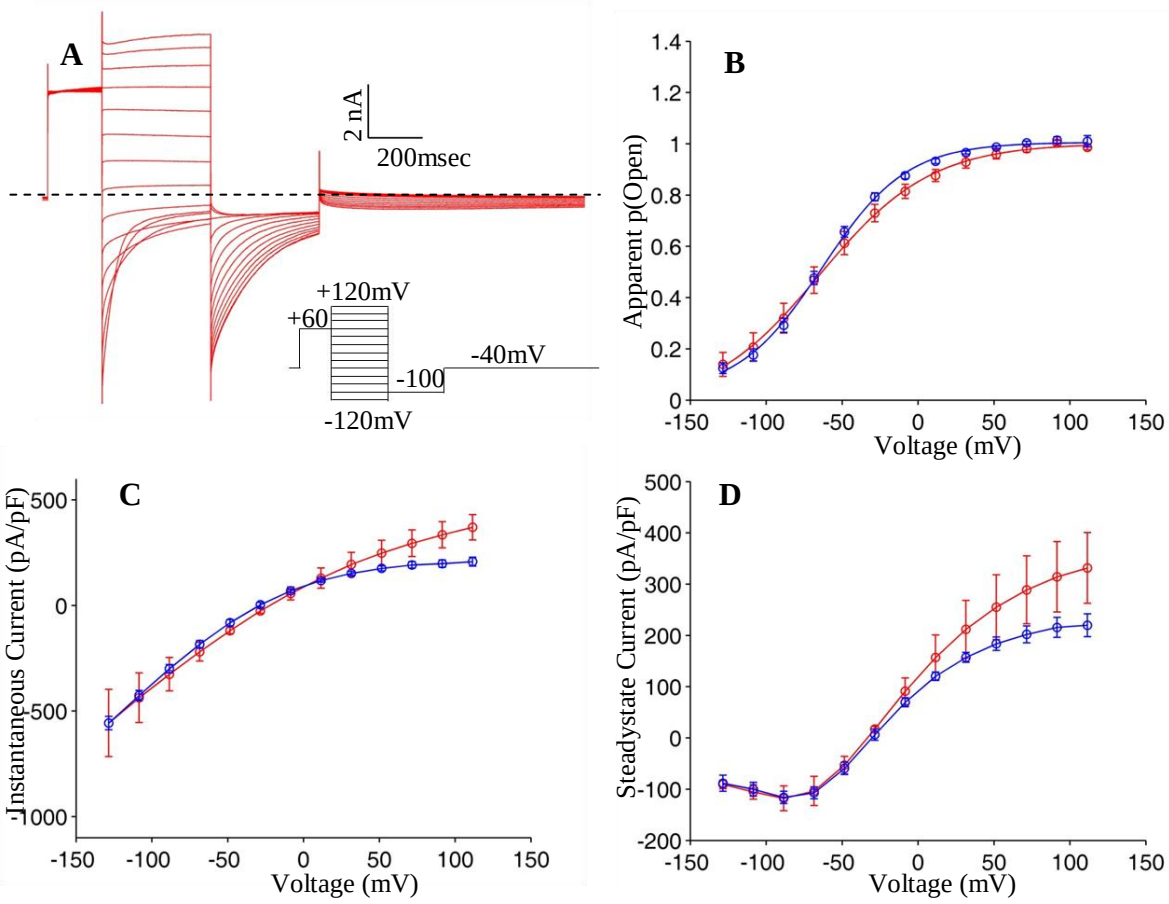

Figure 3.11 Comparison of H369P and wildtype CLCN1.
(A) Representative currents from one HEK293T cell expressing the H369P mutation. **(B)** Apparent open probabilities of wildtype (blue) and S298G (red) derived from tail currents. **(C)** Instantaneous IV relationship. **(D)** Steadystate IV relationship (steadystate was not reached for the most depolarizing pulses). Means ± S.E.M are shown for voltages between -120 and +120 mV. Wildtype n = 8. H369P n = 5. Error bars obscured by symbol in places.

The G523D variant

G523D was identified in heterozygosity with a normal allele in a single individual with no family history. Symptom onset was around age 7, with stiffness, difficulty letting go of objects, and exacerbation by cold temperatures.

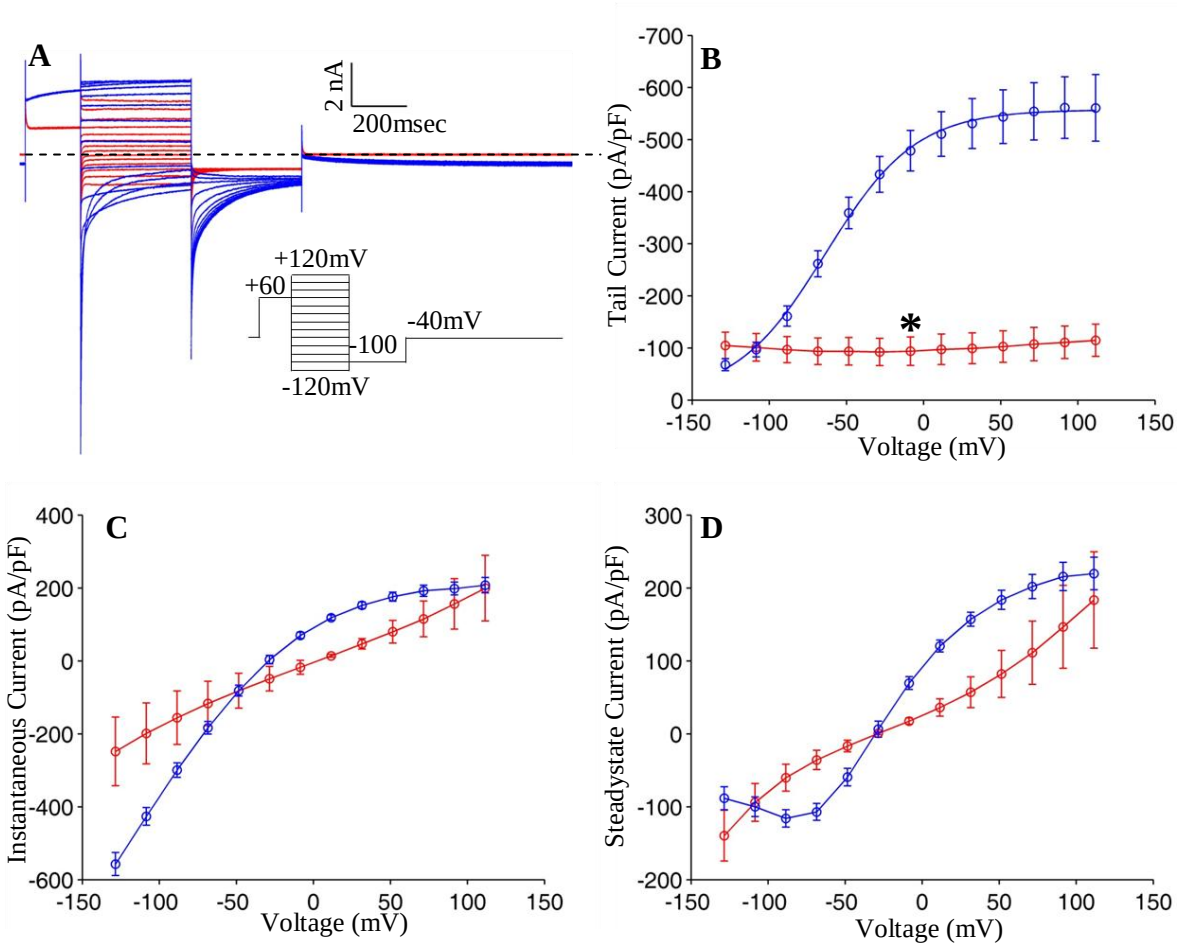

Figure 3.12 Comparison of G523D and wildtype CLCN1.
Representative currents from one HEK293T cell expressing wildtype CLCN1 (blue) and one expressing the G523D mutation (superimposed in red) are shown in **(A)**. Tail currents are presented **(B)** instead of the apparent opening probability because the mutant displayed no voltage-dependence, yielding approximately linear instantaneous **(C)** and steadystate **(D)** IV relationships indistinguishable from background leak artefact. Means ± S.E.M. are shown for voltages between -120 and +120 mV (responses to the -140 mV step in this series of recordings was distorted by artefact in all but 1 of the 5 mutant recordings, not shown). Wildtype n = 8. G523D n = 5. Error bars obscured by symbol in places. Star in **(B)** indicates significant difference between WT and G523D ($p<0.01$, one way ANOVA on WT, G276D and G523D followed by post-hoc pair-wise analysis).

G523D was described in the Korean population a year after the start of this PhD thesis, where it was identified in heterozygosity with a normal allele in a single individual with no family history of myotonia (Moon, Kim et al. 2009). HEK293T cells expressing homodimeric G523D ClC-1 channels (Figure 3.12) yielded no voltage dependent chloride currents; the mutation appears to cause total loss of function.

The A566T variant

A566T has been published by our group before (Fialho, Schorge et al. 2007), but its function has not previously been studied. So far the clinical genetics lab has seen this variant in samples from 4 autosomal recessive pedigrees, 3 of which are consanguineous. The probands are apparent homozygotes for the variant, but parental DNA was only available for one and MLPA has not been performed in any to rule out the presence of a large *in cis* indel. One of these families (where parental DNA was available) also suffers from type 2 myotonic dystrophy, but family members who are homozygous for A566T and do not also have myotonic dystrophy still have severe myotonia In this family the mother carries a single copy of the variant, while the father is an apparent homozygote, therefore there is a possibility of a large deletion in the father and the proband. In the HEK293T assay the A566T variant behaved as wildtype.

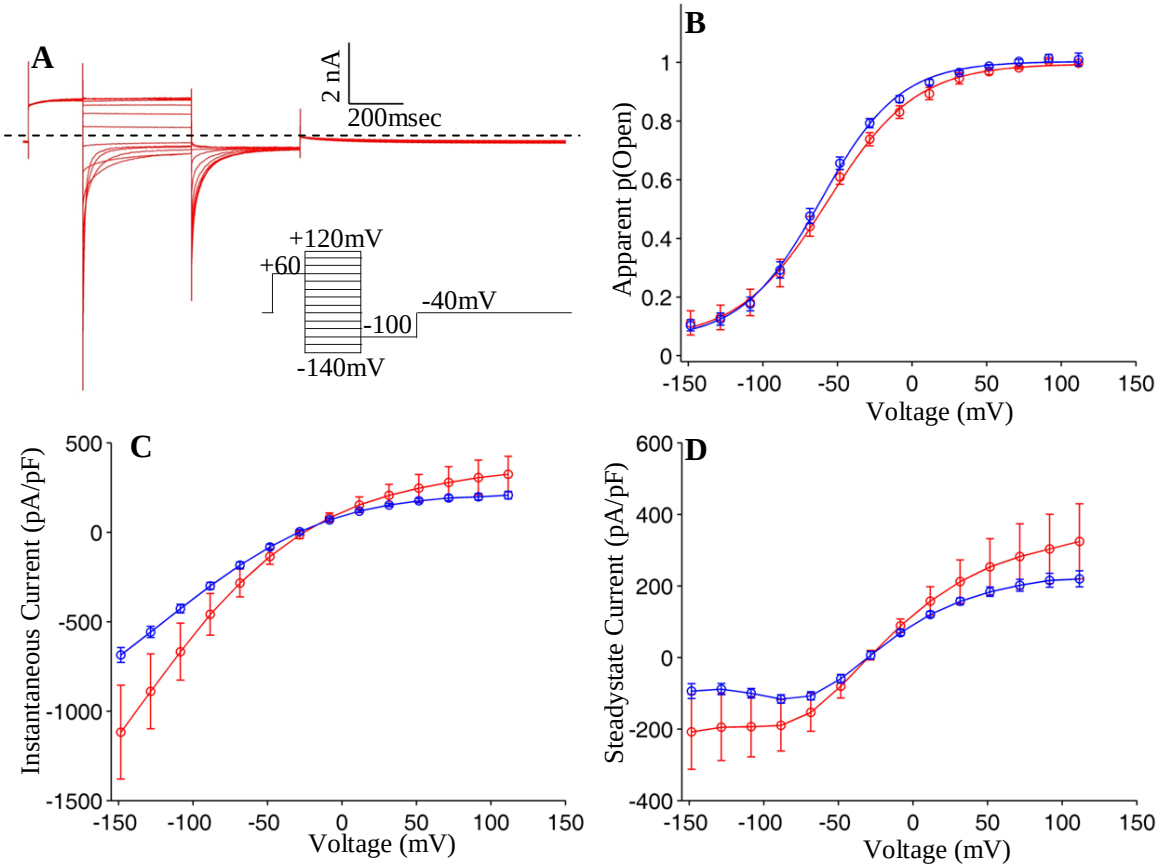

Figure 3.13 Comparison of A566T and wildtype CLCN1.
Representative currents from a HEK293T cell expressing the A566T CLCN1 mutant are shown in **(A)**. Apparent open probabilities **(B)**, instantaneous IV relationship **(C)** and steadystate IV relationship **(D)** of the mutant (red) were not significantly different from wildtype (blue). Means ± S.E.M. are shown for voltages between -140 and +120mV. Wildtype n = 8. A566T n = 5. Error bars obscured by symbol in places.

The M646T variant

M646T was identified in two pedigrees. The first consists of two siblings, both homozygous for the variant. Their symptoms were relatively early onset and severe, and the parents are asymptomatic, consistent with recessive Myotonia Congenita. The presence of a large indel *in cis* with the variant has not been excluded by MLPA in this family. In the second pedigree the variant appears to be acting dominantly. The proband noticed symptoms in adulthood. The phenotype is relatively mild and there was no clinically detectable myotonia, but EMG disclosed characteristic myotonic discharges. The patient's adult children were not affected but one parent may have been symptomatic. It should, however, be noted that neither family has been tested for mutations in SCN4A. The M646T mutation could not be distinguished from wildtype ClC-1 in the HEK293T cell assay.

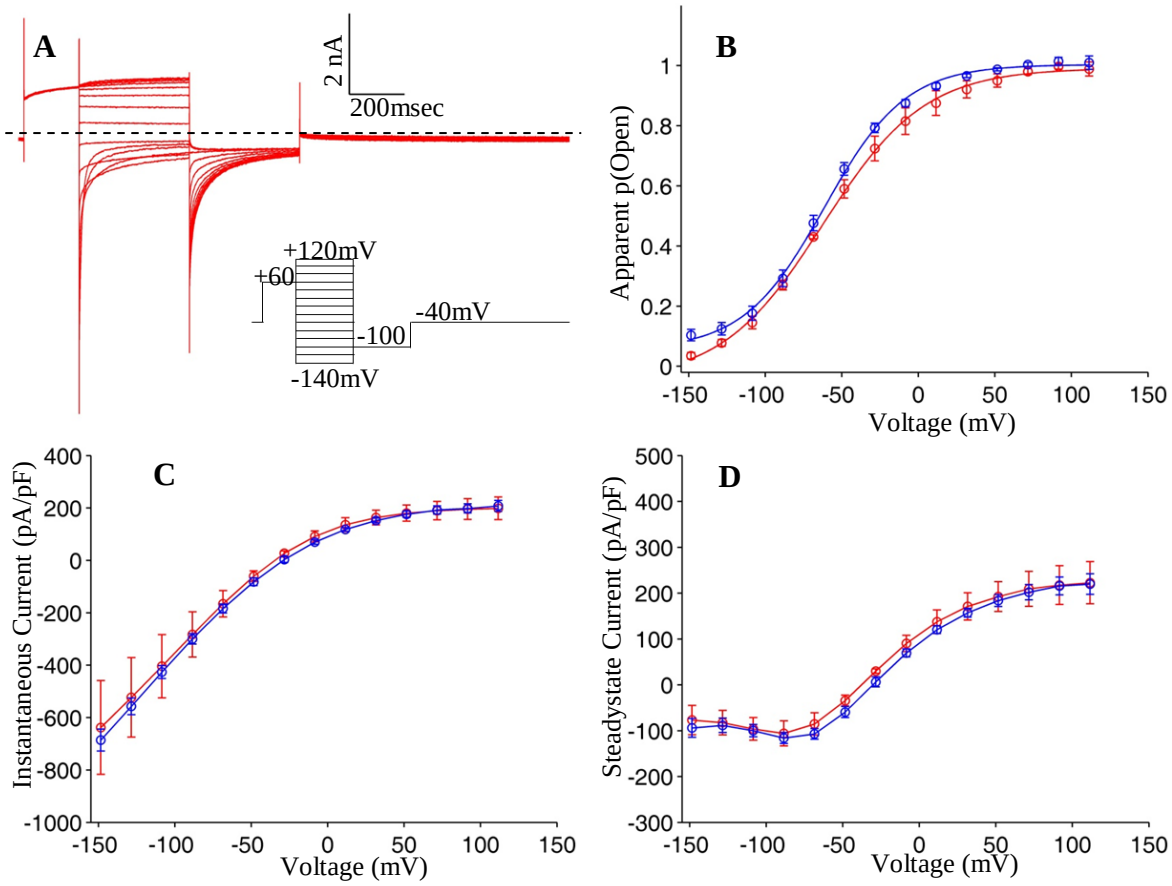

Figure 3.14 Comparison of M646T and wildtype CLCN1.
Representative currents from a HEK293T cell expressing the M646T CLCN1 mutant are shown in **(A)**. Apparent open probabilities **(B)**, instantaneous IV relationship **(C)** and steadystate IV relationship **(D)** of the mutant (red) were not significantly different from wildtype (blue). Means ± S.E.M. are shown for voltages between -140 and +120mV. Wildtype n = 8. M646T n = 3. Error bars obscured by symbol in places.

The P744T variant

P744T was identified in apparent homozygosity in two families not known to be related to each other but from the same ethnic group. Patient 578 is a member of a large consanguineous family of Iraqi Kurds (parents 2nd cousins, paternal grandparents 1st cousins). One parent and three siblings are similarly affected. Patient 619 is similarly affected with typical Myotonia Congenita, and two out of six siblings are affected. However, the P744T variant was not significantly different from wildtype in the HEK293T assay, and the patients were subsequently found by the genetics laboratory to harbour homozygous duplications in CLCN1 involving exons 8-14.

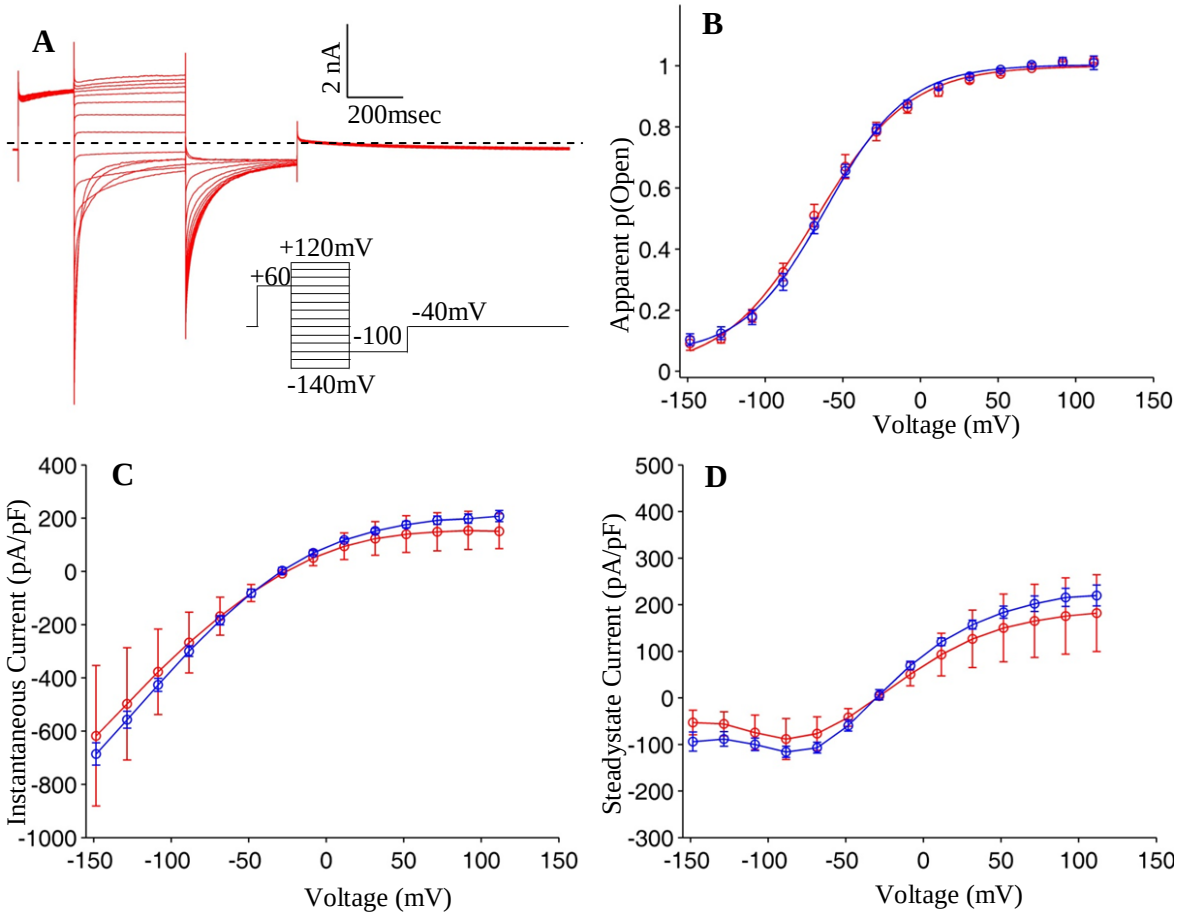

Figure 3.15 Comparison of P744T and wildtype CLCN1.
Representative currents from a HEK293T cell expressing the P744T CLCN1 mutant are shown in **(A)**. Apparent open probabilities **(B)**, instantaneous IV relationship **(C)** and steadystate IV relationship **(D)** of the mutant (red) were not significantly different from wildtype (blue). Means ± S.E.M. are shown for voltages between -140 and +120mV. Wildtype n = 8. P744T n = 5. Error bars obscured by symbol in places.

3.7 Summary of results

The functional consequences of the eight variants, studied as homodimers by voltage clamp of HEK293T cells, are compared below in Figure 3.16, Table 3.3 and Table 3.4.

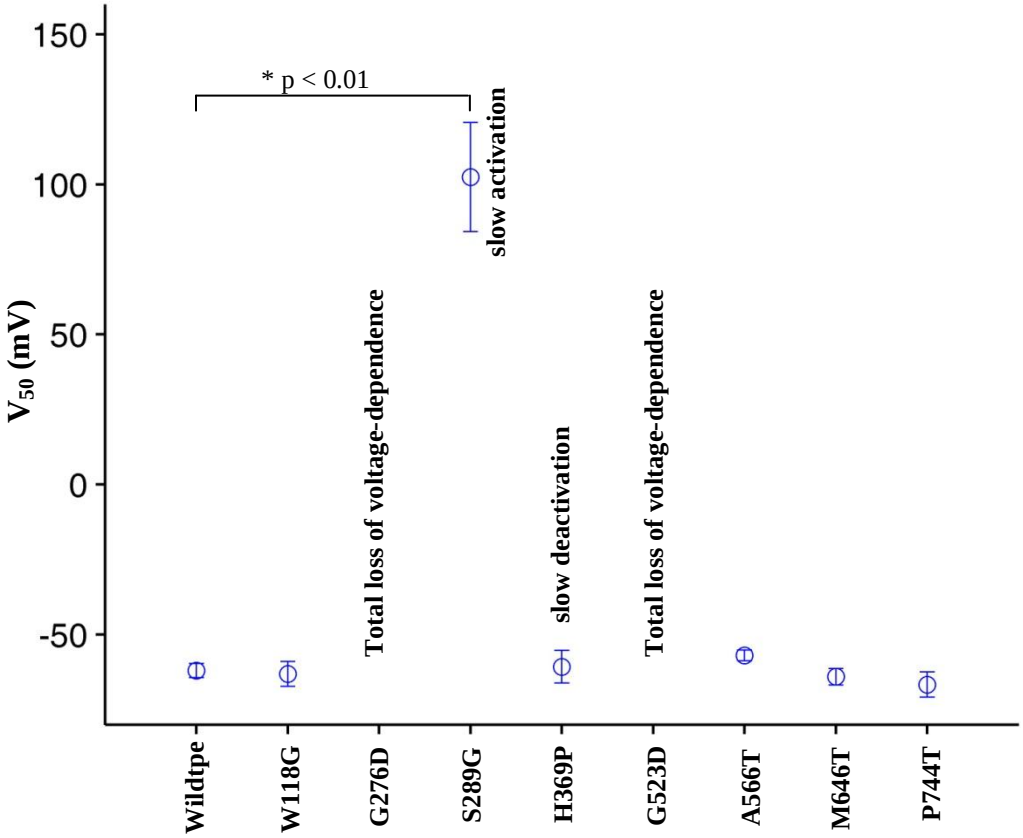

Figure 3.16 Comparison of CLCN1 sequence variants studied.
Mean ± S.E.M. of the voltage of half maximal activation for wildtype and each of the variants (n = 8 for wildtype, n = 3 for M646T, n = 5 for all others). G276D and G523D showed total loss of function (no voltage dependence). S289G showed a significant ($p < 0.01$) depolarizing shift in voltage dependence and slowed channel activation. H369P showed normal voltage dependence but slow deactivation. See also Table 3.3 and Table 3.4. Statistical analysis by one way ANOVA with post-hoc pairwise comparison.

Table 3.3 ClC-1 Boltzmann parameters (mean ± S.E.M.)

	n	V_{50} (mV)	Slope (mV)
WT	8	-62.0 ± 2.4	26.3 ± 1.7
W118G	5	-63.1 ± 4.2	22.9 ± 1.1
G276D	5	No voltage dependence	
S289G	5	**102.4 ±18.2***	34.1 ± 6.7
H369P	5	-60.7 ± 5.4	34.5 ± 3.1
G523D	5	No voltage dependence	
A566T	5	-57.0 ± 1.8	30.7 ± 2.9
M646T	3	-64.1 ± 2.7	30.7 ± 7.0
P744T	5	-66.7 ± 4.2	29.2 ± 1.7

Table 3.4 Time constants of macroscopic current activation and deactivation (mean ± S.E.M.)

		Activation		Deactivation	
	n	τ_{slow} (msec)	n	τ_{fast} (msec)	τ_{slow} (msec)
WT	8	127.6 ± 10.4	4	7.3 ± 1.0	82.1 ± 8.3
W118G	5	141.7 ± 5.9	5	3.6 ± 0.8	70.7 ± 10.5
G276D	-	No voltage dependence	-	No voltage dependence	
S289G	5	**402.4 ± 27.2***	5	6.8 ± 1.2	37.6 ± 6.9
H369P	3	140.2 ± 5.4	5	**14.1 ± 2.1***	98.0 ± 11.2
G523D	-	No voltage dependence	-	No voltage dependence	
A566T	4	118.3 ± 24.7	5	5.4 ± 0.6	58.0 ± 14.1
M646T	3	139.1 ± 10.3	3	10.1 ± 2.0	100.4 ± 5.4
P744T	5	180.4 ± 13.1	5	7.6 ± 1.1	104.8 ± 8.0

For activation the fast time constant is omitted because the fast component of current activation was obscured by capacitative transients in most recordings.

In both tables, **bold*** indicates $p < 0.01$ in post-hoc pairwise comparison against WT after one way ANOVA on WT and all variants.

The results suggest that G276D, G523D and S289G are pathogenic. G276D and G523D both appear to cause complete loss of function when expressed in the homozygous state in HEK293T cells; no voltage-dependent chloride current was detectable for either variant. The patients are heterozygotes with one wildtype and one variant allele. While for both of these variants the residual voltage-independent chloride currents were slightly larger than observed for healthy, un-transfected HEK293T cells, it is difficult to distinguish this leak from artefact caused by an imperfect seal or an unhealthy cell membrane (as sometimes results from transfection). With hindsight, a comparison against cells transfected with empty vector might have helped to resolve this question, but there is little doubt from the results that these variants drastically reduce chloride conductance at physiological potentials compared to wildtype. S289G produced a marked alteration of kinetics along with a depolarizing shift in voltage-dependence. The patient is homozygous and the parents are known to each carry one copy of the variant. H369P produced a small alteration in kinetics of deactivation, which is of dubious physiological significance. The remaining variants were indistinguishable from wildtype. In the patients with P744T, an alternative explanation for myotonia (a large homozygous duplication in CLCN1) emerged from research using MLPA. The possibility that the other variants that tested normal in HEK293T cells are *in cis* with large indel mutations has not been excluded. However, normality of function in HEK293T cells may reflect shortcomings of the assay. Therefore, although the pathogenicity of variants testing normal in the HEK293T cell assay remains in question, they cannot be classified with certainty as benign. These ideas will be expanded in Chapter 6 (the discussion).

Chapter 4 Modulation of CLCN1 by sex hormones

4.1 Chapter summary

The actions of progesterone and oestrogen on endogenous chloride currents through the wildtype ClC-1 of mouse skeletal muscle were investigated by whole cell patch clamp. Progesterone and oestrogen rapidly reduced the chloride conductance and shifted its voltage dependence. It is concluded that a rapid, non-genomic mechanism exists in skeletal muscle that would enable these hormones to modulate the excitability, and to exacerbate myotonia during pregnancy. Further work will be required to clarify the physiological role and the components of this signaling pathway.

4.2 Aims

The major aim of this chapter was to characterise the effect of progesterone and oestrogen on ClC-1 in its native cellular environment, skeletal muscle. A secondary aim was to establish the techniques for whole cell patch clamp of dissociated skeletal muscle fibres in the laboratory of the MRC Centre for Neuromuscular Diseases.

4.3 Motivation

Phenotypic variability arises not only from differences in genotype between patients, but probably also from differences in both the cellular milieu and the wider external environment. Myotonia Congenita is often exacerbated during pregnancy, and progesterone is known to shift the voltage-dependence of human ClC-1 expressed in *Xenopus* oocytes through a rapid, and therefore non-genomic, pathway. These observations led to the suggestion that sex hormones play a role in the regulation of skeletal muscle excitability

and could be responsible for the exacerbation of myotonia during pregnancy, and the more severe phenotype that is often observed in males as compared to females. However, the hypothesis has not been tested in skeletal muscle before.

4.4 Whole cell patch clamp of isolated skeletal muscle fibres

Muscle tissue was obtained from animals that were being sacrificed for brain tissue by colleagues working in the department of experimental epilepsy. Given this readily available source of FDB muscle fibres, in accordance with the principles of 'reduce, replace, and refine' in animal research, the author preferred to share animals rather than to purchase additional animals for his own use. However, it should be noted that some of the mice included in this PhD were genetically modified with a point mutation in the voltage gated potassium channel, Kv1.1 (a mouse model of Episodic Ataxia type 1). Although Kv1.1 is expressed in skeletal muscle, the presence of the mutation in some but not other cells could not directly contribute to cell to cell differences in current magnitude because potassium currents were blocked (by cesium and TEA) to enable recordings of pure chloride currents. While the possibility of an indirect effect was considered, for example an alteration on the responsiveness to hormones or the abundance of chloride channels in the membrane, no consistent differences beyond were observed between wildtype and Kv1.1 mutant mice with respect to chloride currents or their response to progesterone or oestrogen.

Stable whole-cell recordings from FDB muscle fibres required low series resistance, minimal contraction of the muscle fibres, firm adherence of the muscle fibres to a surface and minimal floating debris in the bath. Establishment of the technique was greatly facilitated by email correspondence with Dr. John Lueck (post-doctoral fellow at The University of Iowa Carver College of Medicine, Iowa City, USA). The program of muscle

fibre experiments was initiated in October 2010 and the first acceptable recording in the presence and absence of hormone was achieved 5 months later in March 2011.

Cell adherence

The initial technique adopted was based on that used for HEK cells. After incubation in collagenase the muscle was triturated in Ringer and the resulting suspension of single fibres was divided among glass coverslips coated with either PDL or collagen. Each coverslip was lifted with forceps and transferred to a 35mm dish containing extracellular solution, and then to the stage of the microscope of the patch clamp rig. This unfortunately resulted in loss of virtually all the fibres, which were not sufficiently adherent to the coverslip to withstand lifting with forceps and movement through two air-liquid interfaces even if they were allowed 24 hours to attach. Muscle fibres adhered more tightly to Nunclon-coated 35mm tissue culture dishes so the final technique was to triturate the muscle briefly in a series of 35mm dishes and patching the muscle directly in these dishes after carefully exchanging the Ringer for recording solution. It was necessary to trim the walls of the dishes to about half their original height with scissors to allow the microelectrode access to the whole dish without abutting the rim.

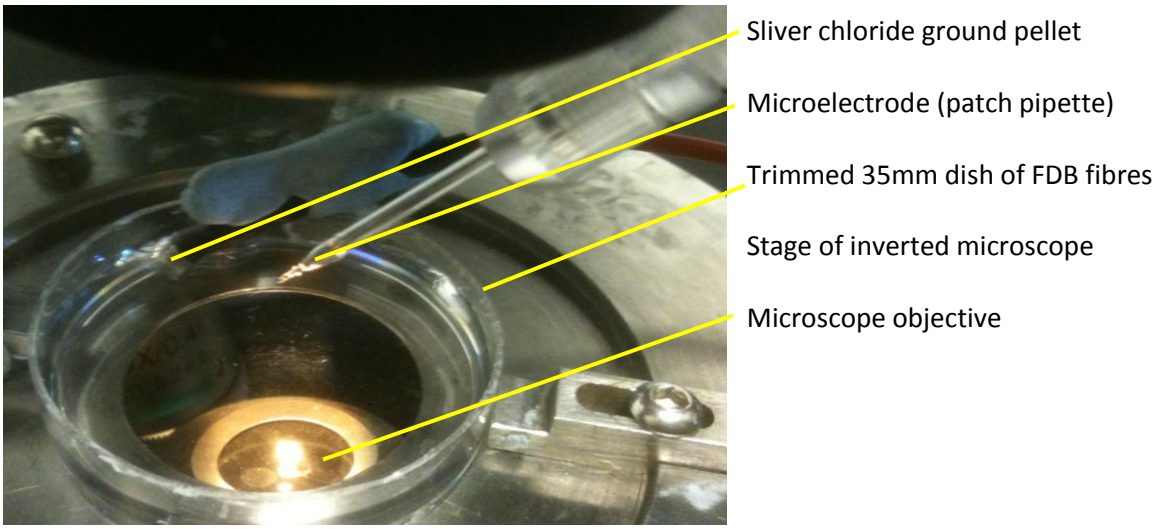

Figure 4.1 Trimmed 35mm tissue culture dish of muscle fibres ready for patch clamp.
The dish is sitting on the stage of an inverted microscope. It contains muscle fibres, adhering to its floor, and external recording solution. The ground electrode is held in place with blue-tack. A glass microelectrode is ready to descend into the dish to record from a cell. The light source above the dish can be seen as a reflection in the objective lens below.

Enzymatic digestion and trituration

The initial concentration of collagenase employed was 2mg/ml and incubation was for 2 hours, but this tended to result in damaged fibres that were difficult to patch. For juvenile animals (post-natal day 20) incubation in 1mg/ml for 40 minutes was sufficient to allow dissociation of muscle fibres by trituration. For older animals 1mg/ml for 1.5 hours was necessary.

Muscle contraction

Healthy FDB muscle fibres with clear striations were contractile; it was helpful to inhibit contraction as far as possible in order to achieve stable recordings. During preliminary experiments positive pressure was maintained on the micropipette as it approached the muscle fibre, but the efflux of intracellular solution in the vicinity of a fibre often stimulated contraction, presumably by depolarizing the membrane and initiating action

potentials. Positive pressure was therefore only applied as the electrode entered the bath (in order to discourage debris floating on the surface from sticking to the electrode tip) and was turned off again to approach the targeted muscle fibre. Voltage clamp of a muscle fibre to depolarized potentials also stimulated contraction. Sometimes recordings could be achieved in spite of contraction and relaxation of the fibre, but often the seal between electrode and the membrane was disrupted. A number of techniques have been employed by other groups to prevent contraction including osmotic shock to detubulate the fibres, stretching of intact muscle to reduce actin-myosin filament overlap, and drugs that block calcium release from sarcoplasmic reticulum (Macdonald, Pedersen et al. 2005) . BTS was selected because it inhibits actin-myosin interaction without significantly affecting membrane excitability or calcium signalling (Macdonald, Pedersen et al. 2005), which may be important in the pathway linking hormonal stimulation to altered chloride conductance. The internal environment was already markedly disturbed by the pipette solution and further disturbance by disconnecting t-tubules (by osmotic shock) or inhibiting calcium release (with dantrolene) was undesirable. Although BTS reduces the force of an isometric contraction (e.g. when a myofibre is firmly attached to the tissue culture dish), it does not suppress unloaded contraction (Cheung, Dantzig et al. 2002). Myofibres that were not firmly adherent to the tissue culture dish were still able to contract. This significantly reduced the yield of experiments.

Achieving a seal and going whole cell

Microelectrodes were fire-polished on the day of the experiment to improve the success rate of achieving seals and stored in a dust-free box during the experiment. The dish of muscle fibres was rotated to orientate the targeted fibre with its long axis in a north-south

direction so that the microelectrode would approach from the side. This seemed to be the best orientation for achieving seals. After zeroing the current offset with the electrode close to the cell, positive pressure was applied as the electrode was lowered onto the side of the cell and then gentle negative pressure was applied to encourage seal formation. Seals were sometimes established within seconds, but often took several minutes and required turning the suction off and on again and/or gently pressing the electrode more firmly against the cell. To enter the whole cell configuration the suction was carefully and only moderately increased. A brief, strong pulse of suction, as was used for HEK293T cells, was not effective for breaking into FDB muscle fibres. With sustained hard suction it was possible to go whole cell within seconds, but the seals were usually disrupted. The most successful method was to apply moderate suction and to wait. With this approach the whole cell configuration was usually entered after a minute or two, often with a rather high series resistance at first that would subsequently fall over the course of the next 10 minutes while the pipette solution was allowed to dialyze the cell. Early whole cell recordings were plagued by series resistance errors and by the cell re-sealing after establishment of the whole cell configuration. It was necessary to maintain suction for the duration of the recording to prevent re-sealing.

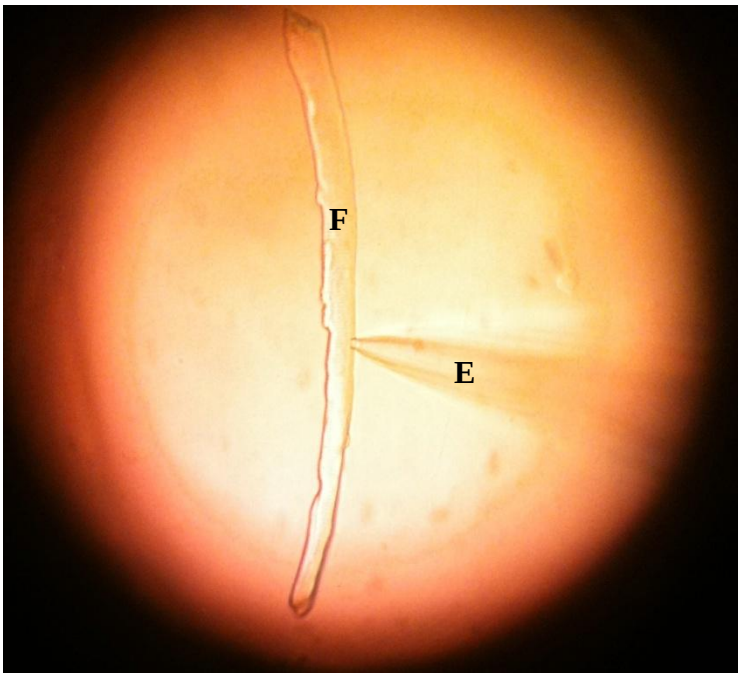

Figure 4.2 Glass microelectrode (E) sealed on to a mouse FDB muscle fibre (F).
Magnification approx. 400x. FDB muscle fibres are relatively short. The whole fibre can be seen within the field of view in this image. Striations were visible down the microscope but are not faithfully captured by the camera.

Capacitance cancellation and series resistance compensation

Experiments were performed using thin glass microelectrodes to produce low series resistance (1 – 3MΩ). In addition, 90% series resistance compensation was applied. The Axopatch 200b was able to partially cancel capacitative transients of the muscle cells. Residual capacitative artifact was tackled by measuring tail currents after the end of the capacitative current. Current were compared in the same cells before and after application of hormone using absolute current magnitudes rather than current density.

Stability of recordings

As recordings from FDB fibres are frequently unstable, several measures were taken to monitor the stability of each recording. The acceptability of each recording with respect to

its stability was assessed during recording, and then again during analysis by comparing currents elicited near the beginning and near the end of each run through the voltage protocol. Over time the current magnitude recorded from a cell tended to decrease. To distinguish normal rundown of currents from the effect of hormone, washout was measured wherever possible.

4.5 Range of current magnitude in mouse FDB muscle fibres

Consistent with their range of sizes, and the difficulty of space clamp, FDB muscle fibres yielded current magnitudes that varied over a wide range. Because of the large size of the cells it was not possible to accurately measure the capacitance, and so current densities could not be compared. Very large currents (e.g. >50 nA) introduced artefacts into the current traces as can be seen from the rounding of currents in the blue trace of figure 4.3A. However, when currents were relatively small (e.g. < 2 nA; figure 4.3A red traces), capacitative artefact was proportionately larger.

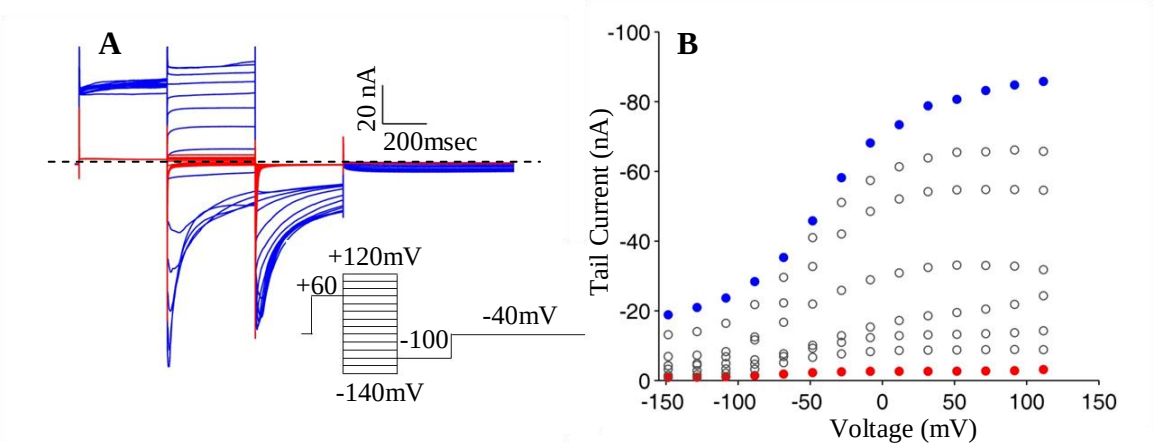

Figure 4.3 Range of tail current magnitudes from mouse FDB muscle fibres.
(A) Superimposed examples of the largest (blue) and smallest (red) chloride currents recorded from FDB muscle fibres.

(B) Tail currents plotted against prepulse voltage for 8 different FDB muscle fibres including the two shown in A.

Cell to cell variability precluded a comparison of cells treated with hormone against different control cells. Instead the effects of hormones were measured in each cell compared to control currents in that cell prior to addition of hormone. While the protocol was being refined, recordings tended not to last long enough to allow complete solution exchanges. In addition, contraction of muscle cells was only partly resolved by the addition of BTS. Thus sample sizes are small.

4.6 Results

ClC-1 gating parameters in HEK293T and in mouse FDB muscle fibres treated with different hormones are presented in below, which summarizes the four experiments presented in this section.

Table 4.1 Gating parameters for ClC-1 in FDB muscle cells (mean ± S.E.M.)

	n	V_{50} (mV)	Slope (mV)	τ_{fast} (msec)	τ_{slow} (msec)
Experiment 1: Comparison of ClC-1 in HEK293T against mouse FDB muscle fibres					
HEK293T	8	-62.0 ± 2.4	26.3 ± 1.7	7.3 ± 1.0	82.1 ± 8.3
FDB	5	-51.5 ± 4.3	27.9 ± 1.2	9.8 ± 3.3	91.4 ± 15.5
				Note: n = 4 for τ measurements in HEK293T cells (artifact in 1 recording)	
Experiment 2: Action of 100 µM progesterone on ClC-1 in mouse FDB muscle fibres					
Baseline	5	-52.6 ± 9.3	31.0 ± 2.6	5.4 ± 1.4	76.5 ± 25.0
Progesterone	5	35.5 ± 6.7* *(p < 0.01)*	53.1 ± 2.5	4.2 ± 1.6	52.7 ± 5.0
Experiment 3: 100 µM oestrogen, washoff, 100 µM progesterone in mouse FDB					
Baseline	5	-57.2 ± 7.6	23.7 ± 1.8	4.9 ± 0.7	52.1 ± 8.3
Oestrogen	5	-40.5 ± 9.8* *(p < 0.05)*	28.0 ± 2.5	4.9 ± 1.1	43.3 ± 5.1
Progesterone after Oest.	3	36.1 ±16.5	42.6 ± 3.1	11.5 ± 4.4	29.3 ± 3.6
Experiment 4: 1 µM progesterone, washoff, 10 µM progesterone in mouse FDB					
Baseline	4	-36.1 ± 15.5	33.7 ± 1.0	4.0 ± 0.8	36.7 ± 3.2
1 µM Prog	4	-35.6 ± 9.2	31.0 ± 1.1	3.2 ± 0.3	31.4 ± 5.2
10 µM Prog	4	-3.0 ± 5.9* *(p < 0.05)*	42.9 ± 4.2	5.0 ± 2.0 *Note: n = 3 for all τ measurements in experiment 4 (artifact in 1 recording)*	30.2 ± 2.4

Time constants were measured by fitting a double exponential function to the deactivating current on stepping from +60mV to -80mV. Stars indicate statistically significant differences from baseline. Unpaired t-tests were used to compare parameters in HEK293T and FDB (experiment 1). Pre- and post-hormone parameters for progesterone and oestrogen (experiments 2 and 3) were compared in paired t-tests. Progesterone after oestrogen was compared against progesterone or oestrogen alone in a one way ANOVA (discussed in the text).

Experiment 1: Human ClC-1 in HEK293T cells vs. mouse ClC-1 in FDB muscle fibres

In order to characterise ClC-1 by voltage clamp, the region of membrane being studied should ideally be clamped uniformly to the same voltage so that all the channels experience the same electric field and are set to the same state for each voltage being tested. If some channels fail to be clamped to the test voltage, the currents recorded will not reliably reflect the response of the channel to that voltage, distorting the measured current-voltage relationship. For a cylindrical cell to be studied by a single microelectrode, axial resistance to current flow along the length of the cell will result in potential differences between regions of membrane close and far away from the electrode (poor space clamp). The shorter the muscle fibre the better. Space clamp of HEK293T cells, which are smaller and more symmetrical than muscle cells, is likely to be much better. The muscle fibres from mouse FDB are relatively short, and it was possible that imperfect space clamp would not distort the recordings of ClC-1. A second potential problem was that large currents in muscle fibres could lead to large series resistance errors. In order to assess the adequacy of whole-cell patch clamp for characterising ClC-1 in FDB fibres a comparison was made between chloride currents from FDB fibres recorded with low resistance electrodes, and chloride currents from recombinant human ClC-1 expressed in HEK293T cells (figure 4.4).

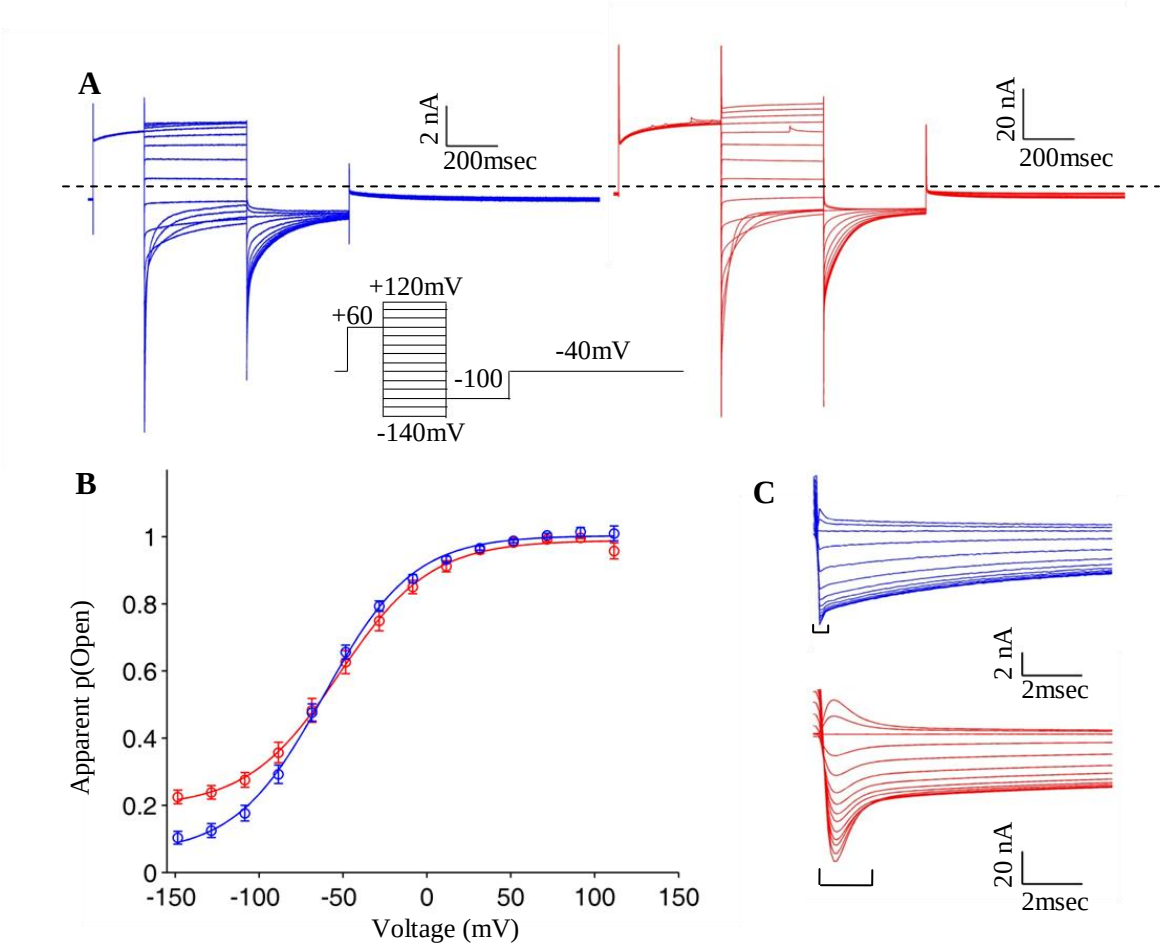

Figure 4.4 Comparison of cloned human ClC-1 in HEK293T with the endogenous chloride conductance of isolated mouse FDB muscle fibres.
(A) Chloride currents from a HEK293T cell expressing hClC-1 (blue) and from a mouse FDB fibre (red). **(B)** Normalized tail currents plotted as a function of pre-pulse voltage. Means ± S.E.M. are shown for voltages between -140 and +120mV. Wildtype human ClC1 in HEK293T (blue, n = 8), mouse FDB (red, n = 5). Error bars obscured by symbol in places. The voltage dependence of activation is very similar. The difference at hyperpolarized voltages probably arises from the need to measure tail currents slightly later in FDB muscle fibres to avoid capacitative artifact. **(C)** Expanded view of tail currents to show capacitative artifact (indicated by brackets below each trace) lasts longer in the FDB (red) than the HEK (blue) recording.

The characteristics of chloride currents from wildtype human ClC-1 in HEK293T cells and mouse FDB muscle fibres are compared in figure 4.4 (above) and (last section of the results chapter). There were no statistically significant differences between V50 of the Boltzmann fit, slope factor of the Boltzmann fit, or time constants of current deactivation

on stepping from +60 to -80 mV (paired t-tests). The FDB chloride currents resembled those reported in the literature (Lueck, Mankodi et al. 2007).

Experiments 2 & 3: 100 μM progesterone or 17β-oestradiol

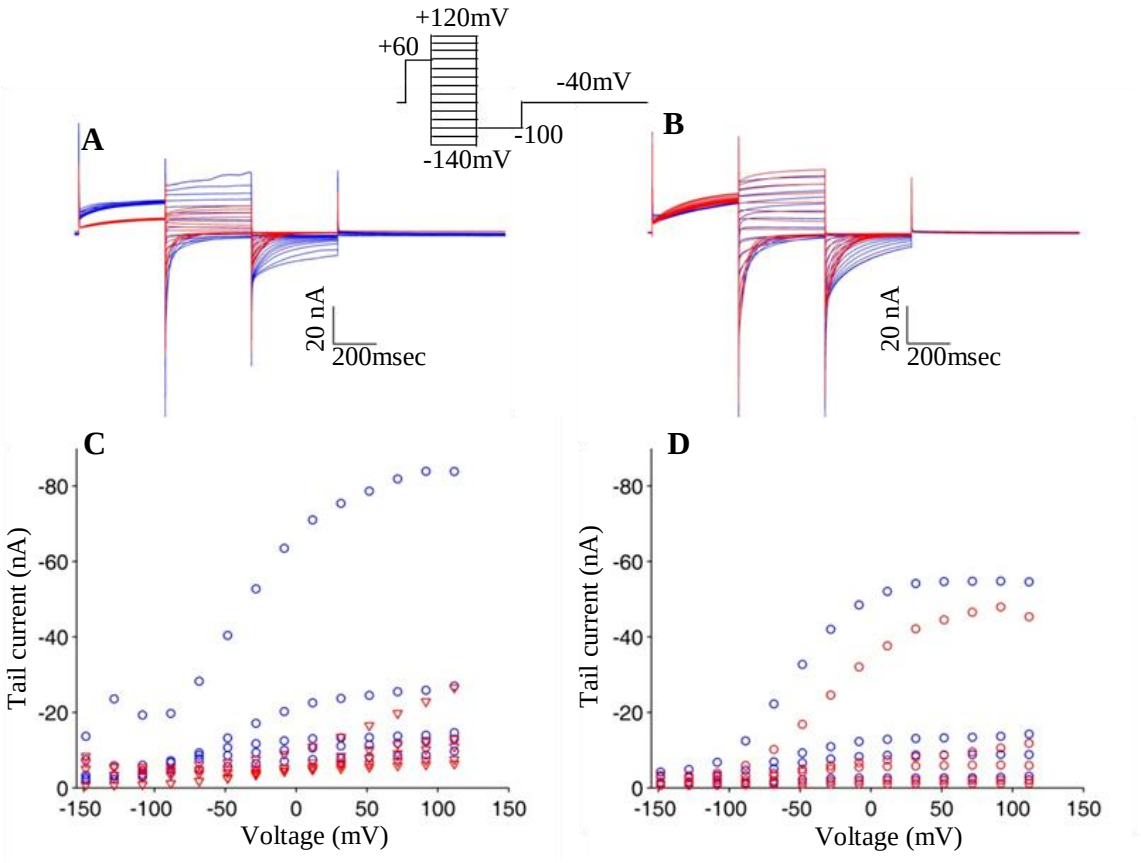

Figure 4.5 Raw data from FDB muscle fibres before/after 100μM progesterone or 17β-oestradiol. **(A)** Examples of chloride currents before (blue) and after (red) progesterone in the same cell. **(B)** Example of chloride currents before (blue) and after (red) 17β-oestradiol in the same cell (different cell from **A**). **(C)** and **(D)** show raw data (tail currents) from experiments with 100 μM progesterone or 17β-oestradiol to show cell-to-cell variability. Tail currents were plotted against prepulse voltage for every cell included in the analysis (n = 5 for each hormone). Note the inverted y-axis so that curves have same orientation as an opening probability curve. **(C)** Tail currents before (blue circles) and after (red triangles) progesterone in 5 cells. **(D)** Tail currents before (blue circles) and after (red circles) 17β-oestradiol in 5 cells (different cells from **C**). NB. The within-cells analysis is presented in figure 4.7 below.

There was considerable cell to cell variability in the magnitude of chloride currents as can be seen from the raw data in figure 4.5 above. As confirmation that the fall in chloride

current observed when hormone was applied, the effect of washing hormone off in two different cells is presented in figure 4.6 below:

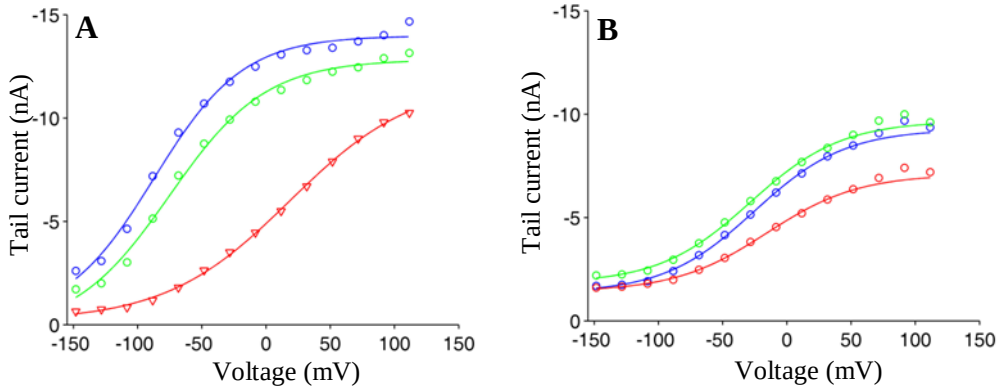

Figure 4.6 Reversibility of hormone action on chloride tail currents of two FDB muscle fibres.
The effects of progesterone (**A**, red triangles) and 17β-oestradiol (**B**, red circles) are reversed by washing hormone off (incompletely in the case of progesterone). Before hormone (blue), after 100 μM hormone (red), wash (green), n = 1 for each graph.

These effect of hormone exposure was complete within the time it took to exchange the solutions (minutes) and could be reversed by washing the hormone off with a similar timescale, implying a non-genomic mechanism. The effect of hormone on tail currents in a given cell was measured by establishing the proportion of the peak current before hormone that remained in presence of hormone. Peak current was estimated using a fitted Boltzmann function (figure 4.7). This procedure enables an assessment of the reduction in maximal current at depolarized potentials after application of hormone, as well as measurement of any change in voltage dependence of chloride conductance.

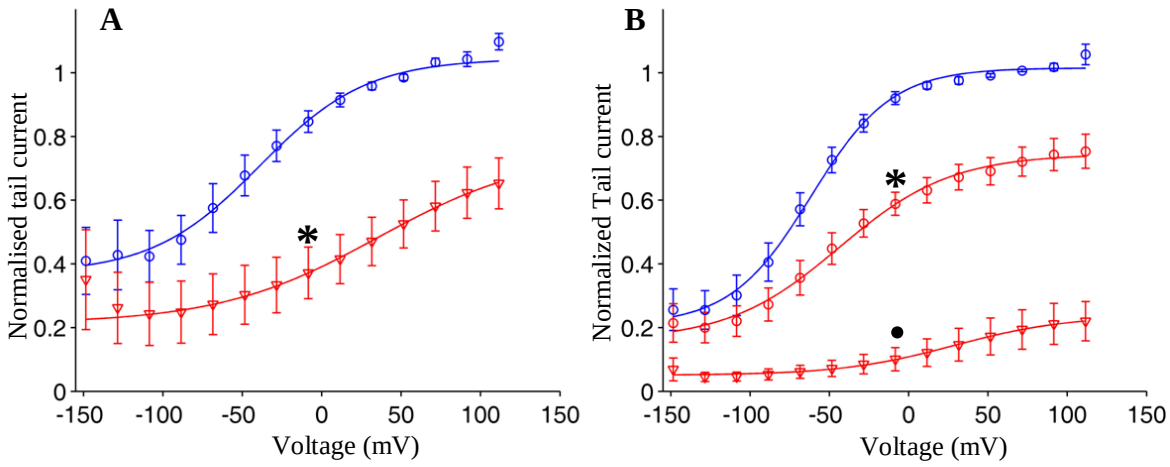

Figure 4.7 Analysis of the effects of 100µM progesterone (A) or 17β-oestradiol (B) on chloride tail currents of the FDB muscle fibres.
Blue circles correspond to currents measured before application of hormone, red triangles are data from cells in progesterone (n = 5). In **(B)** 17β-oestradiol was applied first (red circles) and after washoff, progesterone was applied (red triangles; n = 3). Tail currents in the absence of hormone were fitted with Boltzmann functions. For each cell, the maximal pre-hormone current (top of a Boltzmann fit) was used to normalize both the pre-hormone and post-hormone currents. Means ± S.E.M. are displayed with Boltzmann fits. The fractional tail current at 0 mV as a proportion of pre-hormone maximal current was significantly smaller in the presence progesterone or oestrogen than before hormone application (stars, $p < 0.01$, paired t-tests). Progesterone after prior exposure to oestrogen produced significantly smaller fractional tail currents after 0mV than either progesterone or oestrogen alone (dot, $p<0.01$, one way ANOVA and post-hoc pairwise analysis) but the difference between the latter two did not reach significance.

Experiment 2, comparing FDB muscle fibre chloride currents before and after 100 µm progesterone, is illustrated in panel A of Figure 4.7. Experiment 3, exposing FDB muscle fibres first to 100 µm 17β-oestradiol and then to 100 µm progesterone after washing off the oestrogen, is illustrated in panel B of Figure 4.7. In the presence of 100µM progesterone the chloride conductance activation curve appears shallower, with a right-shift, reducing chloride currents at -50mV and more positive. 17β-oestradiol at the same concentration appears to have a similar but smaller effect. The fractional tail current at 0mV as a proportion of pre-hormone maximal current was significantly smaller in the presence progesterone or oestrogen than before hormone application (stars, $p < 0.01$, paired t-tests). Progesterone and 17β–oestradiol at 100µM concentration both induced significant

depolarizing shifts in voltage dependence (V50 change from baseline of +88.1 ± 10.3 mV, $p<0.05$, and +16.7 ± 4.7 mV, $p<0.01$, respectively). Progesterone after prior exposure to oestrogen produced significantly smaller fractional tail currents at 0mV than either progesterone or oestrogen alone (dot, $p<0.01$, one way ANOVA and post-hoc pairwise analysis) but the difference between the latter two did not reach significance. There was, however a significant difference in the V50 change induced by the two hormones. In a comparison of the effect on V50 of 17β–oestradiol, progesterone, and progesterone after prior 17β–oestradiol treatment (one way ANOVA, $p<0.01$ that mean V50 is the same in all three conditions), 17β–oestradiol shifted voltage dependence significantly less than progesterone ($p < 0.01$, post-hoc, pairwise analysis with Matlab's muilticompare function). There was a trend towards application of progesterone after washing off 17β-oestradiol producing a larger effect than application of progesterone without 17β-oestradiol (figure 4.7), implying that the 17β-oestradiol may remain bound to its oestrogen receptors after washout. However, the difference between progesterone with or without prior 17β–oestradiol treatment did not reach significance, possibly because of the small number of cells ($n = 3$) in which the latter experiment was achieved. The same comparisons and statistical analyses as performed for V50 in experiments 2 and 3 were applied to the slope factor of the Boltzmann fit to the tail currents, and to the fast and slow time constants of current deactivation on stepping from +60 to -80 mV; there were no significant differences for these parameters.

Experiment 4: 1 μM and 10 μM progesterone

The highest concentration of progesterone that occurs naturally is in the last trimester of pregnancy when it reaches about 0.2 μM (Soldin, Guo et al. 2005). Thus the experiments presented above used non-physiological concentrations of progesterone, about 500 times higher than occur naturally. Therefore 1 μM and 10 μM concentrations were tested on the FDB fibres to look for an effect closer to physiological levels. Each myofibre was first exposed to 1 μM, then washed and next exposed to 10 μM followed by a wash. The results from four cells are presented below.

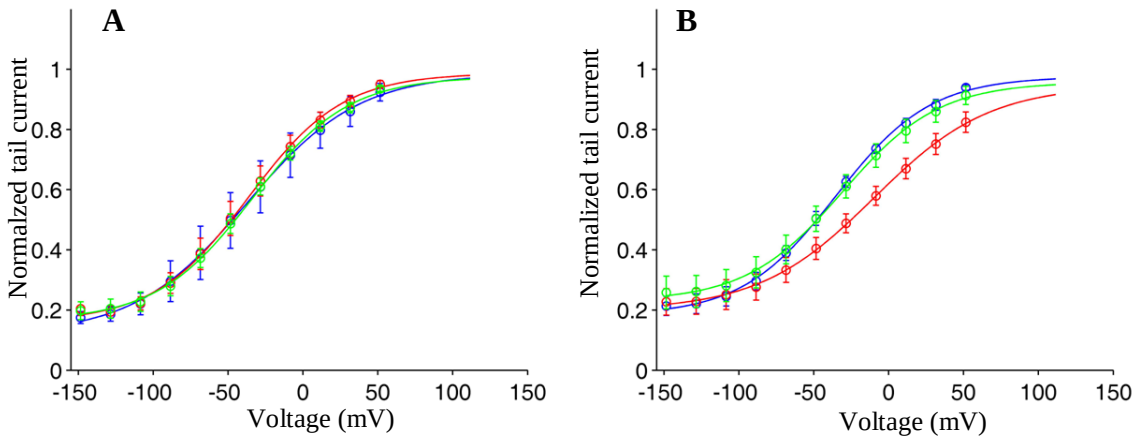

Figure 4.8 The actions of 1 μM and 10 μM progesterone on normalized chloride tail currents in muscle. Means ± S.E.M. were fitted with Boltzmann functions. **(A)** 4 cells before (blue) and after 1 μM progesterone (red), followed by wash (green). B. The same cells before (blue) and after 10 μM progesterone (red), followed by wash (green). The most depolarized steps were distorted by capacitative artifact and had to be excluded from the analysis. Fractional tail currents as a proportion of pre-hormone maximal current appeared smaller in the presence of 10 μM progesterone but the largest difference (after the 0 mV step) did not reach statistical significance (two way ANOVA without replication comparing pre-hormone, 1 μM and 10 μM progesterone).

It was possible to complete the experiment in four cells, however the most depolarized steps had to be excluded because of capacitative artefacts. There were no significant differences between 0 and 1 μM progesterone (see Figure 4.8 panel A and Table 4.1). In Figure 4.8 panel B chloride currents appear slightly smaller in the presence of 10 μM

progesterone but the largest difference (after the 0mV step) did not reach statistical significance (two way ANOVA without replication comparing pre-hormone, 1 μM and 10 μM progesterone). However, an analysis of the voltage-dependence of chloride currents from the same FDB fibres treated successively with 0, 1 and 10 μM progesterone (two way ANOVA without replication, $p = 0.02$ that mean V50 is the same in all three treatments), the right-shift produced by 10 μM progesterone in comparison to baseline 0 μM was significant ($+30.1 \pm 4.4$ mV, $p < 0.05$, post-hoc, pairwise analysis with Matlab's muilticompare function). The same comparisons and statistical analyses as performed for V50 were applied to the slope factor of the Boltzmann fit to the tail currents, and to the fast and slow time constants of current deactivation on stepping from +60 to -80 mV; there were no significant differences for these parameters.

4.7 Summary of results

The experiments in this section tested the response of the endogenous chloride conductance of mammalian skeletal muscle to progesterone and 17β-oestradiol by whole cell patch clamp of isolated mouse FDB fibres.

First comparison of the endogenous chloride conductance from mouse skeletal muscle with that of human ClC-1 expressed in HEK29T cells indicated that whole cell patch clamp was adequate for the planned hormone experiments. Whole cell patch clamp is not a traditional method for studying muscle cells, but the data are in agreement with the recent work of a relatively few others (Lueck, Mankodi et al. 2007) showing that the whole cell patch clamp technique can be successfully applied to characterizing ion channels in skeletal muscle cells. It should be noted that others have used off-line leak subtraction of residual currents

after application of 9-AC (an inhibitor of ClC-1), and have expressed currents per unit capacitance measured in the presence of 9-AC in order to cope with cell-to-cell size differences (Lueck, Mankodi et al. 2007). In preliminary experiments with 9-AC in this project the time taken for chloride currents to be inhibited was around 10 minutes, which when added to the time taken to complete hormone applications was generally longer than a stable recording could be maintained. As a result, the comparisons of hormone effects were measured in the same cells before and after hormone.

In *Xenopus* oocytes sex hormones at high concentration rapidly reduce the conductance of heterologously expressed human ClC-1 (Fialho, Kullmann et al. 2008); the results here suggest that the endogenous chloride conductance in mammalian skeletal muscle responds similarly. However, as in the oocyte experiments, the concentration of hormone that was effective in the muscle experiments is much higher than occurs physiologically in plasma. The data therefore support the existence of a mechanism in skeletal muscle through which sex hormones at high concentrations can rapidly modulate ClC-1, but the influence of these hormones on muscle excitability *in vivo* at physiological concentrations remains an open question.

Chapter 5 Computer simulation of ClC-1 and myotonic muscle

5.1 Chapter summary

The macroscopic chloride conductance of a membrane expressing wildtype ClC-1 was simulated in Matlab. The simulation improves on published models by recapitulating both time-dependence and voltage-dependence of the channel through a method based on independent representations of the fast and the slow gates. The applicability of the model for the purposes of exploring the effects of specific mutations was assessed by attempting to simulate the currents through S289G homodimers that had been recorded in chapter 3 by whole cell patch clamp. Three published models of chloride channel myotonia were re-evaluated in Matlab. The mechanism of low chloride conductance myotonia and electrical factors likely to impact on its severity are discussed in the context of a critical review of each of the models.

5.2 Aims

Develop a model of the macroscopic, time-dependent and voltage-dependent chloride currents through a membrane expressing ClC-1 channels.

Develop a model of the skeletal muscle action potential that exhibits both the early (potassium-independent) and the late (potassium-dependent) phases of the after-depolarization in order to improve on existing models of myotonia.

Use the model ClC-1 channel to explore the differential effects of altered kinetics versus shifts in voltage dependence on the propensity to myotonic discharges.

5.3 Motivation

Mathematical models of excitable membranes complement empirical enquiry because macroscopic electrical behaviour depends not only on the particular electrophysiological properties of an excitable membrane, but also on the geometry of the dynamical system as a whole. Interactions between ionic currents are often complex, and computer models can help to disentangle the various interdependencies. The relationship between ClC-1 and the wider skeletal muscle dynamical system is highly relevant to the self-sustaining voltage oscillations that occur in myotonia. It is desirable to improve on existing models of the muscle chloride conductance (which is often represented as a linear time- and voltage-independent leak), to enable a more faithful representation of specific CLCN1 variants.

5.4 Scope

A multitude of factors downstream from the primary electrical abnormality of autonomous sarcolemmal action potentials are likely to impact to some degree on the patient's experience of myotonia from excitation-contraction coupling all the way through to the individual's state of mind. In the discussion of phenotypic variability it is therefore important to be clear at the outset as to what is meant by 'severity of myotonia'. The present discussion is concerned with electrical phenomena, and the severity of myotonia is defined not in terms of the clinical symptoms or impact on a patient's life, but in terms of the behaviour of the muscle cell membrane. The easier it is to elicit a train of involuntary, autonomous muscle fibre action potentials or the longer that train, the more severe the myotonia. The warm-up phenomenon is not considered because its mechanism remains unknown.

5.5 Critique of three published models of myotonia

In myotonic muscle the last in a train of neurally-driven action potentials is followed by further autonomous muscle action potentials instead of a return to resting potential. For the surface membrane to depolarize again instead of returning to resting potential, net current at the surface (which is outward during repolarization) must overshoot zero and turn inward.

The Barchi model

Barchi showed that in an isolated region of membrane containing sodium, delayed rectifier potassium and leak conductances raised external potassium could drive a paradoxical inward current through the delayed rectifier in the second half of repolarization (Barchi 1975). Reducing the opposition by chloride to this depolarizing potassium current caused repetitive discharges. Barchi's simulation can be considered to represent the state of the t-tubule at the end of a contraction during which the tubule lumen has accumulated potassium. The response of the tubular membrane in this state to one further neural stimulus (the final action potential of the voluntary contraction) is simulated by injection of a square pulse of current to elicit an action potential, after which the tubular membrane potential either returns to rest or further autonomous discharges occur depending on the chloride conductance.

Parameters for the sodium and delayed rectifier conductances are derived from voltage clamp experiments in amphibian muscle (Adrian, Chandler et al. 1970). The chloride conductance is represented as a linear leak, with a reversal potential of -95mV, so that it conducts a hyperpolarizing current at the membrane voltages encountered during an action potential, promoting repolarization. A brief depolarizing after-potential occurs in Barchi's

model because the potassium reversal, E_k, is set rather positive at -70mV (as would be the case if potassium had accumulated in the tubule lumen). At the start of action potential repolarization both the leak current (representing the chloride current) and the delayed rectifier potassium current are outward, promoting a return to resting potential. But in the second half of repolarization the delayed rectifier current turns inward (membrane potential drops below the potassium reversal potential), opposing but not completely overcoming the leak current, and delaying repolarization (Figure 5.1). Varying the potassium reversal potential (to simulate different degrees of potassium accumulation) changes the size of the after-depolarization (Figure 5.2), and varying the leak conductance changes its duration. When the leak conductance is sufficiently reduced (simulating myotonic muscle's low chloride conductance) it can be overcome by the inward potassium current turning net membrane current inward at a time when sodium channels have recovered from inactivation, and autonomous action potentials are set off (Figure 5.3).

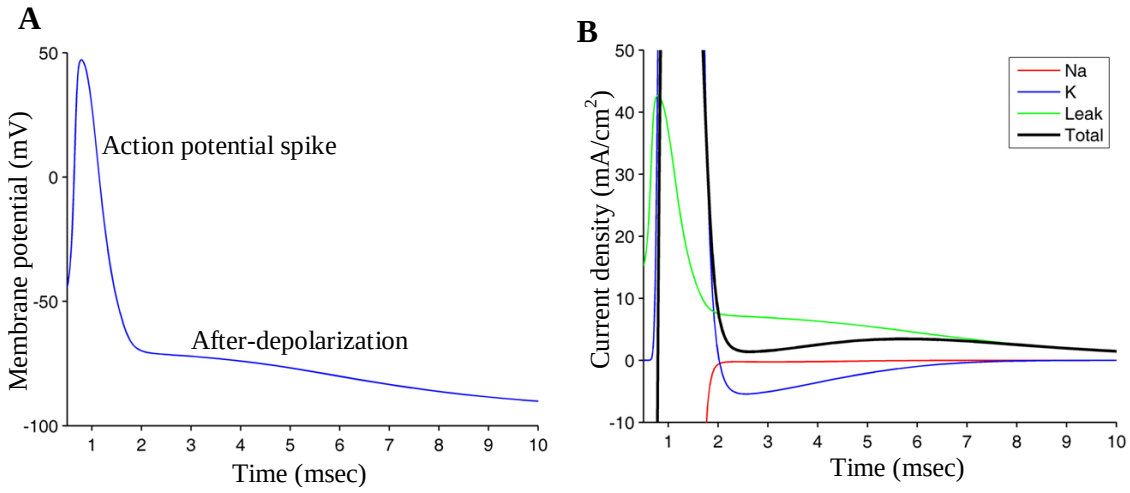

Figure 5.1 Mechanism of the after-depolarization in the Barchi model.
The Barchi model (parameters given in the methods section) was implemented in Matlab and stimulated with a 0.5 msec duration square current pulse at t = 0 msec. The response is plotted here starting at the end of the pulse. **(A)** Membrane potential. The action potential is followed by a brief after-depolarization. **(B)** Ionic currents. At each time point net current though ion channels (black) is the sum of the sodium, potassium and leak currents (red, blue and green respectively). Rate of change of the membrane potential is proportional to the magnitude of the total current – zero current causes steady, unchanging voltage, outward current (positive values on the y-axis) causes repolarization, inward current (negative values on the y-axis) causes depolarization. A phase of inward potassium current starting around 2 msec opposes the outward leak current and slows repolarization almost to a halt (net current close to zero).

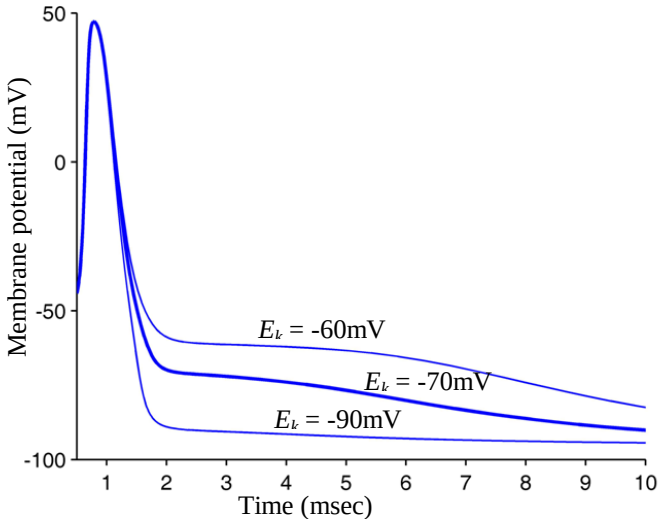

Figure 5.2 Effect of potassium accumulation in the Barchi model.
The Barchi model was stimulated with a 0.5 msec square current pulse at t = 0 msec. The response is plotted here, starting at the end of the pulse. The after-potential is enhanced by shifting the potassium reversal potential (E_k) to a more depolarized value of -60 mV (simulating potassium accumulation) and reduced by shifting it to -90 mV.

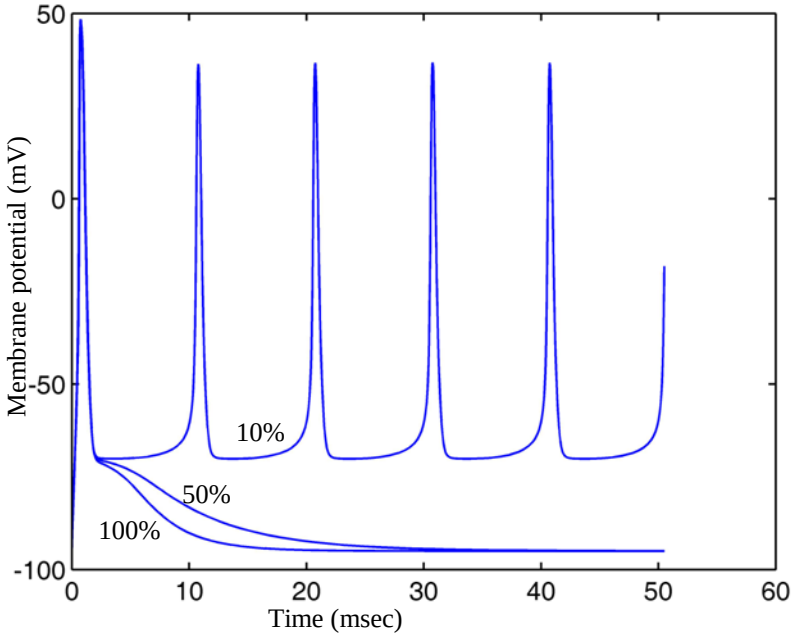

Figure 5.3 Effect of reducing the leak conductance in the Barchi model.
The Barchi model was stimulated with a 0.5 msec duration square current pulse at t = 0 msec. The potassium reversal potential was -70 mV. The leak conductance was changed from 100% to 50% and then 10% of normal. The duration of the after-potential increases as the leak conductance is reduced and at 10% of normal leak autonomous action potentials occur.

The absence from the Barchi model of a way for accumulated potassium to influence membrane potential at voltages around the resting potential is a significant departure from real muscle. While the resting chloride conductance of skeletal muscle is large, there is relatively little active transport of chloride ions (Aickin, Betz et al. 1989), which are predominantly driven into their concentration gradient by the resting potential that the actively pumped potassium ions establish (Kwiecinski, Lehmann-Horn et al. 1984). Inward rectifier potassium channels, including *Kir2.1*, are important for coupling the resting potential to the potassium equilibrium potential (Jurkat-Rott, Fauler et al. 2006; Struyk and Cannon 2008). However, the focus of the Barchi model is on events critical to the onset of myotonia, when the muscle membrane 'takes the decision' whether to return to rest or

continue with autonomous discharges; the aim was not to describe diffusion of potassium out of the tubule, the termination of the myotonic discharge, or the resting state of the membrane. At depolarized potentials the potassium channels primarily responsible for coupling the resting potential to the potassium concentration gradient (inward rectifier channels, including *Kir2.1*) are non-conductive (Anumonwo and Lopatin 2010) and so their absence from a model of events during the descending phase of the action potential is not unreasonable.

Asynchrony between t-tubules and the surface membrane

Models that represent the interaction between tubular and surface membranes (Adrian and Marshall 1976; Cannon, Brown et al. 1993) offer an alternative to Barchi's hypothesis that myotonia is triggered by paradoxical inward current through the delayed rectifier. The imbalance of currents at the surface membrane which sets off a myotonic discharge in the context of low chloride conductance might arise from asynchrony between action potentials at the surface and in the t-tubules. Figure 5.4 shows an equivalent circuit representing a region of surface membrane connected to a region of t-tubule. A potential difference between $V_{surface}$ and V_{tubule} drives current across the access resistance and around a loop between the surface and tubule membranes.

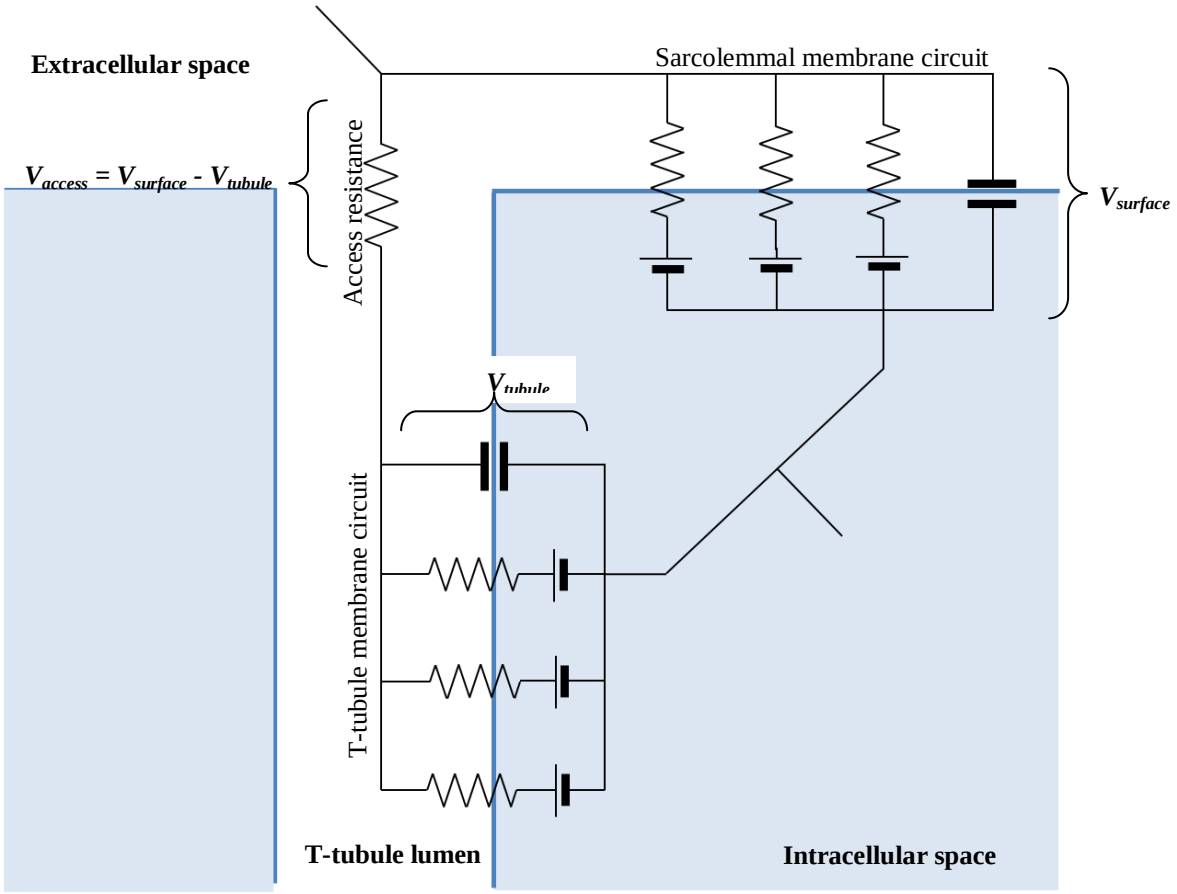

Figure 5.4 Paths of current flow between intracellular and extracellular space in muscle.
Current can flow between the intracellular and extracellular spaces directly through the sarcolemma (right hand branch of the circuit diagram) or indirectly by first crossing into the space inside t-tubule lumens through the tubular membrane (left hand branch of the circuit diagram). Current through each membrane can pass through channels or across a capacitor. Capacitative currents change the membrane potential because positive charge accumulates on one side and departs from the other side of the membrane. Resistance to current flow between the lumen of the t-tubule system and the extracellular fluid (caused by narrow, sparse tubule openings on the sarcolemma) is represented as an 'access resistance'. Current through the access resistance is the net (capacitative plus all ion channels) current through the tubule membrane and is driven by the difference in tubular and surface membrane potentials (*Vtubule – Vsurfac*e).

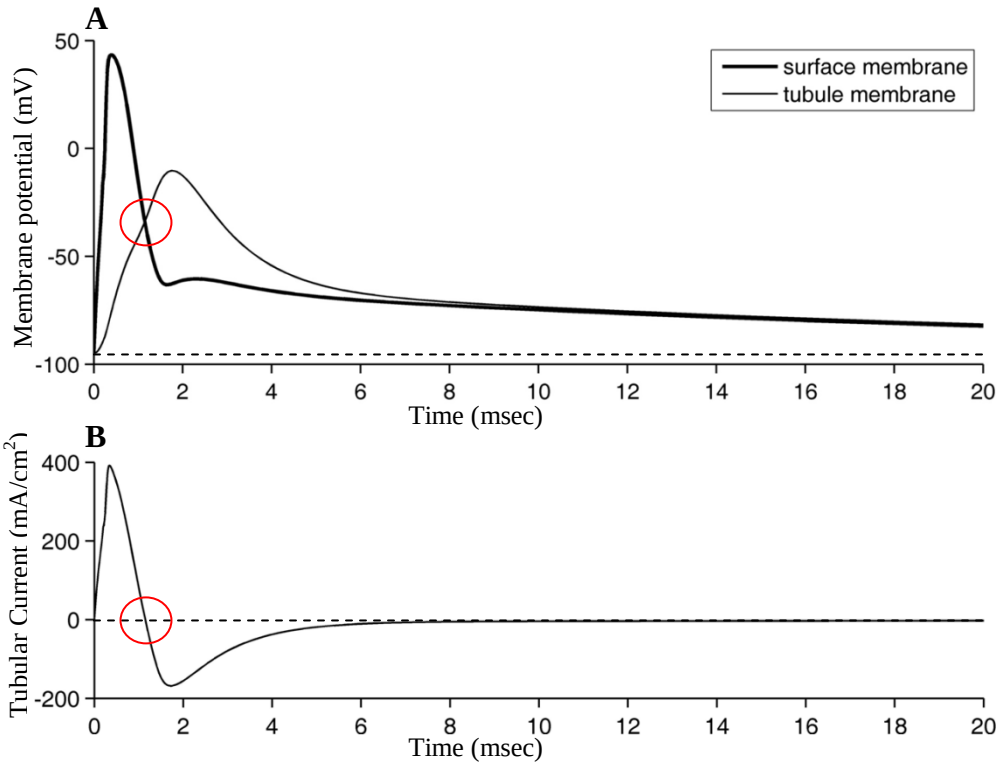

Figure 5.5 Mechanism of the early after-depolarization.
The Adrian & Marshall model was implemented in Matlab and used to simulate a 300 μm long segment of a 70 μm diameter cylindrical muscle fibre with an appropriately scaled region of tubular membrane (equivalent circuit shown in Figure 5.4). A 0.1 msec depolarizing current stimulus (450 $\mu A/cm^2$) was injected at t = 0 msec. From a resting potential of -95 mV (**A**, dotted line) an action potential occurred at the surface (**A**, heavy black line) and, later, in the t-tubule (**A**, thin black line). The action potential's return to resting potential suddenly slows at around 2 msec – this is the onset of the early after-depolarization. The current passing across the access resistance at the mouth of the tubule is shown in **(B)**. At 1.1 msec (red circles) the tubular and surface membrane potentials are equal, and current across the access resistance current (**B**, thin black line) hits zero (no potential difference to drive current across the access resistance). Thereafter the difference in potential between surface and tubule membranes drives an inward current across the access resistance, through the tubular membrane into the cell, and out across the surface membrane. At this time the surface membrane is 'trying' to repolarize with a capacitative current that carries positive charge off its inner aspect and out through surface channels. The access resistance current competes with the surface membrane to be accommodated by the outward channel current (whose value is fixed by the membrane potential and state of the channels). As the access resistance current reaches its maximum inward value, it swamps the outward channel current through surface channels, and the excess current from the tubules must flow via the surface capacitance which stops repolarizing and starts depolarizing again at around t = 2 msec. This is thought to be the basis of the notch that was observed in the early after-depolarization of amphibian muscle fibres.

The t-tubules have a large area of membrane relative to the area of sarcolemma on the surface of a muscle fibre (Peachey 1965) and hence a higher capacitance that takes longer to charge to threshold for an action potential. An example is presented in Figure 5.5. The large tubule capacitance in series with the access resistance means that V_{tubule} lags behind $V_{surface}$ and peaks when $V_{surface}$ is repolarizing.

For the majority of the upstroke of the tubular action potential, a potential difference across the access resistance causes clockwise current flow around the loop connecting the surface and tubular membranes. The surface membrane supplies charge to the tubule even while the tubule's own sodium channels are supplying current to drive its action potential. The clockwise current through the access resistance peaks at the time of greatest difference between V_{tubule} and $V_{surface}$ and then declines as the surface begins to repolarize and the tubular continues to depolarize. The rising phase of the tubular action potential meets the descending phase of the surface action potential shortly after 1 msec (Figure 5.5 red circles). At this instant there is zero current around the loop between surface and tubule. At the tubule all the inward current through channels goes into charging its membrane. At the surface, all the repolarization current flowing off the capacitance is exiting via surface channels.

V_{tubule} continues to rise for a short time after its meeting with $V_{surface}$, indicating a continued outward capacitative current, but as V_{tubule} grows more positive than $V_{surface}$ current is driven counter-clockwise through the access resistance. Some of the inward tubular sodium current that is driving the upstroke of the tubular action potential is sucked into the cell and out across the surface membrane. When the tubular membrane repolarizes, some of the repolarization current flows out through the surface membrane. Thus tubular currents

compete for the potassium and chloride (leak) channels through which the surface membrane is 'trying' to discharge. The effect on the surface membrane can be seen in Figure 5.5 at around 2 msec – surface repolarization is briefly halted and reversed as surface channels are swamped and some current has to flow out across the surface capacitance, charging it up again. To make matters worse, at these surface potentials, the delayed rectifier is beginning to close. The later the tubule potential peaks (the further the surface has repolarized) the more closed the delayed rectifier, so the less accommodating the surface channels can be and the more of this charge must flow as capacitative current, depolarizing the membrane. The surface chloride conductance could be critical in providing an alternative exit route from the delayed rectifier. If this current was large enough and late enough it might in theory cause a further action potential, with exactly the same process occurring again and again (myotonia) at the end of each action potential.

In summary, asynchrony between the tubule and surface action potentials causes a delay in the return to resting potential, which manifests as the early after-depolarization. Chloride channels at the surface may be critical in providing an exit route for current flowing in through the tubule and out across the sarcolemma at a time when the sarcolemmal delayed rectifier is beginning to close (Adrian and Marshall 1976).

The Adrian & Marshall model

Adrian & Marshall (Adrian and Marshall 1976) built on earlier models of the interaction between tubular and surface membranes (Falk and Fatt 1964; Adrian, Chandler et al. 1969; Adrian and Peachey 1973). They accounted for accumulation and diffusion of potassium in the t-tubular system as well as propagation of an action potential both longitudinally along the surface membrane, and radially into the depths of a muscle fibre. The muscle fibre was

represented by a cylinder of surface membrane divided into isopotential segments. Propagation of the surface membrane action potential longitudinally between adjacent segments was implemented by calculating intracellular currents axially between segments from the segment-to-segment potential differences and intracellular resistivity. Each segment of surface membrane was connected to an appropriately scaled area of t-tubule membrane and volume of t-tubule lumen. Radial propagation of the t-tubular action potential from the surface of the fibre (outer t-tubule segment) to its centre (inner t-tubule segment) was calculated in a similar fashion using tubular lumen resistivity (Figure 5.6). Potassium was allowed to accumulate in the lumens and to diffuse between the lumens of adjacent t-tubule segments (Figure 5.6B).

Low chloride conductance myotonia was simulated by reducing the leak conductance at the surface membrane, without changing the t-tubule (which in the model has a rather small leak conductance anyway). Figure 5.7 shows the effect of reducing the surface chloride conductance on the model's response to stimulation with $200\mu A/cm^2$ for 150msec, as was presented in figure 5 of the original paper (Adrian and Marshall 1976). The normal fibre responds with a single action potential at short latency, as occurs in normal muscle fibres. Reducing chloride conductance to half normal produces 10 action potentials during the stimulus but no autonomous action potentials afterwards. Further reduction to 10% of normal chloride conductance produces 13 action potentials during the stimulus, and 2 autonomous action potentials after the stimulus (myotonia).

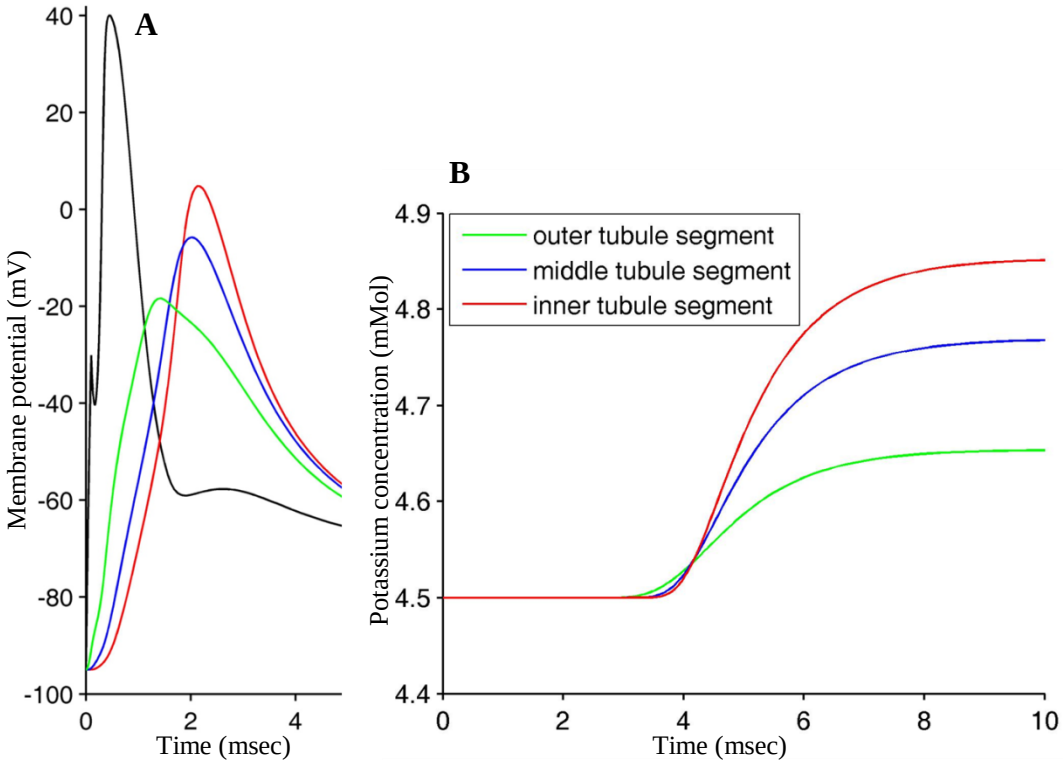

Figure 5.6 Adrian model action potential shape, and potassium accumulation.
Reconstruction of figures 2b and 3a of Adrian's original report – the Matlab program faithfully replicates Adrian's results.

A) Action potential at surface and tubule membranes in a single 300 μm-long segment of cylindrical muscle (100μm diameter, tubule divided into 3 segments running radially into the fibre, potassium accumulation disabled – see figure 2b of Adrian's paper). Adrian does not specify the stimulus current he used, but a square current pulse 0.1msec long of 750μA/cm^2 reproduced the stimulus artefact in his figure.

B) Tubular potassium accumulation at the 7th segment of a 15 segment, 4.5 mm-long fibre (100 μm diameter, each segment 300 μm long, tubule divided into 3 segments running radially into the fibre, potassium accumulation enabled – see figure 3a from Adrian's figure). Potassium accumulates during repolarization, flowing out through delayed rectifier channels into the tubule lumen.

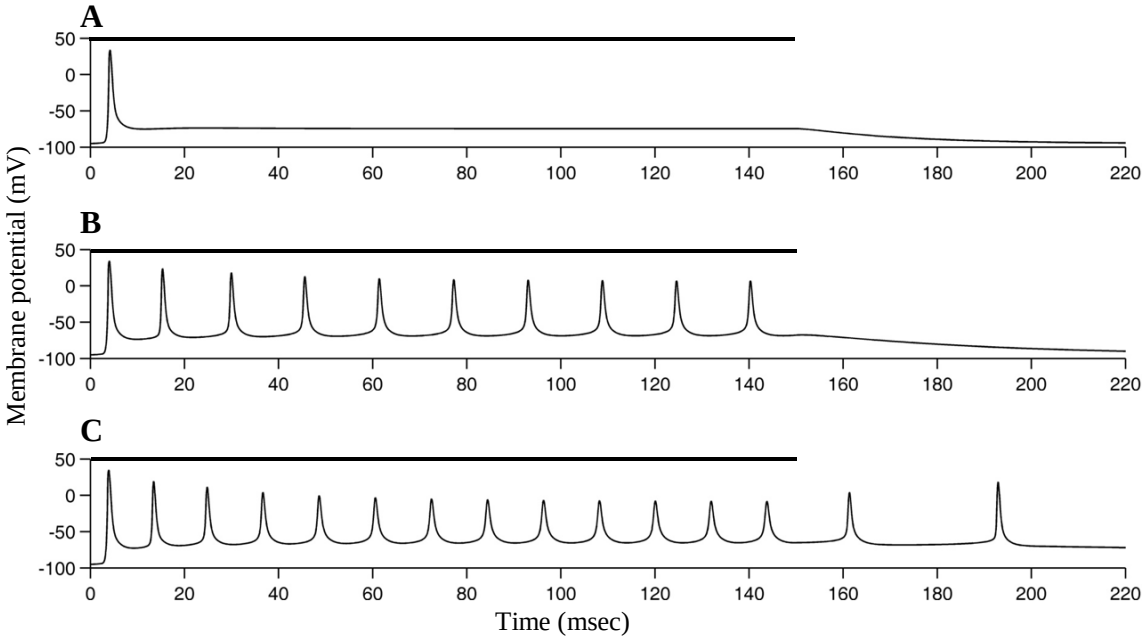

Figure 5.7 Reconstruction of the Adrian model of myotonia.
Reconstruction of figure 5 from Adrian's original report. A 4.5mm long model fibre, 70 μm diameter, divided into 15 segments each containing 3 t-tubule segments was stimulated at one end with a constant current pulse lasting 150 msec starting at t = 0. The membrane potential in mV of the middle (7th) segment is plotted against time in msec. A black bar above each plot indicates the period of stimulation. The original paper does not divulge the magnitude of the current stimulus. A 200 $\mu A/cm^2$ stimulus produced identical results as reported in the paper. With normal leak a single action potential occurred **(A)**. Halving the leak resulted in 10 action potentials during the stimulus **(B)**. Reducing the leak to a tenth of normal produced 13 action potentials during the stimulus, and two autonomous action potentials after the stimulus **(C)**. The authors commented on the difficulty of eliciting autonomous action potentials in their model and tackled the problem by slowing deactivation of sodium channels.

As in Barchi's model, the only potassium conductance is through the delayed rectifier, which is not conductive at voltages around the resting potential. Thus while accumulated potassium affects repolarization currents during the action potential downstroke, it has no influence over the resting potential. The resting potential is set by the leak conductance, representing chloride channels, whose equilibrium potential is fixed and independent of the potassium equilibrium potential.

Cannon's model of sodium channel myotonia

Cannon's model was designed to recapitulate sodium channel myotonia, which is also critically dependent on the t-tubular system (Cannon and Corey 1993). The sodium channel in mammalian muscle is active at rather more hyperpolarized potentials than its equivalent in amphibian muscle (Fu, Struyk et al. 2011), from which Barchi and Adrian & Marshall took their parameters. The circuit for Cannon model is exactly as presented in Figure 5.4. A single isopotential region of tubule membrane is associated with a single isopotential region of surface membrane in a simplification of the multi-segmented Adrian and Marshall model. The ratio of tubular to surface membrane areas is 4.8, and concentration changes in the tubule lumen are calculated assuming a tubular volume to tubular membrane area ratio of 10^{-6} cm. These structural parameters originated in the Adrian & Marshall model (assuming a cylindrical fibre of 32 μm radius), which used measurements from amphibian muscle (Peachey 1965). A replication in Matlab of figure 3 from the original paper (Cannon and Corey 1993) is presented below in Figure 5.8.

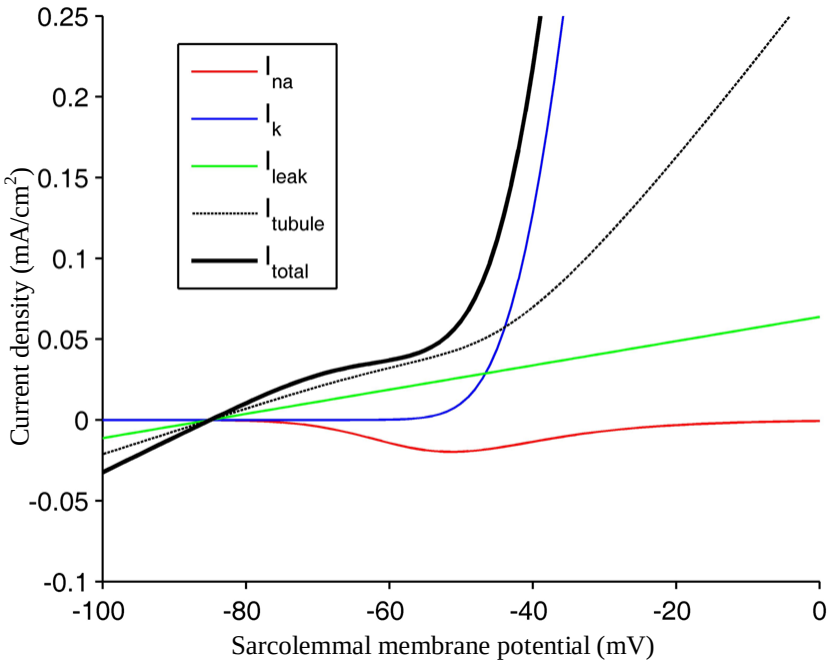

Figure 5.8 Replication of Cannon's model for comparison against figure 3 from his paper.
I_{na}, I_k and I_{leak} are respectively the currents at steadystate through sodium, potassium and leak conductances of the sarcolemmal membrane. I_{tubule} is the steadystate current across the access resistance of the t-tubule system. I_{total} is the sum of all these currents. Itotal crosses the y-axis at the resting potential, approximately -85mV.

Unlike the models of Barchi and Adrian & Marshall, resting potential in the Cannon model is strongly coupled to the potassium equilibrium potential (see Table 5.2). Cannon achieved this by calculating the equilibrium potential for the leak conductance (the only active conductance around the resting potential) from the potassium concentration gradient. The influence of t-tubular potassium on resting potential is illustrated in Figure 5.9. The late after-depolarization that results from tubular potassium accumulation during a train of action potentials muscle (Freygang, Goldstein et al. 1964) is illustrated in Figure 5.10.

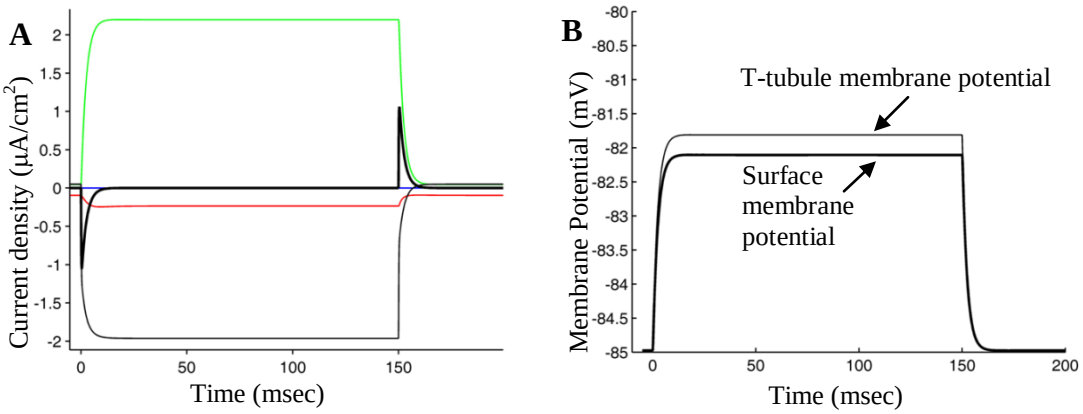

Figure 5.9 Influence of tubular potassium on surface membrane resting potential in Cannon's model. Tubular potassium was stepped from 4 to 5 mM at t = 0 msec and stepped back at t = 150 msec. Surface membrane currents are shown in **(A)**. Potentials across surface t-tubular membranes are shown in **(B)**. The change in leak reversal potential increased the tubule membrane potential, which drew an inward current via the access resistance (**B**, grey line), across the tubule membrane into the cell to charge the surface membrane (the capacitative component is seen as a brief spike in the net surface membrane current: **A** – heavy black line). The new surface membrane potential **(B)** in turn drove an outward leak current (A, green line) that rose to balance the inward tubular current, until a new equilibrium was established. The tubular and surface membrane potentials shifted from around -85mV to around -82mV **(B)**. Sodium (**A**, red) and potassium (**A**, blue) currents are small at these potentials. Stepping potassium back to 4mM reversed the process.

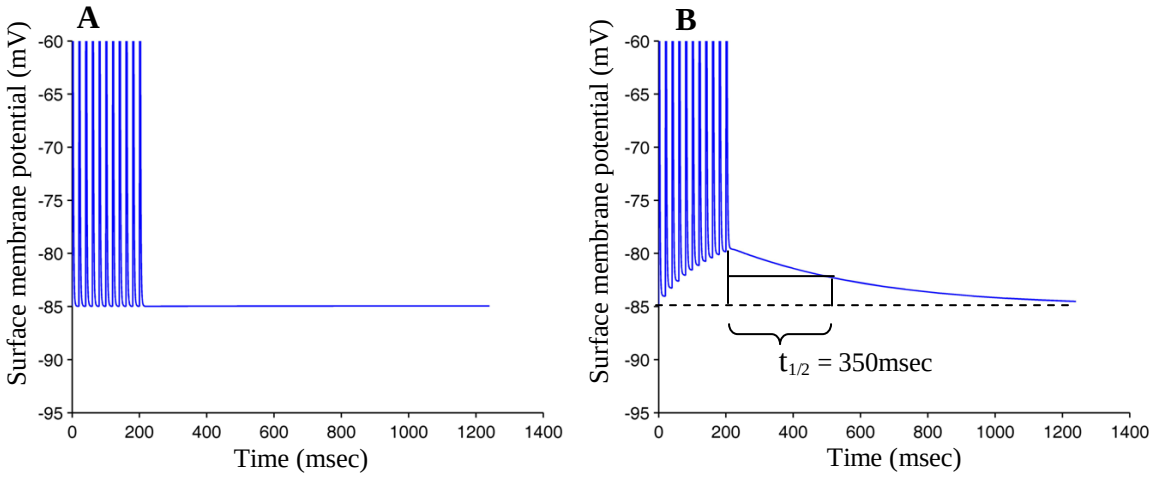

Figure 5.10 Late-afterdepolarization in the Cannon model. Tetanic muscle contraction lasting 200msec was simulated by stimulating the model at 50 Hz with square current pulses of 0.5msec duration (one pulse every 20 msec). The y scale is set to zoom in on the base of the action potentials to highlight effects on the resting potential. **(A)** With potassium accumulation disabled (constant tubular potassium of 4mMolar) membrane potential returns immediately to rest (approximately -85mV). **(B)** When potassium is allowed to accumulate in the tubular lumen, a late after-depolarization follows the train of action potentials. Its amplitude is about 0.5mV per action potential.

While Cannon's model captures important aspects of sodium channel myotonia, it was not designed to recapitulate low chloride conductance myotonia; when the leak conductance is reduced (Figure 5.11 below) the system becomes inexcitable rather than myotonic. Inexcitability occurs because as the leak conductance is reduced the current-voltage curve becomes increasing N-shaped, and the right hand knee of the N crosses the zero-current level (Figure 5.12 below) at a voltage where inactivation of sodium channels makes the membrane refractory to action potentials. This effect is an intrinsic property of the simulation membranes, independent of potassium in the t-tubule.

Summary

Barchi's hypothesis that accumulated tubular potassium might drive a paradoxical inward current through the delayed rectifier is compatible with Adrian & Marshall's ideas about tubular and surface membrane asynchrony since the former process, by delaying tubular repolarization, would exacerbate the latter. The late after-depolarization caused by tubular potassium accumulation, as captured by the Cannon model, might additionally contribute to the initiation of a myotonic discharge by maintaining the system near threshold for action potential. A major aim for this chapter was to develop a model with all these features by using the equivalent circuit of Adrian & Marshall, but replacing the leak with an inward rectifier potassium conductance and a voltage gated ClC-1 conductance. While a similar approach has been adopted in the past for the description of t-tubular potassium fluxes (Wallinga, Meijer et al. 1999), it has not been used to model low chloride conductance myotonia, and nor have the two gates of ClC-1 been represented. An *in silico* assay for estimating physiological consequences of ClC-1 abnormalities would complement a cell-based voltage clamp assay for CLCN1 variants.

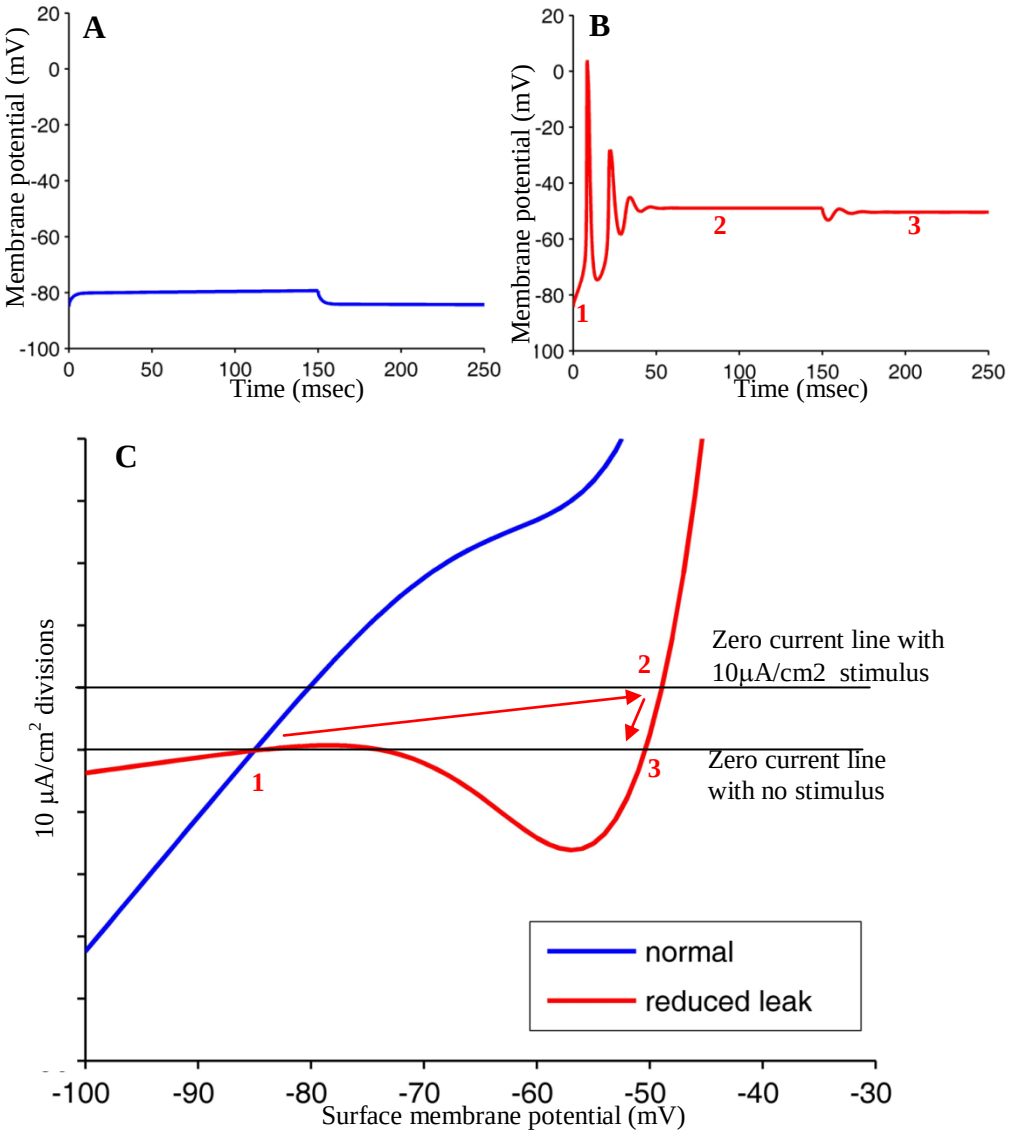

Figure 5.11 Equilibria in the Cannon model with reduced leak conductance.
Responses of the Cannon model to stimulation with 10 µA/cm^2 for 150 msec at constant t-tubular potassium (4 mM). **(A)** Normal leak conductance. Small shift in potential during stimulation followed by return to original resting potential after stimulation. **(B)** Leak conductance reduced to 10% of normal. From resting at -85mV (point 1), action potentials are elicited (hyperexcitability) but do not persist. Membrane potential settles near -50mV during stimulation (point 2) but fails to return to the original resting potential afterwards, instead remaining close to -50mV (point 3). **(C)** Total steadystate current (excluding capacitative current) at the surface membrane under normal conditions (blue) and with leak reduced to 10% of normal (red). Total current is the sum of sodium, potassium, leak and tubular currents plus stimulus - stimulation shifts the curve vertically. Horizontal lines show zero current levels in the absence and presence of stimulation. Stable equilibria occur at voltages where the curve passes upward through a zero line. With normal leak there is a single stable equilibrium irrespective of stimulation (blue curve – single zero crossing). When leak is reduced to 10% of normal (red curve) there are two stable equilibria in the absence of stimulation (points 1 and 3), and only one in the presence of stimulation (point 2). From equilibrium 1 application of the stimulus causes the abnormal fibre to jump to equilibrium 2. When the stimulus is removed the zero crossing slides down the right hand branch of the red curve and the cell comes to rest at point 3 (hysteresis). Inactivation of sodium channels at this potential means that the fibre cannot fire action potentials.

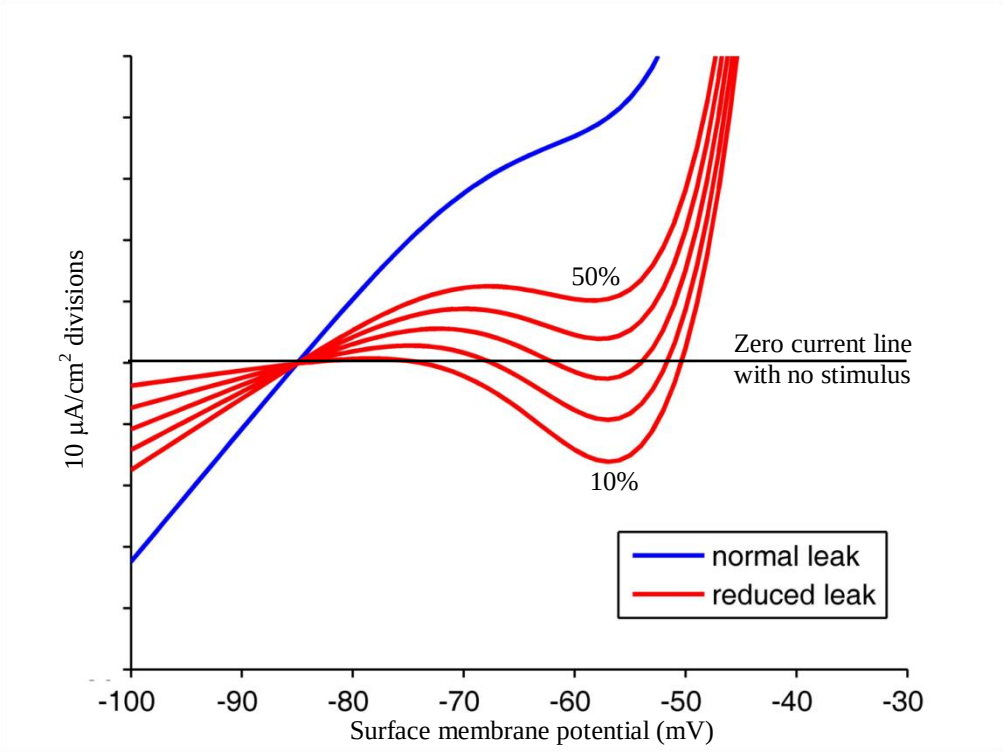

Figure 5.12 Effect of progressive reductions in leak on steadystate currents.
Steadystate current-voltage curves for the Cannon model are plotted with normal leak conductance (blue), and when leak is reduced down to 50%, 40%, 20%, 30% and 10% of normal (red). In the absence of a stimulus current, all curves pass upwards through the zero current line at -85mV (the 'normal' equilibrium potential). In addition the 30%, 20% and 10% curves pass upward through the zero current line between -50 and -60mV – a second, more depolarized stable equilibrium potential (the downward crossings of the zero current line are unstable equilibria since a small deviation in voltage from such a point drives current in a direction that promotes further deviation in the same direction, continuing the shift away from the point). Inactivation of sodium channels means that the membrane is inexcitable at the depolarized equilibrium. This type of phenomenon underlies attacks in familial periodic paralysis, and may also be the mechanism of transient weakness in severe Myotonia Congenita. A qualitative change in the behaviour of a system as a parameter is varied is known as a bifurcation in dynamical systems theory.

5.6 Methods

The models published by Barchi, Adrian & Marshall, and Cannon were implemented in Matlab and their differential equations solved with the Matlab function, ode15s. The parameters from the three models are summarised below in Table 5.1 and 5.2. The representation of an excitable membrane by an equivalent circuit containing parallel conductances (ion channels), capacitances (plasma membrane itself) and batteries (ionic

equilibrium potentials) is covered in textbooks on ion channels, electrophysiology, or biophysics (Jack, Noble et al. 1983; Johnston and Wu 1995; Hille 2001; Izhikevich 2007). Briefly, the surface and tubular membranes are represented as cylindrical, isopotential segments. In the Barchi model there is just one segment of membrane, representing a region of t-tubular membrane. The membrane potential, *V*, of a given segment was calculated by solving the differential equation for the capacitative current *CdV/dt*, which is the current remaining after accounting for transmembrane currents through ion channels and axial currents to/from connected segments of tubular or surface membrane. Net transmembrane current through sodium, potassium and leak channels is given by:

$$I_{\text{channels}} = G_{\text{max\_}Na} m^3 h (V - E_{Na}) + G_{\text{max\_}K} n^4 (V - E_K) + G_{\text{Leak}} (V - E_{Leak})$$

G_{max_ion} is the maximal conductance when all channels to that ion are open, G_{Leak}, is the leak conductance and E_{ion} is the equilibrium potential for an ion. Values for these parameters are given in Table 5.2. Values for the gating variables *m*, *h* and *n* are calculated by solving the differential equations below with parameters as shown in Table 5.1.

$$\frac{dm}{dt} = \alpha_m (1 - m) - \beta_m (m) \text{ where } \alpha_m = \frac{\bar{\alpha}_m (V - \bar{V}_m)}{1 - e^{-(V - \bar{V}_m)/K_{\alpha m}}};\ \beta_m = \bar{\beta}_m e^{-(V - \bar{V}_m)/K_{\beta m}}$$

$$\frac{dh}{dt} = \alpha_h (1 - h) - \beta_h (h) \text{ where } a_h = \bar{\alpha}_h e^{-(V - \bar{V}_h)/K_{\alpha h}};\ \beta_h = \frac{\bar{\beta}_h}{1 - e^{-(V - \bar{V}_h)/K_{\beta h}}}$$

$$\frac{dn}{dt} = \alpha_n (1 - n) - \beta_n (n) \text{ where } a_n = \frac{\bar{\alpha}_n (V - \bar{V}_n)}{1 - e^{-(V - \bar{V}_n)/K_{\alpha n}}};\ \beta_n = \bar{\beta}_n e^{-(V - \bar{V}_n)/K_{\beta n}}$$

Table 5.1 Gating parameters for sodium and potassium channels of published models

	Cannon	Barchi	Adrian & Marshall
$\bar{\alpha}_m$	0.288	0.25	0.2392
$\bar{\beta}_m$	1.38	2.5	2.08
$\bar{V}_m$	-46	-42 or -46	-42
$K_{\alpha m}$	10	10	10
$K_{\beta m}$	18	18	18
$\bar{\alpha}_h$	0.0081	0.0187	0.0156
$\bar{\beta}_h$	4.38	4.06	3.38
$\bar{V}_h$	-45	-41	-41
$K_{\alpha h}$	14.7	14.7	14.7
$K_{\beta h}$	9	7.6	7.6
$\bar{\alpha}_n$	0.0131	0.0275	0.0229
$\bar{\beta}_n$	0.067	0.1156	0.0961
$\bar{V}_n$	-40	-40	-40
$K_{\alpha n}$	7	7	7
$K_{\beta n}$	40	40	40

Note: Barchi states $\bar{V}_m$ is -42 in his table, but presents figures where it is shifted to -46. Adrian & Marshall adjusted their rate constants assuming a Q_{10} of 2.5 but quote the figures before adjustment – the figures here are presented after adjustment for ease of comparison with the other two models.

Table 5.2 Concentration gradients, conductances & resting potentials of published models

	Cannon		Barchi		Adrian & Marshall	
Concentration gradients and equilibrium potentials						
$[Na]_{out}$	150		not specified		not specified	
$[Na]_{in}$	24		not specified		not specified	
E_{na}	46.6		50		50	
$[K]_{out}$	4		not specified		4.5	
$[K]_{in}$	156		not specified		130	
$[E]_k$	-93.1		-70		-85	
$[Leak]_{out}$	$[K]_{out}+0.01[Na]_{out}$		not specified		not specified	
$[Leak]_{in}$	$[K]_{in}$		not specified		not specified	
E_{leak}	-85.0		-95		-95	
Resting potential of surface membrane						
Vrest	-85Mv		-95Mv		-95mV	
Limiting surface conductances (G_{max}) mS/cm^2 of surface membrane (%of total)						
Total	127.35				221.74	
G_{max_na}	150	(87.0%)	-		180	(81.2%)
G_{max_k}	21.6	(12.5%)	-		41.5	(18.7%)
G_{leak}	0.75	(0.4%)	-		0.24	(0.1%)
(Note: Barchi's model is assumed to represent the t-tubule not the surface)						
Limiting tubular conductances in mS/cm^2 of tubular membrane (%of total)						
Total	24.0		155.3		10.3	
$G_{max\_na\_tub}$	15	(62.5%)	110	(70.8%)	9.0	(87.6%)
$G_{max\_k\_tub}$	8.64	(36.0%)	45	(29.0%)	1.27	(12.4%)
G_{leak_tub}	0.375	(1.6%)	0.3	(0.2%)	0.0067	(0.7%)
(Note: Cannon specifies each tubular conductance as a fraction of the equivalent surface conductance : 0.1, 0.4, and 0.5 for Na, K and Leak conductances respectively)						
Capacitance per unit area of surface or tubule membrane (pF/cm^2)						
Surface	1		1		0.9	
Tubule	1		1		0.9	

Modification of the Adrian & Marshall model with Kir and ClC-1 conductances

The Adrian & Marshall model was modified as shown in Table 5.3 in order to introduce a late after-depolarization that would trigger myotonia after a train of impulses. Gating parameters for the sodium channel and delayed rectifier potassium channel were not changed.

Table 5.3 Comparison of parameters in the original and modified Adrian & Marshall models

	Original		**Modified**	
Concentration gradients and equilibrium potentials				
E_{na}	50		50	
$[K]_{out}$	4.5		4.0	
$[K]_{in}$	130		130	
$[E]_k$	-85		-88	
E_{leak}	-95		-	
E_{cl}	-		-88	
Resting potential of surface membrane				
Vrest	-95mV		-88 mV	
Limiting surface conductances (G_{max}) mS/cm^2 of surface membrane (%of total)				
Total	221.74		222.17	
G_{max_na}	180	(81.2%)	150	(81.0%)
G_{max_k}	41.5	(18.7%)	21.6	(18.7%)
G_{leak}	0.24	(0.1%)	-	-
G_{max_kir}	-	-	0.32	(0.04%)
G_{max_cl}	-	-	1.8	(0.27%)
(Note: G_{max_kir} varies with external K conc. The value here is for 4.0 mM K_{ext})				
Limiting tubular conductances in mS/cm^2 of tubular membrane (%of total)				
Total	10.3		10.4	
$G_{max\_na\_tub}$	9.0	(87.6%)	9.0	(86.8%)
$G_{max\_k\_tub}$	1.27	(12.4%)	1.27	(12.2%)
G_{leak_tub}	0.0067	(0.7%)	-	-
$G_{max\_kir\_tub}$	-	-	0.32	(0.95%)
$G_{max\_cl\_tub}$	-	-	0	(0%)

Simulation inward rectifier potassium (Kir) conductance

The inwardly rectifying potassium conductance of a macroscopic region of membrane was simulated with a published blocking-particle model (Standen and Stanfield 1978), as has previously been employed for modeling t-tubular potassium fluxes in mammalian muscle (Wallinga, Meijer et al. 1999). The model equations for g_{kir} (below) capture the closure of Kir channels with reduction of external potassium concentrations and at outward driving forces (Anumonwo and Lopatin 2010). Parameters for the equations are described in Table 5.4.

$$g_{kir}(V,[K_{ext}) = g_{max\_kir}\ ([K]_{ext}) \times y(V,[K]_{ext})$$

$$g_{max\_kir}([K]_{ext}) = \frac{G_k\ {K_R}^2}{{K_K}+\ {K_R}^2} \quad \text{where} \quad [K]_R([K]_{ext}) = [K]_{ext} e^{-\delta E_k F/RT}$$

$$y(V,K_{ext}) = 1 - \left[1 + \frac{K_S}{{[S]_i}^2 e^{2(1-\delta)VF/RT}}\left(1 + \frac{{[K]_R}^2}{K_K}\right)\right]^{-1}$$

Table 5.4 Parameters for inward rectifier conductance

Parameter	Value	Units	Description
δ	0.4	dimensionless	Fraction of electrical distance through membrane from outside where binding site is placed
G_k	1.5 / 1.5	mS/cm^2	Surface/Tubule max. conductance when binding sites fully occupied (calculated so that at resting potential g_{kir} is 20% of leak conductance in Cannon's model)
K_K	950	mM^2	Potassium dissociation constant at binding site
$[S]_i$	12	mM	Intracellular oncentration of blocking cation S
K_S	1	mM^2	Dissociation constant for blocking cation, S, at binding site

The derivation for the equations above can be found in the original paper (Standen and Stanfield 1978). Briefly, inward rectification is accounted for by competition for a binding site, *R*, between potassium and an intracellular cation, *S*, which is carried into the channel

and accumulates at the binding site (cannot pass out to the extracellular side) when driving force is outward. $[K]_R$ is the concentration of potassium at the binding site, R. $[S]_i$ is the intracellular concentration of the competing cation. It is now thought that not one, but several intracellular cations (the polyamines spermine, spermidine, and putrescine) are responsible for inward rectification of Kir channels (Anumonwo and Lopatin 2010).

Simulation of the skeletal muscle chloride channel, ClC-1

The macroscopic chloride conductance of a region of membrane containing ClC-1 channels was simulated by representing ClC-1 as a double-barreled channel with three gates. Each pore was given an independent fast gate with open probability, *f*, while a common slow gate with open probability, *s*, regulated both pores simultaneously. The fraction of conductive ClC-1 pores in the membrane was calculated as the product, *fs*. The rational for this simple multiplication of *f* and *s* derives from a consideration of the two conductive states a ClC-1 channel can adopt (Figure 5.13) – slow gate open and both fast gates open (state1), or slow gate open and only one fast gate open (state2).

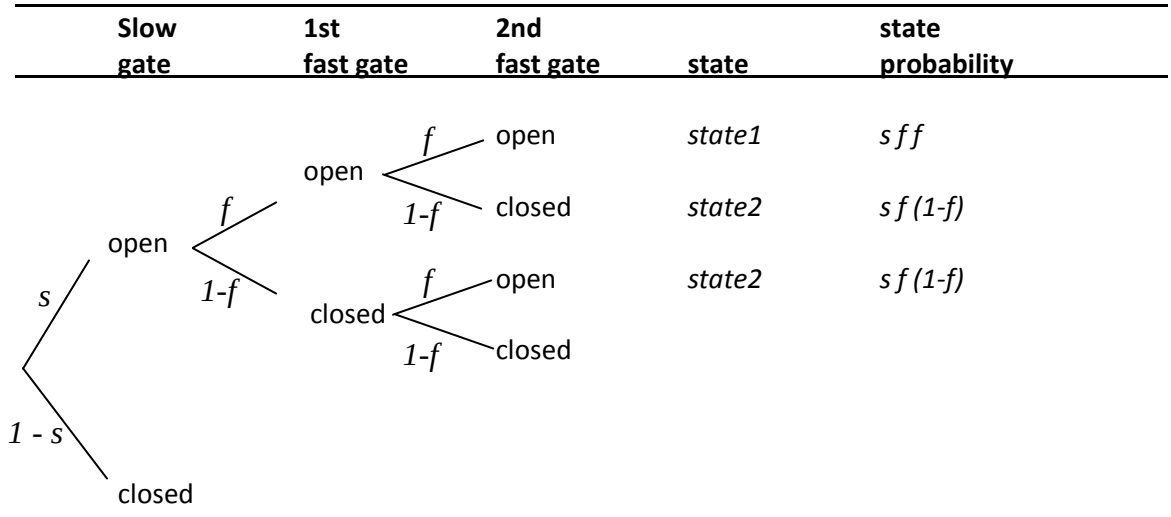

Figure 5.13 Probability tree diagram for ClC-1 fast and slow gate open probabilities.

State 1 has twice the conductance of state 2 (two open pores in state 1 vs. one open pore in state 2), but there are 2 ways of arriving at state 2 (one for each of the fast gates). Thus it follows that membrane chloride conductance is proportional to:

$2\,p(state1) + p(state2)$ where $p(state1) = s\,f\,f$

$p(state2) = 2sf\,(1 - f)$

The above simplifies as follows:

$$2\,s\,f\,f + 2sf\,(1 - f) = 2\,s\,f\,[\,f + (\,1 - f)\,] = 2\,s\,f$$

The factor of 2 can be removed without disturbing proportionality; the membrane chloride conductance, *g*, is equal to *sf* multiplied by a constant of proportionality and the 2 can be incorporated into that constant.

$$g = constant\ x\ 2sf = G_{max\_cl}sf$$ (*g*, *f*, *s* are functions of voltage and time)

The new constant of proportionality, G_{max_cl}, represents the maximal conductance of a region of membrane when all its ClC-1 channels have all of their gates open, and the product *sf* gives the fraction of ClC-1 pores that are conductive (*sf* = 1 when all the pores are conductive and 0 when all are non-conductive) at a given time and membrane potential.

The fast and slow gate probabilities, *s* and *f*, were modelled as functions of voltage and time using parameters derived from voltage clamp experiments on human ClC-1 heterologously expressed in *Xenopus* oocytes. The functions, $s(V,t)$ and $f(V,t)$, were defined implicitly by two first order differential equations:

$$\frac{ds}{dt} = \frac{s_\infty(V) - s(V,t)}{\tau_s(V)} \quad \text{and} \quad \frac{df}{dt} = \frac{f_\infty(V) - f(V,t)}{\tau_f(V)}$$

The time constants (τ_s and τ_f) and the steadystate open probabilities (s_∞ and f_∞) in the above equations are voltage dependent; their functional representation in Matlab was based on data in the literature (Accardi and Pusch 2000). When voltage is fixed $1/\tau_f$ and $1/\tau_s$ are constants of proportionality relating the rate of change of the fast and slow gate open probabilities respectively to the deviation of those open probabilities from their steadystate values (s_∞ and f_∞) at that voltage.

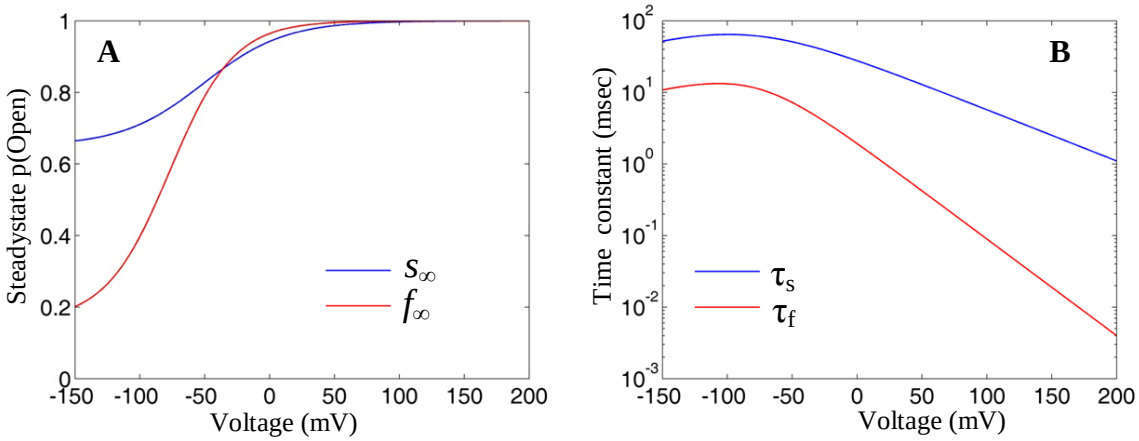

Figure 5.14 Steadystate open probabilities and time constants for ClC-1 fast and slow gates.
Fast and slow gate steadystate open probability functions **(A)** and time constants **(B)** were reconstructed in Matlab using parameters reported in the literature found by voltage clamp of ClC-1 heterologously expressed in *Xenopus* oocytes (Accardi and Pusch 2000). The steadystate open probabilities are given by the following Boltzmann functions:

$$s_\infty(V) = 0.65 + \frac{1-0.65}{1+\exp\left(\frac{0.81(-51-V)F}{RT}\right)} \qquad f_\infty(V) = 0.16 + \frac{1-0.16}{1+\exp\left(\frac{1.08(-77-V)F}{RT}\right)}$$

where R is the gas constant, F is Faraday's constant, T is a temperature of 295 Kelvin.

The time constant functions were created by trial and error to yield curves that closely approximate the data in the figure from Accardi & Pusch with the following equations:

$$\tau_s(V) = \frac{1000}{a+b} \quad \text{where} \quad a = 2.8\exp\left(-0.3\,\frac{VF}{RT}\right);\ b = \frac{\exp\left(0.42\,\frac{VF}{RT}\right)}{0.03}$$

$$\tau_f(V) = \frac{1000}{c+d} \quad \text{where} \quad c = 20\exp\left(-0.25\,\frac{VF}{RT}\right);\ b = \frac{\exp\left(0.79\,\frac{VF}{RT}\right)}{0.002}$$

In order to represent the characteristic inward rectification displayed by currents through ClC-1, a heuristic approach based on the authors own recordings was adopted. Four high

quality whole cell patch clamp recordings from HEK293T cells expressing wildtype ClC-1 (Figure 5.15) were used as the inspiration for the rectification function, *r(V):*

$$r(V, E_{Cl}) = \begin{cases} 1, & V \leq E_{Cl} \ \ (inward\ or\ zero\ driving\ force) \\ 0.6e^{-0.01(V - E_{Cl})} + 0.07, & V > E_{Cl} \ \ (outward\ driving\ force) \end{cases}$$

Where V is membrane potential and E_{Cl} is the chloride equilibrium potential. The term (V-E_{Cl}) is the driving force for chloride across the membrane.

For each cell, the conductance at different voltages with all channels fully open was calculated by dividing the instantaneous current at different voltages after a prepulse to +60mV by the driving force at each voltage (chloride reversal potential was calculated from the internal and external solutions to be -36mV). The conductances for each cell were normalized, and plotted against the driving force (Figure 5.15).

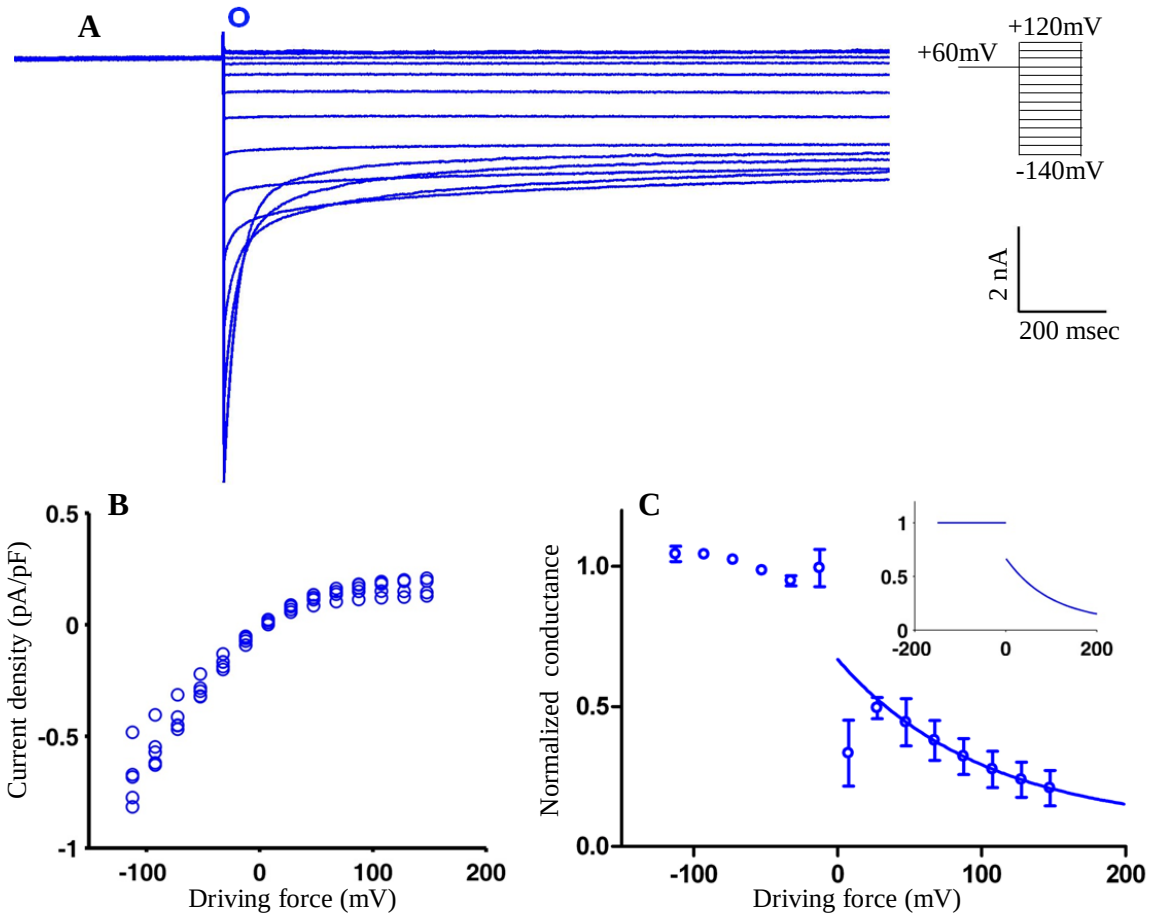

Figure 5.15 normalized conductance of the open ClC-1 channel.
(A) Raw current traces from a HEK293T cell expressing wildtype ClC-1. **(B)** Instantaneous currents (time point indicated by blue circle above the traces) at different voltages after a pre-pulse to +60mV plotted against driving force (V - E_{Cl}) for 4 different cells. The +60 mV pre-pulse was used to maximally open all the ClC-1 gates so that the instantaneous current during the subsequent voltage step reflects the conductance of the open pores at each test voltage. **(C)** Mean conductance ± S.E.M. (instantaneous current divided by driving force) from the 4 cells plotted against driving force. For positive driving forces conductance of the open channel falls (inward rectification) and its decay was fitted with a single exponential: $y = 0.6\exp(-0.01x) + 0.07$ (parameters rounded to a single significant digit). The fit was performed in GraphPad Prism using the last 6 (most depolarized) data points. Inset is the rectification function adopted for the simulation, *r(V)*, against driving force. It is set to 1 for negative and zero driving force and to the exponential for positive driving force.

In summary, the macroscopic current, I_{Cl}, through a membrane containing ClC-1 was simulated as the product of rectification, conductance and driving force:

$$I_{Cl}(V,t) = r(V,E_{Cl}) \cdot g_{cl}(V,t) \cdot (V - E_{Cl})$$

Rectification, *r*, was a function of voltage and the chloride equilibrium potential:

$$r(V,E_{Cl}) = \begin{cases} 1, & V \le E_{Cl} \ \ (inward\ or\ zero\ driving\ force) \\ 0.6e^{-0.01(V-E_{Cl})} + 0.07, & V > E_{Cl} \ \ (outward\ driving\ force) \end{cases}$$

Conductance, *g*, was the product of a constant, G_{max}, (used to set the density of channels in the membrane) and opening probabilities *f* and *s*:

$$g_{cl} = G_{max\_cl} \cdot s(V,t) \cdot f(V,t)$$

Opening probabilities for the fast and slow gates, *f* and *s*, were functions of voltage defined implicitly by differential equations, which were expressed in terms of steadystate functions of voltage, and time constant functions:

$$\frac{df}{dt} = \frac{f_\infty(V) - f(V,t)}{\tau_f(V)}, \qquad \frac{ds}{dt} = \frac{s_\infty(V) - s(V,t)}{\tau_s(V)}$$

$$s_\infty(V) = 0.65 + \frac{1-0.65}{1+\exp\left(\frac{0.81(-51-V)F}{RT}\right)}, \qquad f_\infty(V) = 0.16 + \frac{1-0.16}{1+\exp\left(\frac{1.08(-77-V)F}{RT}\right)}$$

$$\tau_s(V) = \frac{1000}{a+b} \quad where \quad a = 2.8\,exp\left(-0.3\,\frac{VF}{RT}\right); \quad b = \frac{exp\left(0.42\,\frac{VF}{RT}\right)}{0.03}$$

$$\tau_f(V) = \frac{1000}{c+d} \quad where \quad c = 20\,exp\left(-0.25\,\frac{VF}{RT}\right); \quad b = \frac{exp\left(0.79\,\frac{VF}{RT}\right)}{0.002}$$

5.7 Results

Comparison of simulated ClC-1 with real ClC-1

A simulated voltage clamp experiment is illustrated in Figure 5.16 (below) using the same voltage protocol as was employed in the whole cell patch clamp experiments presented in Chapter 3. Each gate was initialized to its steadystate value at the holding potential. The chloride equilibrium potential was set to -36mV. The in-built Matlab ordinary differential equation solver, ode15s, was used to solve the differential equations representing the fast and slow gates. The resulting set of values for *s* and *f* at each time point were used together with the rectification function, the voltage at each time point, the equilibrium potential, and a maximal membrane conductance of 1 to reconstruct the chloride current at each time point. No attempt was made to scale the magnitude of the simulated chloride current for these simulations, since the main point of interest was the general form and kinetics of the currents. The simulation did not include a representation of series resistance error. Appropriate scaling of the chloride currents becomes important when the channel is inserted into a membrane with other conductances.

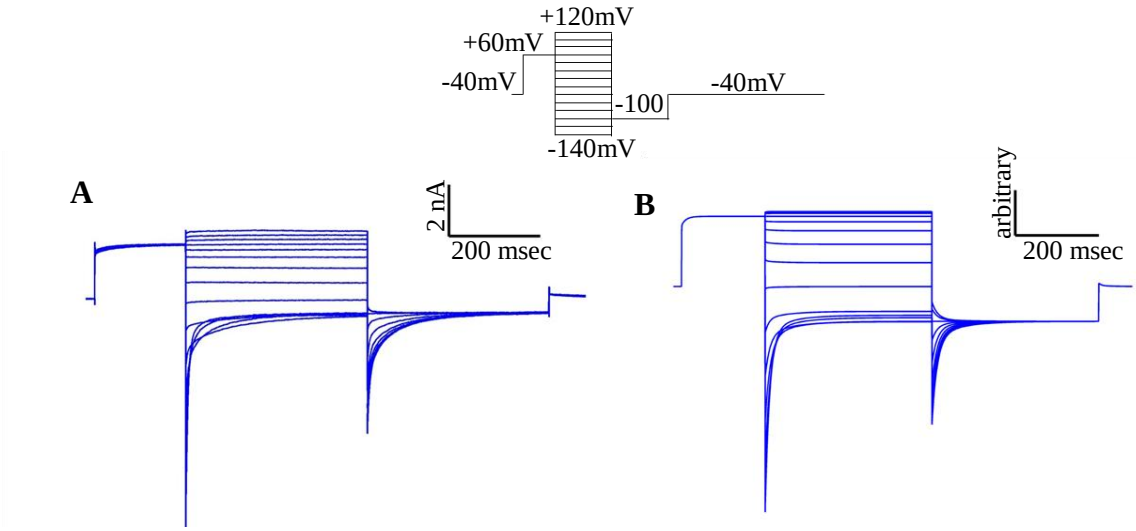

Figure 5.16 Current traces from ClC-1 expressed in a HEK293T cell and from the model channel. **(A)** Raw current traces from one HEK293T cell expressing wildtype ClC-1 recorded by whole cell patch clamp. **(B)** Simulation ClC-1 current. In the simulation there is no leak current, capacitative artefact or series resistance error, voltage steps are instantaneous and voltage clamp is perfect.

The simulation produced currents that were similar to those observed from ClC-1 in HEK293T cells. The model's kinetics were slightly faster and there was slightly less overlap of the deactivating currents at hyperpolarized potentials. Nevertheless the simulation is a better approximation to the non-linear, voltage- and time-dependent currents through ClC-1 than the linear, time-independent and voltage-independent conductance traditionally used to represent ClC-1 in models of myotonic muscle.

The opening probability curves from human ClC-1 in HEK293T cells and from the simulation ClC-1 were similar, although the model is slightly more conductive at hyperpolarized potentials (Figure 5.17).

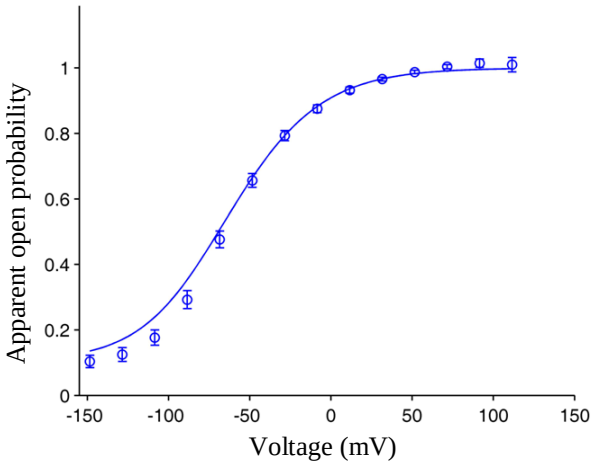

Figure 5.17 Apparent open probabilities of model ClC-1 and real ClC-1.
Control data points from chapter 3 (means ± S.E.M. from 8 HEK293T cells), were plotted together with the combined steadystate open probability of the ClC-1 model (continuous line). Error bars obscured by symbol in places. The apparent open probability of the real ClC-1 was obtained by normalizing the tail currents at -100 mV after pre-pulses to different voltages as discussed in chapter 3. For the model the apparent open probability is calculated as *sf*, the product of the steadystate open probabilities of the fast and slow gates.

T-tubular asynchrony is sufficient for myotonia in large diameter model fibres

A major aim of this chapter was to assess simulated normal and variant ClC-1 channels in a model of skeletal muscle capable of sustained myotonic discharges. Adrian & Marshall commented that a large reduction of the leak conductance (to 10% of normal) elicited rather few post-stimulus myotonic discharges in their 70µm diameter model muscle fibre (see Figure 5.7). One way to exacerbate myotonia was to alter the sodium channel kinetics (Adrian and Marshall 1976). Another potential source of variability in the severity of myotonia is muscle fibre diameter. The larger the diameter of the muscle fibre, the larger the capacitance of the tubular membrane associated with each unit area of surface membrane and the more asynchrononous the tubular action potential should be. Figure 5.18 (below) summarizes results from a new experiment using the original Adrian & Marshall model, in which fibre diameter was increased from 70 to 100µm in the context of

50% reduced leak conductance using a similar experimental protocol as presented in Figure 5.7. This time potassium accumulation was disabled in order to test the hypothesis that myotonia could theoretically arise purely from asynchrony between the surface and tubular membranes. A 150 msec stimulus of 100 μA/cm^2 produced a sustained myotonic discharge that lasted for as long as the experiment was continued.

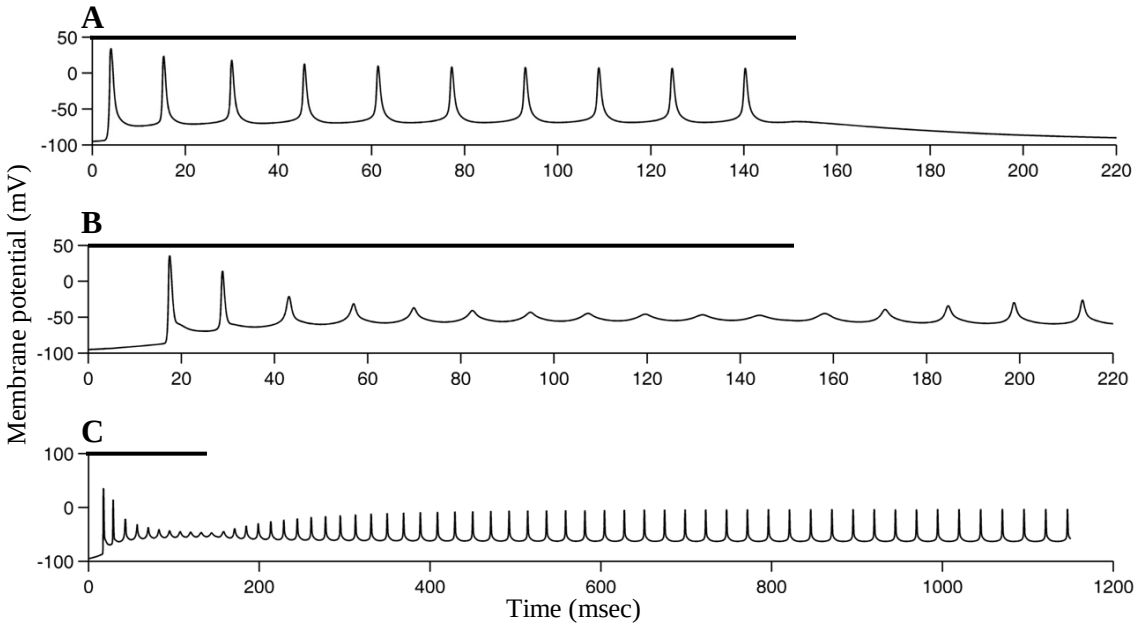

Figure 5.18 Increasing muscle fibre diameter exacerbates myotonia in the Adrian & Marshall model
A 4.5 mm long model fibre divided into15 segments each containing 3 t-tubule compartments was stimulated at one end with a constant current pulse for 150 msec starting at t = 0. A black bar above each plot indicates the period of stimulation The membrane potential in mV of the middle (7th) segment is plotted against time in msec. **(A)** Copy of Figure 5.7B showing a 70 μm diameter fibre with 50% of normal leak conductance stimulated with 200 μA/cm^2. No myotonia occurs. **(B)** Diameter increased to 100 μm. Same time-scale as **(A)**. The stimulus was 100 μA/cm^2. C Same experiment as **(B)** viewed on a longer time-scale. Self-sustaining action potentials continued after the end of the stimulus for as long as the simulation was run (1200 msec). The myotonia was independent of potassium accumulation, which was disabled for the experiments in **(B)** and **(C)** (but not for **A**).

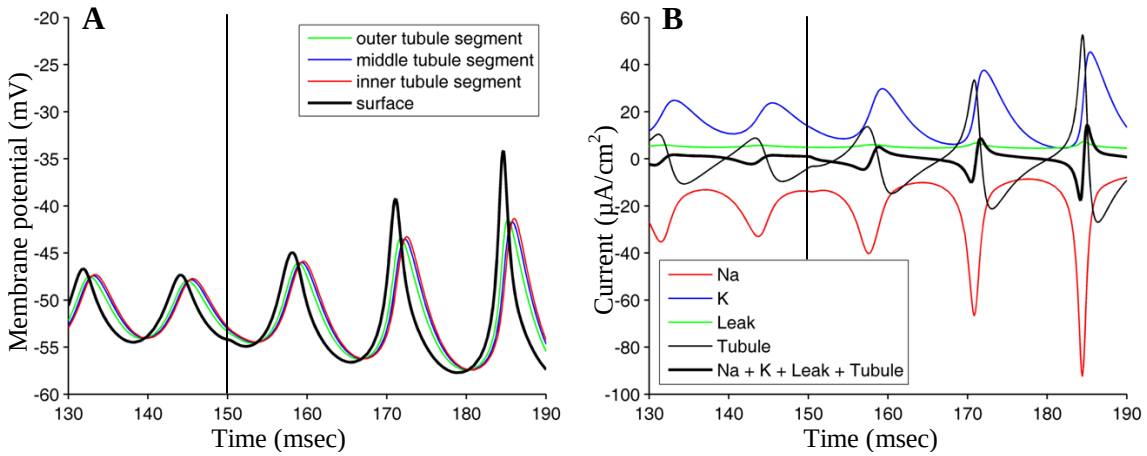

Figure 5.19 T-tubular asynchrony and surface membrane currents during myotonia
Membrane potentials and currents in the middle of the muscle fibre from the simulation experiment presented in Figure 5.18 **(B)** and **(C)** shortly before and after the end of stimulation at 150 msec (vertical black lines). **(A)** T-tubule action potentials (coloured) are delayed relative to surface membrane action potentials (black). **(B)** Currents at the surface membrane, including net tubular current (the current across the access resistance). Immediately after the 150 msec mark, the sum of the inward currents (tubular + sodium) exceeds the sum of the outward currents (sodium + leak) as can be seen from the total (thick black line is below zero). This is because the potassium current is diminishing and the leak is abnormally small (simulating abnormal ClC-1), while the net tubular current (the current across the access resistance) is still inward. The resultant depolarization of the membrane re-activates sodium channels (the sodium current immediately after the 150 msec mark starts off heading towards zero, but then re-activates, turning inward again and generating an action potential).

In the 100μm diameter fibre (Figure 5.19) the tubular action potential is delayed long enough that the inward current arriving at the surface from the tubule (the access resistance current) is still present at a time when outward surface currents have become too small to accommodate it (owing to closure of the delayed rectifier and an abnormally small leak conductance). Current must therefore flow across the surface capacitance, depolarizing the cell and reactivating sodium channels. The process is independent of potassium accumulation in the tubule.

The late after-depolarization in the original and modified Adrian & Marshall models

Adrian & Bryant hypothesized that accumulation of potassium in t-tubules combined with membrane hyperexcitability to trigger myotonia after a train of action potentials (Adrian

and Bryant 1974). *In vivo*, muscle action potentials are elicited by repetitive, brief current influxes through acetylcholine receptors at the motor endplate. In the original model myotonia cannot be elicited by repetitive stimulation with brief current pulses because there is no late after-depolarization (Figure 5.20). The original model was therefore modified to promote myotonia. Potassium accumulation was increased by raising the abundance of delayed rectifier channels in the tubular membrane to match Cannon's model, and the equations for potassium diffusion out of the tubule were changed to those from Cannon's model. The resting membrane potential was coupled to the potassium equilibrium potential by insertion of an inward rectifier potassium conductance. After 50Hz repetitive stimulation the modified model exhibits a late after-depolarization whose size is dependent upon the number of action potentials (Figure 5.21 A and C). When the chloride conductance of the modified model is reduced, the late after-depolarization triggers myotonia after the period of stimulation (Figure 5.21 B and D). The dependence of the late after-depolarization on potassium accumulation and chloride conductance is further illustrated in Figure 5.22.

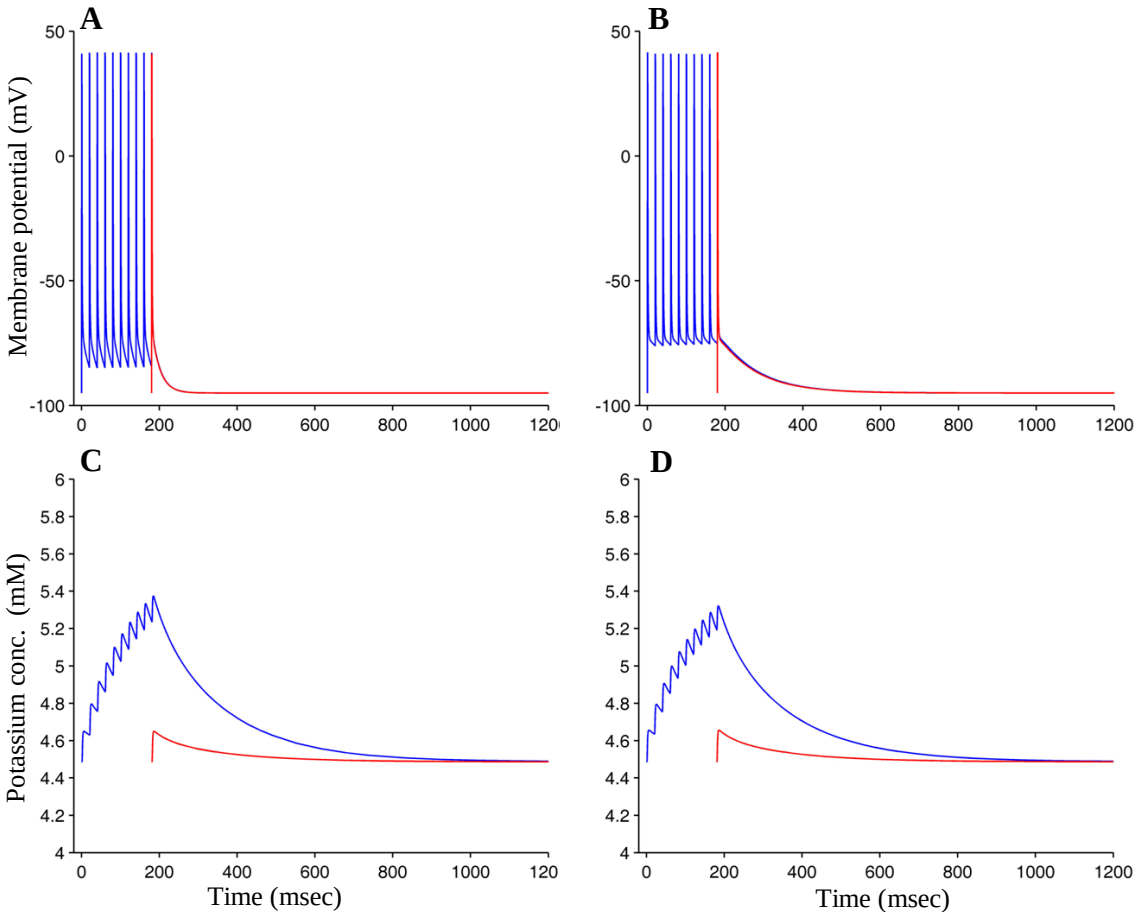

Figure 5.20 After-depolarization in the original Adrian & Marshall model
A single 300µm long, 70 µm diameter segment of the original Adrian & Marshall model containing 3 t-tubule compartments was stimulated at 50 Hz with 10 square current pulses of 0.2 msec duration and 500 µA/cm2 intensity (blue). Superimposed with the final pulse is the response to a single stimulus (red). Upper panels show surface membrane potential when the leak is normal **(A)** or reduced to 10% of normal **(B)**. Lower panels show potassium concentration in the outer t-tubule segment in the normal **(C)** and reduced leak **(D)** conditions. Reducing the leak prolongs the early after-depolarization (compare **A** and **B**) but potassium accumulation caused during repetitive stimulation has almost no effect on the after-depolarization (compare red and blue traces).

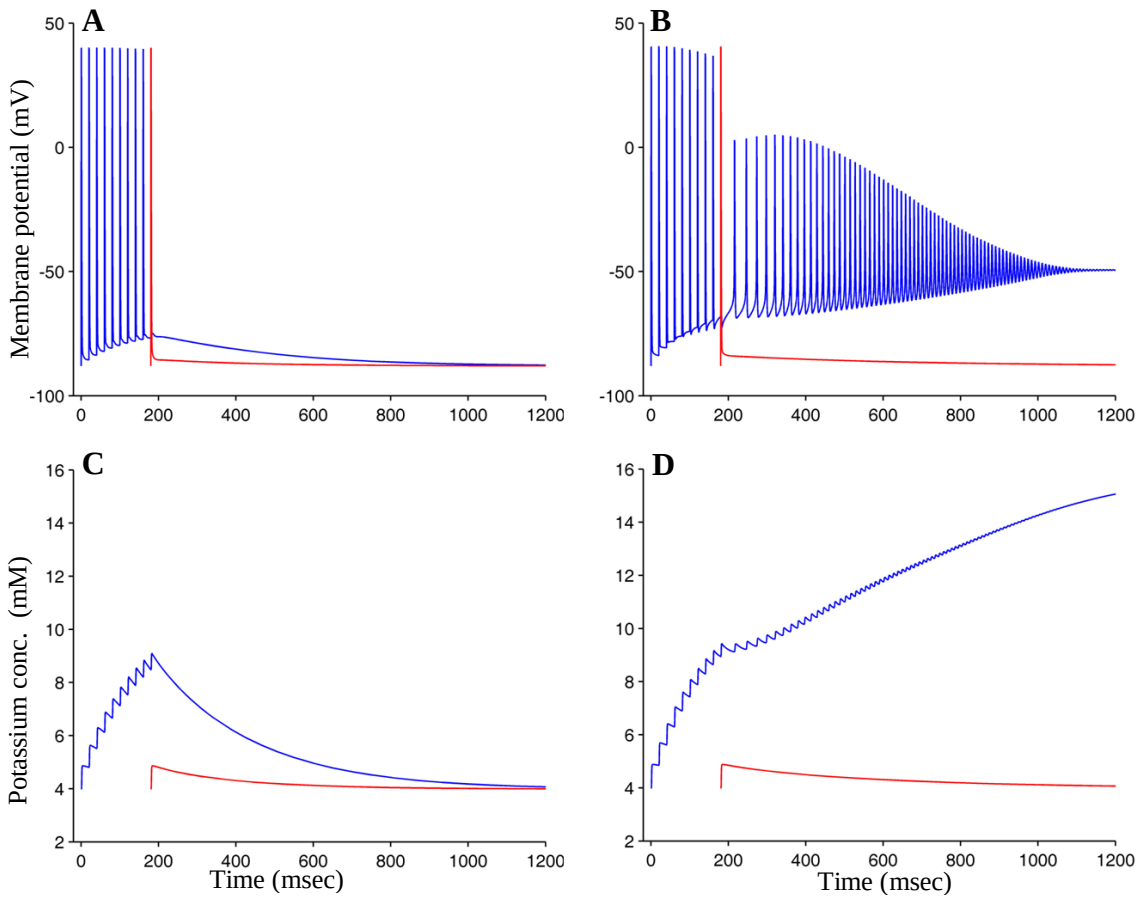

Figure 5.21 After-depolarization in the modified Adrian & Marshall model
A single 300 µm long, 70 µm diameter segment of the modified Adrian & Marshall model containing 3 t-tubule compartments was stimulated at 50 Hz with 10 square current pulses of 0.2 msec duration and 500 µA/cm2 intensity (blue). Superimposed with the final pulse is the response to a single stimulus (red). Upper panels show surface membrane potential when the chloride conductance is normal **(A)** or reduced to 10% of normal **(B)**. Lower panels show potassium concentration in the outer t-tubule segment for normal **(C)** and reduced chloride conductance **(D)**. When chloride conductance is normal, potassium accumulation during repetitive stimulation (**C**, blue) causes a late after-depolarization (**A**, blue). When chloride conductance is reduced to 10% potassium accumulation during repetitive stimulation triggers a myotonic discharge (**B** and **D**).

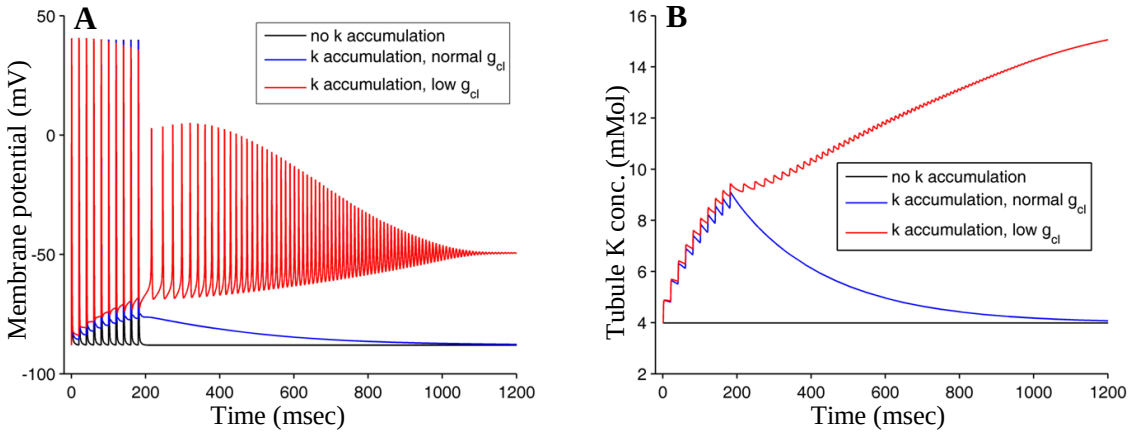

Figure 5.22 Dependence of late after-depolarization on K concentration and Cl conductance
Surface membrane potential **(A)** and potassium concentration in the most peripheral t-tubule segment **(B)** during a simulated brief, strong muscle contraction. A single 300µm long, 70 µm diameter segment of the modified Adrian & Marshall model containing 3 t-tubule compartments was stimulated at 50 Hz with 10 square current pulses of 0.2 msec duration and 500 µA/cm2 intensity (one pulse every 20msec starting at t = 0). When potassium accumulation was disabled (black) there was no late after-depolarization. When potassium was allowed to accumulate in t-tubules in the context of normal chloride conductance (blue) a late after-depolarization followed the last action potential. When the surface membrane chloride conductance was reduced to 10% of normal, myotonia followed the final stimulated action potential and the membrane settled on a new, depolarized resting potential.

Response to long duration stimuli

Both the original model and the modified version differ from the experiments on muscle fibres from normal and myotonic goats in that the normal, non-myotonic models fire repetitively during stimulation over a certain range of injected current (Figure 5.23), whereas real muscle fibres from normal goats fired only once (Adrian and Bryant 1974).

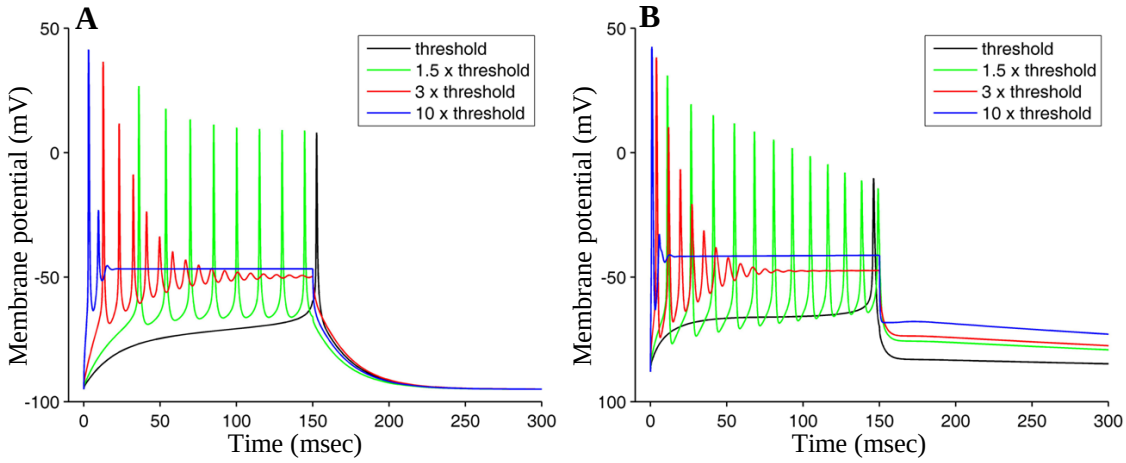

Figure 5.23 Model responses to long duration stimuli
The original **(A)** and modified **(B)** Adrian & Marshall models were stimulated from resting potential at t = 0 msec with 150 msec duration square current pulses of different intensities (shown in different colours). Each model was set up with a single surface segment 70 µm in diameter containing 3 t-tubule segments. The smallest 150 msec duration pulse stimulus that would elicit an action potential (the threshold) was 6.0 µA/cm^2 for the original model and 15.3 µA/cm^2 for the modified model. Both models fired repetitively in response to stimuli 1.5 and 3 x threshold. The latency to the first action potential decreased and the spike amplitude increased with increasing stimulus intensity. Potassium accumulation during stimulation delayed the return to resting potential after stimulus offset in the modified model.

Reducing the surface leak conductance of the original model or surface chloride conductance of the modified model to 10% of normal produced a fall in threshold current for eliciting an action potential (from 6.0 to 1.7 µA/cm^2 in the original model and from 15.3 to 6.4 µA/cm^2 in the modified model). In the modified model, action potentials during stimulation were higher frequency and post-stimulus myotonic action potentials were more sustained than in the original model (Figure 5.24).

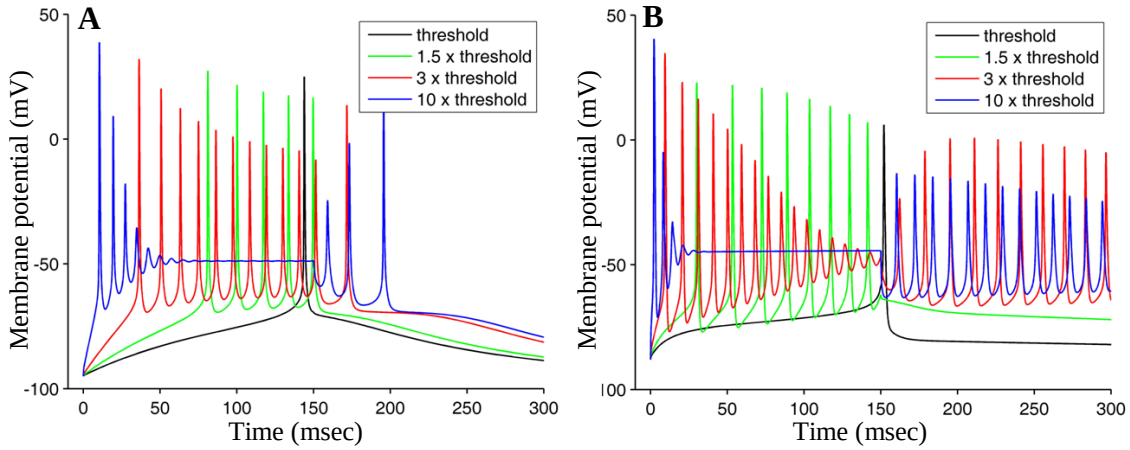

Figure 5.24 Responses to long duration stimuli when leak or chloride conductance is reduced
The original **(A)** and modified **(B)** Adrian & Marshall models were stimulated from resting potential at t = 0 msec with 150 msec duration square current pulses of different intensities. The leak or chloride conductance was reduced to 10% of normal in both. Each model was set up with a single surface segment 70 µm in diameter containing 3 t-tubule segments. The smallest 150msec duration pulse stimulus that would elicit an action potential (the threshold) was 1.7 µA/cm^2 for the original model and 6.4 µA/cm^2 for the modified model. Only two post-stimulus myotonic discharges occurred in the original model, whereas sustained repetitive myotonic discharges could be elicited in the modified model.

Simulating specific defects of ClC-1

The chloride conductance in the modified Adrian & Marshall model can be adapted so that under voltage clamp it passes currents that approximate those passed by a specific ClC-1 variant. This simulated variant can then be tested in the modified Adrian & Marshall model to complement clinical, genetic and electrophysiological enquiry into pathogenicity. To illustrate the process, the question whether slowing of gating altered kinetics alone is sufficient to elicit myotonia is addressed below, and then the effects of the S289G variant are simulated.

Figure 5.25 illustrates the effect of slowing ClC-1 gating. Even a 100,000-fold slowing of both the fast and the slow gates was insufficient to elicit myotonia in the modified Adrian & Marshall model. However, when the abundance of chloride channels at the surface

membrane was reduced to 15% of normal, which alone did not elicit myotonia after a brief stimulus, an additional 100-fold slowing of the fast gate tipped the fibre over the threshold for post-stimulus myotonic discharges.

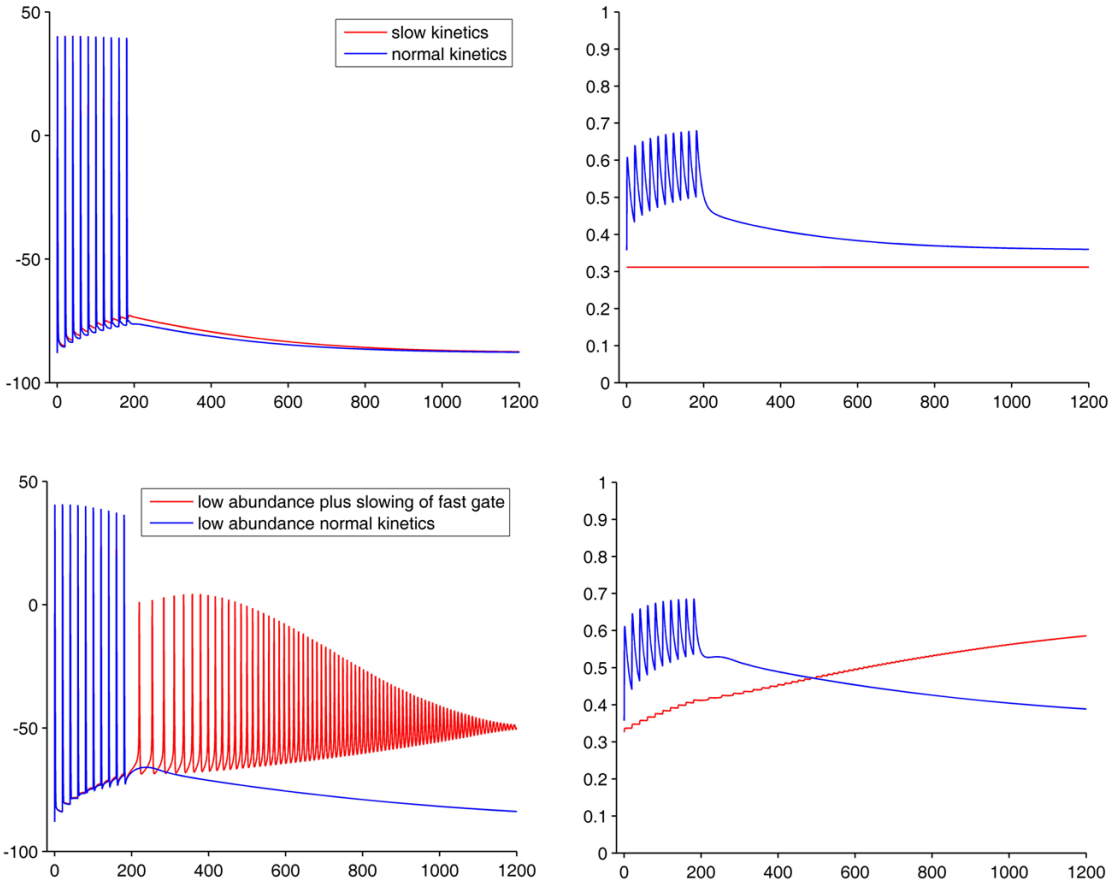

Figure 5.25 Effect of slow ClC-1 kinetics
Surface membrane potential **(A, C)** and overall ClC-1 open probability **(B, D)** during a simulated brief, strong muscle contraction. A single 300 µm long, 70 µm diameter segment of the modified Adrian & Marshall model containing 3 t-tubule compartments was stimulated at 50 Hz with 10 square current pulses of 0.2 msec duration and 500 µA/cm2 intensity (one pulse every 20 msec starting at t = 0). When ClC-1 abundance was normal the reduction in opening probability **(B)** caused by severe (100,000 fold) slowing of both gates did not cause myotonia **(A)**. When ClC-1 abundance was reduced close to threshold for myotonia (15% of normal) the additional drop in open probability caused by 100x slowing of the fast gate alone **(D)** produced myotonia **(C)**.

The S289G variant of ClC-1 presented in Chapter 3 alters both the kinetics and steadystate voltage dependence of ClC-1. The kinetic effect is not a simple slowing because the rate of channel deactivation is relatively fast at negative potentials but its rate of activation at

positive potentials is slow – an inversion of the normal situation. The functional effects of S289G were approximated by shifting voltage dependence of the simulation fast gate, and inverting and slowing the fast gate kinetics (Figure 5.26).

The simulation S298G variant elicited myotonia in the modified Adrian & Marshall model (Figure 5.27, red). The kinetic abnormality of the fast gate and the shift in fast gate steadystate voltage dependence in the simulated S289G variant were tested independently. The shift in voltage dependence was both necessary and sufficient for myotonia in the model; the abnormalities in fast gate kinetics did not cause myotonia (Figure 5.27 black and blue).

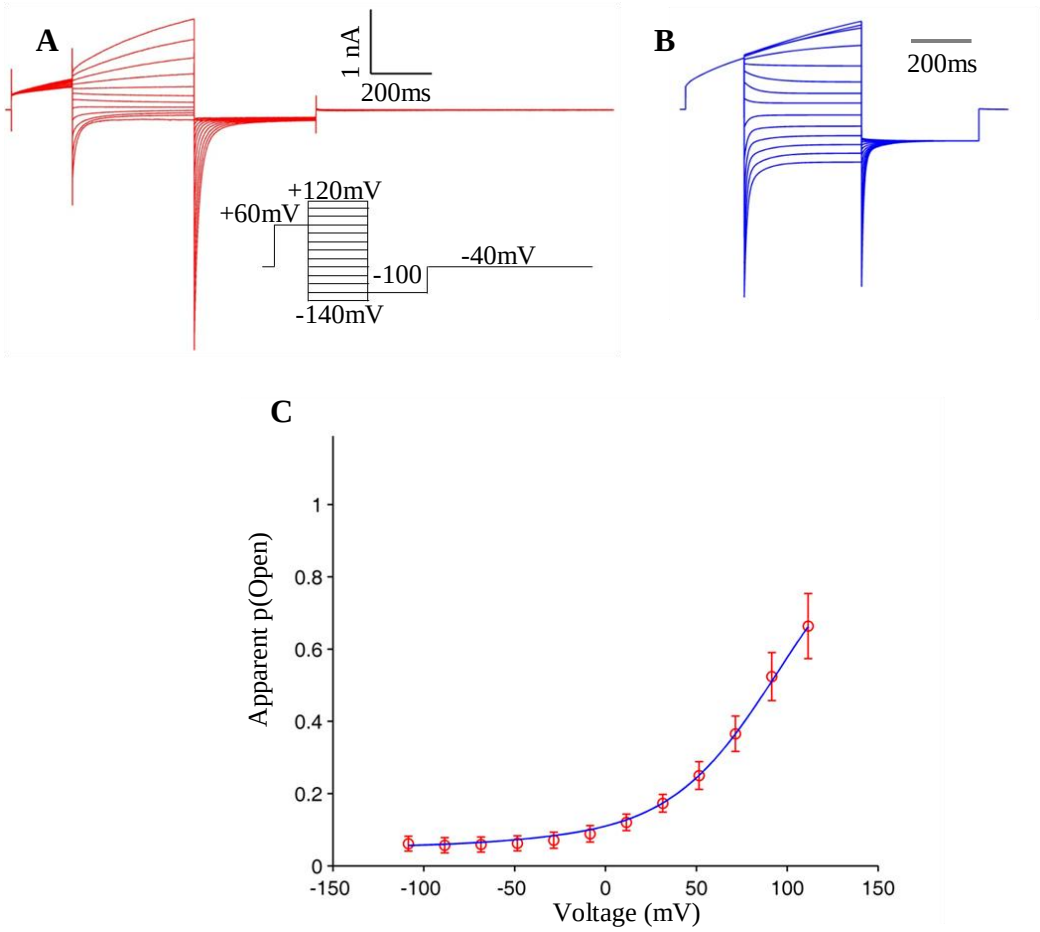

Figure 5.26 Simulation of the S289G mutation in ClC-1.
(A) Copy of the current traces shown in figure 3.10 from human ClC-1 homodimers carrying the S298G variant recorded by whole cell patch clamp in a HEK293T cell. **(B)** Simulation of currents from a membrane containing the S298G mutant channel. C. Red data points are normalized tail currents (mean ± S.E.M.) from 5 HEK293T cells expressing S298G ClC-1 channels. The continuous blue line is the apparent open probability of the simulation. The mutation slows the rate of channel activation during depolarization but deactivating currents during the -100 mV tail current step remain relatively fast. There is also a depolarizing shift in the steadystate apparent opening probability. The shift in voltage dependence was introduced by changing the V50 of the fast gate from -77 to +95. The kinetic effects were simulated by inverting the fast gate time constant function so that the fast gate kinetics get slower with depolarization instead of faster, and by slowing the gate by a factor of 100.

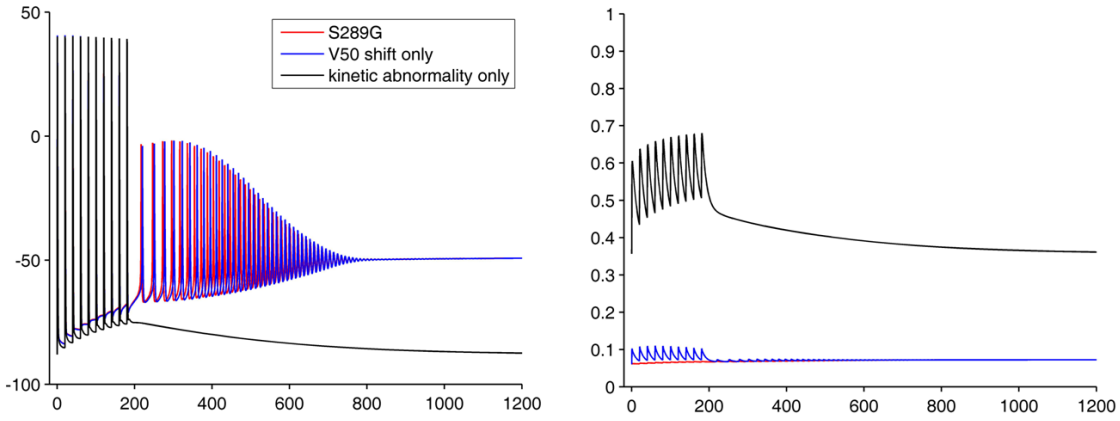

Figure 5.27 In silico analysis of the S289G variant
Membrane potential **(A)** and overall open probability of ClC-1 **(B)** in the modified Adrian & Marshall model containing the simulated ClC-1 S289G variant (red) or its V50 (blue) or kinetic (black) components in isolation. A single 300µm long, 70 µm diameter segment of the modified Adrian & Marshall model containing 3 t-tubule compartments was stimulated at 50 Hz with 10 square current pulses of 0.2 msec duration and 500 µA/cm2 intensity (one pulse every 20msec starting at t = 0). The simulated S289G mutant produced myotonia (**A**, red) by reducing ClC-1 overall open probability to around 0.05 (**B**, red). The shift in V50 was both necessary and sufficient for the effect - it produced myotonia when kinetics were normal (blue). The kinetic abnormality could no elicit myotonia when V50 was normal (black).

5.8 Summary of results

New experiments were conducted with a well-known model of skeletal muscle (the Adrian & Marshall model) showing that variation in the diameter of muscle fibres within the physiological range could lead to differences in the propensity of those fibres to myotonia in the context of reduced chloride conductance. Specifically, a 100 µm diameter model myofibre was more susceptible to myotonia than a 70 µm diameter myofibre owing to more marked asynchrony between tubular and surface action potentials in the former.

It was shown that the Adrian & Marshall model lacks a late after-depolarization, so that although repetitive action potentials lead to t-tubular potassium accumulation this accumulated potassium does not affect return of the sarcolemma to resting potential.

Introduction of an inward rectifier potassium channel into the model remedied this situation by coupling resting potential to the potassium equilibrium gradient.

The model was further modified by designing and incorporating a ClC-1 conductance that contains representations of the protopore and common gating processes as well as rectification. Addition of the new ClC-1 enabled an exploration of the relative effects of altered kinetics and altered voltage dependence of ClC-1 on the liability to myotonia. The results suggest that pure slowing of channel gating is not sufficient to produce myotonia, but that slowing could exacerbate the myotonic propensity caused by reduced channel abundance or a shift in voltage dependence. Finally the model was used to show that the pathogenicity of S289G is more likely to arise from the shift in voltage dependence than from the kinetic abnormality.

Chapter 6 Discussion

6.1 The HEK293T assay for CLCN1 sequence variants

Eight naturally-occurring CLCN1 sequence variants of uncertain clinical significance were tested for pathogenicity by voltage clamp of homodimeric mutant channels in HEK293T cells. The HEK293T assay focused on detection of altered channel function, but was rather insensitive to altered current density, in part because of the wide range of normal current densities observed with wildtype CLCN1 in the transfection-based expression system. Three of the variants (G276D, G523D and S289G) were classified as pathogenic, but pathogenicity could not be proven for the others.

The interpretation of loss of voltage-dependence

HEK293T cells expressing homodimeric G276D or G523D variant ClC-1 channels yielded small, voltage-independent chloride currents that were indistinguishable from leak currents. It is possible that some of the voltage-independent current recorded from these cells was carried by chloride ions through variant ClC-1 channels in which the broken gating processes left the pores partially conductive (a subtotal loss of function). Nonetheless the comparison against wildtype leaves little doubt that these two variants are pathogenic. G276D variant lies in the G helix. Although this helix does not contribute directly to the dimer interface it may still play a role in the common gating process (Duffield, Rychkov et al. 2003). A number of pathogenic variants have been reported in the G helix including T261M (Mailander, Heine et al. 1996), T268M (Duffield, Rychkov et al. 2003), and C271R (Fialho, Schorge et al. 2007). G276D was initially identified in a compound heterozygote and so appeared to be acting recessively (Fialho, Schorge et al. 2007). However it was

subsequently identified in two dominant pedigrees, consisting of an affected parent and an affected child each with single mutations. Symptom onset for one of the probands was during pregnancy; exacerbation of Myotonia Congenita in pregnancy and the possible roles of progesterone and oestrogen are addressed in chapter 4 and discussed later in this chapter. The individuals have typical Myotonia Congenita including the warm-up phenomenon.

G523D is in the O-helix of ClC-1. This helix does not participate directly in the dimer interface. Another known pathogenic ClC-1 variant, A531V, also lies in the O helix (Sun, Tranebjaerg et al. 2001). The patient harbouring G523D has a single copy, the other allele being wildtype. The clinical findings of typical Myotonia Congenita and heterozygosity with a normal allele raise the possibility of a dominant negative interaction. However the referring clinician reported that there is no family history of myotonia (although the parents may not have been formally assessed by EMG, and have not undergone genetic testing to establish whether the variant is *de novo* in the proband). The alternative possibility that the patient has recessive Myotonia Congenita and that the apparently wildtype allele actually harbours a large duplication, undetected by Sanger sequencing, has not been excluded. In the published account of the mutation, inheritance is described as sporadic (Moon, Kim et al. 2009) and the variant was found in heterozygosity with a normal allele in a single individual with no family history, but MLPA was not performed.

Given the possibility of dominant negative interaction raised by the clinical and genetic data on G276D and G523D it would be useful for a diagnostic service to employ an assay that was able to investigate dominant negative interactions or dissect out effects on the common gate. The fact that these mutations cause an apparent complete loss of function in the present assay meant that it was not possible to perform an analysis of common gating

by fitting exponentials to the deactivating currents (because there were no deactivating currents). Co-transfection of a 50:50 mixture of mutant and wildtype CLCN1 on separate plasmids into a population of HEK293T cells is possible but interpretation of currents from any given cell would be difficult since each cell may take up different amounts of the two plasmids instead of the desired 50:50 ratio. One way to tackle this issue would be to create a plasmid containing two copies of ClC-1, one of which is mutated, linked to each other with a short, artificial length of amino acid chain (Wu, Ryan et al. 2002). This approach has the shortcomings that the cloning is difficult and the artificial linker may interfere with channel function. Although HEK293T cells are more closely related to human skeletal muscle cells than *Xenopus* oocytes, the latter have the distinct advantage of control over the amount of genetic material introduced because they are large enough to be injected with a known quantity of mRNA. This means that the cell to be studied can be co-injected with a 50:50 ratio of wildtype and mutant CLCN1 mRNA for an assessment of dominant-negative interaction. In the author's opinion, this single factor of 'injectability' makes *Xenopus* oocytes the best currently available heterologous cell system on which to base a functional assay of CLCN1 sequence variants.

The S289G variant

S289G lies in the H helix of ClC-1, which is one of the helices at the dimer interface and has been implicated in common gating. The second half of the H helix together with the whole I helix are encoded by exon 8. Exon 8 is the region of the CLCN1 gene where pathogenic mutations are most frequently encountered among the patients in our cohort, and in particular is a hotspot for dominant mutations (Fialho, Schorge et al. 2007). S289G was identified in the homozygous child of two first cousins. The parents, who each carry a

single copy of the variant, are said to be asymptomatic but they have not been examined by EMG, according to the referring clinician. The description by the referring clinician of early onset and severe myotonia is typical of autosomal recessive myotonia (i.e. of patients who harbour two mutations). The functional consequences of S289G for the ClC-1 channel are twofold and slightly difficult to disentangle. First there is a marked depolarizing shift in the voltage dependence of channel activation. Secondly there is an effect on the kinetics of the channel which manifests in the protocol adopted for the assay as a prolongation of the time taken for the chloride current to relax to a steadystate value on stepping to depolarized potentials. Failure to reach steadystate during the most depolarized steps may have exacerbated the apparent shift in voltage dependence.

The gating of the wildtype ClC-1 channel is slow relative to the rate of change of membrane potential during an action potential. The role of the channel is not to oppose the rapid change in membrane voltage during an action potential, but to resist slow deviations in the resting potential consequent upon potassium accumulation in t-tubules, and to limit the effect of asynchrony between surface and t-tubule action potentials (discussed in Chapter 5). Potassium accumulation during voluntary muscle contraction would otherwise progressively depolarize muscle fibres leading to fatigue (loss of excitability owing to sodium channel inactivation) and/or runs of autonomous action potentials (myotonia). From this description it is not entirely obvious that ClC-1 ‘needs’ to be voltage-gated; a voltage-independent conductance might perform equally well, and in the majority of mathematical models of skeletal muscle this is precisely how ClC-1 has been represented (Adrian and Peachey 1973; Barchi 1975; Adrian and Marshall 1976; Cannon, Brown et al. 1993). Voltage-gating is the source of much unhappiness when it goes awry. A depolarizing shift

in voltage-dependence leaves the gates of the channels closed when they need to be open, a problem that would not occur for a channel with no gates. The advantage offered by a voltage-gated ClC-1 over a leak conductance may be that a slow non-linear (disproportionately large) increase in chloride conductance in response to depolarization enables very strong resistance to the effects of tubular potassium-accumulation while minimally interfering with the generation of action potentials from normal resting potential. The physiological consequences of slowed channel opening for skeletal muscle ought to depend in part on the rapidity of potassium accumulation. If the channel is too slow to respond to depolarization due to potassium accumulation (for example in response to a brief powerful contraction) this might contribute to myotonia.

Slowed ClC-1 activation has been reported for another Myotonia Congenita mutation, P480T (Tsujino, Kaibara et al. 2011). During a train of brief depolarizations designed to simulate a train of action potentials, the P480T variant impaired the increment in chloride conductance compared to wildtype, exacerbating the effect of a small depolarizing shift in voltage-dependence. The shift in voltage dependence for S289G is much larger than for P480T and so the contribution of slowed kinetics is less clear. Calculations using a mathematical model of myotonic muscle (discussed later) suggest that slowed ClC-1 kinetics is insufficient on its own to produce myotonia.

The interpretation of variants that test normal in HEK293T cells

The pathogenicity of novel CLCN1 variants discovered by Sanger sequencing of DNA from patients with myotonia often cannot be determined from the clinical and genetic data. As discussed above, functional expression in HEK293T cells can, with a few caveats, inform the decision whether a novel variant is pathogenic or not. The main caveat is that,

for reasons discussed later, variants that test normal under voltage clamp in HEK293T cells are not necessarily benign. Nonethelesss, the experience with P744T suggests that normality of function in HEK293T cells should prompt at least a consideration of the possibility that a variant might be benign. In such cases a careful hunt for other possible causes of myotonia in the same or another gene may be rewarding. P744T was identified in homozygosity in members of two different families from the same ethnic minority. Both patients have severe, early onset myotonia and a short exercise test result consistent with Myotonia Congenita. P744T is absent from control chromosomes from the UK population (although its frequency among Iraqi Kurds is not known), and it therefore appeared to be pathogenic. However, P744T was indistinguishable from wildtype under voltage clamp in HEK293T cells, meaning that either P744T is benign, or that the HEK293T assay is not sufficiently sensitive to detect it's effect. The answer came from an independent research project in the clinical genetics laboratory after the functional study in HEK293T cells had finished. Technology in the field of diagnostic genetics has advanced rapidly since 2008 when this thesis was initiated, and the molecular genetics laboratory began to explore (on a research basis) the possibility of large indel mutations in patients with Myotonia Congenita by using MLPA. Sanger sequencing can detect small indel sequence variants but cannot detect large ones. Some patients with likely chloride channel myotonia do not achieve a complete genetic diagnosis even after Sanger sequencing of all 23 exons of CLCN1. These include patients suspected to have recessive disease on the basis of phenotype and lack of family history in whom only a single pathogenic sequence variant is detected. In such cases a second undetected pathogenic CLCN1 variant may be present on the other allele, and may be detectable by MLPA (Raja Rayan, Haworth et al. 2012). In other cases a benign variant

detected by Sanger sequencing may appear to be pathogenic when it is *in cis* with an undetected large indel. This turned out to be the case in the myotonia patients with P744T. MLPA revealed homozygous duplications of exons 8-14 of CLCN1 in these patients (Raja Rayan, Haworth et al. 2012). P744T is likely to be a non-pathogenic marker for the real pathogenic variant, which being a large duplication, went undetected by Sanger sequencing. The portion of the channel harbouring P744T is after the duplicated region and so the variant may not even be expressed in these individuals unless the duplication is in-frame, in which case a very elongated protein may be generated (but a pathological role of P744T in this context is doubtful).

While in this instance an advance in the available technology lead to clarification of the molecular diagnosis, the discovery of new variants of uncertain significance among patients with myotonia, not only in CLCN1 but also in the wider genome, is set to increase dramatically as next generation sequencing technology becomes increasingly accessible. Next generation technologies now offer the possibility of quickly and cost-effectively identifying variants across the whole exome or even the whole genome (although the interpretation of variants in non-coding regions remains problematic) (Bras, Guerreiro et al. 2012). There may, for example, be variants in skeletal muscle sodium and potassium channels that influence t-tubular potassium accumulation and membrane excitability in Myotonia Congenita. Genes important for the development and morphology of the tubular system could equally contribute to differences between patients with myotonia. Functional expression is likely to remain as important as ever in the period when variants are catalogued and classified with respect to pathogenicity. However, simple expression systems like HEK293T cells may not be sufficiently faithful to muscle for this purpose.

The ideal functional expression system would be able to quickly, non-invasively and cost-effectively determine the effect of a particular CLCN1 genotype on the localization, abundance and function of ClC-1 in a particular patient, and in so doing reveal to what extent and by what mechanism different CLCN1 variants predispose to myotonia. Ideally the CLCN1 gene, introns and all, would be expressed in a muscle cell. Muscle regulates expression of ClC-1 at least in part through splicing, controlling the proportion of mRNA that undergoes nonsense mediated decay (Cooper 2007; Lueck, Lungu et al. 2007), and membrane electrical activity is critical for maintained ClC-1 expression at the sarcolemma (Klocke, Steinmeyer et al. 1994). Neither of these can occur when recombinant CLCN1 DNA that lacks introns is transfected into in a cell that lacks action potentials. Because heterologous cells, including HEK293T cells, do not recapitulate post-transcriptional processing of CLCN1 in skeletal muscle, variants that reduce channel abundance in muscle without affecting the function of the channel protein may appear normal. Others have noted that pathogenic mutations of CLCN1 may appear virtually normal under heterologous expression and yet fail to express or traffic normally in skeletal muscle (the F413C mutation, for example) (Zhang, Sanguinetti et al. 2000; Papponen, Nissinen et al. 2008).

A second problem with the HEK293T cell assay is that even if reduced surface channel density was faithfully recapitulated the resulting alteration in channel density could go undetected owing to the very large range of normal current density seen in control cells expressing wildtype CLCN1. There was a 100 fold difference in current magnitude between dimly fluorescent cells and brightly fluorescent cells expressing wildtype ClC-1. Inability to precisely control the amount of genetic material introduced into each HEK293T cell during transfection is a major limitation of this assay. Differences in the number of

copies of CLCN1 taken up by wildtype and mutant-expressing cells tend to confound the differences in current densities attributable to channel function. The vector used for the assay in this study expresses both GFP and CLCN1 so that fluorescence could be used as a surrogate for CLCN1 expression. A semiquantitative assessment of CLCN1 expression by visual estimation of the degree of fluorescence went some way to reducing the problem. However, cell to cell differences in current density were often large. Differences in current density between wildtype- and mutant-expressing cells had to be very large to be detectable, limiting the sensitivity of the assay to mutations in which the channel pore is less conductive than normal without any shift in voltage dependence. The vector carrying CLCN1 also carries the SV40 origin of replication, which enables episomal replication of the plasmid inside mammalian cells (e.g. HEK293T cells) that express the SV40 large T antigen (Cooper, Lippa et al. 1997). Very little CLCN1-bearing plasmid (0.5 µg per 35mm tissue culture dish) was required to yield chloride currents. Small variations in cDNA uptake, amplified by episomal plasmid replication within HEK293T cells, could explain the high variability of wildtype control recordings.

It is possible, therefore, that one or all of H369P, A566T or M644T are pathogenic despite the results from the HEK293T cell assay. W118G, which also tested normal, will be discussed separately later. H369P is a private variant as far we know – it is present in only a single family at our centre, has not been reported in the literature, and is not in any of the control chromosomes at our centre. The proband, Patient 611 in table 3.1 is a compound heterozygote who also carries a deletion (c.1872delG p.E624fs) that has not been reported outside of our centre, but is present in several unrelated individuals with myotonia and appears to act recessively. Patient 611 has severe myotonia, and has taken to using a

wheelchair at times. Carriers of the H369P in the family are not affected by myotonia, suggesting autosomal recessive inheritance (or non-pathogenicity). H369P is situated in the J helix of ClC-1, in which other autosomal recessive variants have been reported, including G355R (Deymeer, Cakirkaya et al. 1998) and R377X (Fialho, Schorge et al. 2007). It changes a positively charged amino acid to a neutral residue, but at a position that is not particularly well conserved among ClC channels. The presence of H369P in a compound heterozygote with a clear Myotonia Congenita phenotype, and its absence from controls, is suspicious of pathogenicity but at present the significance of the variant remains uncertain.

A566T and M646T are located towards the end of the channel, A566T in the Q helix and M646T in the first CBS domain of the C-terminus. Both the Q helix and the CBS domains of ClC-1 are thought to play important roles in the common gating process, and both dominant and recessive variants have been described in these regions (Duffield, Rychkov et al. 2003; Bykova, Zhang et al. 2006; Fialho, Schorge et al. 2007). A566T has been identified in samples from 4 families, three of which are consanguineous, and shows autosomal recessive inheritance in all of them - carriers of a single copy are unaffected, and homozygotes have severe myotonia. In one (Patient 384) EMG showed a degree of myopathy in addition to florid myotonia, as occurs at the severe end of the spectrum of Myotonia Congenita (Colding-Jorgensen 2005). In one of the families there is co-segregation of Myotonia Congenita with type 2 myotonic dystrophy, a phenomenon that has been previously described (Cardani, Giagnacovo et al. 2012). Homozygotes for A566T from this pedigree who do not also have myotonic dystrophy still have severe myotonia. However, parental DNA was not available for three of the four families and MLPA has not been performed.

M646T is apparently dominant in patient 620, who presented as an adult with a mild phenotype, who has a single copy of the variant, and who described grip myotonia in one parent. Patient 222 and her brother are both homozygotes for M464T (and not related to patient 620). They exhibit an earlier onset, more severe phenotype, although the girl is less severely affected than the boy, as is often the case in this disease (Colding-Jorgensen 2005; Fialho, Kullmann et al. 2008). In classical genetics the term 'dominant' refers to a situation where heterozygotes for an allele have the same phenotype as homozygotes. However, clinicians tend to use the term to include any disease-associated allele that produces a phenotype in the heterozygous state, when technically many of these are actually semidominant (meaning that homozygotes have a different, usually more severe, phenotype than heterozygotes) (Wilkie 1994; Zlotogora 1997).

No functional differences between A566T, M646T and wildtype ClC-1 could be found by whole cell patch clamp of HEK293T cells. H369P displayed only an alteration in the kinetics of deactivation of dubious physiological significance. Mathematical modeling (presented in chapter 5 and discussed later in this chapter) suggests that slowing of kinetics is unlikely to be sufficient to cause myotonia on its own. The possibility that these variants are benign markers for large *in cis* indel mutations has not been investigated, but as discussed above normality in the HEK293T cell assay does not completely rule out pathogenicity. It would be interesting to assess A566T, M646T and H369P by two electrode voltage clamp of *Xenopus* oocytes, which can be injected with a precise quantity of mRNA to look for reduced current density compared to wildtype ClC-1. Such a reduction could be caused either by altered channel abundance in the membrane, or by altered function of each channel, or both.

The W118G variant

The patient's own muscle is an obvious choice of expression system that circumvents some of the limitations of an assay in HEK293T cells. Electrophysiological characterization of ClC-1 is possible using biopsied intercostal muscle tissue (Lipicky, Bryant et al. 1971), but the technique is invasive and technically demanding. It is also possible, by immunocytochemistry, to examine the abundance of ClC-1 at the sarcolemma of muscle tissue biopsied from patients with Myotonia Congenita. The W118G variant, which tested normal in the HEK293T assay, has been studied in this way; compound heterozygotes for W118G/R894X or W118G/F413C had less sarcolemmal ClC-1 than patients with R894X or F413C alone (Raheem, Penttila et al. 2012). The relatively normal total cellular ClC-1 content of muscle from the compound heterozygotes carrying W118G, as measured by Western blot, suggested that the reduced sarcolemmal ClC-1 content may be due to a defect in trafficking. However, muscle biopsy is invasive and currently not in use at NHNN for the diagnosis of Myotonia Congenita (which can be achieved in the majority using genetic and clinical neurophysiology tests). While intracellular recordings of membrane potential have been achieved *in vivo* (Brooks and Hongdalarom 1968), it is not currently possible to measure the chloride conductance of muscle cells *in vivo* in the EMG clinic. Recently, induced pluripotent stem (IPS) cell technology has been used to produce patient-specific models of cardiac channelopathies (Park and Fishman 2012) and diseases of skeletal muscle (Tanaka, Woltjen et al. 2013). IPS cells could well prove useful for functional characterization of ClC-1 variants if the cells can be differentiated far enough to express the channels.

W118G (c.352T>G) is present in 2% of control chromosomes but is over-represented in the Myotonia Congenita population (8% of chromosomes), raising the possibility that it acts as a disease modifier. It is present in the online database, dbSNP (refSNP number rs10282312 – NB. the reference CLCN1 sequence is currently stated with the variant (less frequent) base, G, at position c.352 rather than the common, 'normal' base, T). At the time of writing UCSC genome browser, which collates data about the human genome from a number of sources, including dbSNP, gives the observed frequency of the variant allele, G, as 1.325% (95 / 7171). If W118G tends to worsen myotonia it could lead to a selection bias, increasing the likelihood that an individual with myotonia presents to a clinician. Two homozygotes for W118G (patient IDs 622 and 746) in the CLCN1 database had incomplete genetic explanations for myotonia unless W118G is pathogenic in its own right. While Patient 746 harboured no CLCN1 variants other than W118G, it is not absolutely certain that this individual's symptoms are attributable to myotonia. If this individual does have myotonia it must be very mild since the only clinical sign detected was a hint of percussion myotonia and when the author performed electromyography on the patient there were just one or two brief runs of spontaneous activity. Such mild myotonia cannot necessarily account for the symptoms in this individual. In patient ID 622 a known pathogenic variant (c.1872delG) was present together with c.1401+17T>C. The latter variant is unlikely to be pathogenic in its own right; it is present in controls and an unaffected homozygote is known. There is no doubt that patient 622 has myotonia. Either the summed functional effect of the three variants is sufficient to produce myotonia or there is another explanation, for example a deletion or duplication on one CLCN1 allele (which would not be picked up by Sanger sequencing), or an SCN4A mutation.

The W118G variant need not be pathogenic in its own right to produce an exacerbation of myotonia in a patient with a background low chloride conductance. The threshold chloride conductance for myotonia has been estimated (Furman and Barchi 1978) to be around 40% of normal (a 60% reduction from normal). If each W118G allele caused a 5% reduction of muscle chloride conductance then a homozygote might have a total of 10% reduction in chloride conductance, which is insufficient to cause myotonia. Even if one allele had lost function entirely (contributing at most 50% loss of the total membrane chloride conductance assuming no dominant negative interaction and equal allelic expression), then an additional 5% loss of chloride conductance from W118G on the other allele would not be sufficient for myotonia. However, on a background of an already >60% reduced chloride conductance, an extra 5 or 10% loss of function might produce more severe symptoms on average in a group of individuals (except in those whose background genotype was already such that chloride conductance was completely abolished). The reasoning in the above scenario is based on several assumptions; the threshold chloride conductance for myotonia may differ between patients and may not be sharp, the propensity to myotonic discharges may not scale linearly with the percentage loss of chloride conductance below the threshold for myotonia, and allelic expression may not be equal. Nevertheless the scenario serves as an illustration of how a CLCN1 variant could theoretically act as a modifier without being frankly pathogenic and without violating our current understanding of the pathophysiology of myotonia.

6.2 Whole cell patch clamp of skeletal muscle

Whole cell patch clamp is not a traditional approach to studying ion channels in skeletal muscle, but the experiments here confirm observations by others that with large diameter (low resistance) patch pipettes and 90% series resistance compensation, the whole cell patch clamp technique can be successfully applied to the small, relatively stubby muscle fibres of mouse FDB (Lueck, Mankodi et al. 2007). A voltage clamp experiment asks the question 'what transmembrane current must be applied in order to maintain a constant transmembrane voltage (the command potential)?' A negative feedback circuit rapidly and automatically adjusts the applied current so as to maintain a constant voltage, and changes in membrane resistance caused by opening or closing of ion channels are measured as changes in the applied current (Johnston and Wu 1995). The population of channels under study should be exposed to the same test voltage ('good space clamp'), which in a homogenous membrane requires that current density across the membrane be the same everywhere. Microelectrodes, as were used for this project, inject current at a point. For an isolated small, symmetrical cell (a HEK293T cells for example) current can spread fairly evenly to all parts of the membrane and space clamp is not a problem (except when the cell being studied is attached to another). Long cells have an appreciable internal axial resistance so that a microelectrode at one end cannot effectively control the membrane potential at the other end. Flow of current down the length of the cell produces a potential difference between membrane regions near the electrode tip and at the cell's extremities. Instead of using a microelectrode to inject current at a point, for some long cylindrical cells a wire electrode can be threaded internally down the length of the cell, but this is only possible with cells of large diameter (the giant axon of the squid for example (Hodgkin,

Huxley et al. 1952)). The traditional approach to voltage clamp experiments in skeletal muscle cells is to limit errors due to poor space clamp by restricting recordings to a limited area. A small region of membrane can be electrically isolated, for example by Vaseline gap technique (Hille and Campbell 1976)), or two electrodes very close to each other can be used, one to inject current and the other to record voltage (two electrode voltage clamp (Kao and Stanfield 1968; Fu, Struyk et al. 2011)). These techniques preceded the availability of whole cell patch clamp (continuous single electrode voltage clamp), in which the same electrode is used to simultaneously monitor both current and voltage.

6.3 The actions of progesterone and oestrogen on ClC-1 in mammalian muscle

Myotonia congenita is often exacerbated by pregnancy, is sometimes first noticed by patients during pregnancy (as occurred for Patient 675, described in chapter 3, table 3.1), and in some of these individuals the myotonia resolves after the pregnancy (Wagner, Deymeer et al. 1998; Colding-Jorgensen 2005). If the mechanism is a further reduction in sarcolemmal chloride conductance via altered function or expression of ClC-1, it might occur in patients whose genotype causes partial, but not total loss of ClC-1 function (since no further reduction of chloride conductance would be possible in the latter). Exacerbation of myotonia in pregnancy is particularly observed in autosomal dominant disease (which tends to be milder than recessive disease) (Fialho, Kullmann et al. 2008).

In voltage-clamp experiments on human ClC-1 expressed in *Xenopus* oocytes, 100 μM progesterone shifted the channel's voltage dependence by about +30 mV (Fialho, Kullmann et al. 2008), but the effect of oestrogen was smaller (a shift of only about 7 mV). In the above experiments using mouse FDB muscle fibres, progesterone shifted the voltage

dependence of chloride currents by 88 mV, and oestrogen produced a 16 mV shift. Reversibility of the effect on washing off the hormone supports the idea that the effect is attributable to the hormones, not to a recording artifact that develops over time or is produced by the process of exchanging solutions. Given that ClC-1 is the primary source of the skeletal muscle chloride conductance it can be concluded from these observations that, at least in mouse skeletal muscle, there is a rapid mechanism linking these two sex hormones at high concentrations with the function and/or expression of ClC-1. The effects are too rapid to be explained by the classical mechanism of steroid hormone action, which involves binding to nuclear receptors and alteration of gene transcription (Hammes and Levin 2007).

Rapid, non-genomic actions of steroid hormones, mediated by extra-nuclear receptors, are well described (Hammes and Levin 2007), but have not received much attention in skeletal muscle. Interestingly, physiological concentrations of dihydrotestosterone modulate the maximal isometric contractile force of small bundles of mouse skeletal muscle with a time course of about 30 minutes (Hamdi and Mutungi 2010). In these experiments inhibiting the androgen receptor had no effect on the response to testosterone, which appeared instead to be mediated by the epidermal growth factor receptor and involved phosphorylation of myosin light chain kinase. The precise mechanism of the effect of sex hormones on the chloride conductance of skeletal muscle will require further experiments. A reasonable stating point would be to test the hypotheses that the effect on ClC-1 is mediated though surface receptors for hormones and that the signal involves protein kinase C (PKC). ClC-1 is known to be regulated by PKC, at least when expressed in HEK293T cells (Rosenbohm, Rudel et al. 1999), and activators of PKC cause myotonia by reducing the chloride

conductance of muscle (Brinkmeier and Jockusch 1987). Mutagenesis experiments suggest the interaction between PKC and ClC-1 occurs at a region in the channel's C-terminal after the second CBS domain (Hsiao, Huang et al. 2010). Furthermore in brain tissue sex hormones are known to have non-genomic actions that are mediated via PKC (Balasubramanian, Portillo et al. 2008).

The physiological role of rapid modulation of muscle excitability by steroid hormones remains an open question given that in both *Xenopus* oocytes (Fialho, Kullmann et al. 2008) and in the experiments presented here on skeletal muscle, the effects of progesterone were only statistically significant at concentrations 50 to 500x higher than the highest concentration that occurs in the circulation (0.2 μM during the last trimester of pregnancy (Soldin, Guo et al. 2005)). Perhaps a very small additional fall in chloride conductance on a background of a loss of ClC-1 function is sufficient to produce a clinically significant exacerbation of symptoms, for example if the muscle membrane is in a state close to the threshold for myotonia, and the whole cell patch clamp assay employed here was not able to resolve such a small effect. Progesterone and oestrogen are poorly soluble in water, and the actual concentration of free hormone in the bath solution around the muscle cells in the present experiments is not known. In the circulation these hormones are mainly bound to albumen and sex hormone-binding globulin, with a small percentage free in aqueous solution (Zumoff, Strain et al. 1990; Ford, Cooke et al. 1992), but their free concentration in the extracellular milieu around skeletal muscle fibres *in vivo* is not known. There are a large number of intermediates and metabolites in the metabolic pathways of sex hormones, several of which are known to play roles as neuroactive steroids in the central and peripheral nervous systems (Roglio, Giatti et al. 2008; Melcangi, Panzica et al. 2011). It is

possible that the compound responsible for exacerbation of symptoms in Myotonia Congenita is one of these substances and that it has a more potent effect than progesterone or oestrogen. The trend towards a larger effect of progesterone after prior exposure to oestrogen is worth further investigation; synergistic effects of more than one steroid hormone may be important.

6.4 Mathematical modelling of myotonia and choice of model parameters

Reducing the chloride conductance of skeletal muscle causes a bifurcation in muscle membrane dynamics (Izhikevich 2007). When chloride conductance is normal, membrane potential always returns to a stable equilibrium after an action potential. As chloride conductance is reduced a new, oscillatory state becomes possible (myotonia). Oscillations may give way to a return to normal resting potential, or to a third condition in which the membrane enters a depolarized, inexcitable state (Rudel, Ricker et al. 1988). Geometrical analysis of a dynamical system in terms of equilibria and bifurcations is a powerful approach to understanding the behaviour of excitable membranes, but is only feasible when the phase space (an abstract space whose axes represent each independent variable) can be reduced to two or three dimensions (Izhikevich 2007). Cannon reduced his model of sodium channel myotonia to two dimensions by considering an isolated region of t-tubule membrane at different fixed luminal potassium concentrations and by focusing on the state of the system during the down stroke of the action potential (Cannon, Brown et al. 1993). However in his reduced model the action potential is driven solely by the abnormal fraction of sodium channels that fail to inactivate, and so this approach is not applicable to low chloride conductance myotonia. Specific defects of ClC-1 gating, and asynchrony between t-tubules and the surface membrane, (Adrian and Peachey 1973; Adrian and Marshall 1976)

would be difficult to capture in a reduced model. For this reason the Adrian & Marshall model was extended rather than reduced, and was analysed with simulation current camp experiments rather than with the geometrical tools of dynamical systems theory.

The spike of a skeletal muscle action potential is followed by a delay in the return to resting potential (an after-depolarization) that can be divided into early and late phases (Freygang, Goldstein et al. 1964). The late after-depolarization, which becomes apparent after a train of impulses, is thought to be caused by potassium accumulation in t-tubule lumens (Freygang, Goldstein et al. 1964; Adrian and Bryant 1974). Experiments with muscle from the myotonic goat lead to the idea that in myotonia the late after-depolarization becomes large enough initiate self-sustaining activity (Adrian and Bryant 1974). Subsequent results from mathematical modeling raised the possibility of an additional mechanism based on asynchrony between t-tubules and the surface membrane (Adrian and Peachey 1973; Adrian and Marshall 1976). T-tubular potassium accumulation in the original Adrian & Marshall model did not produce a late after-depolarization (as demonstrated here with new experiments - see Figure 5.20) because the model's resting potential was set by a leak conductance whose reversal potential was independent of the potassium concentration gradient. However, by reducing repolarization currents through delayed rectifier channels, potassium accumulation delayed t-tubular repolarization, exacerbating asynchrony between tubular and surface action potentials, which in turn drove myotonic discharges (Adrian and Marshall 1976). Modification of Adrian & Marshall's model by insertion of an inward rectifier potassium conductance successfully introduced a late after-depolarization.

The model Kir and ClC-1 conductances

Skeletal muscle expresses *Kir2.1* and *Kir2.2* channels at the surface and in the t-tubules (Dassau, Conti et al. 2011). The density of inward rectifier channels in the model was set equal in at the surface and in the t-tubules as in the model of potassium fluxes by Wallinga (Wallinga, Meijer et al. 1999). The chloride conductance in the modified Adrian & Marshall model was based on voltage clamp data from heterologously expressed human ClC-1 (Accardi and Pusch 2000). The modified Adrian & Marshall model contains all its chloride channels at the surface and none in the t-tubules as, most recently, was suggested by voltage clamp experiments in mouse FDB muscle fibres before and after de-tubulation (Lueck, Rossi et al. 2010). However, the literature is divided on the topic of the distribution of ClC-1 (Difranco, Herrera et al. 2010; Fahlke 2010; Zifarelli and Pusch 2010). While sarcolemmal ClC-1 may provide a shunt for depolarizing currents driven across the surface by asynchronous t-tubular action potentials (Adrian and Marshall 1976), tubular ClC-1 channels could carry some of the tubular repolarization current, limiting potassium accumulation (Coonan and Lamb 1998; Dutka, Murphy et al. 2008).

Sodium and delayed rectifier channels

Gating parameters for sodium and delayed rectifier channels were the same values (derived from amphibian muscle) as employed by the original Adrian & Marshall model. Sodium channels in mammalian muscle activate and inactivate at more hyperpolarized potentials (Fu, Struyk et al. 2011) than those from frog muscle (Adrian, Chandler et al. 1970). However, when the mammalian gating parameters from Cannon's model were tested in the context of low chloride conductance the model became inexcitable rather than myotonic (data not shown for the modified Adrian & Marshall model, but illustrated in Figure 5.11

for Cannon's model). The densities of sodium and delayed rectifier potassium channels were altered to match the model by Cannon (Cannon, Brown et al. 1993), which entailed an increase in the abundance of the t-tubular delayed rectifier. Cannon calculated that the density of delayed rectifier channels might be 40% that of the surface membrane (Cannon, Brown et al. 1993), and more recently it has been suggested there might be an even higher density (Difranco, Quinonez et al. 2012). The resultant increase in repolarization current density caused a larger increase in tubular potassium concentration per action potential and contributes to the myotonia exhibited by the new model. Potassium concentrations in the extracellular space of working muscle can reach 10mM, and in the confined space of the t-tubule lumen may reach even higher levels (Kristensen and Juel 2010). The modified Adrian & Marshall model does not faithfully represent all the mechanisms that contribute to export of potassium from the t-tubule lumen and may over-estimate tubular potassium concentrations. In particular, the sodium-potassium pump is not included in the model.

6.5 In silico assessment of specific ClC-1 defects

Failure of the normal increment of chloride conductance during repetitive action potentials owing to slowing of ClC-1 activation has been suggested to contribute to the pathogenicity of certain mutations that produce mild shifts in voltage-dependence (Tsujino, Kaibara et al. 2011). However, in the modified Adrian & Marshall model even 100,000 fold slowing of ClC-1 gating was insufficient to cause myotonia on its own (although it could exacerbate myotonia caused by reduced ClC-1 abundance). Calculations using the modified Adrian & Marshall model suggested that the S289G mutation studied in Chapter 3, causes myotonia primarily by shifting voltage-dependence, not as a consequence of its kinetic effects. Although *in silico* assessment of specific ClC-1 mutations is possible with the model, there

are reasons to be cautious. Low chloride conductance myotonia is strongly influenced by the gating behaviour of sodium channels, and the sodium channels of the modified Adrian & Marshall model are based on voltage clamp experiments from amphibian muscle (Adrian, Chandler et al. 1970). In a model containing gating parameters from mammalian muscle channels (Cannon, Brown et al. 1993), reducing the chloride conductance (represented by a leak conductance in the model) produced inexcitability, not myotonia (Figure 5.11).

6.6 The influence of muscle fibre size on the severity of myotonia

Differences in muscle fibre diameter could contribute to phenotypic variability in Myotonia Congenita. Myotonia in the original Adrian & Marshall model is exacerbated by increasing the diameter of the muscle fibre owing to worsening of the asynchrony between action potentials at the surface and in the t-tubule system. The original and modified Adrian & Marshall models are based on the assumption that muscle fibres are approximately cylindrical (Adrian and Marshall 1976). The area of surface membrane in a section of model muscle cell increases in proportion with the circumference of the cylinder's circular ends. The area of tubular membrane contained in the segment scales with the segment's volume. In this scheme, the surface membrane area scales with the radius (since circumference is $2\pi r$), while the tubular membrane area scales with the square of the radius (volume is proportional to the area, πr^2, of a cross-section through the fibre). Increasing the radius of the model causes a disproportionate rise in tubular membrane area (an increase in the area of tubular membrane per unit area of surface membrane). Small diameter model muscle fibres exhibit less asynchrony between tubular and surface action potentials than large diameter fibres as a direct consequence of this effect. The rise in tubular capacitance

per unit area of surface increases the time it takes to charge the tubule to threshold for an action potential and exacerbates the delay between surface and tubular action potentials. Furthermore, the radial distance over which potassium must diffuse from the centre to the periphery of the fibre is longer in larger diameter fibres, and so potassium accumulation is predicted to be larger and to last longer in large fibres.

The earliest that symptoms of severe, recessive Myotonia Congenita are noticed by parents is around the time the affected infant begins to walk. The onset of Thomsen's disease is generally later in the first of second decade (Colding-Jorgensen 2005). Symptoms usually start in the large muscles of the legs (Fialho, Schorge et al. 2007) and affect activities like running or climbing stairs. At birth human muscle fibres average about 10 μm in diameter and increase to an average of about 40 μm diameter by age 13 (Fung; Brooke and Engel 1969). On average, adult human muscle fibre diameters vary between 40 μm and 100 μm, with proximal muscles being larger than distal muscles, and muscles from women about 10 μm smaller than those from men (Fung; Brooke and Engel 1969). Expression of ClC-1 is temporally coupled with maturation of the t-tubule system, and in rodents is upregulated over the first few weeks after birth (Conte Camerino, De Luca et al. 1989; Franzini-Armstrong 1991; Wischmeyer, Nolte et al. 1993; Lueck, Lungu et al. 2007). This suggests that the small, immature muscle fibres of very young animals may not suffer from t-tubular potassium accumulation or asynchronous action potentials that occur in larger, mature muscle fibres. The age at onset of Myotonia Congenita may, at least partially, be determined by the relationship between the developmental increase in muscle fibre diameter and the severity of loss of ClC-1 function. Differences between men and women might also be accounted for by larger muscle fibre diameters in men.

6.7 Conclusions

On the basis of the HEK293T results it is suggested that the functional expression service should characterise not only the behaviour of homodimeric variant ClC-1 channels, but also check for dominant negative interactions, and develop an assay of ClC-1 abundance and localization. While normality of a homodimeric variant ClC-1 channel in the HEK203T assay does not necessarily rule out pathogenicity, it should prompt a search for an alternative genetic explanation.

The clinical/physiological significance of functional abnormalities observed in voltage clamp studies of ClC-1 is not always clear. Mathematical modeling presented here suggests that slowing of gating is not sufficient on its own to produce myotonia.

Phenotypic variability arises not only from differences between CLCN1 variants, but also from differences in the muscle cell and wider environment that surround them. Progesterone and 17β-oestradiol reduce the chloride conductance of mammalian muscle at high concentrations. This may be relevant to male-female differences and to the exacerbation of myotonia that can occur in pregnancy. The currently accepted mechanism of myotonia predicts more severe myotonia in larger diameter muscle fibres, which may also be relevant to male-female differences.

Chapter 7 Mathematical Appendix

The potential difference across a region of cell membrane changes at a rate proportional to the rate of charge addition/removal from its surfaces by transmembrane currents through ion channels in that region, and by axial currents along the cell to and from more distant regions. The models presented in this chapter for the most part represent (experimentally desirable but difficult to achieve) conditions of space-clamp in which the entire membrane under consideration experiences the same, uniform conditions and there are no potential differences to drive axial currents between different regions. Propagation of action potentials in space can be modeled by connecting several such isopotential segments of membrane in series. The models discussed below all represent the muscle membrane using the equivalent circuit shown in Figure 7.1. In those models that represent both the tubular and surface membranes, two of these equivalent circuits are connected together via a resistor that represents the narrow and sparsely distributed tubular mouths on the sarcolemma (Figure 5.4). In an isolated, space-clamped patch of surface membrane (Figure 7.1), current entering the system at the intracellular side (Itotal) of the membrane (synaptic current entering through the endplate in response to neural stimulation, or current injected by a microelectrode), only has two possible paths. Either it flows through the ion channels of the membrane ($I_{channels}$), or it flows across the membrane itself (I_{cap}) which acts like a capacitor, accumulating charge on one side and repelling it from the other side. When there is no injected current (i.e. when the system is space-clamped to zero net current) $I_{channels}$ and I_{cap} are balanced (equal and opposite, summing to zero). If transmembrane potential is rising then there must be an outward I_{cap} (positive charge deposited on the intracellular surface of the membrane and repelled off the extracellular surface of the membrane); in the

absence of a stimulus current, all the charge exiting via I_{cap} must be entering by an equal and opposite $I_{channels}$ (for example the inward sodium current that drives the upstroke of the action potential). To apply a depolarizing stimulus, an additional current is added to the system. There are two ways to think of the stimulus in a simulation – as a an extra inward current through some channels or receptors (e.g. opening of acetylcholine receptors at the endplate) or in terms of a current clamp experiment where microelectrodes are used to fix the net transmembrane current to a net outward value (i.e. extra current out across the capacitor). The difference is simply what convention is adopted for sign of the stimulus current (positive or negative) in the equations. In the following explanation of the equations underlying a simulated excitable membrane, a current clamp experiment will be in mind. The net transmembrane current flowing from inside the cell, out across the membrane to the ground electrode is fixed ('clamped') to I_{total}. From Figure 7.1 I_{total} has two possible routes across the membrane, via the capacitor or the channels ($I_{total} = I_{channels} + I_{cap}$). The stimulus current does not directly enter into the calculation of $I_{channels}$ because current though channels is determined entirely by the conductivity of those channels and the transmembrane voltage at each instant (the stimulus can indirectly affect $I_{channels}$ by altering the membrane potential). At the instant when I_{total} is stepped from zero to a net outward transmembrane current, the transmembrane voltage has had no time to change, so $I_{channels}$ is unchanged, and all of the new net outward current flows across the capacitance. As the capacitor charges, the resulting change in voltage begins to alter the channel current. If axial currents are permitted up and down the length of a cell, or radial currents can flow between the surface and the t-tubule, then I_{total} includes these extra currents as well, but they are also determined by potential differences not directly by the stimulus current itself.

For the moment the discussion will continue to focus on an isolated, space-clamped patch of membrane (no axial or radial currents).

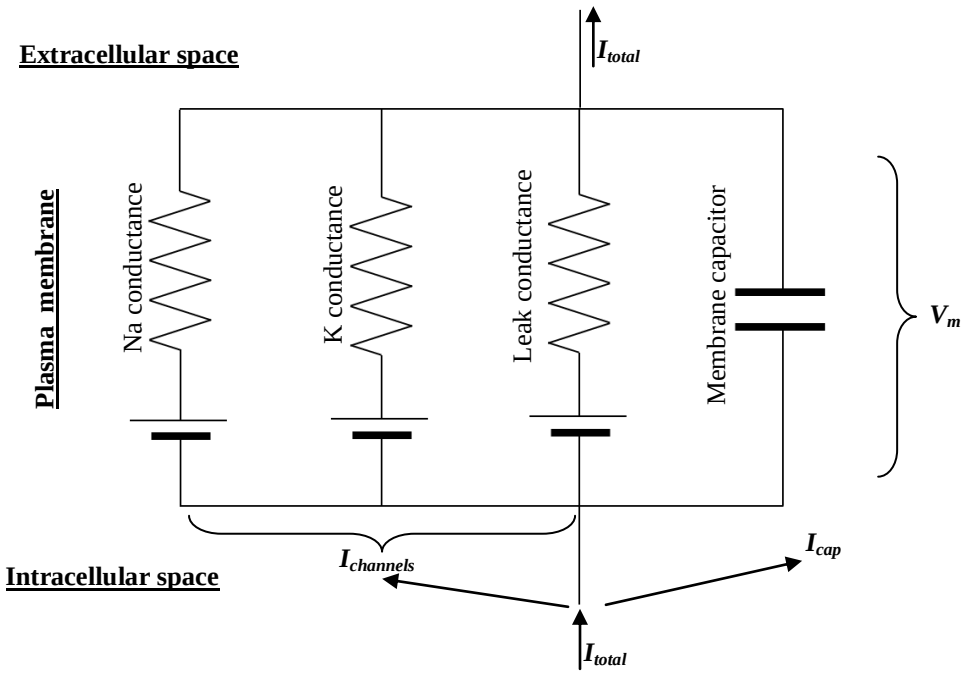

Figure 7.1 Circuit representation of space clamped excitable membrane.
Current injected intracellularly can either flow through the channels of the membrane (represented as resistors) or charge the membrane capacitance. Three types of channel (resistors) are shown, but any number could be included. The battery in series with each channel represents the effect of each ion's concentration gradient. The net driving force producing flow of a particular ion across the membrane is the deviation of the membrane potential, V_m, from the reversal or equilibrium potential, E_{ion} , that would exactly oppose its concentration gradient (driving force = $V_m - E_{ion}$). When a constant current is injected (Itotal) at first the majority flows onto the capacitor (large I_{cap}, small $I_{channels}$). As the capacitor charges, its voltage changes – this is the membrane potential, which drives an increasing proportion of the total current through membrane's channels. Eventually a potential is reached (equal to the product of total membrane resistance and the total current, $V = It_{otal}R_{total}$) at which all the current is flowing through the channels ($I_{channels} = I_{total}$) and none onto the capacitor (I_{cap} = 0). No further charge accumulates on the capacitor and from this point onwards membrane potential remains constant so as long as Itotal is held constant.

The proportion of net transmembrane current, I_{total}, that flows through the membrane's channels is determined by the membrane potential (see legend to Figure 7.1) and by the states of the different ion channels. Whatever is left over flows across the membrane as capacitative current, I_{cap}, charging or discharging the membrane:

$$I_{cap} = I_{total} - I_{channels}$$

The potential difference across the membrane is proportional to the amount of charge, *Q*, stored on its surfaces. The larger the area of the membrane, the more thinly each unit of charge gets spread over its surface, and so the larger the total quantity of charge must be deposited to effect a given change in voltage. The constant of proportionality is the capacitance, *C* (the larger the area, the larger the capacity for storing charge at a given voltage).

$$Q = CV$$

The capacitative current, Icap, is the speed that charge flows onto or off the membrane and is equal to the rate of change of the charge stored on the membrane, dQ/dt. Differentiating both sides of the above equation yields an expression for Icap in terms of membrane potential:

$$\frac{dQ}{dt} = C\frac{dV}{dt} \qquad = I_{cap}$$

Substituting CdV/dt into equation 1 yields the following:

$$C\frac{dV}{dt} = I_{total} - I_{channels}$$

The aim of the simulation is to solve this differential equation and thereby obtain an explicit function for the membrane potential as it varies over time, *V(t),* during and/or after a stimulus. In a simulation of skeletal muscle the ion channels in the membrane can be

manipulated to investigate the types of abnormality that predispose to repetitive, autonomous action potentials (myotonia) after cessation of a brief stimulus.

Because $I_{channels}$ depends on the state of various voltage-gated ion channels, the simulation involves solving not one, but a system of coupled non-linear differential equations. The presence of voltage-gated channels means that voltage determines current flow, which in turn controls the voltage. Analytical solutions (using pencil and paper to integrate the equations) to such systems are generally not possible, but there are various numerical methods that can be run as a computer program. Matlab contains a suite of routines for solving systems of differential equations.

The classic model of an excitable membrane by Hodgkin and Huxley includes a representation of the voltage-dependent gates on sodium (m and h gates) and delayed rectifier potassium (n gate) channels. The gating variables are not necessarily intended to correspond to physical components of ion channels, but are a convenient way to reconstruct the time- and voltage-dependencies of macroscopic ionic currents recorded in voltage clamp experiments. The variables m, n and h, can take on any value from 0 to 1 and are used in a representation of the fraction of open channels. A typical system of equations has the form:

$$C\frac{dV}{dt} = I_{total} - I_{channels}$$

$$where\ I_{channels} = G_{max\_na} m^3 h(V - E_{Na}) + G_{max\_K} n^4 (V - E_K) + G_{Leak}(V - E_{Leak})$$

$$\frac{dm}{dt} = \frac{m_\infty(V) - m(V,t)}{\tau_m(V)}, \quad \frac{dh}{dt} = \frac{h_\infty(V) - h(V,t)}{\tau_h(V)}, \quad \frac{dn}{dt} = \frac{n_\infty(V) - n(V,t)}{\tau_n(V)}$$

The first equation simply states the conditions of space-clamp. If current cannot go

anywhere other than through channels or onto the capacitance, then the current that flows via the membrane capacitance, *CdV/dt*, must be whatever is left over from the total current, I_{total} , after transmembrane current, $I_{channels}$, has exited though the ion channels. The total current, I_{total}, is used to stimulate the system. Setting it positive simulates injection of current at the intracellular side of the membrane by a microelectrode, or as a result of a synaptic input. The proportion of the net transmembrane current that flows through channels at the instant of stimulus onset is pre-determined by the state of the ion channels and the membrane potential at that instant, so the extra outward current initially crosses entirely through the capacitance, depolarizing the membrane. The channel current is the sum of sodium, potassium and leak currents in this example system (other currents and channels can be added depending on the system to be simulated). The fraction of open channels, a number between 0 (none) and 1 (all open), is given by n^4 for the delayed rectifier potassium channels or m^3h for sodium channels, after Hodgkin and Huxley. At a given voltage each gate (m, n or h) relaxes towards an equilibrium or steadystate determined by that voltage (the steadystate values for the m, n and h gates are represented as Boltzmann functions). When voltage is altered, the speed that a gate changes towards its new steadystate value is proportional to the distance between its current state and the new steadystate – the further it has to travel the faster it goes. The constant of proportionality is expressed as a time constant (which is different at different voltages). The time constants and steadystate functions of m, h and n have been measured in skeletal muscle by voltage clamp (Adrian, Chandler et al. 1970; DeCoursey, Bryant et al. 1982; Almers, Roberts et al. 1984; Fu, Struyk et al. 2011).

Although the rates of change of each gate can be represented directly and intuitively in terms of time constants and steadystates as above, traditionally the gating equations are expressed in terms of rate constants α and β (both functions of voltage), as follows:

$$\frac{dm}{dt} = \alpha_m(1-m) - \beta_m(m)\ ,\quad \frac{dh}{dt} = \alpha_h(1-h) - \beta_h(h),\quad \frac{dn}{dt} = \alpha_h(1-n) - \beta_h(n)$$

The two systems are equivalent. The rate constant functions *α(V)* and *β(V)* for each gate are derived from the experimentally measured time constant and steadystate functions, based on following relationships:

$$m_\infty = \frac{\alpha_m}{\alpha_m + \beta_m} \qquad \tau_m = \frac{1}{\alpha_m + \beta_m}$$

The equations for *α(V)* and *β(V)* for the gates are of the form:

$$a_m = \frac{\bar{\alpha}_m(V - \bar{V}_m)}{1 - e^{-(V-\bar{V}_m)/K_{\alpha m}}} \qquad \beta_m = \bar{\beta}_m e^{-(V-\bar{V}_m)/K_{\beta m}}$$

$$a_h = \bar{\alpha}_h e^{-(V-\bar{V}_h)/K_{\alpha h}} \qquad \beta_h = \frac{\bar{\beta}_h}{1 - e^{-(V-\bar{V}_h)/K_{\beta h}}}$$

$$a_n = \frac{\bar{\alpha}_n(V - \bar{V}_n)}{1 - e^{-(V-\bar{V}_n)/K_{\alpha n}}} \qquad \beta_n = \bar{\beta}_n e^{-(V-\bar{V}_n)/K_{\beta n}}$$

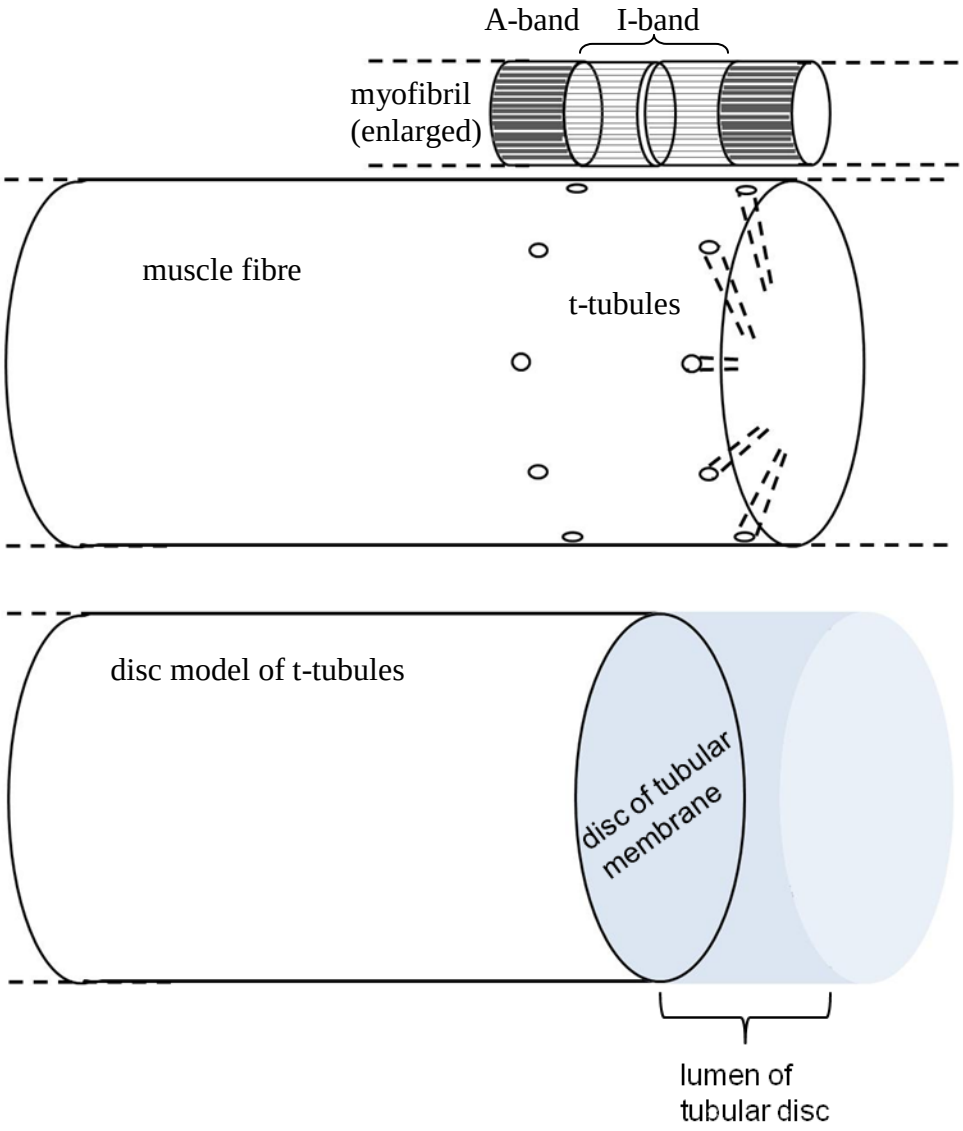

The cylindrical muscle cell is divided into segments of equal length. The surface membrane within a segment is assumed to be homogenous (same membrane potential and current density at all points), as is the membrane of the system of t-tubules associated with that segment. In mammalian muscle, the mouths of the t-tubules occur in rings around the circumference of muscle fibre coinciding with A-I junctions of the sarcomeres. The Adrian & Marshall disc model of t-tubular propagation starts with the assumption that as the t-tubules pass radially into the fibre, interconnections form a network in the cross-sectional

plane of the fibre. The model focuses exclusively on tubular action potentials conducting radially into the fibre, perpendicular to the surface membrane, and ignores longitudinal t-tubules. Rather than attempting to represent each individual radially-conducting t-tubule and its lumen, all of the membrane from radially-oriented t-tubules within a segment of muscle fibre is considered at once, as if each t-tubule had been incised down its length, laid flat and joined to its neighbours in a large disc of membrane. Only those sections of the t-tubule network that conduct in a radial direction (perpendicular to the surface) are included in the disc. It assumed that in the network of t-tubules, only half of them are orientated perpendicular to the surface membrane (Adrian, Chandler et al. 1969). The area of the disc and volume of its lumen are scaled according to the volume of the muscle fibre segment. The volume of tubular lumen is assumed to be 0.3% of the volume of the muscle fibre segment and the ratio of the tubular volume to the tubular surface area is 10^{-6}. These parameters were estimated by electron microscopy of frog muscle (Peachey 1965). To simulate propagation of the tubular action potential radially from the surface to the centre of the cylindrical segment of muscle fibre, the action potential must propagate from the outer rim of the circular disc of tubular membrane to its centre. The disc is therefore divided into concentric rings and a central disc.

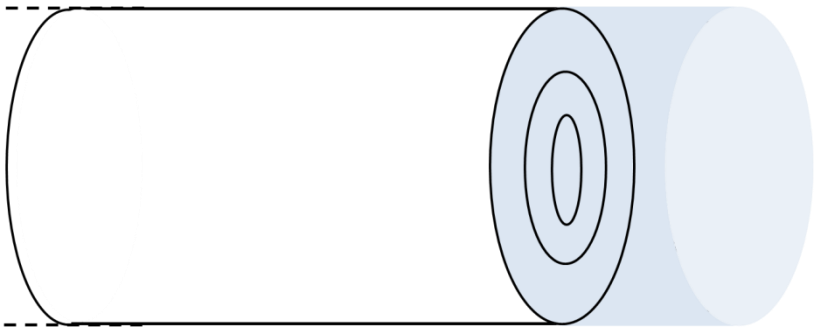

The membrane within a ring is homogenous (all points within a ring are the same potential and same current density). The luminal surface of the different rings can take different membrane potentials to simulate the action potential passing down the t-tubule. The cytoplasmic surfaces are assumed to all be at the same potential as the cytoplasmic aspect of the surface membrane (i.e. the resistance to radial current flow through the cytoplasm inside the fibre is assumed to be negligible). The equations for radial action potential propagation from one ring to the next within a segment are analogous to those for longitudinal action potential propagation at the surface from one segment to the next.

$$I_{total} = C\frac{dV}{dt} + I_{channels} + I_{\text{axial}}$$

When a segment depolarizes, the potential difference between its membrane and the membranes of its neighbours drives axial current through the cytoplasm into its neighbouring segments. Considering propagation from left to right, the current that flows across the membrane of a segment (through channels and the capacitance) is whatever remains of the current flowing in from the left after subtracting current that is driven away to the right:

$$I_{channels} + C\frac{dV}{dt} = I_{\text{in\_from\_left}} - I_{\text{out\_to\_right}}$$

So the transmembrane voltage can be found by solving the differential equation:

$$C\frac{dV}{dt} = I_{\text{in\_from\_left}} - I_{\text{out\_to\_right}} - I_{channels}$$

The segment can be stimulated by adding an additional stimulus current on the left hand side of the equation. The axial currents from left and to the right are calculated from the resistivity of the cytoplasm and the potential differences between the segment under consideration and its neighbours (current = voltage/resistance). The longer each segment of muscle, the higher the resistance to current flow between segments. In the t-tubule, the resistivity of the tubule lumen is used, and in the outer most tubular ring the access resistance is added to the tubular resistivity. For each segment or tubular ring there are 4 differential equations to solve – one for the voltage (above) and one for each of the gates (m, n and h). Thus for a muscle fibre divided into 15 segments each with 3 t-tubular rings there are 15 x 3 x 4 = 180 coupled differential equations to solve. Matlab running on a standard modern laptop computer was able to compute solutions within seconds or minutes.

References

Accardi, A. and C. Miller (2004). "Secondary active transport mediated by a prokaryotic homologue of ClC Cl- channels." Nature **427**(6977): 803-7.

Accardi, A. and M. Pusch (2000). "Fast and slow gating relaxations in the muscle chloride channel CLC-1." J Gen Physiol **116**(3): 433-44.

Adrian, R. and M. Marshall (1976). "Action potentials reconstructed in normal and myotonic muscle fibres." Journal of Physiology **258**: 125-143.

Adrian, R. H. and S. H. Bryant (1974). "On the repetitive discharge in myotonic muscle fibres." J Physiol **240**(2): 505-15.

Adrian, R. H., W. K. Chandler, et al. (1969). "The kinetics of mechanical activation in frog muscle." J Physiol **204**(1): 207-30.

Adrian, R. H., W. K. Chandler, et al. (1970). "Voltage clamp experiments in striated muscle fibres." J Physiol **208**(3): 607-44.

Adrian, R. H. and L. D. Peachey (1973). "Reconstruction of the action potential of frog sartorius muscle." J Physiol **235**(1): 103-31.

Aickin, C. C., W. J. Betz, et al. (1989). "Intracellular chloride and the mechanism for its accumulation in rat lumbrical muscle." J Physiol **411**: 437-55.

Almers, W., W. M. Roberts, et al. (1984). "Voltage clamp of rat and human skeletal muscle: measurements with an improved loose-patch technique." J Physiol **347**: 751-68.

Anumonwo, J. M. and A. N. Lopatin (2010). "Cardiac strong inward rectifier potassium channels." J Mol Cell Cardiol **48**(1): 45-54.

Aromataris, E. C., G. Y. Rychkov, et al. (2001). "Fast and slow gating of CLC-1: differential effects of 2-(4-chlorophenoxy) propionic acid and dominant negative mutations." Mol Pharmacol **60**(1): 200-8.

Arreola, J., J. A. De Santiago-Castillo, et al. (2008). "Gating and trafficking of ClC-2 chloride channel without cystathionine beta-synthase domains." J Physiol **586**(Pt 22): 5289.

Balasubramanian, B., W. Portillo, et al. (2008). "Nonclassical mechanisms of progesterone action in the brain: I. Protein kinase C activation in the hypothalamus of female rats." Endocrinology **149**(11): 5509-17.

Barchi, R. L. (1975). "Myotonia. An evaluation of the chloride hypothesis." Arch Neurol **32**(3): 175-80.

Bardouille, C., D. Vullhorst, et al. (1996). "Expression of chloride channel 1 mRNA in cultured myogenic cells: a marker of myotube maturation." FEBS Lett **396**(2-3): 177-80.

Bateman, A. (1997). "The structure of a domain common to archaebacteria and the homocystinuria disease protein." Trends Biochem Sci **22**(1): 12-3.

Beck, C. L., C. Fahlke, et al. (1996). "Molecular basis for decreased muscle chloride conductance in the myotonic goat." Proc Natl Acad Sci U S A **93**(20): 11248-52.

Bekoff, A. and W. Betz (1977). "Properties of isolated adult rat muscle fibres maintained in tissue culture." J Physiol **271**(2): 537-47.

Bell J, B. D., Sistermans E, Ramsden S.C. (2008) "Practice guidelines for the interpretation and reporting of Unclassified Variants (UVs) in clinical molecular genetics." CMGS e-publication **Volume**, DOI:

Bennetts, B., G. Y. Rychkov, et al. (2005). "Cytoplasmic ATP-sensing domains regulate gating of skeletal muscle ClC-1 chloride channels." J Biol Chem **280**(37): 32452-8.

Bischoff, R. and H. Holtzer (1968). "The effect of mitotic inhibitors in myogenesis in vitro." J Cell Biol **36**(1): 111-27.

Blatz, A. L. and K. L. Magleby (1983). "Single voltage-dependent chloride-selective channels of large conductance in cultured rat muscle." Biophys J **43**(2): 237-41.

Blatz, A. L. and K. L. Magleby (1985). "Single chloride-selective channels active at resting membrane potentials in cultured rat skeletal muscle." Biophys J **47**(1): 119-23.

Boldin, S., U. Jager, et al. (1987). "Cultivation, morphology, and electrophysiology of contractile rat myoballs." Pflugers Arch **409**(4-5): 462-7.

Bras, J., R. Guerreiro, et al. (2012). "Use of next-generation sequencing and other whole-genome strategies to dissect neurological disease." Nat Rev Neurosci **13**(7): 453-64.

Bretag, A. H. (1987). "Muscle chloride channels." Physiol Rev **67**(2): 618-724.

Brinkmeier, H. and H. Jockusch (1987). "Activators of protein kinase C induce myotonia by lowering chloride conductance in muscle." Biochem Biophys Res Commun **148**(3): 1383-9.

Brooke, M. H. and W. K. Engel (1969). "The histographic analysis of human muscle biopsies with regard to fiber types. 1. Adult male and female." Neurology **19**(3): 221-33.

Brooke, M. H. and W. K. Engel (1969). "The histographic analysis of human muscle biopsies with regard to fiber types. 4. Children's biopsies." Neurology **19**(6): 591-605.

Brooks, J. E. and T. Hongdalarom (1968). "Intracellular electromyography. Resting and action potentials in normal human muscle." Arch Neurol **18**(3): 291-300.

Brown, J. C. (1974). "Muscle weakness after rest in myotonic disorders; an electrophysiological study." J Neurol Neurosurg Psychiatry **37**(12): 1336-42.

Bryant, S. H. (1969). "Cable properties of external intercostal muscle fibres from myotonic and nonmyotonic goats." J Physiol **204**(3): 539-50.

Bykova, E. A., X. D. Zhang, et al. (2006). "Large movement in the C terminus of CLC-0 chloride channel during slow gating." Nat Struct Mol Biol **13**(12): 1115-9.

Camerino, D. and S. H. Bryant (1976). "Effects of denervation and colchicine treatment on the chloride conductance of rat skeletal muscle fibers." J Neurobiol **7**(3): 221-8.

Camerino, D., D. Tricarico, et al. (2007). "Ion channel pharmacology." Neurotheraputics: The Journal of the American Society for Experimental NeuroTherapeutics **4**: 184-198.

Cannon, S. C., R. H. Brown, Jr., et al. (1993). "Theoretical reconstruction of myotonia and paralysis caused by incomplete inactivation of sodium channels." Biophys J **65**(1): 270-88.

Cannon, S. C. and D. P. Corey (1993). "Loss of Na+ channel inactivation by anemone toxin (ATX II) mimics the myotonic state in hyperkalaemic periodic paralysis." J Physiol **466**: 501-20.

Cardani, R., M. Giagnacovo, et al. (2012). "Co-segregation of DM2 with a recessive CLCN1 mutation in juvenile onset of myotonic dystrophy type 2." J Neurol.

Chen, M. F. and H. Jockusch (1999). "Role of phosphorylation and physiological state in the regulation of the muscular chloride channel ClC-1: a voltage-clamp study on isolated M. interosseus fibers." Biochem Biophys Res Commun **261**(2): 528-33.
Chen, T. Y. (2005). "Structure and function of clc channels." Annu Rev Physiol **67**: 809-39.
Chen, T. Y. and C. Miller (1996). "Nonequilibrium gating and voltage dependence of the ClC-0 Cl- channel." J Gen Physiol **108**(4): 237-50.
Cheung, A., J. A. Dantzig, et al. (2002). "A small-molecule inhibitor of skeletal muscle myosin II." Nat Cell Biol **4**(1): 83-8.
Chua, M. and W. J. Betz (1991). "Characterization of ion channels on the surface membrane of adult rat skeletal muscle." Biophys J **59**(6): 1251-60.
Colding-Jorgensen, E. (2005). "Phenotypic variability in myotonia congenita." Muscle & Nerve **32**: 19-34.
Conte-Camerino, D., S. H. Bryant, et al. (1985). "The influence of inactivity on membrane resting conductances of rat skeletal muscle fibres undergoing reinnervation." J Exp Biol **115**: 99-104.
Conte Camerino, D., A. De Luca, et al. (1989). "Membrane ionic conductances in normal and denervated skeletal muscle of the rat during development." Pflugers Arch **413**(5): 568-70.
Coonan, J. R. and G. D. Lamb (1998). "Effect of transverse-tubular chloride conductance on excitability in skinned skeletal muscle fibres of rat and toad." J Physiol **509 (Pt 2)**: 551-64.
Cooper, M. J., M. Lippa, et al. (1997). "Safety-modified episomal vectors for human gene therapy." Proc Natl Acad Sci U S A **94**(12): 6450-5.
Cooper, T. (2007). "Regulation of chloride ion conductance during skeletal muscle development and in disease. Focus on "Chloride channelopathy in myotonic dystrophy resulting from loss of posttranslational regulation for CLCN1"." American Journal of Physiology Cell Physiology **292**: 1245-1247.
Dassau, L., L. R. Conti, et al. (2011). "Kir2.6 regulates the surface expression of Kir2.x inward rectifier potassium channels." J Biol Chem.
DeCoursey, T. E., S. H. Bryant, et al. (1982). "Sodium currents in human skeletal muscle fibers." Muscle Nerve **5**(8): 614-8.
Desaphy, J. F., S. Pierno, et al. (2005). "Recovery of the soleus muscle after short- and long-term disuse induced by hindlimb unloading: effects on the electrical properties and myosin heavy chain profile." Neurobiol Dis **18**(2): 356-65.
Deymeer, F., S. Cakirkaya, et al. (1998). "Transient weakness and compound muscle action potential decrement in myotonia congenita." Muscle & Nerve **21**: 1334-1337.
Difranco, M., A. Herrera, et al. (2010). "Chloride currents from the transverse tubular system in adult mammalian skeletal muscle fibers." J Gen Physiol.
Difranco, M., M. Quinonez, et al. (2012). "The delayed rectifier potassium conductance in the sarcolemma and the transverse tubular system membranes of mammalian skeletal muscle fibers." J Gen Physiol **140**(2): 109-37.
Duffield, M., G. Rychkov, et al. (2003). "Involvement of helices at the dimer interface in ClC-1 common gating." J Gen Physiol **121**(2): 149-61.
Duno, M., E. Colding-Jorgensen, et al. (2004). "Difference in allelic expression of the CLCN1 gene and the possible influence on the myotonia congenita phenotype." European Joural of Human Genetics **12**: 738-743.

Dutka, T. L., R. M. Murphy, et al. (2008). "Chloride conductance in the transverse tubular system of rat skeletal muscle fibres: importance in excitation-contraction coupling and fatigue." J Physiol **586**(3): 875-87.

Dutzler, R. (2007). "A structural perspective on ClC channel and transporter function." FEBS letters **581**: 2839-2844.

Dutzler, R., E. B. Campbell, et al. (2002). "X-ray structure of a ClC chloride channel at 3.0 A reveals the molecular basis of anion selectivity." Nature **415**(6869): 287-94.

Eisenberg, R. S. and P. W. Gage (1969). "Ionic conductances of the surface and transverse tubular membranes of frog sartorius fibers." J Gen Physiol **53**(3): 279-97.

Estevez, R. and T. J. Jentsch (2002). "CLC chloride channels: correlating structure with function." Curr Opin Struct Biol **12**(4): 531-9.

Estevez, R., M. Pusch, et al. (2004). "Functional and structural conservation of CBS domains from CLC chloride channels." J Physiol **557**(Pt 2): 363-78.

Fahlke, C. (2010). "Chloride channels take center stage in a muscular drama." J Gen Physiol.

Fahlke, C., E. Zachar, et al. (1992). "Single-channel recordings of chloride currents in cultured human skeletal muscle." Pflugers Arch **421**(2-3): 108-16.

Fahlke, C., E. Zachar, et al. (1993). "Chloride channels with reduced single-channel conductance in recessive myotonia congenita." Neuron **10**(2): 225-32.

Falk, G. and P. Fatt (1964). "Linear Electrical Properties of Striated Muscle Fibres Observed with Intracellular Electrodes." Proc R Soc Lond B Biol Sci **160**: 69-123.

Fialho, D., D. M. Kullmann, et al. (2008). "Non-genomic effects of sex hormones on CLC-1 may contribute to gender differences in myotonia congenita." Neuromuscul Disord **18**(11): 869-72.

Fialho, D., S. Schorge, et al. (2007). "Chloride channel myotonia: exon 8 hot-spot for dominant-negative interactions." Brain **130**(Pt 12): 3265-74.

Fong, P., A. Rehfeldt, et al. (1998). "Determinants of slow gating in ClC-0, the voltage-gated chloride channel of Torpedo marmorata." Am J Physiol **274**(4 Pt 1): C966-73.

Ford, H. C., R. R. Cooke, et al. (1992). "Serum levels of free and bound testosterone in hyperthyroidism." Clin Endocrinol (Oxf) **36**(2): 187-92.

Fournier, E., M. Arzel, et al. (2004). "Electromyography guides toward subgroups of mutations in muscle channelopathies." Ann Neurol **56**(5): 650-61.

Fournier, E., K. Viala, et al. (2006). "Cold extends electromyography distinction between ion channel mutations causing myotonia." Ann Neurol **60**(3): 356-65.

Franzini-Armstrong, C. (1991). "Simultaneous maturation of transverse tubules and sarcoplasmic reticulum during muscle differentiation in the mouse." Dev Biol **146**(2): 353-63.

Freygang, W. H., Jr., D. A. Goldstein, et al. (1964). "The after-Potential That Follows Trains of Impulses in Frog Muscle Fibers." J Gen Physiol **47**: 929-52.

Fu, Y., A. Struyk, et al. (2011). "Gating behaviour of sodium currents in adult mouse muscle recorded with an improved two-electrode voltage clamp." J Physiol **589**(Pt 3): 525-46.

Fukada, J. (1975). "Voltage clamp study on inward chloride currents of spherical muscle cells in tissue culture." Nature **257**(5525): 408-10.

Fung, K. "How to work up a muscle biopsy." Retrieved 13 July, 2012, from http://moon.ouhsc.edu/kfung/JTY1/NeuroHelp/ZNEWWU10.htm.

Furman, R. E. and R. L. Barchi (1978). "The pathophysiology of myotonia produced by aromatic carboxylic acids." Ann Neurol **4**(4): 357-65.
Gurnett, C. A., S. D. Kahl, et al. (1995). "Absence of the skeletal muscle sarcolemma chloride channel ClC-1 in myotonic mice." J Biol Chem **270**(16): 9035-8.
H.P. Rang, M.M. Dale, et al. (1995). Pharmacology, Churchill Livingston.
Hamdi, M. M. and G. Mutungi (2010). "Dihydrotestosterone activates the MAPK pathway and modulates maximum isometric force through the EGF receptor in isolated intact mouse skeletal muscle fibres." J Physiol **588**(Pt 3): 511-25.
Hammes, S. R. and E. R. Levin (2007). "Extranuclear steroid receptors: nature and actions." Endocr Rev **28**(7): 726-41.
Harris, G. and W. Betz (1987). "Evidence for active chloride accumulation in normal and denervated rat lumbrical muscle." The Journal of General Physiology **90**: 127-144.
Heiny, J. A., J. R. Valle, et al. (1990). "Optical evidence for a chloride conductance in the T-system of frog skeletal muscle." Pflugers Arch **416**(3): 288-95.
Herson, P. S., M. Virk, et al. (2003). "A mouse model of episodic ataxia type-1." Nat Neurosci **6**(4): 378-83.
Hille, B. (2001). Ion channels of excitable membranes. Sunderland, Mass., Sinauer.
Hille, B. and D. T. Campbell (1976). "An improved vaseline gap voltage clamp for skeletal muscle fibers." J Gen Physiol **67**(3): 265-93.
Hodgkin, A. L. and P. Horowicz (1959). "The influence of potassium and chloride ions on the membrane potential of single muscle fibres." J Physiol **148**: 127-60.
Hodgkin, A. L. and P. Horowicz (1960). "The effect of sudden changes in ionic concentrations on the membrane potential of single muscle fibres." J Physiol **153**: 370-85.
Hodgkin, A. L., A. F. Huxley, et al. (1952). "Measurement of current-voltage relations in the membrane of the giant axon of Loligo." J Physiol **116**(4): 424-48.
Hsiao, K. M., R. Y. Huang, et al. (2010). "Functional study of CLC-1 mutants expressed in Xenopus oocytes reveals that a C-terminal region Thr891-Ser892-Thr893 is responsible for the effects of protein kinase C activator." Cell Physiol Biochem **25**(6): 687-94.
Izhikevich, E. M. (2007). Dynamical systems in neuroscience : the geometry of excitability and bursting. Cambridge, Mass., MIT Press.
Jack, J. J. B., D. Noble, et al. (1983). Electric current flow in excitable cells. Oxford, Clarendon Press.
Jentsch, T. J., K. Steinmeyer, et al. (1990). "Primary structure of Torpedo marmorata chloride channel isolated by expression cloning in Xenopus oocytes." Nature **348**(6301): 510-4.
Jentsh, T. (2008). "CLC chloride channels and transporters: from genes to protein structure, pathology and physiology." Critical Reviews in Biochemistry and Molecular Biology **43**: 3-36.
Johnston, D. and S. M.-s. Wu (1995). Foundations of cellular neurophysiology. Cambridge, Mass., MIT Press.
Jurkat-Rott, K., M. Fauler, et al. (2006). "Ion channels and ion transporters of the transverse tubular system of skeletal muscle." J Muscle Res Cell Motil **27**(5-7): 275-90.
Kao, C. Y. and P. R. Stanfield (1968). "Actions of some anions on electrical properties and mechanical threshold of frog twitch muscle." J Physiol **198**(2): 291-309.

Karteris, E., S. Zervou, et al. (2006). "Progesterone signaling in human myometrium through two novel membrane G protein-coupled receptors: potential role in functional progesterone withdrawal at term." Mol Endocrinol **20**(7): 1519-34.

Klocke, R., K. Steinmeyer, et al. (1994). "Role of innervation, excitability and myogenic factors in the expression of the muscular chloride channel ClC-1." Journal of Biological Chemistry **269**(44): 27635-27639.

Koch, M. C., K. Steinmeyer, et al. (1992). "The skeletal muscle chloride channel in dominant and recessive human myotonia." Science **257**(5071): 797-800.

Kristensen, M. and C. Juel (2010). "Potassium-transporting proteins in skeletal muscle: cellular location and fibre-type differences." Acta Physiol (Oxf) **198**(2): 105-23.

Kwiecinski, H., F. Lehmann-Horn, et al. (1984). "The resting membrane parameters of human intercostal muscle at low, normal, and high extracellular potassium." Muscle Nerve **7**(1): 60-5.

Kwiecinski, H., F. Lehmann-Horn, et al. (1988). "Drug-induced myotonia in human intercostal muscle." Muscle Nerve **11**(6): 576-81.

Lacomis, D., J. T. Gonzales, et al. (1999). "Fluctuating clinical myotonia and weakness from Thomsen's disease occurring only during pregnancies." Clin Neurol Neurosurg **101**(2): 133-6.

Lamb, G. D. (2005). "Rippling muscle disease may be caused by "silent" action potentials in the tubular system of skeletal muscle fibers." Muscle Nerve **31**(5): 652-8.

Lamb, G. D., R. M. Murphy, et al. (2011). "On the localization of ClC-1 in skeletal muscle fibers." J Gen Physiol **137**(3): 327-9; author reply 331-3.

Lipicky, R. and S. Bryant (1966). "Sodium, potassium, and chloride fluxes in intercostal muscle from normal goats and goats with hereditary myotonia." The Journal of General Physiology **50**: 89-111.

Lipicky, R. J., S. H. Bryant, et al. (1971). "Cable parameters, sodium, potassium, chloride, and water content, and potassium efflux in isolated external intercostal muscle of normal volunteers and patients with myotonia congenita." J Clin Invest **50**(10): 2091-103.

Lisal, J. and M. Maduke (2009). "Review. Proton-coupled gating in chloride channels." Philos Trans R Soc Lond B Biol Sci **364**(1514): 181-7.

Lorenz, C., M. Pusch, et al. (1996). "Heteromultimeric CLC chloride channels with novel properties." Proc Natl Acad Sci U S A **93**(23): 13362-6.

Ludewig, U., T. J. Jentsch, et al. (1997). "Analysis of a protein region involved in permeation and gating of the voltage-gated Torpedo chloride channel ClC-0." J Physiol **498 (Pt 3)**: 691-702.

Lueck, J. D., C. Lungu, et al. (2007). "Chloride channelopathy in myotonic dystrophy resulting from loss of posttranscriptional regulation for CLCN1." Am J Physiol Cell Physiol **292**(4): C1291-7.

Lueck, J. D., A. Mankodi, et al. (2007). "Muscle chloride channel dysfunction in two mouse models of myotonic dystrophy." J Gen Physiol **129**(1): 79-94.

Lueck, J. D., A. E. Rossi, et al. (2010). "Sarcolemmal-restricted localization of functional ClC-1 channels in mouse skeletal muscle." J Gen Physiol.

Macdonald, W. A., T. H. Pedersen, et al. (2005). "N-Benzyl-p-toluene sulphonamide allows the recording of trains of intracellular action potentials from nerve-stimulated intact fast-twitch skeletal muscle of the rat." Exp Physiol **90**(6): 815-25.

Macias, M. J., O. Teijido, et al. (2007). "Myotonia-related mutations in the distal C-terminus of ClC-1 and ClC-0 chloride channels affect the structure of a poly-proline helix." Biochem J **403**(1): 79-87.
Mailander, V., R. Heine, et al. (1996). "Novel muscle chloride channel mutations and their effects on heterozygous carriers." Am J Hum Genet **58**(2): 317-24.
Maljevic, S., T. V. Wuttke, et al. (2010). "KV7 channelopathies." Pflugers Arch **460**(2): 277-88.
Mankodi, A., M. P. Takahashi, et al. (2002). "Expanded CUG repeats trigger aberrant splicing of ClC-1 chloride channel pre-mRNA and hyperexcitability of skeletal muscle in myotonic dystrophy." Mol Cell **10**(1): 35-44.
Markovic, S. and R. Dutzler (2007). "The structure of the cytoplasmic domain of the chloride channel ClC-Ka reveals a conserved interaction interface." Structure **15**(6): 715-25.
Melcangi, R. C., G. Panzica, et al. (2011). "Neuroactive steroids: focus on human brain." Neuroscience **191**: 1-5.
Miller, C. (2006). "ClC chloride channels viewed through a transporter lens." Nature **440**: 484-489.
Moon, I. S., H. S. Kim, et al. (2009). "Novel CLCN1 mutations and clinical features of Korean patients with myotonia congenita." J Korean Med Sci **24**(6): 1038-44.
Palade, P. T. and R. L. Barchi (1977). "Characteristics of the chloride conductance in muscle fibers of the rat diaphragm." J Gen Physiol **69**(3): 325-42.
Papponen, H. (2008). The muscle specific chloride chanel CLC-1 and myotonia congenita in northern finland, University of Oulu.
Papponen, H., T. Kaisto, et al. (2005). "Regulated sarcolemmal localization of the muscle specific ClC-1 chloride channel." Experimental Neurology **191**: 163-177.
Papponen, H., M. Nissinen, et al. (2008). "F413C and A531V but not R894X myotonia congenita mutations cause defective endoplasmic reticulum export of the muscle-specific chloride channel CLC-1." Muscle & Nerve **37**: 317-325.
Park, D. S. and G. I. Fishman (2012). "Forever young: induced pluripotent stem cells as models of inherited arrhythmias." Circulation **125**(25): 3055-6.
Peachey, L. D. (1965). "The sarcoplasmic reticulum and transverse tubules of the frog's sartorius." J Cell Biol **25**(3): Suppl:209-31.
Pusch, M. (2002). "Myotonia caused by mutations in the muscle chloride channel gene CLCN1." Hum Mutat **19**(4): 423-34.
Pusch, M., U. Ludewig, et al. (1997). "Temperature dependence of fast and slow gating relaxations of ClC-0 chloride channels." J Gen Physiol **109**(1): 105-16.
Pusch, M., K. Steinmeyer, et al. (1994). "Low single channel conductance of the major skeletal muscle chloride channel, ClC-1." Biophys J **66**(1): 149-52.
Raheem, O., S. Penttila, et al. (2012). "New immunohistochemical method for improved myotonia and chloride channel mutation diagnostics." Neurology **79**(22): 2194-200.
Raja Rayan, D. L., A. Haworth, et al. (2012). "A new explanation for recessive myotonia congenita: exon deletions and duplications in CLCN1." Neurology **78**(24): 1953-8.
Ritchie, A. K. and D. M. Fambrough (1975). "Electrophysiological properties of the membrane and acetylcholine receptor in developing rat and chick myotubes." J Gen Physiol **66**(3): 327-55.

Roglio, I., S. Giatti, et al. (2008). "Neuroactive steroids and peripheral neuropathy." Brain Res Rev **57**(2): 460-9.
Rosenbohm, A., R. Rudel, et al. (1999). "Regulation of the human skeletal muscle chloride channel hClC-1 by protein kinase C." J Physiol **514 (Pt 3)**: 677-85.
Rudel, R. and F. Lehmann-Horn (1985). "Membrane changes in cells from myotonia patients." Physiol Rev **65**(2): 310-56.
Rudel, R., K. Ricker, et al. (1988). "Transient weakness and altered membrane characteristic in recessive generalized myotonia (Becker)." Muscle Nerve **11**(3): 202-11.
Rychkov, G. Y., M. Pusch, et al. (1996). "Concentration and pH dependence of skeletal muscle chloride channel ClC-1." J Physiol **497 (Pt 2)**: 423-35.
Saviane, C., F. Conti, et al. (1999). "The muscle chloride channel ClC-1 has a double-barreled appearance that is differentially affected in dominant and recessive myotonia." J Gen Physiol **113**(3): 457-68.
Schmidt-Rose, T. and T. J. Jentsch (1997). "Reconstitution of functional voltage-gated chloride channels from complementary fragments of CLC-1." J Biol Chem **272**(33): 20515-21.
Soldin, O. P., T. Guo, et al. (2005). "Steroid hormone levels in pregnancy and 1 year postpartum using isotope dilution tandem mass spectrometry." Fertil Steril **84**(3): 701-10.
Standen, N. B. and P. R. Stanfield (1978). "Inward rectification in skeletal muscle: a blocking particle model." Pflugers Arch **378**(2): 173-6.
Statland, J. M., B. N. Bundy, et al. (2012). "Mexiletine for symptoms and signs of myotonia in nondystrophic myotonia: a randomized controlled trial." JAMA **308**(13): 1357-65.
Statland, J. M., B. N. Bundy, et al. (2012). "A quantitative measure of handgrip myotonia in non-dystrophic myotonia." Muscle Nerve **46**(4): 482-9.
Steinmeyer, K., R. Klocke, et al. (1991). "Inactivation of muscle chloride channel by transposon insertion in myotonic mice." Nature **354**(6351): 304-8.
Steinmeyer, K., C. Lorenz, et al. (1994). "Multimeric structure of ClC-1 chloride channel revealed by mutations in dominant myotonia congenita (Thomsen)." EMBO J **13**(4): 737-43.
Steinmeyer, K., C. Ortland, et al. (1991). "Primary structure and functional expression of a developmentally regulated skeletal muscle chloride channel." Nature **354**(6351): 301-4.
Streib, E. W., S. F. Sun, et al. (1982). "Transient paresis in myotonic syndromes: a simplified electrophysiologic approach." Muscle & Nerve **5**: 719-723.
Struyk, A. F. and S. C. Cannon (2008). "Paradoxical depolarization of BA2+- treated muscle exposed to low extracellular K+: insights into resting potential abnormalities in hypokalemic paralysis." Muscle Nerve **37**(3): 326-37.
Sun, C., L. Tranebjaerg, et al. (2001). "Spectrum of CLCN1 mutations in patients with myotonia congenita in Northern Scandinavia." Eur J Hum Genet **9**(12): 903-9.
Tan, S. V., E. Matthews, et al. (2012). "Refined exercise testing can aid dna-based diagnosis in muscle channelopathies." Ann Neurol **69**(2): 328-340.

Tanaka, A., K. Woltjen, et al. (2013). "Efficient and Reproducible Myogenic Differentiation from Human iPS Cells: Prospects for Modeling Miyoshi Myopathy In Vitro." PLoS One **8**(4): e61540.

Trip, J., G. Drost, et al. (2006). "Drug treatment for myotonia (Review)." Cochrane Database of Systematic Reviews(1).

Trip, J., G. Drost, et al. (2009). "Redefining the clinical phenotypes of non-dystrophic myotonic syndromes." J Neurol Neurosurg Psychiatry **80**(6): 647-52.

Tsujino, A., M. Kaibara, et al. (2011). "A CLCN1 mutation in dominant myotonia congenita impairs the increment of chloride conductance during repetitive depolarization." Neurosci Lett **494**(2): 155-60.

Wagner, S., F. Deymeer, et al. (1998). "The dominant chloride channel mutant G200R causing fluctuating myotonia: clinical findings, electrophysiology, and channel pathology." Muscle Nerve **21**(9): 1122-8.

Wallinga, W., S. L. Meijer, et al. (1999). "Modelling action potentials and membrane currents of mammalian skeletal muscle fibres in coherence with potassium concentration changes in the T-tubular system." Eur Biophys J **28**(4): 317-29.

White, M. M. and C. Miller (1979). "A voltage-gated anion channel from the electric organ of Torpedo californica." J Biol Chem **254**(20): 10161-6.

Wilkie, A. O. (1994). "The molecular basis of genetic dominance." J Med Genet **31**(2): 89-98.

Wischmeyer, E., E. Nolte, et al. (1993). "Development of electrical myotonia in the ADR mouse: role of chloride conductance in myotubes and neonatal animals." Neuromuscul Disord **3**(4): 267-74.

Wu, F. F., A. Ryan, et al. (2002). "Novel CLCN1 mutations with unique clinical and electrophysiological consequences." Brain **125**(Pt 11): 2392-407.

Zachar, E., C. Fahlke, et al. (1992). "Whole-cell recordings of chloride currents in cultured human skeletal muscle." Pflugers Arch **421**(2-3): 101-7.

Zhang, J., S. Bendahhou, et al. (2000). "Functional consequences of chloride channel gene (CLCN1) mutations causing myotonia congenita." Neurology **54**(4): 937-42.

Zhang, J., M. C. Sanguinetti, et al. (2000). "Mechanism of inverted activation of ClC-1 channels caused by a novel myotonia congenita mutation." J Biol Chem **275**(4): 2999-3005.

Zhu, G., Y. Zhang, et al. (1998). "Identification of endogenous outward currents in the human embryonic kidney (HEK 293) cell line." J Neurosci Methods **81**(1-2): 73-83.

Zifarelli, G. and M. Pusch (2010). "Relaxing messages from the sarcolemma." J Gen Physiol **136**(6): 593-6.

Zlotogora, J. (1997). "Dominance and homozygosity." Am J Med Genet **68**(4): 412-6.

Zumoff, B., G. W. Strain, et al. (1990). "Plasma free and non-sex-hormone-binding-globulin-bound testosterone are decreased in obese men in proportion to their degree of obesity." J Clin Endocrinol Metab **71**(4): 929-31.